Summer 8-15-2019

Aging of the Reproductive System and of Germline Stem Cells in Caenorhabditis

Zuzana Kocsisova
Washington University in St. Louis

WASHINGTON UNIVERSITY IN ST. LOUIS

Division of Biology and Biomedical Sciences
Program in Molecular Genetics and Genomics

Dissertation Examination Committee:
Kerry Kornfeld, Chair
Tim Schedl, Co-Chair
Tom Baranski
Kristen Kroll
Kelle Moley
Zachary Pincus
Joan Riley

Aging of the Reproductive System and of Germline Stem Cells in *Caenorhabditis*

by
Zuzana Kocsisova

A dissertation presented to
The Graduate School
of Washington University in
partial fulfillment of the
requirements for the degree
of Doctor of Philosophy

August 2019
St. Louis, Missouri

Table of Contents

List of Figures

List of Tables

List of Abbreviations

4',6-Diamidino-2-Phenylindole, Dihydrochloride (DAPI)
5-ethynyl-2'-deoxyuridine (EdU)
Caenorhabditis elegans (*C. elegans*)
cell diameters (c.d.)
Distal Tip Cell (DTC)
Endomitotic Phenotype (Emo)
Green Fluorescent Protein (GFP)
Paraformaldehyde (PFA)
Phosphate Buffered Saline (PBS)
Progenitor Zone (PZ)
Proliferating cell nuclear antigen (PCNA)
Single molecule fluorescence in situ hybridization (smFISH)
untranslated region (UTR)

C. elegans gene name conventions

Phenotypes:	Daf	(first letter uppercase, roman)
		Dauer formation abnormal
Genes:	*daf-2*	(lowercase, italic, letters-number)
		Number in order of discovery
Alleles:	*e1370*	(lowercase, italic, follows gene name in parentheses)
		Letter designates where isolated (Jonathan Hodgkin, Oxford)
		Number in order of discovery
Proteins:	DAF-2	(uppercase, roman, same as gene name)
Strains:	CB1370	(uppercase, roman)
		Letters designates where isolated (Jonathan Hodgkin, Oxford)
		Number in order of assignment
		Note: the wild-type strain is N2

Acknowledgments

I would like to thank Swathi Arur for rabbit-anti-GFP antibodies; the *E. coli* stock center for MG1693; Wormbase; the *Caenorhabditis* Genetics Center which is funded by the National Institutes of Health Office of Research Infrastructure Programs (P40OD010440) for strains; Mike Nonet and Scott Dour for advice, reagents, and microscope use for CRISPR/Cas9 genome engineering; Zach Pincus for statistical advice and injection microscope use; Aiping Feng and Luke Schneider for laboratory reagents; Ariz Mohammad for the *am315/nT1g* balanced strain; Charles Baer for the VX02253 strain; the Kimble lab for the JK5500 strain; and several anonymous reviewers (and several who chose not to remain anonymous) for suggestions that greatly improved the manuscripts.

This work was supported in part by NIH grant R01 AG02656106A1 to KK, NIH grant R01 GM100756 to TS, and a NSF predoctoral fellowship DGE-1143954 and DGE-1745038 and the Douglas Covey Fellowship to ZK. The NIH and the NSF would like to make it known that neither had any role in the design of the studies, collection, analysis, and interpretation of data, nor in writing the manuscripts. I would also like to thank the Ellison Medical Foundation, Matt Kaeberlein, Daniel Promislow, Scott Leiser, Matt McCormick, and Hillary Miller for an intense introduction to Aging Biology and R programming at Woods Hole.

I would also like to thank Kurt Warnhoff and Sandeep Kumar for introducing me to *C. elegans* and to aging research; Ariz Mohammad and especially John Brenner for teaching me how to work with the germline and confocal microscopy; Jesús Santiago and Elena Bagatelas for being the sharpest and hardest-working undergraduate researchers one could ask for; Luke

Schneider, Andrea Scharf, James Tan, Brian Earley, Brian Egan, and the rest of the Kornfeld and Schedl labs for training, advice, support, reagents, and helpful discussion about scientific literature, classic science fiction, Chinese history, world politics, and anything in-between; and my Wash U classmates who welcomed me to St. Louis like family, joined me for study hours, which turned to teatimes, which turned to potlucks and Secret Santa get-togethers. Also, I would like to thank my undergraduate advisors, especially Joyce Stamm, for her advice to go to graduate school (heeded) and advice not to work with worms or antibodies (unheeded).

Although I have not met most of them, I would like to thank Stacey Hughes for exploring *C. elegans* reproductive aging in the first place and setting up this research question; Jim McCarter, Paul Fox, Ariz Mohammad, and many others for developing the tools that made these experiments possible, and Sydney Brenner for picking the worm over 50 years ago.

Most importantly, I would like to thank my PhD advisors. Kerry Kornfeld, who introduced me to this research question at a poster session in 2013, I would like to thank for his patience, calm-yet-contagious motivation, immense knowledge, big-picture discussions, and continuous support no matter if experiments "worked" or if "quals" turned out to be a bigger hurdle than anticipated. Since this project is at the intersection of aging biology and germline biology, I was lucky to have Tim Schedl as a co-mentor; I would like to thank him for his deep knowledge, attention to detail and the latest (often yet-unpublished) advances in the field, practical advice when I was troubleshooting finicky experiments, and insistence on weekly updates that helped me bring this project where it is today. Besides my primary advisors, I would like to thank the rest of my thesis committee: Tom Baranski, Kristen Kroll, Zachary Pincus, Joan Riley, and Kelle Moley for their insightful comments, questions, encouragement, and insistence on prioritizing impactful experiments.

Last but not the least, I would like to thank my family: my parents for putting such high value on education and science and for taking the risk in 1999 to move 8,000 kilometers from Bratislava to Atlanta; my two sisters and two brothers for being so good at what they do, fun to be around, and occasionally just the right level of mischievous. Every letter, phone call, and visit from you made me homesick. And Ben Wolf, for making every campsite under the stars feel like home; for turning conversations about gardens, companies, and other projects into adventures; and for becoming my best friend.

Zuzana Kocsisova

Washington University in St. Louis

August 2019

Dedicated to my teachers

ABSTRACT OF THE DISSERTATION

Aging of the reproductive system and of germline stem cells in *Caenorhabditis*

by

Zuzana Kocsisova

Doctor of Philosophy in Biology and Biomedical Sciences

Molecular Genetics and Genomics

Washington University in St. Louis, 2016

Professor Kerry Kornfeld, Chair

Professor Tim Schedl, Co-Chair

C. elegans hermaphrodites display dramatic age-related decline of reproduction early in life while somatic functions are still robust. To understand why the germline fails so early, we analyzed the assembly line of oocyte production that generates fertilized eggs in mated hermaphrodites with sufficient sperm. Aging germlines displayed both sporadic and population-wide changes. A small fraction of aging animals displayed endomitotic oocytes in the germline and other defects. By contrast, all animals displayed age-related decreases in germline size and function. As early as day 3 of adulthood, animals displayed fewer stem cells and a slower cell cycle, which combine to substantially decrease progenitor zone output. The *C. elegans* germline is the only adult tissue that contains stem cells, allowing the analysis of stem cells in aging. To investigate the mechanism of the decrease in stem cell number, we analyzed the Notch signaling pathway. The Notch effectors LST-1 and SYGL-1 displayed age-related decreases in expression domains, suggesting a role for Notch signaling in germline aging. The results indicate that while sporadic defects account for the sterility of some animals, population-wide changes account for the overall pattern of reproductive aging.

Moderate caloric restriction and specific mutations in the insulin pathway result in extended reproductive span, albeit with decreased peak reproduction. We found that while the germline of these mutant animals started out smaller and meiotic entry was lower than in wild-type, the slope of decline was more gradual than in wild-type. This was consistent with the hypothesis that an age-related decrease in progenitor function leads to a decrease in meiotic entry and causes the age-related decrease in progeny production. We also identified mid-life reproductive improvement, a pattern of increased progeny production on days 5-7 of adulthood in *che-3(lf)* and *sygl-1(tg)*, and found that certain mutants extended lifespan without compromising early progeny production and that other mutants increased reproductive ability without extending lifespan. These results showed that while reproductive function and somatic lifespan are inter-linked, they are also separable.

Chapter 1:

Introduction

Reproductive aging is a key component of age-related decline that is important for human health but not well characterized. *C. elegans* is a powerful model system for analyzing reproductive biology, since sophisticated assays have been developed to measure germ line function. The germ line is the only tissue in adult *C. elegans* that contains stem cells, making this an attractive model to study the role of adult stem cells during aging. Reproductive aging is a fundamental feature of the overall aging phenotype that is understudied. *C. elegans* hermaphrodites must be sperm-replete to rigorously analyze reproductive aging and avoid the complications of sperm depletion.

Every scientific endeavor builds on an immense foundation of prior research. Aging researchers have described countless age-related changes in wild-type *C. elegans* (summarized in **Chapter 2**) as well as numerous mutations and pharmacological interventions that extend *C. elegans* lifespan. Hughes (2005) described progeny production in wild-type and mutant sperm-replete *C. elegans* hermaphrodites and defined how reproductive aging would be studied in *C. elegans*. Germline researchers, including Fox *et al.* (2011), defined the gold-standard techniques to study the development and peak function of the *C. elegans* germline. In the following chapters, I describe how we were able to build on this foundation to advance our understanding of reproductive and germline aging in the genus *Caenorhabditis*.

At the outset of these experiments, we hypothesized that cell cycle arrest in germline stem cells was the cause of reproductive senescence in sperm-replete *C. elegans* hermaphrodites. In order to test this hypothesis, we needed reliable and easy-to-use markers of the cell cycle. While markers of M-phase were readily available, the only method to label S-phase required feeding EdU, a nucleoside analog that becomes covalently incorporated into newly replicated DNA and can be visualized using click chemistry, as described in **Chapter 4**. In mammals,

antibody staining against the proliferating cell nuclear antigen has been used as a marker of S-phase. We hypothesized that the presence of *C. elegans* homolog of the proliferating cell nuclear antigen, *pcn-1*, in the nucleus may provide a more convenient marker of S-phase. As described in **Chapter 3**, we found that *pcn-1* is present in the nucleus during S-phase and G2 phase in the *C. elegans* germline. This unexpected pattern of expression was interesting, but made epitope-tagged *pcn-1* useless as a marker of S-phase. For this reason, we used EdU-based techniques, described in **Chapter 4**, to measure the duration of S-phase and of the cell cycle in the *C. elegans* aging germline.

C. elegans hermaphrodites display dramatic age-related decline of reproduction early in life while somatic functions are still robust (Huang *et al.* 2004; Hughes *et al.* 2007), a pattern that holds true in other species in this genus (**Chapter 6**). To understand reproductive aging, we analyzed the assembly line of oocyte production that generates fertilized eggs in wild-type animals (**Chapter 5**). Germlines displayed both sporadic and population-wide changes in function and morphology at ages preceding the age-related decline in progeny production. We also found that, unlike our prediction, older germline stem cells do not arrest in G2-phase. Instead, we found that all germline stem cells progressed through the entire cell cycle more slowly. When Lee *et al.* (2016) and Shin *et al.* (2017) reported that *sygl-1* and *lst-1* are the key effectors of the Notch pathway that maintains germline stem cells (and thus potential stem cell markers), we used CRISPR/Cas9 genome editing to engineer epitope-tagged alleles of these two genes. Using these reagents, we found that the number of stem cells decreases with age. Since all of these changes occurred before the decline in progeny production, we hypothesized that these age-related changes cause the decline in reproduction.

We used long-reproductive mutants to test this hypothesis in **Chapter 6**. First, we measured germline function in several long-reproductive mutants. We found that the pattern of age-related decline in meiotic entry mirrors the pattern of progeny production in long-lived mutants. Second, we tested a prediction of the model in Chapter 5: that increasing Notch signaling would delay reproductive aging. We found that a transgenic strain with increased SYGL-1 expression resulted in increased mid-life progeny production. Next, we performed a candidate-based screen for mutants that extend reproduction. We found that a mutation in *che-3*, which affects chemosensory function, led to increased mid-life progeny production. Both *sygl-1(tg)* and *che-3(p801)* displayed a previously unfamiliar pattern of progeny production (it was called the "magic-mutant" in our experimental proposals): increased progeny production on days 5-7 without a decrease in peak progeny production (days 1-4).

The techniques and results in **Chapters 2 - 6** provide tools to analyze the cell cycle and aging germline, a detailed description of stochastic and pervasive age-related changes in the germline, and several leads regarding molecular mechanisms of reproductive aging. These results also raise new questions and open several avenues for future research. In **Chapter 7** I propose five approaches to continue the study of the molecular and cellular basis of reproductive aging, including approaches to identify additional genetic and pharmacological interventions to increase late-life progeny production and approaches to dissect the Notch signaling pathway to determine the role of the *lag-2* ligand in the DTC during age-related decline.

Chapter 2:

Measuring age-related changes in *C. elegans*

The work presented in Chapter 2 is in preparation for submission with the following authors:

Kocsisova Z., Egan B.E., Scharf A., Anderson X., Kornfeld K.

It is an update of the below-listed chapter for the fourth edition of Wormbook:

Collins J. J., Huang C., Hughes S., Kornfeld K., **2008** The measurement and analysis of age-related changes in *Caenorhabditis elegans*. WormBook : the online review of *C. elegans* biology: 1–21.

Abstract

Aging is characterized by progressive degenerative changes in tissue organization and function that increase the probability of mortality. Major goals of aging research include elucidating the series of events that cause degenerative changes and analyzing environmental and genetic factors that modulate these changes. The bases for mechanistic studies of aging are accurate and precise descriptions of age-related changes, since these descriptions define the aging phenotype. Here we review studies that describe age-related changes in *C. elegans* including measurements of integrated functions such as behavior, reproduction, microscopic analyses of tissue organization, and biochemical studies of macromolecules. Studies that analyze the relationships between different age-related changes are discussed. Together these studies provide fundamental insights into aging in *C. elegans* that may be relevant to aging in other animals.

Introduction

Aging is a fundamental aspect of animal biology that resonates deeply with people, because people experience their own aging and they witness others aging. Because aging is characterized by degenerative changes that progressively diminish function, and increase the probability of death from intrinsic causes people have a strong desire to understand aging so that it can be modified or delayed (Medawar 1952; Jemielity *et al.* 2005). Compared to many synthetic processes in biology that are known to be mediated by complex patterns of gene expression and intricate molecular machines, aging is not well characterized. The causes of aging and the potential plasticity of age-related degeneration are active research areas.

While understanding human aging is an important goal, the experimental challenges of studying aging in humans or other vertebrates are substantial. By contrast, the free-living nematode *Caenorhabditis elegans* is a leading model system for studies of aging based on the identification of mutations, drugs, and environmental factors that extend the adult lifespan significantly. Mechanistic studies of how these factors influence aging are critical, and the foundation for these studies are measurements of age-related changes. Here we review the current understanding of age-related changes in *C. elegans*.

This chapter is divided into three sections: (1) a consideration of the approaches used to measure age-related changes, (2) a description of the specific age-related changes that have been reported for *C. elegans*, and (3) conclusions about aging that have emerged from these studies.

The first section focuses on (a) which age-related changes should be measured; (b) why it is important to measure age-related changes; (c) how age-related changes are measured; (d) tools and methods (e) how these measurements provide a foundation to study mutations and treatments which delay aging; and (f) how these measurements can define the relationships between age-related changes.

The second section describes specific age-related changes that occur in *C. elegans* including behaviors mediated by the neuromuscular system, reproduction, tissue morphology, and biochemical properties (**Table 1**). As is common in *C. elegans* research, most studies focus on the hermaphrodite. Several studies have examined age-related changes in the *C. elegans* male, specifically focused on the behavior and tail morphology (**Table 2**). This section also describes the relationships between age-related changes (**Table 3**).

The third section highlights major conclusions from these studies including the significance of relationships between age-related changes and the relevance of these studies to evolutionary theories of aging.

a) Distinguishing age-related changes pertinent to development and senescence

Changes over time are widespread, yet not every change is due to aging or senescence, and not every change is an appropriate focus for aging studies. It is important to draw a distinction between age-related changes that represent development and growth and age-related changes that represent senescence. While several criterial are useful for distinguishing these changes, establishing definitions that precisely distinguish these two types of changes is challenging.

One useful criterion is whether the age-related change increases organization or function (typical of development) or decreases organization and function (typical of aging). While this is a robust criterion, it is not definitive. For example, older adults display an induction of stress response genes, which seems likely to be a functional response that improves survival. However, this is typically considered an aging change. By contrast, young hermaphrodites lose the ability to generate sperm when the gonad switches to egg production, but this change results in a loss of functional capacity is typically considered development.

A second criterion is the point in the life cycle when the change occurs. Events in the embryo will typically be developmental whereas changes in older adults will typically be aging. While the onset of reproductive maturity is often used as the final event of development and earliest point of comparison for aging studies, it is clear that the distinction is artificial, since the peak of function typically occurs at a time after the onset of reproductive maturity in a variety of

organisms. In fact, there is no time in midlife that clearly separates development from aging, and it is likely that developmental changes and aging changes occur simultaneously. For example, damage accumulation, which is typically considered an aging change, begins in young animals that are undergoing development and growth.

A third criterion is the existence of a genetic program that specifies the change. Age-related developmental changes require a genetic program. If age-related degenerative changes also require a genetic program, then this criterion cannot distinguish development from aging. By contrast, if aging changes do not require a genetic program, then this would be a distinguishing characteristic. As the relationships between genetic programs and age-related changes are better characterized, this criterion may become valuable.

The passage of time results in not only aging, but other changes in the organism. For example, adult hermaphrodites have a limited number of sperm and with time experience both aging and feminization due to sperm depletion (**Figure 7C**). Some studies separate these two variables by using female animals or by providing sperm through mating to avoid feminization (Angeles-Albores *et al.* 2017).

Although a consideration of these issues does not lead to a definition of age-related changes that represent aging, these criteria are useful and most studies focus on changes that occur late in adult life and diminish tissue function or organization.

b) Measuring age-related changes is the foundation for mechanistic aging studies

Measuring age-related changes is important for several reasons. First, these studies provide a description of normal aging in wild-type animals, and this description is the basis for the current understanding of aging. These descriptive studies have revealed that age-related

changes are widespread, affecting many different tissues. Furthermore, age-related changes occur at all levels of organization. At the level of integrated systems that require multiple tissues, there are declines in survival, stress resistance, and function, such as diminished body movement and reproduction. At the level of tissues and cells, there are changes in morphology, such as a decline in intestinal and vulval integrity, and increased disorganization of the nucleus and mitochondrial networks. At the molecular level there are structural changes of macromolecules, such as DNA, proteins, and metabolites.

Second, the identification of specific age-related changes has been the source of hypotheses regarding the causes of aging. For example, the observation of age-related increases in oxidative damage to macromolecules such as proteins and nucleic acids suggests the hypothesis that these structural changes are a cause of age-related functional declines (Balaban *et al.* 2005). Similarly, the observation of age-related increases in yolk protein in the body cavity or apoptotic corpses in the germline suggests the hypothesis that some developmental processes may become detrimental when they continue during adulthood and are this a cause of age-related functional declines (de la Guardia *et al.* 2016; Ezcurra *et al.* 2018).

Third, measurements of age-related changes can provide markers of aging. Such markers allow assessments of the extent of aging in live animals and can be used to predict lifespan or used to evaluate short-lived strains for evidence of premature aging (Baker and Sprott 1988; Garigan *et al.* 2002; Huang *et al.* 2004; Gerstbrein *et al.* 2005; Pincus and Slack 2010).

Fourth, the measurement of age-related changes is a necessary starting point for studies that can define causal relationships during aging. The ultimate goal of aging research is to provide a comprehensive description of age-related changes that includes the causal relationship between the different changes. While measurements of age-related changes alone do not define

the causal relationships, these measurements are an essential element of experiments that have the potential to define causal relationships. These experiments include the analysis of genetic, environmental, dietary, and pharmacological factors that influence aging and longitudinal studies that define relationships between different age-related changes (Huang *et al.* 2004). In the past decade, a vast number of genetic and pharmacological factors have been reported to influence aging. In this chapter, we will focus on descriptions of age-related changes in wild-type animals and on longitudinal studies that define the relationships between age-related changes.

For these reasons, measurements of age-related changes are a critical component of every mechanistic aging study.

c) How to measure age-related changes

Any property of a biological system that can be measured can in principle be analyzed as a function of time during the animal's life stages.

The **first** important issue is the time axis; relevant considerations are the starting time, the ending time, and the number of intermediate times that are analyzed (**Figure 5**). For *C. elegans*, the starting times that are frequently selected are egg deposition, the emergence of the L1 larvae or the L4 larvae, or the appearance of the first embryos in the uterus, since these developmental stages can be accurately determined by morphological criteria. The simplest study involves measuring one time point. If two or more time points are analyzed, then it is possible to derive a graph of the property versus time. Two time points can be analyzed with a linear regression, more time points can be analyzed with a linear, polynomial, or exponential regression (**Figure 5**). *C. elegans* studies frequently involve daily measurements until the end of life. For example, a lifespan analysis typically involves daily assessments of whether the animal is alive or dead.

When designing a study, the tradeoffs between temporal resolution, sample size, and statistical power should be carefully considered (Petrascheck and Miller 2017). In this chapter, we summarize the reported age-related changes regardless of the number of time points analyzed in the study.

The **second** important issue is whether the study has a longitudinal or cross-sectional study design. Cross-sectional studies typically involve a single measurement of each young individual and a single measurement of each old individual (**Figure 2**). Any differences between the group of young animals and the group of old animals are attributed to age. However, it is not possible to rule out that differences existed between the groups for reasons other than age. Cross-sectional studies are used for invasive measurements, such as electron microscopy, and for experiments that require combining multiple animals (bulk measurements), such as protein analysis by mass spectrometry or Western blot.

In a longitudinal study, individual animals are observed at a young age and the same individuals are observed again later at an old age (**Figure 2**). Because the same individual is observed at all time points, it is more straightforward to distinguish which changes existed between individuals and which changes occurred as a result of age. Because longitudinal studies involve serial measurements of the same individual, the measurements must be non-invasive (except for the final measurement, which can be invasive). Longitudinal studies provide the same information as cross-sectional studies, but also tighter correlations and opportunities for data analysis that are not possible with cross-sectional studies. *C. elegans* are well suited to longitudinal studies because of the relatively short lifespan.

The **third** important issue is the measurement itself. While in principle any measurable property of the animal can be analyzed as a function of time, in practice aging studies of *C.*

elegans tend to focus on rhythmic behaviors, tissue and cell morphology, and changes in biochemical properties. Each of these measurements is discussed in detail below.

A general issue is the extent to which the measurement is quantitative. (i) Some measurements are highly quantitative, such as the rate of pharyngeal pumping or the number of copies of a particular mRNA. For highly quantitative measurements, it is possible to graph the quantity versus time (**Figure 3A**). Image analysis tools like ImageJ and FIJI can be vital in extracting quantitative information from microscopic analyses. (ii) For measurements that are not highly quantitative, the typical approach is to establish ordered categories (**Figure 3G**). For example, tissue organization is not easily quantified, so categories such as well organized, partly disorganized, and highly disorganized might be used (Garigan *et al.* 2002; Herndon *et al.* 2002; Chow *et al.* 2006). Numbers may be assigned to these ordered categories (e.g. well organized = 1, partly disorganized = 2, highly disorganized = 3) to allow the generation of summary statistics. However, because these numbers are assigned somewhat arbitrarily, this approach is limited to non-parametric statistics. (iii) Other non-quantitative measurements may not lend themselves to ordered categories, so unordered categories are used. For example, germline defects include cavities, misshapen oocytes, mislocated oocytes, and cellularization, among other, yet is it not clear which defect is more severe than another. (iv) Finally, some measurements are binary. For example, vitality is not easily quantified or categorized, so animals are classified as alive or dead. Statistical methods developed for survival analysis are often used with binary measurements.

A **fourth** important issue in analyzing these data is the generation of summary statistics for the purpose of making comparisons. **Figure 3** shows the basic approaches that have been used to generate summary statistics. One approach is to analyze the pattern of the declining

function. For example, the data can be fit to a straight line and the slope of the line and intercepts where the line crossed the X or Y-axis can be used as summary statistics (Bolanowski *et al.* 1983; Johnson 1987). An important issue with the approach of fitting data to a straight line is that these data may fit better to another shape. A second approach is to predetermine a time and then compare the values (see **Figure 3A,B**). This approach is almost always used for studies of biochemical properties and tissue morphology, and is often used for studies of behavior. A third approach is to predetermine a transition point in the value and then compare the times (see **Figure 3C,D**). A related approach is to predetermine the value and compare the number of individuals in the population above or below the value (see **Figure 3E,F**). This is the approach used for lifespan, where the predetermined value is the transition from alive to dead. This approach can also be used to analyze other transitions, such as the cessation of pharyngeal pumping or reproduction (Huang *et al.* 2004; Hughes *et al.* 2007; Wang *et al.* 2014). Several transitions can be combined to represent stages of aging (**Figure 3G**), and the time axis can be normalized to maximum lifespan to show the proportion of life spent in each stage (**Figure 3H**; Huang *et al.* 2004; Bansal *et al.* 2015).

d) Tools and methods

Classical tools for measuring age-related changes in *C. elegans* include microscopy, biochemistry, and sequencing. As discussed above, some techniques lend themselves to **quantitative** measurements while others are qualitative. As previously mentioned, some techniques like counting pharyngeal pumping are non-invasive, some like Nomarski microscopy are invasive but non-lethal, while others like immunohistochemistry are lethal and **invasive**. Some methods such as microscopy provide **spatially-resolved** information, while other methods

such as Western blot analysis and RNA-seq require homogenization of the tissue, thus losing the spatial aspects. A related aspect of such techniques is the amount of tissue required for analysis. Due to recent advances in DNA sequencing technologies, it is becoming possible to use techniques like RNA-seq on individual *C. elegans*. Other techniques, like mass spectrometry, require pooling several hundred, thousand, or million animals in order to obtain a **bulk measurement** on a sufficiently large sample. This chapter highlights the features and limitations of the method as each method is introduced and in the fourth column of **Table 1 and 2**.

An important advancement in this field has been the development of tools and methods for **automating measurements**. Automated techniques help researchers achieve larger sample size and more consistent environment than when working manually. These techniques generally rely on automated serial image capture and image recognition tools which must separate information about the animal from background information. In order to make this possible, modifications had to be made to the culture conditions of *C. elegans*. Standard Petri dishes with nematode growth medium seeded with *E. coli* OP50 and placed on a dissecting microscope work well when manipulated by human hands and observed directly by human eyes, but are difficult to automate. Stroustrup *et al.* (2013) continued to use Petri dishes, but substituted scanners instead of the dissecting microscope. Solis and Petrascheck (2011) turned to liquid culture to increase throughput of lifespan assays, and placed animals in 96-well microtiter plates which can be observed under a microscope manually or automatically. Hulme *et al.* (2010) also use liquid culture of animals, but each individual is maintained in a separate microfluidics chamber for lifelong microscopic observation. Zhang *et al.* (2016) isolated individual animals in droplets of *E. coli* OP50 in sealed polymer compartments for lifelong microscopic observation. Churgin *et al.* (2017) also isolated individual animals in droplets of *E. coli* OP50 for lifelong microscopic

observation, but used a molded polymer. Additional automation and culture techniques are reviewed by Kamili and Lu (2018). All of these techniques have been demonstrated to automate the measurement of lifespan, and those techniques which maintain animals under near-constant surveillance can measure additional age-related changes non-invasively.

The analysis of survival data requires special techniques and non-parametric statistics, because survival data rarely fit a normal distribution or the assumptions of parametric tests. The survival curve displays the probability of being alive at a particular age and is often displayed as a Kaplan-Meier survival curve, which accounts for censored events explained below (Kaplan and Meier 1958). A survival curve can be summarized by its mean (or median), maximum, and variance. The amount of variation in lifespan of individuals can be described by how "steep" or "square" the survival curve appears: a steep curve means less variation. Two or more survival curves can be compared based on these parameters. When very large sample sizes are available, it may be possible to mathematically model the survival curve, for example by fitting a Gompertz or a Weibull function (Pletcher *et al.* 2000), or to compare whether two survival curves scale (Stroustrup *et al.* 2016).

Statistical analysis of lifespans

Whether one is measuring a nematode's lifespan or another binary phenotype, some animals which started in the study never reach the measured endpoint. They may crawl off the petri dish, die for a reason not under study (e.g. matricide or vulval extrusion), or may not have reached the endpoint (death) by the time the result is being analyzed. This poses a challenge to analyzing survival datasets. These animals can be excluded from the entire dataset (purple) or, because the fact that they were alive at earlier timepoints is, in fact informative, the animals can

be included until the time they bag, extrude, flee, or the experiment ends (green). The second approach is called censoring. Both approaches are commonly used in the *C. elegans* literature.

Not including censored data leads to under-estimates of lifespan, and could lead to bias if the censored events occurred in a non-random way. For example, if censoring occurs due to animals crawling off the Petri dish, the genotype with the healthiest and most motile animals may be more prone to crawl off the Petri dish than wild-type controls. Excluding, rather than censoring, these animals biases the dataset and decreases the sample size. Even when these events occur in a random fashion, exclusion decreases the sample size, leading to reduced statistical power. On the other hand, censoring animals requires the assumption that their likelihood of natural death at any age was the same as the rest of the population (Kaplan and Meier 1958). Optimally, very few animals would be excluded or censored.

In wild-type unmated animals, ~8% die due to matricidal hatching (Shaw *et al.* 2007). Animals which died due to matricide or vulval extrusion are typically excluded or censored because their early death may not be informative about the aging process under study. However, several recent studies have examined matricide and vulval extrusion, finding them to be predictive of lifespan (Pickett and Kornfeld 2013; Leiser *et al.* 2016). Sterilizing animals chemically or genetically may reduce the number that need to be censored for matricidal hatching.

Animals which crawl off the NGM onto the edge of the dish and desiccate are also censored. When an experimental treatment increases the rate of "fleeing" to intolerably high levels or unequally among treatments, adjusting culture conditions may reduce fleeing. A physical barrier of palmitic acid applied to the border of NGM dishes works admirably well (Angelo and Van Gilst 2009; Fletcher and Kim 2017). Worm Corrals, WorMotels, microfluidics,

and liquid culture also prevent fleeing to make censoring and excluding nearly unnecessary (Hulme *et al.* 2010; Solis and Petrascheck 2011; Zhang *et al.* 2016; Churgin *et al.* 2017).

Software is available to perform survival analyses. The *survival* library in the R software environment can be used for all statistical analyses and basic graphing. Additional libraries, such as *ggplot2*, *ggfortify*, and *survminer* are useful for adjusting the graphics. The same R analysis can be performed without needing to learn R by using the Online Application for Survival analysIS OASIS (Yang *et al.* 2011; Han *et al.* 2016). In Python, the relevant library is *lifelines*. Finally, commercial software for statistical analysis also contains tools for survival analysis.

Because of variation in approaches to censoring and excluding, it is important to pay attention to the methods used by each study. It is helpful to the reader when the methods clearly state whether animals were censored or excluded, the censoring criteria, and the number of animals censored or excluded by group, in addition to the sample size. It is also helpful to cite the software used for graphing and statistical analysis.

Important aspects of nematode culture

A powerful aspect of *C. elegans* studies is a single defined wild-type genotype and a unified set of culture conditions: Bristol-N2 grown at 20 °C on Petri dishes with Nematode Growth Medium inoculated with *E. coli* OP50 (Brenner 1974; Stiernagle 2006). However, many studies of age-related changes have modified the reference genotype or culture condition for various reasons.

Temperatures besides 20 °C may be used so that experimental time-points align more conveniently with the typical work day and work week, or because the genotypes and phenotypes are most robust at temperatures other than 20 °C.

In aging studies it is important to separate the animals under study from their progeny. One method to achieve this requires moving the adult animals away from their progeny daily. This method is labor-intensive, thus prohibitive to large sample sizes and in techniques that limit access to the animals. An alternate approach is to use only female or sterile animals which cannot produce progeny. Common genotypes include: *fog-2, spe-8, spe-9, daf-2, glp-1, glp-4,* etc. While convenient, these genotypes are not neutral to aging. For example, the temperature-sensitive *daf-2(e1370)* allele in the dauer entry pathway provides a convenient method to separate the parental generation from progeny and also causes the animal to live twice as long as wild-type (Kenyon *et al.* 1993). Studies of the aging male sometimes use *him-5* strains in order to make the collection of males easier.

Another method to avoid mixing generations involves using drugs to selectively kill or sterilize progeny. The antimetabolite drug floxuridine (FUdR) has been used since the earliest aging studies in nematodes (Gershon 1970). FUdR at concentrations up to 400 μM does not affect the lifespan in wild-type animals, but causes a lifespan extension in some mutants, including *gas-1* and *tub-1* (Aitlhadj and Stürzenbaum 2010; van Raamsdonk and Hekimi 2011; reviewed in Amrit *et al.* 2016). FUdR can make aging experiments possible in strains otherwise prone to extremely high levels of matricidal hatching (Shaw *et al.* 2007)

While *E. coli* OP50 has historically been the primary food source for nematode culture, many other dietary conditions can cause changes in lifespan (reviewed in (Amrit *et al.* 2014)). It has long been known that decreasing caloric intake can increase the lifespan in *C. elegans* (Klass 1977; Hosono *et al.* 1989; Lakowski and Hekimi 1998). Common methods of inducing dietary restriction in nematodes are food dilution (Klass 1977), reducing bacterial growth (Hosono *et al.* 1989; Greer *et al.* 2007), and removal of food (Lee *et al.* 2006; Kaeberlein *et al.* 2006).

Feeding *E. coli* OP50 that has been killed via heat, antibiotics, or UV-light treatment can increase lifespan in adult animals (Gems and Riddle 2000; Garigan *et al.* 2002). Some have suggested caloric restriction as a cause, but no difference in morphology or fecundity has been observed in animals fed dead *E. coli* (Gems and Riddle 2000), and this effect is still observed with bacteria grown on carbenicillin, which simply arrests bacterial growth (Garigan *et al.* 2002). Variability in male lifespan of animals grown on crowded plates was reduced when animals were fed dead *E. coli*, and also reduced when males were maintained on the same bacterial lawn for their whole life compared to transferring every few days (Gems and Riddle 2000).

Other bacterial food sources can increase or decrease lifespan compared to *E. coli* OP50. *E. coli* strains HB101 and HT115 increase lifespan compared to OP50 (Soukas *et al.* 2009; Brooks *et al.* 2009; Maier *et al.* 2010), and *E. coli* HB101 can also reduce reproductive lifespan, but not brood size (Sowa *et al.* 2015). Bacterial species other than *E. coli* can extend lifespan (Garsin *et al.* 2003; Ikeda *et al.* 2007; Sánchez-Blanco and Kim 2011; Sánchez-Blanco *et al.* 2016; Kato *et al.* 2018) or reduce lifespan (Tan *et al.* 1999; Labrousse *et al.* 2000; Sifri *et al.* 2003). The soil bacteria *Comamonas* DA1877 has been shown by some to reduce fecundity and lifespan in adult animals and accelerate their development (Macneil *et al.* 2013), while others have found no effect on fecundity or lifespan (Kauffman *et al.* 2010; Kumar *et al.* 2019).

Besides bacterial diet, other conditions can affect *C. elegans* lifespan. Gems and Riddle (2000) showed that isolated males lived longer that males raised with other males; this effect occurred even with as few as 2 males living on the same plate, and was not observed in hermaphrodites. Avery and Shtonda (2003) found that bacterial cell size affected growth rate; animals raised on larger bacteria grew slower than animals raised on smaller bacteria.

The bacterial food source is often used to deliver double-stranded RNA for RNAi feeding experiments (Timmons and Fire 1998; Kamath *et al.* 2000, 2003). Previously, *E. coli* HT115 was used for this purpose, but recent advancements have made it possible for *E. coli* OP50 to be used for RNAi feeding (Xiao *et al.* 2015).

e) Using measurements of age-related changes to characterize factors that influence aging.

In *C. elegans*, factors that have been demonstrated to influence aging include mutations, drugs, diet, and environmental conditions such as temperature. A major goal of aging research is to characterize the mechanisms that cause these factors to influence aging. One important approach to addressing these mechanisms of action is the analysis of how these factors affect age-related changes. A typical approach is to compare an age-related change in wild-type and mutant animals. In, for example, animals with a loss-of-function mutation display a delay of the age-related change, then it suggests that the gene activity causes an acceleration of that age-related change.

So many genes, drugs, and environmental manipulations have been found to extend lifespan and delay age-related changes, that describing them in full is now beyond the scope of this chapter. (Son *et al.* 2018) provides an excellent review of mutations and treatments which delay aging.

f) How to define relationships between age-related changes

A fundamental question in this field is: what are the relationships between age-related changes? In principle, two age-related changes might be independent, they might share a common cause, or they might be linked in a causal relationship such that one age-related change

causes the second age-related change (**Figure 6**). This issue is particularly important for the age-related increase in the probability of mortality that is measured by lifespan; a major goal of aging studies is to identify the age-related changes that contribute to the increasing probability of mortality. Thus, studies that distinguish age-related changes that are independent of survival probability from age-related changes that are correlated with survival probability are important.

Several approaches can be used to experimentally address the relationship between two age-related changes. First, in some cases it is possible to use an experimental intervention to specifically modify one age-related change, and then then measure the effect on the second age-related change. For example, a drug with antioxidant activity might be used to specifically delay age-related oxidative damage and the effects on lifespan could be monitored. This approach is conceptually appealing, but in practice it is difficult to specifically affect age-related degenerative changes – especially to prevent, delay, or decrease the extent of a single specific age-related change.

A second approach is to characterize the correlation between two age-related changes. For example, Johnson (1987) analyzed multiple recombinant inbred strains and showed that strains with an extended lifespan also displayed an extended period of body movement. Another method is to use longitudinal studies to analyze variation within a genetically homogeneous population. Huang *et al.* (2004) used this approach to show that animals with an extended period of pharyngeal pumping also displayed an extended period of body movement. This chapter highlights experimentally determined relationships as each age-related change is considered, and Table 3 summarizes the relationships between age-related changes that have been defined using these approaches.

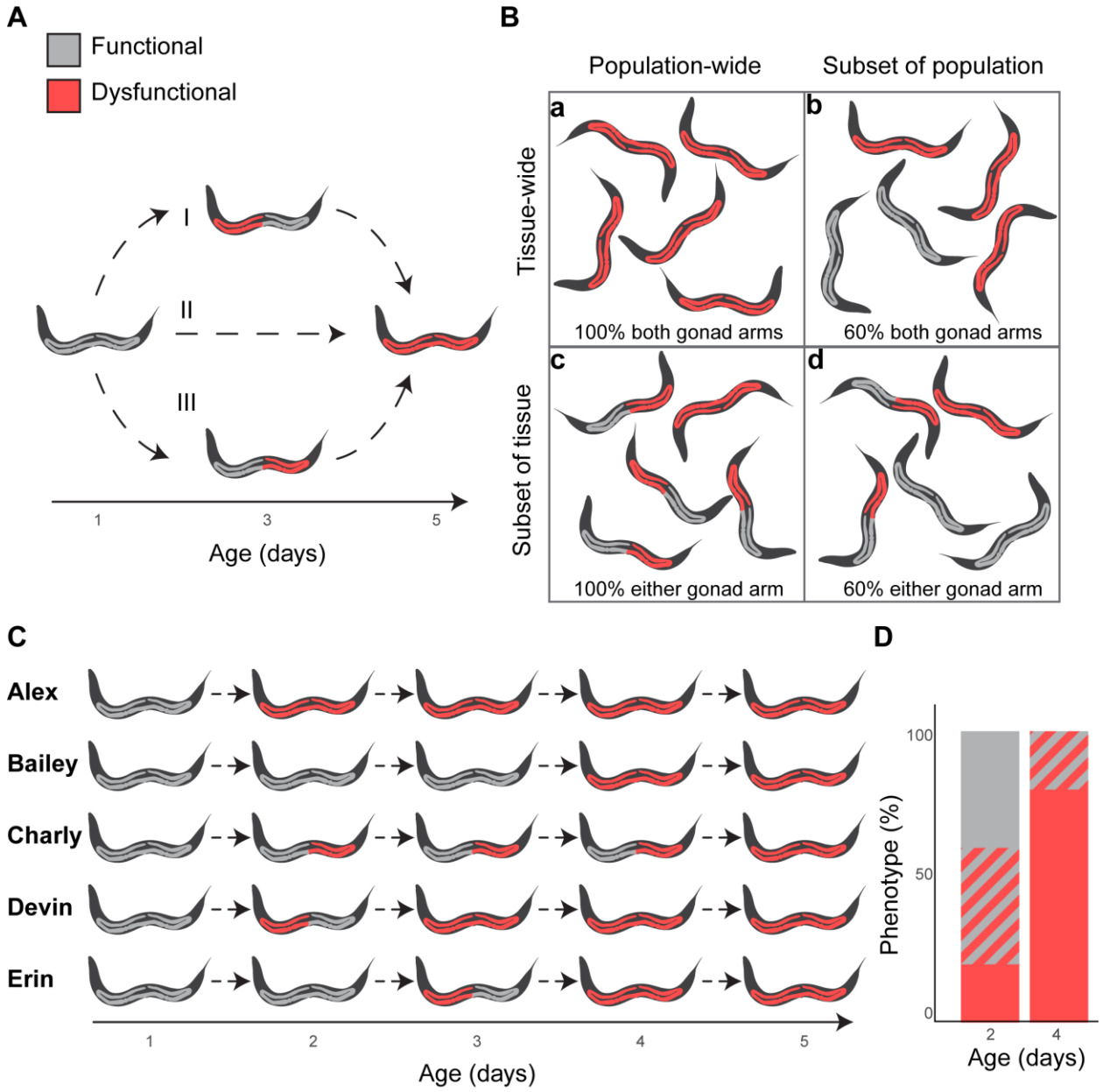

Figure 1: The stochastic nature of some aging phenotypes.
Functional germlines are illustrated in gray; dysfunctional germlines in red. A) Body plan symmetry provides a platform to study tissue heterogeneity in aging. An animal which develops defects in both germlines could have developed the defects simultaneously (II), first in the anterior arm, then the posterior arm (I), or first in the posterior arm, then the anterior arm (III). B) While some phenotypes appear in every part of a tissue in every individual in a population, other age-related phenotypes display some stochasticity. The stochasticity can be at the level of the population: 100% of animals display germline defects in (a), but only 60% of animals display germline defects in (b). In other instances, the stochasticity can be at the level of the tissue: the defects can affect both gonad arms in (a), but affect either or both gonad arms in (c). When stochasticity occurs at both the level of the population and at the tissue level, only some animals are affected, and affected animals may only display defects in part of the tissue, as shown in (d). For example, the Endomitotic oocyte phenotype, described in Kocsisova *et al.* (2019) affects only ~10% of day 5 animals, but typically affects both gonad arms (b). In contrast, Herndon *et al.* (2002) find that

sarcomere, hypodermis, and intestinal integrity often suffer random but extreme local crises and report “wide variability in both the time of onset and the rate of apparent deterioration within an isogenic population reared under uniform environmental conditions,” as illustrated in (d). Longitudinal observations with fine time resolution reveal the full pattern while cross-sectional observations or sparse timepoints reveal only snapshots. C) The diagram shows five individuals (Alex, Bailey, Charly, Devin, and Erin) develop age-related germline defects over five days. D) The stacked bar graph summarizes the data in C by plotting the percentage of individuals at day 2 and day 4 which display two functional germlines (gray), one functional and one dysfunctional germline (striped), and two dysfunctional germlines (red).

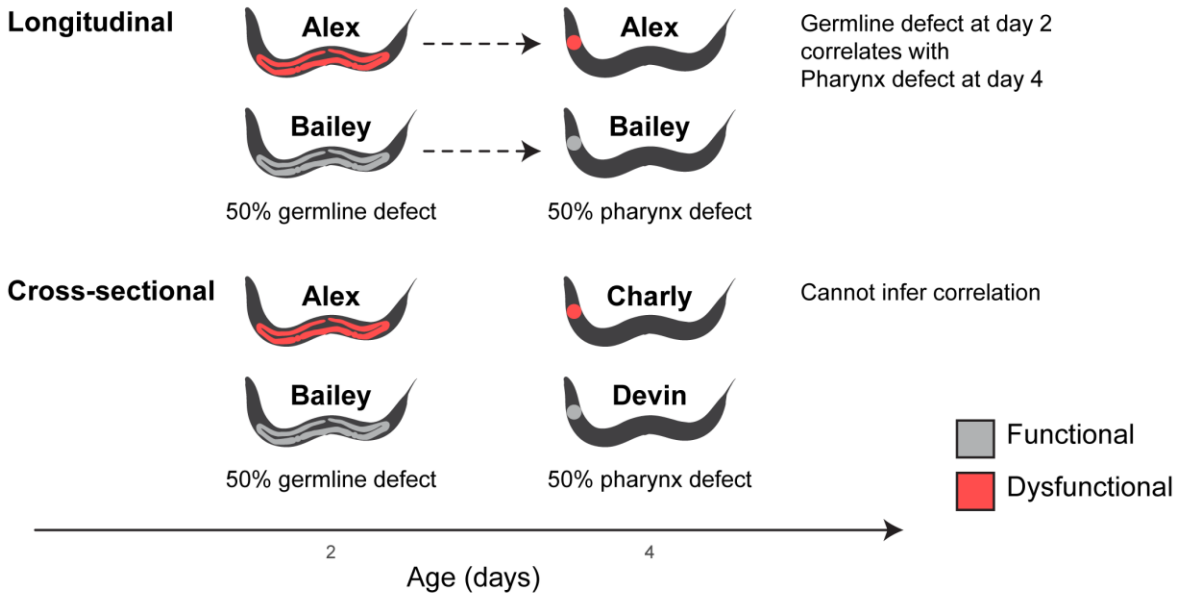

Figure 2: Aging studies can be longitudinal or cross-sectional
In this fictional study, a longitudinal and a cross sectional approach was used to detect germline defects at day 2 and pharynx defects at day 4. Both approaches used two time points and two animals per time point. Both studies detected that 50% of day 2 animals exhibited the germline defect and that 50% of day 4 animals exhibited the pharynx defect. In the cross-sectional study, different individuals were measured at day 2 (Alex and Bailey) and at day 4 (Charly and Devin), and no additional correlations could be inferred. In the longitudinal study, the same individuals (Alex and Bailey were identified and observed at day 2 and at day 4. Because traits could be matched to individuals and correlated over time, the longitudinal study identified a correlation between an individual having a germline defect at day 2 developing a pharynx defect by day 4.

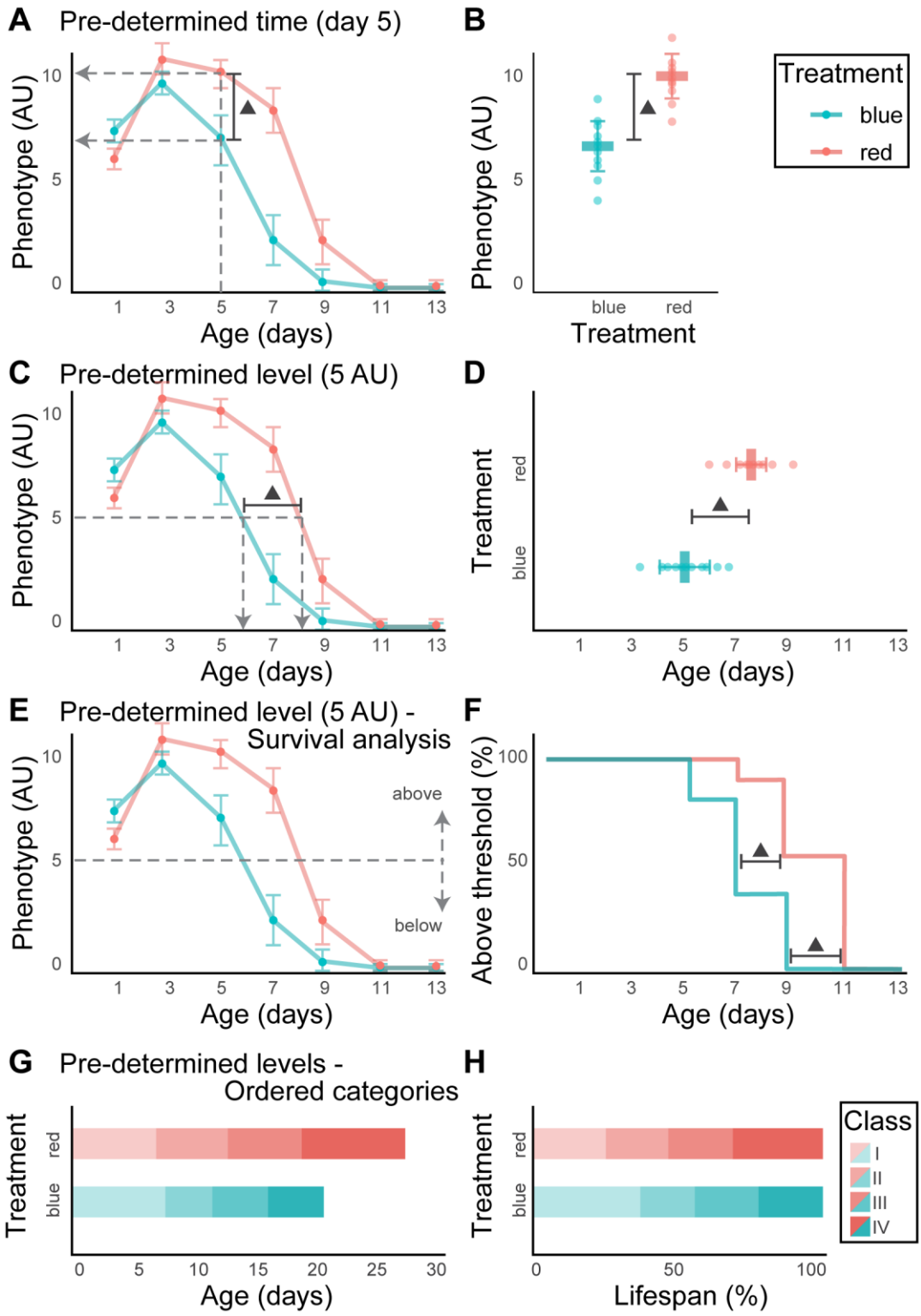

Figure 3: Analysis of age-related changes

A comprehensive description of an age-related decline involves a large set of phenotypic measurements taken at many different times. These data sets can be analyzed, summarized, and compared using several approaches illustrated here. A,C,E) Blue and red lines are hypothetical examples of data sets generated by measuring a quantitative phenotype as a function of time for two groups of animals. The blue animals displayed a more rapid

age-related decline than the red animals. B) Red and blue animals were compared by determining the phenotypic value for each group at one pre-determined time (e.g. day 5). The typical summary statistic is the average phenotypic value at the predetermined time (bold horizontal line), +/- the standard deviation (whiskers). For data which are not normally distributed, the median and inter-quartile range may be more appropriate and may be visualized as a box and whiskers plot. In either case, individual data points may be displayed. Black triangle indicates the difference between the means of the blue group and the red group. The average phenotypic value of the blue group is lower, indicating a more rapid decline. D) Blue and red animals were compared by analyzing the time when each group transitioned to a predetermined phenotypic value (e.g. 50%). The typical summary statistic is the average (or median) span of time from the start of the experiment to the transition time. Black triangle indicates the difference between the means of the blue group and the red group. The transition time of the blue group occurred at an earlier time, indicating a more rapid decline. F) If a phenotypic value is predetermined as shown in panels C and D, then each animal can be classified as above or below that value. The fraction of animals above the value can be plotted. This is the standard approach for survival data, where the predetermined phenotypic value is alive (versus dead), and the typical summary statistic is the mean (or median) lifespan. In addition, this approach can be used for other binary phenotypes such as fertility (e.g. 1 or more eggs produced), pharyngeal pumping (e.g. 10 or more pumps per minute), or body movement (e.g. 5 or more bends per minute). A staircase-style graph is often used to indicate that the data represent a "survival" analysis. Non-parametric statistics, such as the Kaplan-Meier estimator, are typically used because survival data rarely fit a normal distribution or the assumptions of parametric tests and often contain "censored" events. Black triangle indicates the difference between the medians of the blue group and the red group. The graph shows that the fraction of animals above the predetermined value declines more rapidly in the blue group. G) If more than one predetermined value is used to set thresholds for one phenotype, or if multiple phenotypes are employed, animals can be classified into several consecutive stages of aging. This approach was used by (Huang *et al.* 2004). Stage I is a period from onset of adulthood until the end of self-fertile progeny production; Stage II is a post-reproductive period characterized by vigorous motor activity; Stage III is a period of reduced motor activity with continued pharyngeal pumping; Stage IV is a period of minimal motor activity until the end of lifespan. A similar approach was used by Herndon *et al.* (2002 and Newell Stamper *et al.* (2018) to classify animals into three stages: voluntary coordinated mobility, uncoordinated mobility in response to stimulation, and head/tail mobility in response to stimulation. The blue group spent a longer time in stage I. H) The stages of aging over chronological time (G) can be normalized to maximum lifespan to show the proportion of life spent in each stage (Huang *et al.* 2004). This type of approach was used by (Bansal *et al.* 2015) to compare the proportion of life in healthspan versus gerospan. The blue group spent a larger percentage of its life in healthspan.

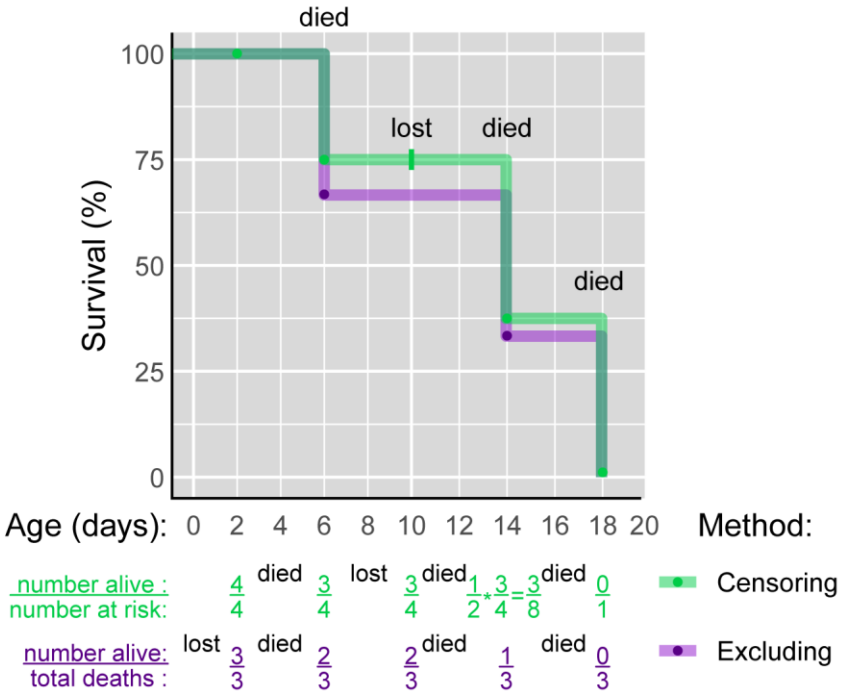

Figure 4: Survival analysis.
The survival curve illustrates a single lifespan dataset analyzed using either excluding (purple) or censoring (green) (Kaplan and Meier 1958) of animals which did not reach the measured endpoint (death). 'died' indicates death occurred at that time point. 'lost' indicates that an animal was lost and its death could not be determined. Censored events are indicated with a '|' on the graph. Fractions below the plot indicate the calculation of the survival curve. Notice the effect on the survival curve at day 8, 12, and 16.

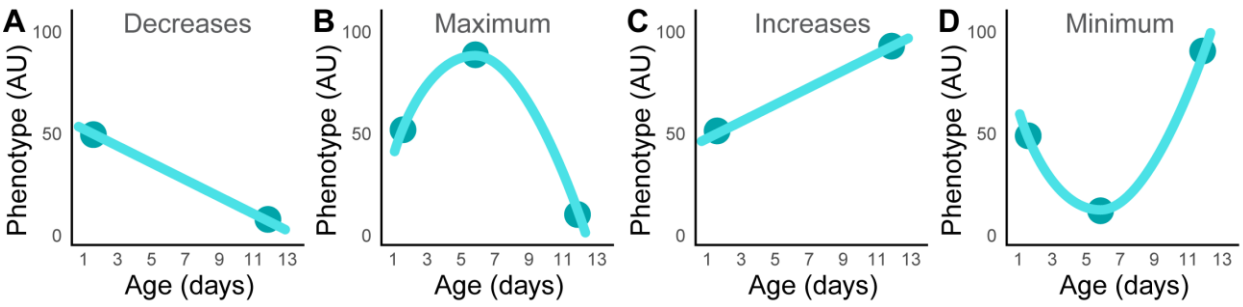

Figure 5: Phenotypes may increase, decrease, or achieve a maximum or minimum.
Only two points are required to define a line (A,C), but three or more points are required to define a more complex pattern (B,D). When a study only measured a phenotype at two time points and reported a decrease (A), it is possible that a later study with increased temporal resolution may uncover an initial increase, followed by a decrease (B).

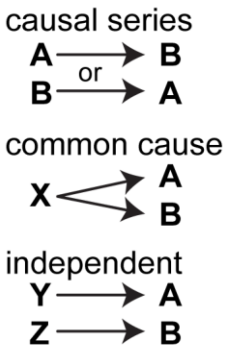

Figure 6: Correlation and Causation
Two age-related changes, A and B, can be found in a causal series, share a common cause (X), or be independent.

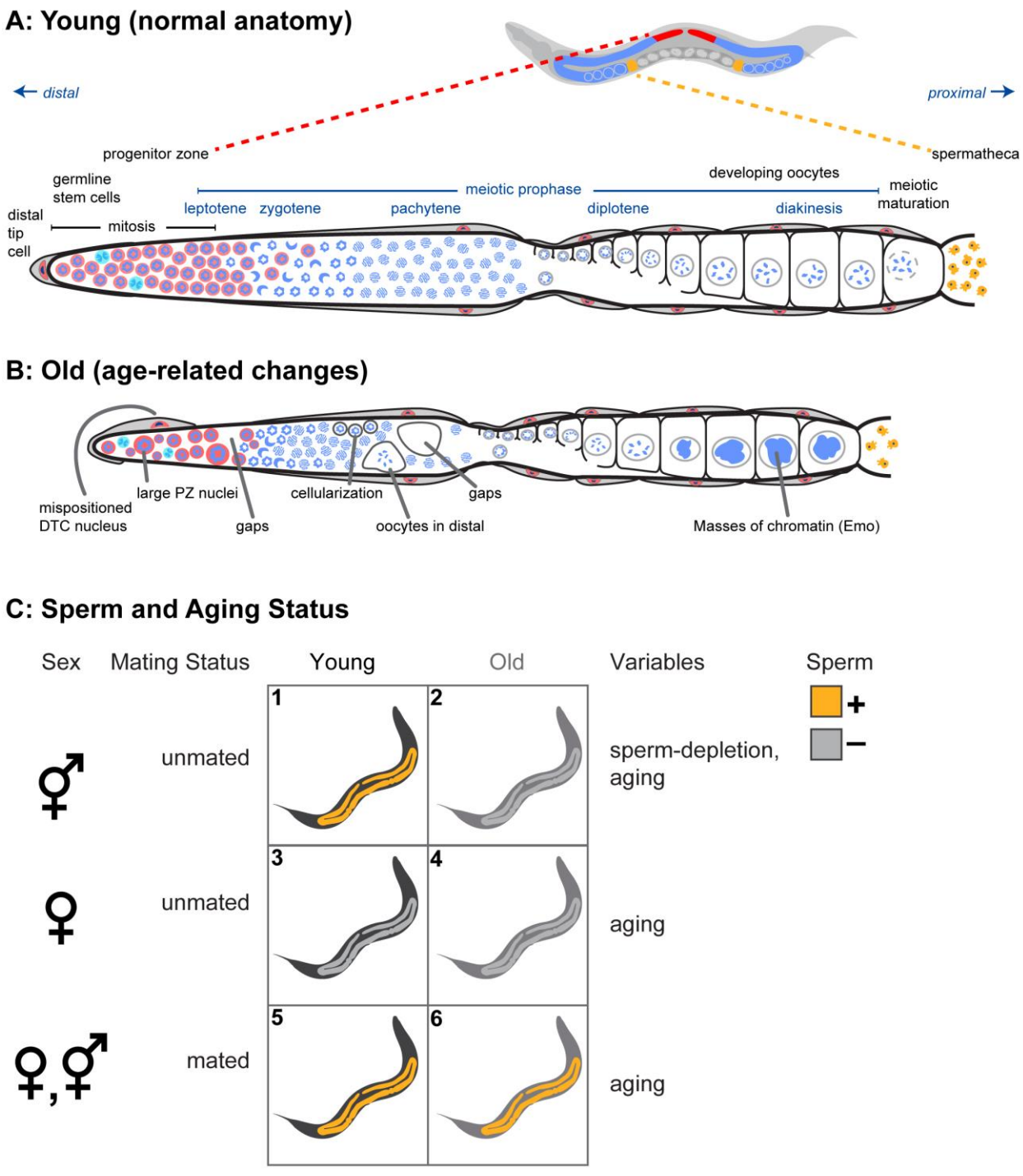

Figure 7: Germline develops defects with age

A) Normal anatomy of *C. elegans* germline. Top: *C. elegans* hermaphrodites have two U-shaped germlines (red and blue). The spermatheca is shown in yellow and the uterus with developing embryos is shown in dark gray. Bottom: Diagram of one unfolded *C. elegans* hermaphrodite germline. Nuclear morphology can be visualized by staining DNA with DAPI (blue). The distal progenitor zone (red) contains mitotically cycling stem and progenitor cells. The distal tip cell (DTC) provides the GLP-1/Notch ligand to maintain the stem cell fate of these cells. As cells migrate away from the DTC, they exit the progenitor zone and enter meiotic prophase. B) Numerous age-related changes in

the germline have been reported. Several are illustrated here. C) In wild-type hermaphrodites, the number of sperm is limiting. Therefore two major changes occur with the passage of time: aging and sperm-depletion.

Results

SURVIVAL

The most overt age-related change is survival; the cumulative probability of death eventually reaches 100%. Gershon (1970) chose the nematode as a convenient model for aging studies and measured the lifespan of *Turbatrix aceti* nematodes. Shortly after, Epstein, Himmelhoch, and Gershon (1972) measured the lifespan of *Caenorhabditis briggsae* in axenic culture. *C. elegans* lifespans were measured in both axenic and standard NGM culture by Klass (1977) and Croll *et al.* (1977). Since then, countless studies have measured the lifespan of millions of *C. elegans* with numerous genotypes and under varied environmental conditions.

It can be difficult to distinguish death, the permanent cessation of all vital functions, because we are not able to measure all vital functions non-invasively at all times in *C. elegans* aging experiments. The working definition of death in a lifespan analysis is the cessation of movement, either voluntary or in response to a stimulus such as light or prodding with a platinum wire.

Huge variability exists, even among isogenic populations. In homogeneous defined medium (CeMM), the mean lifespan is 30 ± 20 days, with a maximum of 93 days. In standard nematode growth medium NGM and *E. coli* OP50 diet, the mean lifespan is16 ± 6 with a 30 day maximum (Szewczyk *et al.* 2006). Reproducibility within and between laboratories (e.g. in the *Caenorhabditis* Intervention Testing Program) can be a challenge; therefore it is critical to include a concurrent control every time (Lucanic *et al.* 2017).

Stress Response

When an animal dies in a lifespan experiment under optimal stress-free conditions, we assume its death was caused by age. However, any environment, including standard NGM culture, involves fluctuating levels of stress. Death in standard conditions could be thought to occur when an individual's level of stress resistance decreases so low that a tiny fluctuation in the environment kills the individual. Stress resistance experiments intentionally increase the level of a stressor (e.g. heat, oxidation, radiation, pathogens, etc.) at a particular time and measure the ability of individuals to survive the stress. Conceptually, the two approaches are very similar, as they both measure the survival of animals over time.

When an animal dies under high-stress conditions, it is not clear whether that death occurred as a result of stress, or whether the animal would have died of age even under low-stress conditions. For this reason, some studies include a no-additional-stress control (i.e. survival from the starting point with no additional stress) (Darr and Fridovich 1995).

Survival in heat stress and oxidative stress decreases with age (Darr and Fridovich 1995; Labbadia and Morimoto 2015). The transcriptional response to heat stress and the unfolded protein response also decrease with age. The DNA damage response, including transcription of nucleotide excision repair machinery, and survival under DNA damage conditions decrease with age (Klass *et al.* 1983; Meyer *et al.* 2007).

The decline in body movement was positively correlated with sensitivity to the nematicidal effects of nile blue, a presumed measure of stress resistance (Hosono *et al.* 1980; Huang *et al.* 2004). Resistance to stress correlates with lifespan between strains (Bansal *et al.* 2015).

In the laboratory, *C. elegans* is generally fed a diet of *E. coli* OP50. Although this bacteria is often thought of as non-pathogenic, there is evidence that the resistance to its pathogenic effects are age-related (Portal-Celhay *et al.* 2012). Indeed, several studies have shown that *E. coli* OP50 accumulate in the intestines of aged animals (Garigan *et al.* 2002; Chow *et al.* 2006; McGee *et al.* 2011; discussed in more detail below), and this may represent a major cause of death late in life (Podshivalova *et al.* 2017).

C. elegans resists pathogenic stress via activation of an innate immune response (reviewed in Kurz and Ewbank (2003) and Kim (2013)), and the ability to respond to pathogens declines with age. Youngman *et al.* (2011) measured survival of aged animals grown on *E. coli* OP50 then transferred to pathogenic bacteria *P. aeruginosa* (PA14). They observed a steady decrease in survival and an increase in bacterial colonization of the intestine in adults introduced to PA14 at days 3, 6, and 9. Similarly, Laws *et al.* (2006) observed a significant reduction in survival time between animals transferred to four different strains of pathogenic bacteria on days 0 and 7. Conversely, Burns *et al.* (2017) did not observe an age-related decrease in pathogen resistance to *S. enterica,* although this study only measured up to day 5 of adulthood.

BEHAVIOR

Body Movement

The well-coordinated sinusoidal body movement characteristic of young hermaphrodites becomes progressively slower and less coordinated and ultimately ceases altogether in old hermaphrodites. Two approaches have been used to measure body movement during aging. First, it is possible to quantify movement as waves per minute observed with a dissecting microscope. Several studies found that the wave frequency declines regularly with age and fit the data to a

straight line (Croll *et al.* 1977; Bolanowski *et al.* 1981; Johnson 1987; Friedman and Johnson 1988; Glenn *et al.* 2004). Second, it is possible to define categories of movement ability (Hosono *et al.* 1980; Herndon *et al.* 2002; Huang *et al.* 2004). Herndon *et al.* (2002) and Hosono *et al.* (1980) defined three categories: Class A (Herndon) or Type I (Hosono) animals progress with rhythmic sinusoidal movement, Class B (Herndon) or Type II (Hosono) are not active and are uncoordinated, and Class C (Herndon) or Type III (Hosono) are unable to progress but spontaneously move their head or tail and respond to touch (Hosono *et al.* 1980; Herndon *et al.* 2002). Huang *et al.* (2004) defined two categories: fast moving corresponding to Type I/Class A and not fast moving corresponding to type II/class B and type III/class C (Huang *et al.* 2004).

With advances in technology, measuring body movement has become more automated. New methods have been created to measure body movement specifically with swimming assays. Restif *et al.* (2014) identified novel features of age associated changes in swimming and analyzed a variety of phenotypes from wave initiation rate to reverse swimming at day 4 and day 11 using the *C. elegans* swimming Test (CeleST) program. Results showed that some phenotypes like wave initiation rate, travel speed, brush stroke and activity index decline with age while body wave number, asymmetry, and curling increase with age. Other phenotypes such as stretch, reverse swimming, and attenuation barely changed over age. Similar to Restif *et al.* (2014), Bansal *et al.* (2015) measured movement in liquid media by performing a thrashing experiment. This study also compared the distance traveled of individual animals by analyzing tracks during a finite period. Results from both experiments corresponded to previous studies by Herndon *et al.* (2002) and Huang *et al.* (2004): as adults age they move less. Using the same classification system as Herndon *et al.* (2002) and Hosono *et al.* (1980), Newell Stamper *et al.*

(2018) performed a longitudinal study on individual animals, finding that as animals age they gradually traverse from Class A to Class B to Class C until death.

The relationships between the decline of body movement and several other age-related changes have been characterized. Several studies have analyzed the relationship between the age-related change of body movement and the declining survival probability measured by lifespan. Hosono *et al.* (1980) and Herndon *et al.* (2002) showed that dividing wild-type animals into movement classes was predictive of lifespan. Huang *et al.* (2004) showed that the fast body movement span was positively correlated with lifespan in wild-type animals and several mutants. Johnson (1987) analyzed a series of recombinant inbred strains with differing lifespans, and found that the x-intercept of the age-related movement decline positively correlated with the maximum lifespan. By contrast, Bolanowski *et al.* (1981) found no correlation between the rate of decline in movement frequency and the lifespan in a longitudinal study of wild-type animals.

Recently, relationships between lifespan and body movement have become more defined. Hsu *et al.* (2009) performed a longitudinal study of individual wild-type animals from adult day 3 until death and specifically examined the locomotor speed by a nematode tracking system. Locomotor speed inversely correlated with lifespan; animals with a slower rate of motor activity decay have a longer lifespan than those that have a faster rate of decay (Hsu *et al.* 2009). Hahm *et al.* (2015) analyzed the maximum velocity of individual animals over their lifespan using a stereomicroscope. Animals with a higher maximum velocity have a longer lifespan than animals with a lower maximum velocity (Hahm *et al.* 2015). Overall, these studies indicate that the decline in body movement is positively correlated with the decline in the survival probability and can be used to predict lifespan (**Table 3**).

Pharyngeal Pumping

The pharynx is a neuromuscular organ that undergoes rhythmic contractions that facilitate feeding; contractions can be counted using a dissecting microscope (Avery and Thomas 1997). The pharyngeal pumping rate reaches a maximum of approximately 300 pumps per minute in two day old adults. Pharyngeal pumping undergoes an age-related decline and typically ceases by about day 12 (Croll *et al.* 1977; Hosono *et al.* 1980; Huang *et al.* 2004; Chow *et al.* 2006). More recently, Russell *et al.* (2017) performed a similar experiment using an electropharyngeogram in a microfluidic device and found that not only does the frequency of pharyngeal pumping decreases with age, the duration of pharyngeal contractions and the variability of the inter-pump interval increase with age.

Habituation is the ability of an organism's response to decrease after repeated or prolonged presentations of the stimulus. Beck and Rankin (1993) examined spontaneous locomotion and habituation by using a stimulus of tapping to measure the occurrence and magnitude of reversals as well as habituations levels. The magnitude of reversals and occurrence of reversals by tap decreased with age from adult day 4 to adult day 7 and 12. This can also be interpreted that older animals have increased habituation and recover from habituation slower compared to younger animals. Timbers *et al.* (2013) performed a similar experiment: they examined reversal probability and reversal distance of adults at various ages in the presence and absence of food, finding that age-dependent changes in short-term habituation occur during the reproduction period. Day 3 to day 5 adults are less likely to respond to tap both in the presence and absence of food. No age dependent changes in reversal distance were observed (Timbers *et al.* 2013).

Longitudinal studies have been used to characterize the relationships between the decline in pharyngeal pumping and other age-related changes (**Table 3**). The decline in body movement is positively correlated with the decline in pharyngeal pumping (Hosono *et al.* 1980; Huang *et al.* 2004). Hosono *et al.* (1980) showed that older adults that still displayed rhythmic, sinusoidal body movement (type 1) displayed more rapid pharyngeal pumping than animals of the same age that had diminished body movement and were unable to progress (type III), indicating a positive correlation between the declines in pharyngeal pumping and body movement (Hosono *et al.* 1980). Huang *et al.* (2004) showed that both the fast-pharyngeal pumping span and the pharyngeal pumping span were positively correlated with the fast body movement span. The decline in body movement was positively correlated with sensitivity to the nematocidal effects of nile blue, a presumed measure of stress resistance (Hosono *et al.* 1980; Huang *et al.* 2004). Bansal *et al.* (2015) examined how pharygneal pumping over age correlates with lifespan and with chronological and relative physiological healthspan.

Neurobiology

Progressive degeneration of the nervous system and related decline in cognitive function is a hallmark of aging in humans and other mammals. In *C. elegans*, morphological changes in many somatic tissues have been commonly observed, but early studies suggested that degeneration in locomotion and other age-related phenotypes could not be explained by changes in the nervous system (Herndon *et al.* 2002; Collins *et al.* 2008b). Herndon *et al.* (2002) used neuronally expressed GFP reporters and electron microscopic analysis to determine that the nematode nervous system undergoes minimal age-related morphological changes.

In contrast, more recent studies have found that various changes in neuronal structure do occur during aging; these include changes in neuron body morphology, increase in spontaneous branching, and the formation of morphological abnormalities along the axon (Pan *et al.* 2011; Tank *et al.* 2011; Toth *et al.* 2012). Pan *et al.* (2011) used neuronally expressed GFP reporters and fluorescence microscopy to examine structural changes in the ALM and PLM touch receptor neurons. They categorized several classes of defects in the neuronal processes that increased in frequency with age: formation of "bubble"-like lesions, GFP-rich "beads", triangular protrusions ("blebs"), and the formation of small branches from the process. Additionally, they noticed an increased disorganization of microtubule bundles in the soma of ALM neurons. These morphological changes were also observed in AVM and PVM touch receptor neurons.

Toth *et al.* (2012) used similar methods, and noticed several novel neuronal morphologies that progressively increase with age; these include novel branches emerging from neuronal processes, novel outgrowths emerging from the soma, and bending of the neuronal process("wavy" appearance). Additionally, they observed an age-related decrease in the presence of GFP-rich "beads" along the processes; this is in disagreement with Pan *et al.* (2011), which found an age-dependent increase, but only in PLM neurons

Tank *et al.* (2011) further examined age-dependent development of new neuronal outgrowths in mechanosensory neurons and found that this phenotype also occurred in GABAergic motor neurons, indicating that age-related branching occurs in multiple neuronal cell types. Finally, they observed the correlation between physiological age (measured by touch response) and branch outgrowth; they found that, at day 13, low-mobility animals displayed more branches than high-mobility counterparts, suggesting a link between neuronal abnormalities and movement decline.

Pan *et al.* (2011); Tank *et al.* (2011); Toth *et al.* (2012) all observed that neuronal morphological changes were present in most, but not all, aged animals, indicating that this phenotype only occurs in a subset of the population. All three also found differences in which morphological changes occurred in which types of neurons. Overall this indicates that, while most morphological changes appear to increase with age, the frequency of abnormalities differs both between individuals in a population and between neuron types within the same animal.

Toth *et al.* (2012) recognized a correlation between the degree of synaptic deterioration and decrepitude in aged animals, suggesting a link between the decline of locomotory behavior and neuronal function. Indeed, Liu *et al.* (2013) found that motor neurons decline in function with age, exhibiting a progressive decline in the frequency of spontaneous post-synaptic currents in motor (bot not body-wall muscle) receptors. Later, the same group discovered that long-lived *slo-1(js379)* mutants showed a decreased rate of decline for this phenotype (Li *et al.* 2019).

Morsci *et al.* (2016) found that neuronal mitochondria show phasic changes throughout aging, showing increased organization and density in middle age but a reduction in early and late life. The authors measured mitochondrial size, density, and load in day 11 decrepit animals, and saw that these phenotypes are reduced compared to youthful-looking aged animals. Finally, the authors measured a decrease in mitochondrial trafficking along the ALM process from day 1 to day 11.

REPRODUCTION

Self-Progeny and Cross-Progeny Production

Successful reproduction is the ultimate goal of an organism. Therefore the age-related decline of reproductive function is likely to be critical for the evolution of aging. From a single

fertilized egg, the *C. elegans* hermaphrodite develops its entire soma and both arms of its reproductive tract and begins laying eggs at ~65 hours at 20°C (Byerly *et al.* 1976). At the peak of reproduction, oocytes are ovulated every ~23 min (McCarter *et al.* 1999), resulting in an average of ~150 progeny per day .

It is notable that self-fertile reproduction ceases relatively early in life: for wild-type hermaphrodites at 20°C on standard nematode growth medium seeded with live *E. coli* OP50, the self-fertile reproductive span is 5.8 days and the lifespan is 15.2 days (Huang *et al.* 2004).

In self-fertile *C. elegans* hermaphrodites the first ~300 germ cells differentiate as sperm, and the remaining germ cells differentiate as oocytes. Ward and Carrel (1979) showed that there is an age-related decrease in the number of sperm in or near the spermatheca which corresponds with the fertilization of oocytes. Klass (1977) and Croll *et al.* (1977) documented that there is an age-related peak and decline in fertilized eggs laid that corresponds with the depletion of sperm. There is a delayed, slightly overlapping, and much smaller peak of unfertilized oocytes deposited. However, the germline responds to sperm depletion by arresting the development of oocytes, a phenotype known as oocyte "stacking". These age-related changes are modulated by temperature and the self-fertile reproductive span is extended by cold temperatures (Klass 1977; Huang *et al.* 2004). The decline in fertilized eggs laid by self-fertile hermaphrodites is caused by the depletion of self-sperm, since mating to males can significantly increase the number of fertilized eggs laid (Ward and Carrel 1979; Hodgkin and Barnes 1991). Mating increases duration of reproduction, while the peak remains relatively unchanged (Hughes *et al.* 2007; Pickett *et al.* 2013).

Reproduction requires both the germ line and somatic tissues, and it is important to understand how age-related changes in both the reproductive tract and in somatic tissues affect

reproductive function. It is notable that even when sperm are not limiting, reproduction ceases relatively early in life: at 20°C on standard nematode growth medium seeded with live *E. coli* OP50, in wild-type hermaphrodites with excess sperm from mating to males, the reproductive span is 8.8 ± 1.8 days and the lifespan is 15.6 ± 3.3 days (Pickett *et al.* 2013). Further, progeny production declines from a peak of ~150 progeny per day on adult day 2 to ~40 progeny per day on adult day 5 and to ~12 progeny per day on adult day 7, while the animals are all still alive, moving, and feeding (Kocsisova *et al.* 2019). This suggests that the age-related decline in reproductive function may not be caused primarily by a decline in somatic functions that maintain survival.

The relationship between the age-related decline in self-fertile reproduction and other age-related changes has been analyzed. Johnson (1987) analyzed the length of the self-fertile reproductive period in many recombinant inbred lines and found no correlation with the mean lifespan of these lines (see Table 3). Huang *et al.* (2004) conducted a longitudinal analysis of wild-type and mutant hermaphrodites, and there was no correlation between the self-fertile reproductive span and the lifespan, the fast body movement span, or the pharyngeal pumping span (see Table 3). The self-fertile reproductive span appears to be determined by the number of sperm that are generated, which is controlled by a developmental switch and the rate of sperm utilization. The absence of correlation observed in multiple studies (Huang *et al.* 2004; Szewczyk *et al.* 2006) indicates that these processes are independent of the processes that influence the decline of body movement, pharyngeal pumping, and survival probability.

Because self-fertile hermaphrodites completely deplete self-sperm, measurements of live progeny production do not accurately measure the reproductive capacity of these hermaphrodites late in life. To address this issue, Hughes *et al.* (2007) and (Pickett *et al.* 2013) analyzed progeny

production in mated hermaphrodites that have sufficient sperm. Compared to self-fertile hermaphrodites, mated hermaphrodites generate more progeny, but still display an age-related decline in progeny production that results in the cessation of progeny production at ~day 8. These studies demonstrate formally that hermaphrodites undergo an age-related decline of reproductive function that is independent of sperm depletion.

Progeny production is typically assayed on standard NGM petri dishes with lawns of live *E. coli* OP50. Individual P0 animals, "mother worms" are placed on a dish, allowed to produce progeny for 24 hours, then transferred to a fresh dish. Progeny are counted either immediately as eggs and larvae or after 2-3 days when the progeny have developed into adults which are easier to count. Alternate approaches to assaying progeny production include maintaining "mother worms" in: 96-well dishes of *C. elegans* minimal medium CeMM (Szewczyk *et al.* 2006), hanging drops of culture medium (Muschiol *et al.* 2009), or droplets of bacteria sealed in a hydrogel (Zhang *et al.* 2016). Progeny production, when analyzed as the number of progeny produced on each day of life, is a quantitative phenotype. It is possible to analyze it as a discrete phenotype: fertile versus sterile. However, this process essentially equates an animal producing 1 egg per day to an animal producing 150 eggs per day. Another assay of reproduction is the ability to produce progeny when mated after a period of sperm depletion. While nearly 100% of wild-type hermaphrodites regain fertility when mated on adult day 8, only 50% do so when mated on day 10, and none regain fertility when mated on day 15 (Mendenhall *et al.* 2011)

Progeny viability and morphology

C. elegans embryos exhibit a remarkably low rate of lethality: typically under 1%. The lethality of embryos from older mothers can increase for two reasons: extended arrest in

diakinesis (only for embryos which developed from stacked oocytes) and/or due to older germline tissue. Andux and Ellis (2008) detected lethality increased to ~20% in embryos which developed from stacked oocytes. However, lethality among embryos which developed from non-stacked oocytes produced by older mothers was ~3% (Andux and Ellis 2008).

The size of *C. elegans* embryos and L1s is tightly regulated. Hibshman *et al.* (2016) report that L1s hatched from embryos deposited by older mothers are slightly longer.

Gonad morphology

C. elegans contain two U-shaped assembly-line-like germlines in which stem cells proliferate in the distal region (distal to the vulva), which then differentiate into oocytes in the proximal region (proximal to the vulva), which are ovulated into the spermatheca, fertilized, and begin embryonic development in the uterus.

The oocytes and germline viewed by Nomarski microscopy undergo multiple age-related changes in appearance that are suggestive of deterioration. Garigan *et al.* (2002) defined five categories of deterioration and used this scoring system to document progressive, age-related deterioration of germ line morphology.

Proximal germline and oocyte morphology deteriorate with age. In unmated hermaphrodites, the gonad responds to sperm depletion by stopping oocyte maturation and arresting oocytes in diakinesis, a process referred to as oocyte “stacking” or feminization. By Nomarski, stacked oocytes appear as narrow rectangles (Hughes *et al.* 2011). Luo *et al.* (2010) report an increased incidence of small oocytes, clusters of oocytes, and cavities in the uterus of day 8 post-reproductive animals. Clusters of oocytes were also observed in day 8 reproductive animals (Luo *et al.* 2010). Hughes *et al.* (2011) report in increased incidence of debris, vacuole-

like structures, and opaque masses visible by Nomarski in the proximal gonad. By using DAPI to visualize DNA, (Kocsisova *et al.* 2019) reported gaps and oocytes in the pachytene region.

Multiple groups have reported swollen nuclei (detected by Nomarski) and masses of chromatin (detected by DAPI) in the proximal gonad arm and/or uterus of older (day 5, day 8) sperm-depleted animals. These are sometimes called hypertrophic nuclei, hypertrophic oocytes, hypertrophic embryos, hyperplasia, and tumors (Hughes 2005; Golden *et al.* 2007; Luo *et al.* 2010; Riesen *et al.* 2014; de la Guardia *et al.* 2016; Wang *et al.* 2018). It is hypothesized that they result from the endoreduplication of unfertilized oocytes (Hughes 2005). In sperm-replete animals, endomitotic oocytes were reported in 10% of the population at day 5 (Kocsisova *et al.* 2019).

The distal germline contains the mitotic stem cells, progenitor cells, and meiotic cells in leptotene, zygotene, and pachytene. These cells exhibit incomplete separation of the cytoplasm, forming a syncytium, yet maintaining asynchronous cell cycles (Pazdernik and Schedl 2013). Garigan *et al.* (2002) reported increased spacing of mitotic nuclei, nucleoplasm disrupted by cavities and grainy material, and nuclei that appear to be cellularized. Luo *et al.* (2010) also reported cavities, graininess, and cellularization. Hughes *et al.* (2011) reported a narrow distal gonad and swollen nuclei in the distal gonad. de la Guardia *et al.* (2016) reported narrowing of the distal gonad and distal gonad fragmentation. By using DAPI to visualize DNA, (Kocsisova *et al.* 2019) reported enlarged progenitor zone nuclei and small distal germlines.

Meiotic prophase progression and apoptosis

In L4 hermaphrodites germ cells differentiate into sperm while in adult hermaphrodites germ cells differentiate into oocytes. In young adults, the process of meiotic prophase

progression and oogenesis takes ~2 days (Jaramillo-Lambert *et al.* 2007). Measuring meiotic progression requires injecting or feeding a nucleoside analog (such as BrdU or EdU) which is incorporated during S-phase, retained by cells as they differentiate, and detected by fluorescent microscopy. Meiotic progression is defined from the last S-phase in the distal germline to meiotic maturation of the most proximal oocyte. As reported by Jaramillo-Lambert *et al.* (2007) meiotic progression begins to slow by adult day 1.5. Meiotic progression in older sperm-replete animals requires significantly longer than 48 hours (Kocsisova *et al.* 2019).

A large proportion (~87%) of germ cells that enter meiosis in the adult function as nurse cells that provide essential constituents to growing oocytes but do not become oocytes, as they undergo apoptosis in late pachytene (Gumienny *et al.* 1999; Wolke *et al.* 2007; Agarwal *et al.* 2018). The number of apoptotic germ cells per gonad arm (detected by CED-1::GFP) displayed an increase from day 1 to day 4, then a decrease from day 4 to day 8 de la Guardia *et al.* (2016).

Schisa *et al.* (2001) used fluorescence microscopy of the live cell dye Syto-14 and reported increased perinuclear staining of RNA-rich P granules in the germline of aged adult hermaphrodites.

Germ cell number and Progenitor Zone size

The total number of germ cells in the entire germline remains relatively constant for 6 days in unmated hermaphrodites (Crittenden *et al.* 2006) but decreases slightly in sperm-replete mated hermaphrodites (Kocsisova *et al.* 2019).

The progenitor zone, sometimes called the proliferative zone or mitotic zone, is the most distal region of the germline located next to the distal tip cell. This region contains all germ cells which have not yet entered meiosis, including mitotically-cycling germline stem cells and

progenitor cells undergoing pre-meiotic S-phase (**Figure 7A**). The cells in the progenitor zone can be identified by immunohistochemistry and approximated by DAPI morphology (Hansen *et al.* 2004a; Crittenden *et al.* 2006; Fox *et al.* 2011; Korta *et al.* 2012; Fox and Schedl 2015). Methods to accelerate and automate the detection of germ cell nuclei and DNA content have been reported (Seidel and Kimble 2015; Roy *et al.* 2016).

Some variability in progenitor zone measurements exists between laboratories. Crittenden *et al.* (2006) reported that PZ cell number remained unchanged up to day 6 of adulthood (day 1 ~243, day 2 ~227, day 3 ~214) in unmated hermaphrodites. Luo *et al.* (2010) report that the number of cells in the progenitor zone peaks at ~220 at day 2, then decreases to ~150 at day 6 of adulthood in unmated hermaphrodites. Killian and Hubbard (2005) and Qin and Hubbard (2015) report that the number of cells in the progenitor zone peaks at ~250 cells, decreases to ~150 cells by day 3, ~100 cells by day 6, and ~50 cells by day 12 of adulthood in unmated hermaphrodites. Narbonne *et al.* (2015) reported that the number of cells in the progenitor zone peaks at ~190 at day 2 and decreases to ~80 at day 7 in unmated hermaphrodites. Shi and Murphy (2014) noted that 50uM FUdR, which did not affect lifespan, reduced the number of germ cell nuclei.

In mated hermaphrodites, Shi and Murphy (2014) found a decrease in the number of progenitor zone cells with age, from ~150 at day 1 to ~100 at days 2-4. Qin and Hubbard (2015) report that mating, via germ cell flux, accelerates the decline of the progenitor zone to ~60 cells at day 6. Narbonne *et al.* (2015) reported that the number of cells in the progenitor zone peaks at ~190 at day 1 and decreases to ~90 at day 8 in continuously mated hermaphrodites. Kocsisova *et al.* (2019) reported that in mated hermaphrodites the total number of progenitor zone cells was ~220 in day 1 adults, ~160 at day 3 and ~130 at day 5. These experiments indicate that the

progenitor zone may become depleted more rapidly in sperm-replete animals than in sperm-depleted animals (**Figure 7C**).

Progenitor Zone Cell Cycle

In young adult hermaphrodites, the mitotic cell cycle of germline stem cells in the progenitor zone takes 6.5-8 hours and consists of a very short or non-existent G1-phase, long S-phase, long G2-phase, and a short mitotic division (Fox *et al.* 2011). The germ cells do not undergo transit-amplifying divisions (Fox and Schedl 2015), and quiescent cells are not observed (Crittenden *et al.* 2006).

Methods to visualize cell cycle phase in living cells have not been reported to work in the *C. elegans* germline to date (Kocsisova *et al.* 2018b). Cells in M-phase can be detected in fixed tissues by staining with mouse anti-phospho-histone H3 antibody. Cells in S-phase can be detected by feeding the nucleoside analog EdU, which is incorporated into DNA during S-phase and detected by click chemistry in fixed tissues. While the number of cells in each phase and the proportion of the progenitor zone in M-phase (M-phase index) or S-phase (S-phase index) can be calculated for individual animals, the measurement of the rate of the cell cycle requires pooling data from many individuals and several EdU-feeding duration experiments, then performing a regression (Kocsisova *et al.* 2018a).

Narbonne *et al.* (2015) and Qin and Hubbard (2015) reported that the M-phase index gradually decreases with age in unmated hermaphrodites, suggesting the germ cells arrest their cell cycle, likely in G2 phase. Narbonne *et al.* (2015) found that mating hermaphrodites delays the decline of the M-phase index. Kocsisova *et al.* (2019) examined mated hermaphrodites and found no significant difference in either the M-phase or the S-phase index between day 1 and day

5 adults. Rather, they report that the rate of progression through the cell cycle slows with age, requiring ~12 hours in day 3 and 5 adults.

DTC nucleus

The distal tip cell is a somatic cell that alone provides the stem cell niche for the germline. Hughes (2005) reported that the distal tip cell, detected with plag-2::GFP, occasionally shifts and/or disappears in day 6-12 unmated hermaphrodites. Byrd *et al.* (2014) reported that the extent of the distal tip cell plexus, visualized by plag-2::myrGFP, remains unchanged by day 4 in unmated hermaphrodites. Kocsisova *et al.* (2019) reported that the distal tip cell nucleus, detected by antibody staining, occasionally mislocalizes away from the distal tip in day 5 mated hermaphrodites. It is not known whether age-related changes in the distal tip cell affect the level of Notch signaling in germline stem cells.

Notch effector domain (stem cell number)

As germ cells move away from and lose contact with the distal tip cell, they lose Notch signaling, complete their ongoing mitotic cell cycle, and then begin meiotic S-phase (Fox and Schedl 2015). The distal tip cell provides the ligand to activate the Notch signaling pathway which permits the stem cell fate and blocks differentiation and entry into meiosis. Two direct transcriptional targets of GLP-1 are the *sygl-1* and *lst-1* genes, which are redundantly necessary and individually sufficient to promote germline stem cell fate and block differentiation (Kershner *et al.* 2014; Lee *et al.* 2016; Shin *et al.* 2017). Thus the extent of LST-1 and SYGL-1 accumulation provides a readout that is correlated with stem cell identity, though detectable LST-1 and SYGL-1 accumulation cannot currently be used to define the number of stem cells. In

day 1 adults, LST-1 and SYGL-1 are expressed in ~38 and ~81 cells, respectively (Shin *et al.* 2017; Kocsisova *et al.* 2019), but the number of cells expressing these proteins decreased two-fold by day 5 in mated hermaphrodites (Kocsisova *et al.* 2019)

BODY AND TISSUE MORPHOLOGY

Body Size

C. elegans adults display an age-related increase in size (Croll *et al.* 1977; Bolanowski *et al.* 1981). Croll *et al.* (1977) noted a progressive increase from day 3 to day 14 in length (about 70%), width (about 30%), and volume (about 280%). Bolanowski *et al.* (1981) noted an increase in volume from day 3 to day 9 (about 170%) with little further change. The age-related changes in size may be an example of programmed growth rather than a degenerative change, although the period of body growth overlaps with periods characterized by functional declines.

Head and Pharynx

Garigan *et al.* (2002) used Nomarski microscopy to analyze age-related changes in tissue appearance in the region of the head and pharynx. These changes include (1) a progressive lack of definition of nuclear boundaries; (2) progressive loss of the smooth and uniform appearance of the cytoplasm and nucleoplasm and the appearance of necrotic cavities and a curdled texture; (3) accumulation of shiny, mobile particles (likely to be yolk) and less mobile material (Garigan *et al.* 2002). This study defined categories to describe the extent of deterioration (none, low, medium, high, and very high). A cross-sectional analysis showed that there is an age-related increase in the extent of deterioration.

Chow *et al.* (2006) used a similar approach to analyze age-related changes in pharynx morphology by categorizing Nomarski images based on the extent of deterioration (least, somewhat, or most). This analysis revealed an age-related increase in pharynx deterioration (Chow *et al.* 2006). Electron microscopy showed that the pharynx of older adults loses its smooth, rounded shape and has an irregular appearance (Herndon *et al.* 2002).

Shamir *et al.* (2009) described a new method for quantifying age-associated deterioration of pharyngeal tissue. Previous studies have shown a marked decline in pharynx integrity over time, but previous techniques primarily observed pharyngeal pumping rate or non-quantitatively observed tissue disorganization (Garigan *et al.* 2002; Herndon *et al.* 2002; Chow *et al.* 2006). Shamir *et al.* (2009) used an algorithm to quantitatively measure morphological changes in the pharynx by quantifying image entropy to measure the animal's physiological age.

Zhao *et al.* (2017) categorized two separate death-associated pharyngeal bulb morphologies, termed "P" (enlarged) and "p" (atrophied). They observed that animals that displayed enlarged pharynxes at death were more likely to have died earlier than animals with atrophied pharynxes and suggested a role for bacterial infection in pharyngeal pathology (Zhao *et al.* 2017).

Bacterial accumulation

C. elegans is typically cultured with live *E. coli.* There appears to be an age-related increase in the amount of bacteria in the pharynx and the anterior and posterior intestine (Chow *et al.* 2006; Garigan *et al.* 2002). Interestingly, treatments that reduce bacterial proliferation, such as U.V. light treatment and antibiotics, extend lifespan, indicating that live *E. coli* are pathogenic (Garigan *et al.* 2002).These interventions had a minimal effect on the decline of pharyngeal

pumping, leading Chow *et al.* (2006) to conclude that bacterial accumulation is not a major contributor to this functional decline (Garigan *et al.* 2002; Chow *et al.* 2006).

McGee *et al.* (2011) concurred with Garigan *et al.* (2002) that undigested bacteria accumulated in the intestine. The authors used electron microscopy to section and visualize the localization of bacteria and found that bacteria localized to grinder, suggesting that the cause is a decline in pharyngeal pumping. The authors observed that bacteria can move through lumenal membrane or invade via the vulva, and that this is associated with age-related changes in intestinal tissue integrity and morphology.

Body wall muscle

The analysis of Herndon *et al.* (2002) demonstrated that *C. elegans* experience sarcopenia, an age-related decline in muscle structure and function. One approach to visualizing muscle morphology is to express GFP in the nuclei of body wall muscle cells; there is an age-related change in nuclear GFP distribution characterized by a highly fragmented appearance (Herndon *et al.* 2002). The cell bodies of body wall muscles can be visualized by staining with phalloidin. Alternatively, GFP localized to the sarcomeres of the body wall muscles can be used to visualize muscle structure. These approaches reveal a progressive, age-related disorganization of sarcomeres with less dense packing and irregular orientation (Herndon *et al.* 2002; Glenn *et al.* 2004). Electron microscopy revealed multiple changes in sarcomeres including fewer myosin thick filaments, bent or broken thick filaments, shrunken cells due to cytoplasmic loss, and accumulation of lipid droplets (Herndon *et al.* 2002). The disorganization of the body wall muscles was positively correlated with the decline in body movement (see Table 3; Herndon *et al.* 2002).

Tissue appearance

Garigan *et al.* (2002) used Nomarski microscopy to analyze age-related changes in tissue appearance in the region of the head and pharynx. These changes include (1) a progressive lack of definition of nuclear boundaries; (2) progressive loss of the smooth and uniform appearance of the cytoplasm and nucleoplasm and the appearance of necrotic cavities and a curdled texture; (3) accumulation of shiny, mobile particles (likely to be yolk) and less mobile material (Garigan *et al.* 2002). Garigan *et al.* (2002) defined categories to describe the extent of deterioration (none, low, medium, high, and very high). A cross-sectional analysis showed that there is an age-related increase in the extent of deterioration.

Vulval integrity

Leiser *et al.* (2016) quantified a commonly observed phenotype, vulval extrusion, which they termed 'age-associated vulval integrity defects', or "Avid" , first described in Leiser *et al.* (2011). Previously, this phenotype, sometimes described as "vulval rupture" or "vulval extrusion", has been observed to commonly occur under standard culture conditions, and are usually censored from aging experiments (Hansen *et al.* 2007; Greer *et al.* 2007; Chen *et al.* 2009; Zhang *et al.* 2009). Here, the authors argued that Avid is a useful measure of the healthspan of the animal, as Avid-associated animals live significantly shorter than their non-Avid peers. They observed that the frequency of this phenotype increased with age, and primarily occurs in "middle age", after the reproductive period has completed (Leiser *et al.* 2016).

Intestinal Integrity

McGee *et al.* (2011) observed changes in intestinal morphology; degradation of intestinal lumen, loss of microvilli, loss of nuclei, and bacterial invasion, using electron microscopy and DAPI staining. The authors suggested that bacterial invasion was caused by the breakdown of intestinal lumen. This senescent phenotype is defined as intestinal atrophy and correlates positively with the formation yolky lipoprotein pools in the body cavity (Ezcurra *et al.* 2018).

Dambroise *et al.* (2016) reported an age-related onset of the permeability of blue fluorescein dye through the intestine. This "Smurf" phenotype was interpreted as a sudden increase in the overall permeability of the intestine. Significant variation exists in the age of onset of the Smurf phenotype, and the Smurf phenotype correlates positively with lifespan between different wild isolates.

Hypodermis

Golden *et al.* (2007) reported a loss of nuclei in the H9 and H10 hypodermal cells of the tail over time using DAPI staining and fluorescent microscopy. At day 4, most animals had two or 3 visible nuclei, whereas animals at day 14 showed a marked decline in visible nuclei. The authors were unable to visualize any nuclei at this location at day 19. Finally, the authors measured genomic DNA copy number using qPCR, and found that animals display an age-related increase. Wild-type males and FUdR-treated wild-type hermaphrodites showed no change in genome copy number, suggesting that the increase in copy number arose from the germline (Golden *et al.* 2007).

Midsection, Body cavity

Golden *et al.* (2007) observed an accumulation of DAPI-stained material along the midsection of wild-type animals that eventually fill the body cavity, first observed at day 14. BrdU was incorporated into the same region at day 11 compared to day 9, indicating that these masses likely require active DNA synthesis, but co-staining with DAPI was not possible (Golden *et al.* 2007).

In young adult hermaphrodites, yolk protein is found primarily in the intestine where it is synthesized and in late stage oocytes and embryos that accumulate it. Older hermaphrodites accumulate shiny, mobile patches of yolk protein in the body cavity where they form yolky lipoprotein pools (Garigan *et al.* 2002; Herndon *et al.* 2002; Ezcurra *et al.* 2018). For more details see the biochemistry section.

CELLULAR MORPHOLOGY

Mitochondrial Morphology

Using electron microscopy, Yasuda *et al.* (2006) observed that mitochondria in body wall muscles displayed an age-related 'swollen' morphology that was first seen in day 10 adults; this phenotype became more pronounced at day 15. This morphological change correlated with a decrease in oxygen consumption and a decrease in the activities of complex I and II of the mitochondrial electron transport chain. Using qRT-PCR, Gruber *et al.* (2011) observed a decline in mtDNA copy number from day 3 to day 14. The authors correlated mtDNA copy number with decrepitude in aged animals; at day 12, class A (youthful) animals had higher copy number compared to class B and C (decrepit) animals of the same age, suggesting a correlation between physiological decline and mitochondrial number (**Table 3**).

Regmi *et al.* (2014) measured mitochondrial morphology using mitochondrial membrane-targeted GFP. They observed that mitochondrial morphology changes with age from day 1 to day 16; there is an increase in fragmentation, a decrease in length, and an increase in circularity. Additionally, mitochondrial networks in body wall muscle cells become increasingly fragmented over the same time span.

Nucleus

The nucleus harbors the genetic information and exhibits a spatial organization that reflects its multiple functions such as securing DNA integrity, DNA damage repair, replication, transcription, splicing, ribosomal assembly, and controlled import and export. Age-related changes in the spatial organization of the nucleus could have dramatic effects due to the importance of its functions. First evidence that aging affects the nucleus in *C. elegans* is described in Herndon *et al.* (2002). The authors reported that muscle nuclei lose their integrity and shape. In addition, the nucleoli increase in size in relation to the nucleus in day 7 animals. These nuclear changes are correlated with a decline in locomotion: mobility class C animals exhibit a more drastic nuclear misshapen. These findings are supported by Haithcock *et al.* (2005) who focused on the nuclear envelope. Using a LMN-1::GFP reporter, the authors reported a loss of the typical circular nuclear envelope in day 8 animals. With increasing age, up to day 18, the nuclear envelope dramatically lost its integrity and nuclei showed abnormal shapes, fragmentation, and extensive stretching (Haithcock *et al.* 2005). Animals with severely impaired mobility classified as class III showed the more severe changes in nuclear envelope morphology compared to animals that exhibited a more youthful locomotion pattern (**Table 3**).

Another age-related change related to nuclei is a complete loss of nuclei in the tail and intestine that was observed by DAPI staining adults via fluorescent microscopy. Young animals exhibit 2-3 tail nuclei, fewer on day 14 and these nuclei completely lost on day 19 (Golden *et al.* 2007). Young animals have 30 uniform intestinal nuclei. After day 8 the number of intestinal nuclei decreases. Some 20 day old animals have fewer than 10 intestinal nuclei, and the remaining nuclei are smaller. It is important to note that the heterogeneity of animals increases with age and the severity of these age-related changes varies between animals (McGee *et al.* 2011).

The size of the nucleoli is negatively correlated with lifespan. Tiku *et al.* (2017) measured the hypodermal nucleoli of day 1 adult animals, recovered the animals, and monitored the lifespan. Smaller nucleoli in young adults were a predictor of longer lifespans (Tiku *et al.* 2016).

Processing bodies

Processing bodies and stress granules are RNA-protein complexes that are involved in post-transcriptional gene regulation. Using GFP-reporters (dcap-1::GFP) and fluorescence microscopy, Rousakis *et al.* (2014) observed an accumulation of processing bodies with age as well as an increase in their size, from days 1 to 5.

Ectopic fat depositions and lipid droplets

C. elegans develop lipid droplets in the intestine that reach a maximum in the young adult and represent the main fat storage in the animal. Herndon *et al.* (2002) observed via electron microscopy that *C. elegans* accumulate fat with age outside the intestine in muscles, and the

hypodermis. The development by Tserevelakis *et al.* (2014) of a noninvasive and dye-free tool for analysis of lipids in biological samples based on higher harmonic generation imaging techniques allows a more detailed and quantitative study. With this improved technique, the authors visualized and quantified lipid accumulations in L1 and L4 larval stages, and day 1, 5, 10, and 15 adults. Lipid droplets increased during development and decreased during aging in the intestine (Tserevelakis *et al.* 2014). In contrast to this observation, lipid droplets accumulated with age up to threefold in the pharyngeal muscles, body wall muscles, and neurons (Mari *et al.* 2015; Palikaras *et al.* 2016). This age-dependent increase of lipids outside of the intestine, the classic fat storage tissue, is defined as ectopic fat.

Autophagy

Autophagy is one major recycling pathway in cells and associated with longevity. Double-membrane vesicles are formed in the cytoplasm to transport macromolecules to the lysosome where these autophagosomes fuse to autolysosomes. Hydrolases degrade the content of the former autophagosomes. Experiments with GFP::LGG-1 reporter allow the quantification of GFP-LGG-1 positive foci in day 1, 3, 5, 7 and 10 animals in the intestine, body-wall muscles, pharynx, and nerve-ring neurons. The number of foci increased in all tissues, up to 9-fold in muscle cells, which reflects an increase in autophagosomes (Chang *et al.* 2017). The authors developed an additional reporter, mCherry::GFP::LGG1, to distinguish between autophagosomes (red and green foci) and autolysosomes (just red foci) in day 1, 3, 5, 7 and 10 animals. Red and green foci increase in the intestine, muscle, and pharynx with age, whereas red foci just increase until day 5 and then decrease in day 7 and day 10 animals. In contrast to the data from the GFP::LGG-1 reporter strain, green and red foci in neurons first decrease from day 1 to day 3 and

then increase at day 7 to reach a plateau, although the number of green foci decreases in neurons in aging animals. Additional experiments with Bafilomycin A, a drug that inhibits lysosomal acidification, showed a general increase in green and red foci. Interestingly, the age-dependent increase was reduced and suggests a decrease in autophagic activity in aging animals (Chang *et al.* 2017).

BIOCHEMICAL – GENE & CHROMATIN

Genome copy number

Golden *et al.* (2007) reported that masses of DNA accumulate in the midbody and germline of day 14 and day 19 *C. elegans* in comparison to day 4 animals. In addition, as indicated by BrdU incorporation, the regions were transcriptionally active in day 11 animals compared to day 9 animals. The authors also analyzed nuclear genome copy number via qPCR in wild-type from day 4 until day 21. Young adults all have a genome copy number around 4000 – 5000, whereas adults older than 10 days vary between and have genome copy numbers between close to zero and more than 25000 (Golden *et al.* 2007). In contrast to this increase in genome copy number, Gruber *et al.* (2011) found a decline in mitochondrial DNA copy number with age. This decline positively correlated with body movement. Adults that were classified in mobility class A have a higher mtDNA copy number compared to animals of the mobility impaired classes B and C (Gruber *et al.* 2011). In contrast to this data, Brys *et al.* (2010) could not detect any age-related changed in mtDNA copy number.

DNA integrity

Klass et al. (1983) demonstrated multiple age-related changes in DNA. DNA extracted from pools of adults displays an age-related increase in the number of single-stand breaks. Furthermore, there is an age-related decline in the ability of DNA to function as a template for transcription *in vitro* (Klass *et al.* 1983). Whereas Klass *et al.* (1983) described an age-related increase in the levels of 5-methylcytosine, Simpson *et al.* (1986) conducted a sensitive analysis and failed to detect 5-methylcytosine in *C. elegans* during either development or senescence. Melov *et al.* (1995) used a PCR strategy to assess deletions in the mitochondrial genome. The frequency of deleted mitochondrial DNA increases with chronological age in four different populations of *C. elegans*.

Chromatin

Histone modifications have the potential to alter chromatin structure and affect gene expression. Chromatin immunoprecipitation combined with deep sequencing (ChIP-seq) makes it possible to analyze genome-wide pattern changes in histone modifications and their association with gene expression changes.

H3K36m3 is mainly found in gene bodies and is associated with active transcription. Throughout the genome, the H3K36m3 pattern is stable with age in experiments that compared L3 larvae, and day 2, 4, and 12 adults. Nevertheless, 624 genes are newly trimethylated at H3K36, whereas 1930 genes lost the trimethylation in old animals. Furthermore, genes that exhibit age-related expression changes have a low H3K36m3 status (Pu *et al.* 2015).

Similar to the results of the H3K36m3 analysis, the H3K4m3 pattern of L3 larvae, and day 2 and day 12 adults appeared to be stable. H3K4m3 is highly linked with transcription and shows a general enrichment at the transcriptional start site and the 5’ promotor region where it

does not change with age. In contrast, uncommon H3K4 methylation in the gene body appeared to change with age and exhibited a correlation with age-related gene expression changes (Pu *et al.* 2018) (**Table 3**).

mRNA splicing

Splicing is a fundamental step in gene expression and seems to be linked to healthy aging. Using an *in vivo* fluorescent alternative splicing reporter, Heintz *et al.* (2017) reported that day 5 adults already started to change their splicing pattern and become heterogeneous. After day 7 nearly all animals lost their youthful splicing pattern. In addition, the splicing efficiency on day 6 of adulthood can be used as a predictor of lifespan since animals with a youthful splicing pattern have a up to 23% longer lifespan (Heintz *et al.* 2017) (**Table 3**).

Gene Expression

A variety of methods have been used to analyze age-related changes in the levels of specific mRNAs and proteins (microRNAs, and proteome). Fabian and Johnson (1995a) examined the abundance of total RNA, rRNA and poly(A)+ RNA, but no consistent age-related trends were observed in these classes of RNA. Fabian and Johnson (1995b) identified twelve specific transcripts that undergo a change in abundance over the adult life span. Cherkasova *et al.* (2000) used subtractive hybridization to compare gene expression in dauer and non-dauer (L3) larvae. Five genes with higher transcript levels in dauer larvae also displayed an age-related increase in transcript levels. Whole-genome microarrays have been used to analyze age-related changes in gene expression (Lund *et al.* 2002; Golden and Melov 2004). Lund *et al.* (2002) identified 164 genes that displayed statistically significant changes in transcript levels as aging

occurs. Expression of some heat-shock proteins decreased, while expression of certain transposases increased. The functional significance of age-related changes in gene expression remains to be determined. Age-related changes in the responsiveness of gene expression to environmental stimuli have also been noted. The heat shock protein 16 (HSP-16) is induced to accumulate by heat stress. Walker *et al.* (2001) showed that there is an age-related decline in the levels of HSP-16 that can be induced by a heat stress, such that day 16 adults only accumulate HSP-16 to about 50% of the level of day 4 adults. Age-related gene expression changes are covered in more detail in another wormbook chapter (Golden and Melov 2007).

MicroRNAs

Small and noncoding miRNAs have a regulatory function in gene expression and are potential candidates that induce age-related changes. To address whether the expression levels of micro RNAs change during aging, Ibáñez-Ventoso *et al.* (2006) analyzed the miRNA expression pattern of day 6, 8, 11, 13 and 15 animals. 114 miRNAs were cataloged at the time of the study and the authors showed that 50 of them changed expression during aging. At least three of these miRNAs were predictive lifespan as a longitudinal study with *mir-71*, *mir-239*, and *mir- 246* promotor::GFP constructs reported. Single animal vermiculture, daily imaging, and semi-automated data analysis showed that while all three microRNAs increased with age, lifespan was directly correlated with expression levels of *mir-71* and *mir-239* and inversely correlated with expression levels of *mir-246* (Pincus *et al.* 2011).

BIOCHEMICAL - PROTEIN

Posttranslational modifications

Oxygen free radicals and other reactive oxygen species (ROS) can cause damage to macromolecules, and this damage is proposed to cause age-related pathologies (Balaban *et al.* 2005). One specific measure of this damage is the level of protein carbonylation. Adachi *et al.* (1998) measured protein carbonylation per milligram of protein in extracts of pooled animals. In wild-type animals the levels of protein carbonylation increased ~3-fold from day 4-8 to day 20. In a more detailed analysis Yasuda *et al.* (2006) compared mitochondrial and cytoplasmic fractions of day 4, 8, 12, and 15 adults. Both fractions showed an increase of carbonylated proteins with age. Importantly, carbonylated proteins accumulated 4-fold more in the mitochondria as expected due to the production of ROS in this organelle (Yasuda *et al.* 2006).

Carbonylated proteins can also be localized in the animal via freeze-crack, methanol/acetone fixation, and immunostaining after treatment with DNHP. Using this method Goudeau and Aguilaniu (2010) showed that the germline contains more carbonylated proteins than the somatic tissue. In more detail, the most proximal oocytes that are close to fertilization showed less antibody staining then the rest of the gonad, which could be due to a clearing mechanism. Day 2 and 5 adults exhibited an increase in oxidized proteins in both the germline and in somatic tissue with age (Goudeau and Aguilaniu 2010).

Proteome

Quantitative proteomic approaches allow a detailed analysis of the aging proteome in *C. elegans*. Two methods based on the SILAC-approach were used to assemble data sets of proteome composition changes:

(1) *E. coli* cells were labelled with heavy lysine isotopes and fed to *C. elegans* (Walther *et al.* 2015). 22 different *C. elegans* lysates from day 1 to 22 were used and more than 5000

different proteins identified and analyzed. The authors found that about 30% of the analyzed proteins changed their abundance at least 2-fold.

(2) Proteins were labelled with arginine and lysine containing light, medium, or heavy isotopes in *E. coli*; these were fed to *C. elegans* to label the animal's proteome. In addition, *orn-1* was knocked-down via RNAi feeding to prevent the enzymatic conversion of arginine to proline (Narayan *et al.* 2016). Day 1, 5, and 10 adults were used in this study and about 10,000 proteins were identified and analyzed. 627 proteins displayed a significant change in abundance with age.

Combined, these two studies provide an extensive data collection of age-related changes in the proteome. Further analysis to uncover GO groups and protein networks that impacts aging are also available for future studies.

Protein stability

Quantitative analysis of insoluble proteins via mass spectrometry of day 3 versus day 10 adults showed a significant increase of aggregated proteins with age (David *et al.* 2010). These data were confirmed by another study that analyzed proteome-wide changes in protein insolubility of day 1 versus day 11 adults via mass spectrometry (Reis-Rodrigues *et al.* 2012). In a more detailed analysis, aggregated proteins in day 1, 6, 12, and 17 adults were collected and analyzed in relation to their abundance in the proteome at this time points The most abundant proteins were the major part of the insoluble protein fraction (Walther *et al.* 2015). Combined, these quantitative studies of the insoluble proteome provide an extensive data collection for future studies.

In agreement with these quantitative analyses of aggregated proteome, Ben-Zvi *et al.* (2009) reported aggregated paramyosin in muscles of day 12 adults of a temperature-sensitive

fluorescent reporter strains. All together these data show that the stability of the proteome is reduced with age in *C. elegans*.

Enzymatic activity

The activity of specific enzymes has been shown to display age-related changes. Protein tyrosine kinase activity in *C. elegans* extracts decreases about 60% from day 5 to day 15 of adulthood (Vanfleteren *et al.* 1998). The activity of several acid hydrolases that are likely to be localized to lysosomes were examined in aging hermaphrodites by Bolanowski *et al.* (1983). b-N-Acetyl-D-glucosaminidase, b-glucosidase, a-mannosidase and acid hydrolase displayed age-related increases in activity. These changes are somewhat specific, since several other lysosomal enzymes did not display age-related changes in activity (Bolanowski *et al.* 1983).

Phosphoenolpryruvate carboxykinase activity increases from L4 to adulthood, peaks on day 6, and decreases in older adults. Similar, the abundance of this enzyme increased from L4 to adulthood, peaked on day 3, and decreased in older adults. Another metabolic enzyme, the pyruvate kinase, exhibited a continuous increase in activity with age. Furthermore, phosphoenolpryruvate carboxykinase abundance was positively correlated with motor activity during day 3-12 of adulthood (**Table 3**). The motor activity was measured as locomotory speed (Yuan *et al.* 2016).

Clustered change in protein levels

In young adult hermaphrodites, yolk protein is found primarily in the intestine where it is synthesized and in late stage oocytes and embryos that accumulate it. Older hermaphrodites accumulate shiny, mobile patches of yolk protein in the body cavity (Garigan *et al.* 2002).

Immunoelectron microscopy showed that yolk protein YP170 (vitellogenin) was distributed in electron dense lipid-like droplets and large accumulations throughout the body cavity of older hermaphrodites (Herndon *et al.* 2002). Similar observations have been made by visualizing GFP-tagged yolk protein. These studies suggest that the intestine continues to synthesize and secrete yolk protein after the time when oocyte production declines, resulting in accumulation of yolk protein in the body cavity, a hypothesis which is supported by Ezcurra *et al.* (2018). Herndon *et al.* (2002) suggest that yolk protein expression is left on in older hermaphrodites because there is little (if any) selective pressure to modify patterns of gene expression in post-reproductive animals, as explained by Medawar (1952) and Williams (1957)

Vitellogenin accumulates especially in self-fertile animals after sperm depletion, whereas, mating limits the accumulation of vitellogenin (Hughes 2005).

In a systematic study, Ezcurra *et al.* (2018) analyzed lipid pools in the body cavity. VIT-2 (YP170) and VIT-6 (YP115 and YP88) localized in these pools. Therefore, they were defined as yolky lipoprotein pools. YP170, YP115, and YP88 levels increased with age from day 1 to day 5 of adulthood; in day 5 adults vitellogenin represented 30-40% of all proteins. Furthermore, intestinal atrophy was positively correlated with yolky lipoprotein pools in the body cavity, which supports the hypothesis that intestinal biomass is converted into yolk in older adults via intestinal autophagy (Ezcurra *et al.* 2018).

BIOCHEMICAL - METABOLISM

Autofluorescence

One of the best biomarkers for aging is an increase of autofluorescence in postmitotic cells, because it is consistently observed and can be found across phyla. Lipofuscin, also called

age-pigment, seems to be the most studied fluorescent compound (Porta 2002). Highly oxidized proteins and lipids accumulate with age and build up aggregates that are visible as brown spots and emit yellow-orange fluorescence with wavelength of 570 to 605 nm when excited with UV light (Jung *et al.* 2007).

The first study that mentioned granules in the intestine that could resemble lipofuscin in a *Caenorhabditis* species is Epstein, Himmelhoch, & Gershon, 1972. They analyzed cross-sections of *C. brigsae* via electron microscopy. This work was followed by Klass who discovered an age-related increase of autofluorescence in *C. elegans* extracts measured via fluorometer (Klass 1977). Since then, autofluorescence is an established marker of aging in *C. elegans* and widely used. The recent development of semi-automated microscopic devices that allow longitudinal experiments with higher throughput show that blue fluorescence (excitation:350/50nm, emission 460/50nm) increases specifically 6-12 hours before an animal dies (Coburn *et al.* 2013; Pincus *et al.* 2016), whereas, red fluorescence (excitation: 545/30nm, emission: 610/70nm) increases throughout life and predicts future lifespan (Pincus *et al.* 2016).

There are two main methods to measure autofluorescence as an age-related change. (1) Using *C. elegans* extracts and measuring bulk increase of autofluorescence with an fluorometer (Klass 1977; Davis *et al.* 1982; Hosokawa *et al.* 1994; Braeckman *et al.* 2002a; b) or (2) Using a fluorescence microscope, measuring whole animals and spatial resolved autofluorescence (Hosokawa *et al.* 1994; Garigan *et al.* 2002; Gerstbrein *et al.* 2005; Pincus *et al.* 2011, 2016; Coburn *et al.* 2013).

(1) Using *C. elegans* extract is a simple way to measure pooled animals and to get an average change of autofluorescence. The pooled animal extracts need to be normalized using dry weight and volume or protein concentration (Klass 1977; Hosokawa *et al.* 1994). The

disadvantage is that aside from fractionated samples, it is impossible to get spatial information and to do longitudinal studies.

(2) Fluorescence microscopy has the advantage to allow following the changes in autofluorescence of single individuals over time with spatial resolution. The disadvantage of this technique was that it was limited to a small number of animals, but the recent development of a semi-automated culture system allows longitudinal studies in higher throughput (Pincus *et al.* 2011).

Autofluorescence is positively correlated with an age-related decline in body movement and lifespan (**Table 3**). Gerstbrein et al. (2005) measured autofluorescence in day 11 animals that were divided into three body movement classes. The severely impaired group showed a significant higher level of autofluorescence than the youthful and partially impaired group. Moreover, longer lived animals exhibit lower level of autofluorescence and especially red autofluorescence can be used as a predictor of lifespan as early as 7 days post hatching (Pincus *et al.* 2011, 2016).

Metabolic activity

Several measurements of metabolic activity have been demonstrated to display age-related changes (see Table 1). Carbon dioxide generation by populations of *C. elegans* grown on plates can be measured by gas respirometry. Carbon dioxide generation declines about 50% from day 6 to day 12 (Van Voorhies and Ward 1999). Oxygen consumption by populations of *C. elegans* in liquid culture were monitored polarographically using Clark type electrodes. Oxygen consumption of wild-type animals declines about 60% from adult day 0 to day 12 (Braeckman *et al.* 2002a; b; Brys *et al.* 2010). Heat produced by populations of live *C. elegans* can be

monitored by microcalorimetry, and it is a measure of the rate of catabolic processes. Heat production of wild-type *C. elegans* declines about 80% from adult day 0 to day 12. ATP levels, a measure of instantly available energy, can be monitored in animal extracts using enzyme reactions that require ATP. ATP levels decline about 80% from adult day 0 to day 12 (Brys *et al.* 2010). ADP levels decline about 70% (Brys *et al.* 2010). The amount of superoxide anion, an estimate of the potential for metabolic activity, can be measured in animal extracts using lucigenin-mediated luminescence; this declines about 95% from adult day 0 to day 12.

Metabolites

A few changes in metabolites were reported in aging animals like the loss of cardiolipin accompanied with an increase of phosphatidylcholines in mitochondria (Gruber *et al.* 2011) or the change in lactate pyruvate ratio (Yanase *et al.* 2017). However, the increasing power of mass spectrometry and NMR spectroscopy combined with advanced data processing opened the field of metabolomics and the extensive study of changes of metabolic pathways (Hoffman *et al.* 2017; Meier *et al.* 2017). Several groups started to provide a metabolic footprint of young versus old animals. They used different *C. elegans* culture methods, different animal lysate preparations and different analysis techniques. Pontoizeau et al. (2014) cultured wild-type animals on NGM dishes in the presence of FUdR and used NMR spectroscopy analysis of intact young adults before egg production versus day 7 adults to create a metabolic footprint of 22 metabolites. Copes et al. (2015) cultured *glp-4* animals in liquid media at 25°C and compared day 4 versus day 10 adults via GC-MS. They analyzed 186 metabolites and 1937 proteins to focus on affected pathways. Davies et al. (2015) cultured wild-type animals on NGM dishes with FUdR and used NMR to compare 33 metabolites in animals 2.5, 6, 8, 10,13,16, and 20 days after hatching to

define a metabolic age. Gao et al. (2017) cultured wild-type and *glp-4* on NGM plates with fluorouracil (5-FU) and analyzed 44 fatty acids, 18 amino acids, and over 600 phospholipids via MS, UPLC-MS/MS and HPLC-MS in wild-type eggs, L1, L2, L3, L4, and day 1-10 adults. In addition, they analyzed a fraction of these metabolites in *glp-4* L3, Day1, day 3, 5, 7, 9 to document metabolic changes. Wan et al. (2017) were interested in metabolic changes that occur through reproduction. They cultivated wild-type and *glp-1* animals on NGM dishes with FUdR and used UPLC-MS and NMR to compare 45 metabolites in young adults before egg-laying versus adult after egg-laying on day 10.

The limitations of all of these approaches are the limited biological replicates due to difficulties of running several repetitions of the experiments and the choices of different sets of metabolites. The clear strengths of these approaches are the large and useful databases of metabolic changes that occur during aging of *C. elegans* and enable future aging network analysis.

MALE BEHAVIOR, REPRODUCTION, & MORPHOLOGY

While behavioral, reproductive, and morphological changes in the *C. elegans* hermaphrodite have been studied widely, only a few studies have examined these changes in the *C. elegans* male. Since a male's success of mating is determined by sperm viability and motility as well as the male's ability to interact with hermaphrodites, male reproductive success is interlinked with a male's tail morphology and the male's ability to move.

Aging in *C. elegans* is usually associated with a decrease in body movement, and males move vigorously over various ages even when infertile. It was determined that body movement capability plays a minor part in *C. elegans* reproductive aging (Chatterjee *et al.* 2013).

The male tail structure is the key component of mating and can be damaged. The male tail is comprised of cuticular fans, sensory spicules, and the hook. Chatterjee *et al.* (2013) examined the morphology of male tales on day 1, 3 and 5 and found moderate damage to the tail over age. However, the damage was not proportional to the rapid decline in brood size.

Chatterjee *et al.* (2013) also examined how various behaviors required for reproductive success changed with age from day 1 to 5. They found that in day 5 animals the efficiency of locating the vulva, the percentage of responding males, and the percentage of males that maintained contact with the vulva significantly decreased, while response time increased slightly and difficulty in turning increased dramatically.

Like hermaphrodites, male nematodes also displayed age-related morphological changes. Chatterjee *et al.* (2013) reported that male tail morphology deteriorated by day 5 of adulthood, in *him-5(e1490)* males. The authors observed changes to the cuticle and rays of the tail, although the difference in the number of males with 'normal' tails at day 5 was non-significant. This analysis was non-quantitative, and involved qualifying tails as normal, semi-normal, or abnormal based on visual appearance.

Several age-related phenotypes are affected by mating in hermaphrodites and male animals. It has previously been observed that mating shortens lifespan and reduces body size in wild-type hermaphrodites (Shi and Murphy 2014). Shi *et al.* (2017) found that mated N2 males also are significantly smaller on day 6 of adulthood compared to unmated males, and also had a reduced lifespan. This shrinking phenotype was abrogated by treatment with male pheromone.

Klass *et al.* (1983) examined the viability of sperm in males that were aged in a mating population versus a virgin population. Males were allowed to mate, and after 24 hours, the number of fertilized eggs and the proportion that that hatched were counted. Results showed that

males grown in the virgin population have a higher number of sperm per male, but as males grew older in the virgin condition, they produced fewer viable progeny after mating (Klass *et al.* 1983). Chatterjee *et al.* (2013) conducted a test to determine the how fertility of wild-type males changed with age. Males were mated to wild-type hermaphrodites. Results showed that the proportion of cross-progeny decreased as males aged.

In addition to changes in fertility, aging can also affect the germline. Klass *et al.* (1983) studied sperm depletion and viability in the presence and absence of females. They found that males raised in the absence of females had significantly more sperm at days 10 and 15 of adulthood compared to males raised alongside hermaphrodites, suggesting that sperm accumulate over time in the absence of mating (Klass *et al.* 1983). Additionally, they observed an age-related decline in the percent of viable eggs produced as a result of aged males mating with young (day 3) females; day 10 and 15 males produced fewer viable progeny than day 5 males (Klass *et al.* 1983). This effect was observed in males raised with and without females, and the rate of decline was more pronounced in males raised with females. The authors suggest that decreased viability arises not from an accumulation of aged sperm, but rather from changes in precursor cells, as males raised with females are continually voiding and differentiating new sperm.

TABLE 1: Catalog of changes in hermaphrodites

Age-related change	Description over age	Method	Features and Limitations	References
Survival				
Lifespan	Probability of death increases	Manual observation of animals on NGM with dissection scope	Qualitative Non-invasive	(Gershon 1970; Epstein *et al.* 1972; Klass 1977; Croll *et al.* 1977)
		Automated 1) Lifespan-on-a-chip in microfluidics 2) 96-well plate in liquid medium		1-(Hulme *et al.* 2010) 2-(Solis and Petrascheck 2011)

		3) Lifespan Machine on standard NGM 4) Worm corrals in sealed hydrogel 5) WorMotel on NGM in sealed compartments		3-(Stroustrup *et al.* 2013) 4-(Zhang *et al.* 2016) 5-(Churgin *et al.* 2017)
Stress tolerance and response				
Heat shock response	Decreased survival; decreased transcriptional response	Survival assay; qPCR; hsf-1::gfp with fluorescent microscopy	Invasive	(Labbadia and Morimoto 2015)
Unfolded protein response	Decreased survival; decreased transcriptional response	Survival assay; qPCR	Invasive	(Labbadia and Morimoto 2015)
Oxidative stress response	Decreased survival; decreased transcriptional response; decreased enzymatic response	Survival assay; qPCR; Enzymatic activity	Invasive	(Darr and Fridovich 1995; Labbadia and Morimoto 2015)
DNA damage response	Decreased survival; decline in transcriptional response	Survival assay; Biochemical assays of extracts QPCR	Invasive	(Klass *et al.* 1983; Meyer *et al.* 2007)
Male exposure response	Decreased survival, decrease in body size	Survival assay	Invasive	
Immune response	Decreased survival; decreased transcriptional response	Survival assay qPCR Western Blot	Invasive	(Youngman *et al.* 2011)
Behavior				
Body Movement	Decrease in rate	Dissecting scope, machine vision, CeleST*(C. elegans* Swimming Test)	Quantitative Non-invasive	(Hosono *et al.* 1980; Bolanowski *et al.* 1981; Johnson 1987; Herndon *et al.* 2002; Huang *et al.* 2004; Hsu *et al.* 2009; Restif *et al.* 2014; Bansal *et al.* 2015; Hahm *et al.* 2015; Newell Stamper *et al.* 2018)
Habituation (Spontaneous locomotion)	Decrease in response time and reversal rate	Dissecting microscope and video recording equipment	Quantitative Non-invasive	(Beck *et al.* 1993; Timbers *et al.* 2013)
Chemotaxis	Decrease in response	Dissecting scope, chemical attractant on NGM dish	Quantitative Non-invasive	(Hosono 1978; Glenn *et al.* 2004)
Pharyngeal Pumping	Decrease in rate	Dissecting microscope	Quantitative Non-invasive Non-spatial	(Croll *et al.* 1977; Hosono 1978; Hosono *et al.* 1980; Huang *et al.* 2004; Chow *et al.* 2006; Bansal

				et al. 2015)
Pharynx Deterioration	Increase in entropy	DIC microscope	Quantitative Non-invasive	(Garigan *et al.* 2002; Herndon *et al.* 2002)
Pharynx pumping function	Decrease in function	Electropharyngeogram	Quantitative Invasive	(Russell *et al.* 2017)
Isothermal Tracking	Decrease in response	Dissecting scope + radial thermal gradient	Qualitative Non-invasive (except temperature shift)	(Murakami *et al.* 2005)
Defecation	Decrease in rate	Dissecting scope	Quantitative Non-invasive	(Croll *et al.* 1977; Bolanowski *et al.* 1981; Thomas 1990; Felkai *et al.* 1999)
Neurobiology				
Neuronal Structure	Remains relatively intact for a long time; appearance of morphological defects; increase in neurite branching	Fluorescent reporter protein with microscopy, Electron microscopy	Qualitative Invasive Spatial	(Herndon *et al.* 2002; Pan *et al.* 2011; Tank *et al.* 2011; Toth *et al.* 2012)
Synapse Structure	Decrease in synapse integrity	Fluorescent reporter protein with microscopy, Electron microscopy	Qualitative Invasive Spatial	(Toth *et al.* 2012)
Neural mitochondrial Structure	Size, shape, density, and load of mitochondria peaks between days 4 and 8, then declines; inter-mitochondrial distance troughs at day 8 then progressively increases	Fluorescent reporter protein with microscopy	Quantitative Invasive Spatial	(Morsci *et al.* 2016)
Synapse Function	Progressive decline in rate of spontaneous post-synaptic currents	Patch-clamp recordings	Quantitative Invasive Spatial	(Liu *et al.* 2013)
Neural mitochondrial function	Decrease in mitochondrial trafficking	Fluorescent reporter protein with microscopy, time-lapse imaging	Quantitative Invasive Spatial	(Morsci *et al.* 2016)
Neural mitochondrial oxidative stress tolerance	Decrease in resistance to oxidative stress	Fluorescent reporter protein with microscopy	Quantitative Invasive Spatial	(Morsci *et al.* 2016)
Reproduction				

Self-Progeny Production	Decrease in rate	Dissecting scope	Quantitative Non-invasive	(Klass 1977; Croll *et al.* 1977; Johnson 1987; Huang *et al.* 2004; Szewczyk *et al.* 2006; Hughes *et al.* 2007; Muschiol *et al.* 2009; Zhang *et al.* 2016)
Cross-Progeny Production	Decrease in rate	Dissecting scope	Quantitative Non-invasive	(Hughes *et al.* 2007; Mendenhall *et al.* 2011; Pickett *et al.* 2013)
Embryo viability	Decrease in viability	Dissecting scope	Quantitative Non-invasive	(Andux and Ellis 2008)
Oocyte morphology	Appearance of cavities, misshapen oocytes, small oocytes, oocytes in uterus, fewer late-stage oocytes *masses of chromatin in oocytes (endomitotic) in gonad and/or in uterus	Nomarski microscopy; DAPI DNA stain with fluorescence microscopy	Categorical Invasive (lethal or non-lethal)	(Golden *et al.* 2007; Luo *et al.* 2010; Hughes *et al.* 2011; Riesen *et al.* 2014; de la Guardia *et al.* 2016; Wang *et al.* 2018; Kocsisova *et al.* 2019)
Proximal gonad morphology	Decrease in organization, appearance of debris and opaque masses from day 5	Nomarski microscopy; DAPI DNA stain with fluorescence microscopy	Qualitative Invasive	(Garigan *et al.* 2002; Hughes *et al.* 2011; Kocsisova *et al.* 2019)
Distal gonad morphology	decrease in organization, appearance of cavities, graininess, cellularization, atrophy, narrowing, fragmentation, and swollen nuclei from day 5	Nomarski microscopy; DAPI DNA stain with fluorescence microscopy	Qualitative Invasive	(Garigan *et al.* 2002; Hughes *et al.* 2011; Kocsisova *et al.* 2019)
Apoptosis	decreases from day 4 (in unmated)	CED-1::GFP or SYTO 12 with fluorescence microscopy	Quantitative Invasive (except GFP)	(de la Guardia *et al.* 2016)
RNA granules	Increased periuclear staining of RNA-rich P granules in the germline	Fluorescence microscopy, Syto14 live cell dye	Qualitative Invasive Spatial	(Schisa *et al.* 2001)

	of aged adult hermaphrodites			
Meiotic prophase progression	slows by day 1.5 of adulthood, and continues to slow after that, even in mated animals	DAPI DNA stain, EdU or BrdU labeling of S-phase with fluorescence microscopy	Quantitative Invasive	(Jaramillo-Lambert *et al.* 2007; Kocsisova *et al.* 2019)
Germ cell number	number of germ cells in unmated animals remains relatively constant for 6 days number of rows of cells in distal gonad decreases by day 5	DAPI DNA stain with confocal fluorescence microscopy	Quantitative Invasive	(Crittenden *et al.* 2006) (Kocsisova *et al.* 2019)
Progenitor Zone size	Decreases by day 3 in mated and unmated animals	Antibody staining of progenitor or meiotic markers; DAPI DNA stain with confocal fluorescence microscopy	Quantitative Invasive	(Killian and Hubbard 2005; Crittenden *et al.* 2006; Luo *et al.* 2010; Shi and Murphy 2014; Qin and Hubbard 2015; Roy *et al.* 2016; Kocsisova *et al.* 2019)
Progenitor Zone Cell Cycle	M-phase index decreases in unmated animals; Cell cycle speed decreases by day 3 in mated animals.	pH3 antibody stain, DAPI DNA stain, EdU labeling of S-phase with fluorescence microscopy	Quantitative Invasive (lethal)	(Narbonne *et al.* 2015; Qin and Hubbard 2015; Kocsisova *et al.* 2019)
Notch effector domain (stem cell number)	Domain of expression decreases	antibody stain of tagged Notch pathway effector proteins LST-1 and SYGL-1; fluorescence microscopy	Quantitative Invasive (lethal)	(Kocsisova *et al.* 2019)
DTC nucleus	Mislocalizes away from distal tip	WAPL-1 antibody stain and DAPI DNA stain with fluorescence microscopy	Quantitative Invasive, lethal	(Kocsisova *et al.* 2019)
Body and Tissue Morphology				
Body Size	Increases in early adulthood, then decreases in late adulthood	Dissecting scope with camera, images analyzed in ImageJ with an optional WormSizer plug-in	Quantitative Non-invasive	(Croll *et al.* 1977; Bolanowski *et al.* 1981; Herndon *et al.* 2002)
Head/Pharynx	Decrease in organization	Nomarski microscopy; DIC microscopy, Harlick texture entropy	Qualitative Invasive	(Garigan *et al.* 2002; Chow *et al.* 2006; Shamir *et al.* 2009)
Pharynx size	Enlarged or atrophied pharynx in a subset of	Nomarski microscopy	Quantitative Invasive Spatial	(Zhao *et al.* 2017)

	population			
Body Wall Muscle	Decrease in myosin fiber organization, loss of sarcomeric density	Electron and Nomarski microscopy	Qualitative Invasive	(Herndon *et al.* 2002; Glenn *et al.* 2004)
Bacterial accumulation	Accumulation in pharynx/ intestine	Electron and Nomarski microscopy	Qualitative Invasive*	(Garigan *et al.* 2002; Chow *et al.* 2006; McGee *et al.* 2011)
Intestinal integrity	Loss of intestinal nuclei and breakdown of plasma membrane	Transmission electron microscopy DAPI, Fluorescence microscopy	Qualitative Invasive Spatial	(McGee *et al.* 2011)
Tissue appearance	acquires granular appearance	Dissecting microscope	Qualitative Non-invasive	(Garigan *et al.* 2002)
Vulval integrity	Increase in probability and severity of vulval rupture in a subset of the population	Dissecting microscope	Quantitative Non-invasive	(Leiser *et al.* 2016)
Hypodermis	Lose 3 nuclei in tail	DAPI microscopy	Qualitative Invasive Spatial	(Golden *et al.* 2007)
Midsection, Body cavity	Masses of DNA accumulated	DAPI microscopy, DNA sysnthesis confirmed by BrdU	Qualitative Invasive Spatial	(Golden *et al.* 2007)
Subcellular Morphology				
Mitochondrial morphology – change in fragmentation and fusion	Loss of tubular morphology, mtDNA copying number decline, functional and structural decline	Transmission electron microscopy, quantitative real-time PCR, fluorescent reporter protein and microscopy	Qualitative Invasive Spatial	(Yasuda *et al.* 2006; Gruber *et al.* 2011; Regmi *et al.* 2014)
Nucleus	Reduction of the number of nuclei	DAPI Fluorescent microscopy, fluorescent reporter protein with microscopy	Quantitative Invasive Spatial	(Golden *et al.* 2007; McGee *et al.* 2011)
Nuclear Envelope	Decrease in organization of the nuclear envelope	Fluorescent reporter protein, Confocal microscopy, Electron microscopy	Categorical Invasive Spatial	(Herndon *et al.* 2002; Haithcock *et al.* 2005)
Nucleolus	Increase of size in relation to the whole nucleus	Fluorescent reporter protein with fluorescence microscopy, Nomarski microscopy	Quantitative Invasive, non-lethal Spatial	(Herndon *et al.* 2002)
Processing bodies	Accumulate	Fluorescent fusion protein, fluorescence	Quantitative Invasive	(Rousakis *et al.* 2014)

		microscopy	(lethal)	
Ectopic fat depositions and lipid droplets	Increase; change in spatial distribution	Fluorescence and transmission electron microscopy; Third Harmonic Generation microscopy	Quantitative Invasive Spatial	(Herndon *et al.* 2002; Tserevelakis *et al.* 2014; Mari *et al.* 2016; Palikaras *et al.* 2016)
Autophagy	Increase of the number Autophagosomes	Confocal Microscopy	Quantitative Invasive	(Chang *et al.* 2017)
Biochemical – gene and chromatin				
Genome copy number	increase genome copy number in germline and decrease mitochondrial genome copy number	qPCR DAPI	Quantitative Invasive Non-spatial	(Golden *et al.* 2007; Gruber *et al.* 2011)
DNA integrity	Increase in single strand breaks Methylation increases	*in vitro* assay for single strand breaks HPLC	Quantitative Invasive Non-spatial	(Klass *et al.* 1983)
Chromatin	Histone methylation profile changes	H3K4m3 Chip-Seq	Quantitative Invasive Non-spatial	(Klass *et al.* 1983; Pu *et al.* 2015, 2018)
Gene Expression / Trancriptomics	Gene expression changes	RNA-seq	Quantitative Invasive	Reviewed in wormbook chapter (Golden and Melov 2007), (Kato *et al.* 2011; Rangaraju *et al.* 2015; Angeles-Albores *et al.* 2017; Templeman *et al.* 2018; Rodriguez *et al.* 2019)
mRNA splicing	Splicing efficiency declines	mCherry/GFP reporter and transcriptomics	Quantitative Invasive	(Heintz *et al.* 2017)
microRNAs	Changes in expression profile	microarray	Quantitative Invasive	(Ibáñez-Ventoso *et al.* 2006; Pincus *et al.* 2011)
Biochemical – protein				
Posttranslational modifications	Increase in levels of protein carbonylationcontent especially in mitochondria and germline	Biochemical assays of extracts Immunofluorescence	Quantitative Invasive Spatial	(Adachi *et al.* 1998; Yasuda *et al.* 2006; Goudeau and Aguilaniu 2010)
Proteome	Protein levels increase and decrease	SILAC-based deep Proteome Analysis	Quantitative Invasive	(Walther *et al.* 2015; Narayan *et al.* 2016)

Protein stability	protein misfolding, loss of protein function protein aggregation	Expression of metastable proteins fused to fluorescent proteins (ts mutations), Mass spectrometry microscopy	Quantitative Invasive/non Invasive some spatial	(Ben-Zvi *et al.* 2009; David *et al.* 2010; Labbadia and Morimoto 2015)
Clustered change in protein levels	Yolk redistribution, increase in Yolk	Electron Microscopy, Nomarski Western B,ot	Qualitative Invasive Spatial	(Garigan *et al.* 2002; Herndon *et al.* 2002; Ezcurra *et al.* 2018)
Enzymatic Activity	Decrease in protein tyrosine kinase activity, increase in lysosomal hydrolases	Biochemical assay Enzymatic activity, Western Blot	Quantitative Invasive	(Bolanowski *et al.* 1983; Yuan *et al.* 2016)
Biochemical – metabolism				
Auto-fluorescence	Increase	Spectrofluorometry Fluorescence/ electron microscopy	Quantitative Invasive Spatial	(Epstein *et al.* 1972; Klass 1977; Davis *et al.* 1982; Hosokawa *et al.* 1994; Garigan *et al.* 2002; Gerstbrein *et al.* 2005; Pincus *et al.* 2011, 2016; Coburn *et al.* 2013)
Metabolic activity	Decrease	Various assays	Quantitative Invasive Non spatial	(Van Voorhies and Ward 1999; Braeckman *et al.* 2002b, a; c; Brys *et al.* 2010; Gruber *et al.* 2011)
Metabolites	Changes in metabolites concentrations (Amino acids, Lipids, others)	NMR Mass spectrometry (GC-MS)	Quantitative Invasive Non spatial	(Braeckman *et al.* 2002a; b; c; Gruber *et al.* 2011; Pontoizeau *et al.* 2014; Davies *et al.* 2015; Copes *et al.* 2015; Gao *et al.* 2017; Yanase *et al.* 2017; Wan *et al.* 2017)

TABLE 2: Catalog of changes in males

Age-related change	Description over age	Method	Features and Limitations	References
Behavior				
Mating behavior	Decrease in successfully completed mating events	Dissecting Scope	Quantitative Non-invasive	(Chatterjee *et al.* 2013)
Body Movement	Decrease in rate	Dissecting scope	Quantitative Non-invasive	(Chatterjee *et al.* 2013)
Body and Tissue Morphology				
Male tail morphology	Progressive deterioration of tail structure	DIC microscopy	Quantitative Invasive (non-lethal)	(Chatterjee *et al.* 2013)
Body Size	Mated males show decreased body length later in life compared to unmated males	Dissecting scope with camera and ImageJ	Quantitative Non-invasive	(Shi *et al.* 2017)
Sperm	Decrease in viability	Dissecting scope to measure cross-progeny production after mating to hermaphrodites	Quantitative Non-invasive	(Klass *et al.* 1983)

TABLE 3: Correlations between age-related changes

	Survival probability	**Pharyngeal pumping**	**Body movement**	**Body and Tissue Morphology**
Self-fertile reproduction	no correlation (Johnson 1987; Huang *et al.* 2004)	no correlation (Huang *et al.* 2004)	no correlation (Johnson 1987; Huang *et al.* 2004)	
Mated reproduction	positive (Pickett and Kornfeld 2013; Pickett *et al.* 2013)			
Body movement	positive (Hosono *et al.* 1980; Bolanowski *et al.* 1981; Johnson 1987; Herndon *et al.* 2002; Huang *et al.* 2004; Gerstbrein *et al.* 2005; Hsu *et al.* 2009; Restif *et al.* 2014)	positive (Hosono *et al.* 1980; Huang *et al.* 2004)	positive (Hsu *et al.* 2009; Beck *et al.* 1993)	
Pharyngeal Pumping	positive (Johnson 1987; Huang *et al.* 2004; Wolkow 2006)			
Defecation	no correlation (Bolanowski *et al.* 1981)		no correlation (Bolanowski *et al.* 1981)	
Pharyngeal Morphology	positive (Zhao *et al.* 2017)	positive (Johnston *et al.* 2008; Zhao *et al.* 2017)		positive (Ezcurra *et al.* 2018)
Uterine Morphology				positive (Ezcurra *et al.* 2018)
Synaptic deterioration			positive (Toth *et al.* 2012)	
Spontaneous neurite branching			positive (Tank *et al.* 2011)	
Pseudocoelomic morphology				positive (Ezcurra *et al.* 2018)
Intestinal morphology				positive (Ezcurra *et al.* 2018)
Mitochondria	positive (Hahm *et al.* 2015)	positive (Hahm *et al.* 2015)	positive (Hahm *et al.* 2015)	
Mitochondrial copy number			negative (Gruber *et al.* 2011)	
Nuclear Envelope			positive (Herndon *et al.* 2002)	
Nucleolar size	negative (Tiku *et al.* 2016)			
Body wall muscle			positive (Herndon *et al.* 2002)	
Autofluorescence	positive (Pincus *et al.* 2011, 2016)		positive (Gerstbrein *et al.* 2005)	
Maximum Velocity	positive (Hahm *et al.* 2015)			
Splicing efficiency	positive (Heintz *et al.* 2017)			
Metabolism			positive (Yuan *et al.* 2016)	

Conclusions

What are the relationships between age-related changes?

One major accomplishment of the studies of age-related changes in *C. elegans* is the definition of relationships between age-related changes. Age-related changes in tissue morphology and function have been documented in many animals, but few studies have addressed the relationships between these changes. The experimental advantages of the *C. elegans* system have made it possible to address these issues using rigorous longitudinal studies (**Figure 2**).

Table 3 summarizes the experimentally defined relationships. There is a strong positive correlation between the declines of pharyngeal pumping, body movement, and survival probability. A positive correlation also exists between the decline of body movement and the appearance of disorganized body wall muscles and the accumulation of fluorescent compounds in the body.

These results suggest that these age-related changes may be causally connected. For example, the age-related disorganization of the body wall muscles may cause the decline in body movement. The appearance of endomitotic oocytes in the gonad may cause sterility. Alternatively, there may be a common mechanism that influences the timing of each of these processes. Overall, these results indicate that age-related changes in tissue morphology and function are controlled by common mechanisms and/or causally linked in series (**Figure 6**).

The decline of self-fertile reproduction and the defecation cycle displayed no correlations with other age-related changes. One explanation for these results is that the lack of correlations occurred because the causes of some of these age-related changes are actually developmental or extrinsic and not due to aging. For example, decline in self-fertile reproduction is probably not

due to an age-related decline in fertility, but rather results from depletion of the finite supply of sperm produced during larval development. Another explanation is that the longitudinal studies were performed in the wrong timeframe. For example, it is plausible that defects in the distal tip cell and germline stem cell region do cause decreased progeny production, but the effect may be delayed by several days, hindering the study of this effect with invasive techniques in longitudinal experiments.

What are the evolutionary theories of aging?

The question of the evolution of aging is as old as evolutionary theory itself. Erasmus Darwin, the grandfather of both Charles Darwin and Francis Galton and author of a poem explaining his early theory of evolution, commented "*How short the span of life*," (Darwin 1803). Charles Darwin listed many questions that he hoped his theory of evolution by natural selection would answer, including, "*Why is life short?*" George C. Williams explained the reason we continue to be baffled by the existence of aging: "*It is indeed remarkable that after a seemingly miraculous feat of morphogenesis a complex metazoan should be unable to perform the much simpler task of merely maintaining what is already formed*,"(1957). Is aging a beneficial trait chosen by natural selection, a trait which is harmful in a context where natural selection cannot act against it, a simple result of entropy and limited resources, or a combination of these?

Several arguments are often used to suggest that senescence is influenced by genetics. First, certain mutations and natural polymorphisms affect lifespan in a way that suggests the function of these genes is to regulate lifespan. Long-lived mutants have been isolated in both *Caenorhabditis elegans* (e.g. *age-1*, *daf-2*) and *Drosophila melanogaster* (e.g. *methuselah, indy*)

(Friedman and Johnson 1988; Kenyon *et al.* 1993; Rogina *et al.* 2000). Also, twin studies show that about a quarter to a third of variation in lifespan is likely genetic, which is higher than what one would expect if senescence were entirely stochastic (Cournil and Kirkwood 2001). Experiments show that artificial selection for longevity can extend lifespan, which also suggests that there is a genetic component which determines longevity (Rose 1984; Luckinbill and Clare 1985)

Second, in some species (semelparous organisms including salmon, bamboo, etc.) rapid senescence and death immediately and invariantly follow reproduction. This has been interpreted by various theorists as either an extreme case of disposable soma or as an example of programmed rapid death similar to apoptosis (Kirkwood and Melov 2011).

Third, similarities in the aging process and in the pattern that reproductive senescence precedes somatic senescence in many species has been interpreted as evidence for a conserved mechanism of aging, because a stochastic aging process is not predicted to produce this type of pattern (Hughes *et al.* 2007). Reproductive and somatic senescence are present not only in animals and plants, but also in asymmetrically-dividing unicellular eukaryotes (*Saccharomyces cerevisiae*) and even in prokaryotes (*Escherichia coli*). Also, the genes in which mutations extend lifespan in one species are highly conserved through evolution and mutations in homologous genes also extend lifespan in other species. The interpretation of these observations is that aging is universal to life (Stewart *et al.* 2005; Steinkraus *et al.* 2008).

Fourth, when senescence is accelerated (progerias, certain short-lived mutants) or decelerated (long-lived mutants, castration in Kokanee salmon, caloric restriction), the broad pattern of aging remains the same, which suggests that the treatments do not entirely change aging, but modulate it through existing pathways which normally respond to the nutritional and

reproductive environment (Robertson 1961; Robertson and Wexler 1962; Walker *et al.* 2005; Hughes *et al.* 2011). On the other hand, classical theories argue that aging is only an artifact of captivity, because aging has rarely been observed to contribute to mortality in the wild (Medawar 1952; Kirkwood and Holliday 1979; Kirkwood and Austad 2000). However, observations of antler flies and other species show that senescence reduces mating success of male antler flies in the wild, which is interpreted to mean that senescence is important to fitness even in the wild (Bonduriansky and Brassil 2002).

What does stochasticity mean for evolutionary theories of aging?

An important conceptual issue in the aging field is the role of genetic programs in controlling age-related degenerative changes. Here, we discuss how the analysis of *C. elegans* contributes to understanding this issue by considering **two theories: (1)** that age-related degenerative changes are specified by a genetic program, and **(2)** that age-related degenerative changes are caused by the absence of genetically encoded instructions that permit continued maintenance and organismal survival. According to the **first theory**, age-related degenerative changes should be relatively reproducible in all individuals and in all tissues, similar to age-related developmental changes, since both types of events are genetically specified. Furthermore, it should be possible to identify mutants that do not undergo specific age-related degenerative changes, by mutating genes that specify these changes (barring pleiotropies). According to the **second theory**, age-related degenerative changes should be relatively chaotic and less reproducible than developmental changes. Furthermore, it should not be possible to identify mutants that do not undergo specific age-related changes, since these changes are not specified by a genetic program.

This review includes all reported age-related changes, regardless of the degree to which the changes are reproducible versus chaotic and stochastic. It has, however, emphasized the reproducible aspects of age-related degenerative changes, including the finding that most changes become progressively more severe, occur during a characteristic time window, and affect the majority of individuals studied. On the other hand, the pattern of age-related changes reported by Herndon *et al.* (2002) and Kocsisova *et al.* (2019) suggests that some of these changes are mediated by stochastic events. The evidence that age-related changes are mediated by stochastic events is the degree of heterogeneity among aging individuals and the degree of heterogeneity among aging tissues or cells within an individual. For example, in a group of animals that are the same chronological age, there can be wide variation in the ability to perform a function such as body movement. At the cellular level, Herndon *et al.* (2002) noted that there is substantial variability in degenerative changes. For example, examining a pair of cells that are left-right symmetrical might reveal that the left cell was extensively degenerated whereas the right cell was intact (Herndon *et al.* 2002; Pincus and Slack 2010). In *C. elegans*, the germline provides a useful model for just such studies of symmetry and intraclass correlation (Taylor *et al.* 2016; Kocsisova *et al.* 2019). These studies convincingly document the degree of variability of age-related changes.

However, developmental events that are programmed display some variability. While it appears that age-related changes at the cellular level are more variable than developmental effects, the amount of this variability has not been defined and it is difficult to quantify variability. Despite these caveats, the observation that age-related degenerative changes are highly variable and likely to be mediated by stochastic processes is a significant discovery that suggests that age-related changes result from the absence of a genetic program.

Chapter 3:

PCN-1 is not an S-phase marker in the *C. elegans* germline

The work presented in Chapter 3 is published with the following authors:

Kocsisova Z., Kornfeld K., Schedl T., **2018** Cell cycle accumulation of the proliferating cell nuclear antigen PCN-1 transitions from continuous in the adult germline to intermittent in the early embryo of *C. elegans*. BMC Developmental Biology **18**: 1–12.

Abstract

The proliferating cell nuclear antigen (PCNA or PCN-1 in *C. elegans*), an essential processivity factor for DNA polymerase δ, has been widely used as a marker of S-phase. In *C. elegans* early embryos, PCN-1 accumulation is cyclic, localizing to the nucleus during S-phase and the cytoplasm during the rest of the cell cycle. The *C. elegans* larval and adult germline is an important model systems for studying cell cycle regulation, and it was observed that the cell cycle regulator cyclin E (CYE-1 in *C. elegans*) displays a non-cyclic, continuous accumulation pattern in this tissue. The accumulation pattern of PCN-1 has not been well defined in the larval and adult germline, and the objective of this study was to determine if the accumulation pattern is cyclic, as in other cells and organisms, or continuous, similar to cyclin E.

To study the larval and adult germline accumulation of PCN-1 expressed from its native locus, we used CRISPR/Cas9 technology to engineer a novel allele of *pcn-1* that encodes an epitope-tagged protein. S-phase nuclei were labeled using EdU nucleotide incorporation, and FLAG::PCN-1 was detected by antibody staining. All progenitor zone nuclei, including those that were not in S-phase (as they were negative for EdU staining) showed PCN-1 accumulation, indicating that PCN-1 accumulated during all cell cycle phases in the germline progenitor zone. The same result was observed with a GFP::PCN-1 fusion protein expressed from a transgene. *pcn-1* loss-of-function mutations were analyzed, and *pcn-1* was necessary for robust fertility and embryonic development.

In the *C. elegans* early embryo as well as other organisms, PCN-1 accumulates in nuclei only during S-phase. By contrast, in the progenitor zone of the germline of *C. elegans*, PCN-1 accumulated in nuclei during all cell cycle stages. This pattern is similar to accumulation pattern of cyclin E. These observations support the model that mitotic cell cycle regulation in the

germline stem and progenitor cells is distinct from somatic cells, as it does not heavily rely on cyclic accumulation of classic cell cycle proteins.

Introduction

Regulation of cell proliferation is key to a wide range of health concerns, from infertility to wound healing and cancer. Like Goldilocks, every tissue in every living organism must find the level of cell division that is "just right" in order to survive, develop, and pass on genetic information. The cell cycle coordinates duplication and segregation of both genetic and cellular material to two daughter cells. Cell cycle regulators change abundance or localization at different stages of DNA replication and cell division. For example, cyclin E accumulates during the G1-S-phase transition. This pattern is generally conserved between multiple eukaryotic kingdoms of life. However, the adult *C. elegans* germline accumulates cyclin E in all cell cycle phases, suggesting that this tissue may utilize distinctive mechanisms of cell cycle control (Fox *et al.* 2011).

The distal *C. elegans* hermaphrodite germline contains the only stem cells in the adult *C. elegans* (Figure 1A). The somatic distal tip cell (DTC) surrounds the syncytial distal-most nuclei and provides the niche to maintain these stem cells in their proliferative fate. The ~20 cell-diameter long distal region, which includes the mitotically cycling germline stem and progenitor cells and meiotic S-phase cells but not cells in meiotic prophase, is called the progenitor zone (Crittenden *et al.* 2006; Hansen and Schedl 2013; Pazdernik and Schedl 2013; Fox and Schedl 2015). As germ cells move away from the DTC, the cells finish the mitotic cell cycle, enter the meiotic cell cycle, undergo meiotic S-phase, and enter prophase I of meiosis (Fox and Schedl 2015).

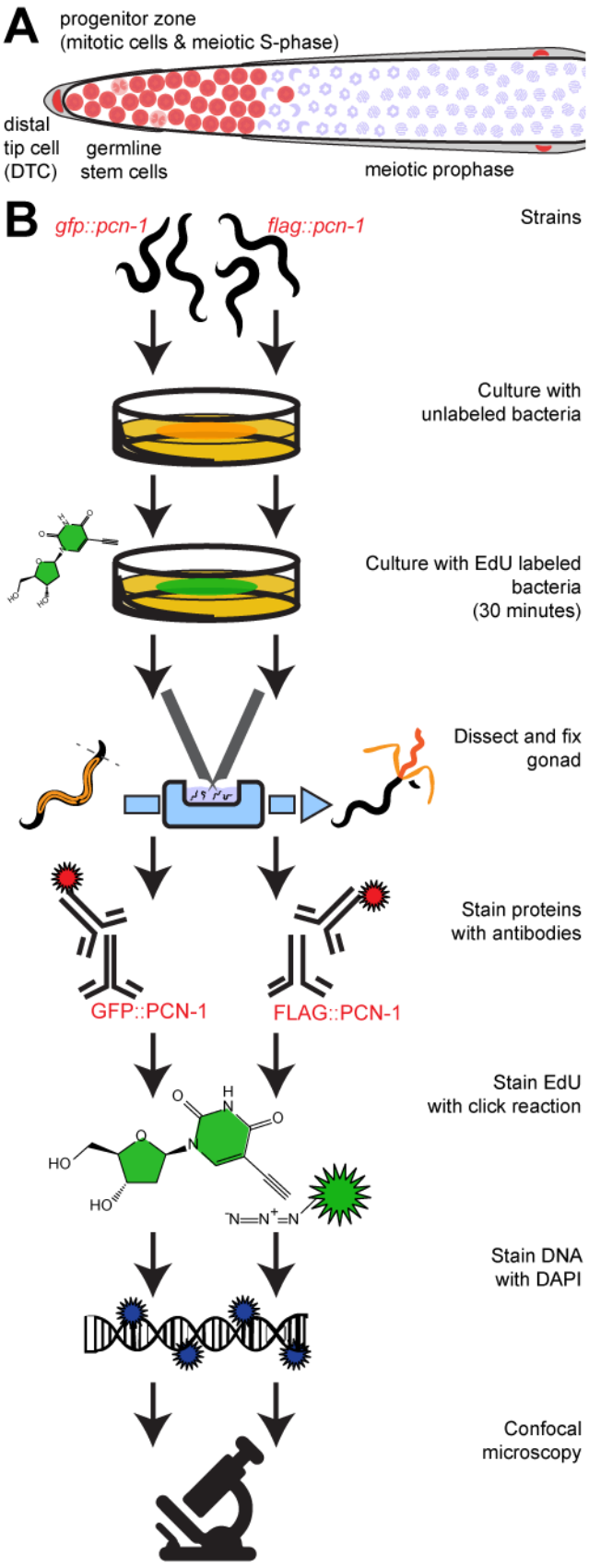
A
progenitor zone
(mitotic cells & meiotic S-phase)
distal
tip cell
(DTC)
germline
stem cells
meiotic prophase
B
gfp::pcn-1
flag::pcn-1
Strains
Culture with
unlabeled bacteria
Culture with EdU labeled
bacteria
(30 minutes)
Dissect and fix
gonad
Stain proteins
with antibodies
GFP::PCN-1
FLAG::PCN-1
Stain EdU
with click reaction
Stain DNA
with DAPI
Confocal
microscopy

Figure 1: Diagram of distal *C. elegans* germline and experimental workflow.

A) The syncytial distal progenitor zone (highlighted in red based on WAPL-1 antibody staining) contains mitotically cycling stem and progenitor cells and cells in meiotic S-phase. The distal tip cell (DTC) provides GLP-1 signal (Notch ligand) to maintain the stem cell fate of these cells. As cells migrate away from the DTC, they exit the progenitor zone and enter meiotic prophase.

B) Workflow used to assay the relationship between PCN-1 accumulation and S-phase (EdU labeling) in the *C. elegans* germline.

The proliferating cell nuclear antigen (PCNA or PCN-1 in *C. elegans*) is an essential processivity factor for DNA polymerase δ (Reviewed in (Moldovan *et al.* 2007)). As its name suggests, PCNA was identified by its nuclear accumulation in proliferating cells (Miyachi *et al.* 1978). In mammals, antibody recognition of PCNA is an often-used technique to identify cells in S-phase (Galand and Degraef 1989). Brauchle *et al.* 2003 established PCN-1 as a useful *in vivo* marker of S-phase in *C. elegans* early embryos, a stage when the cell cycle involves only negligible gap phases. In transgenic worms that express a green fluorescent protein GFP::PCN-1 fusion protein under the control of the *pie-1* promoter, GFP::PCN-1 localizes to the nucleus during S-phase, resulting in a bright fluorescent signal. At nuclear envelope breakdown (beginning of mitosis), GFP::PCN-1 localizes to the cytoplasm, resulting in a diffuse, low level signal (Brauchle *et al.* 2003). Similarly, GFP::PCNA protein injected into the gonad serves as a marker of S-phase in both *C. elegans* pronuclei and early embryonic divisions (Kisielewska *et al.* 2005).

For studies of cell cycle dynamics in the *C. elegans* adult germline, labeling with nucleotide analogs such as 5-ethynyl-2'-deoxyuridine (EdU) or 5-bromo-2'-deoxyuridine (BrdU) has been the gold standard to identify S-phase (Crittenden *et al.* 2006; Fox *et al.* 2011). However, these chemicals must enter *C. elegans* by feeding or soaking, which limits the utility of this approach. For example, some older adult animals fail to label with EdU following a short

(e.g. 30 minute) exposure, which might reflect defects in ingestion and/or transport of EdU (Cinquin *et al.* (2016), our unpublished observations). To clarify the relationships between PCN-1 accumulation and nucleotide analog incorporation as markers of S-phase, we developed methods to combine these two approaches.

To visualize PCN-1 in the adult germline, we used CRISPR/Cas9 genome editing to modify the native *pcn-1* locus to encode a 3xFLAG epitope at the N-terminus of PCN-1. Surprisingly, FLAG::PCN-1 accumulated in all nuclei in the germline progenitor zone. By contrast, a short pulse of EdU revealed that only about half of these nuclei were in S-phase. These results suggest that the accumulation and localization of PCN-1 is regulated differently in the *C. elegans* germline, where it is present in all progenitor zone nuclei, compared to the embryo, where it is restricted to nuclei in S-phase. Furthermore, we demonstrated that *pcn-1* is an essential gene in *C. elegans* necessary for both adult fertility and embryonic development. These results extend the understanding of the accumulation and function of PCN-1 in *C. elegans*, an important model system for studies of germline development and cell cycle regulation.

Methods

C. elegans strains were maintained at 20°C on 6cm dishes of nematode growth media (NGM) seeded with OP50 *E. coli* (Brenner 1974). The wild-type strain was Bristol N2. The GZ264 strain contains the GFP::PCN-1 transgene (*isIs17*) inserted at an undefined location in the genome, and it is wild-type at the *pcn-1* locus (Brauchle *et al.* 2003). To engineer a FLAG epitope tag into the endogenous *pcn-1* locus, we used the co-CRISPR approach (Arribere *et al.* 2014). The injection mix contained Cas9-expressing pDD162 (gift from Mike Nonet) at 50ng/µl, *dpy-10* guide plasmid (pMN3153) at 20ng/µl, *dpy-10(cn64)* ssDNA repair template AFZF827 at

500nM, *pcn-1* guide plasmids (pZK21 and pZK23) at 40ng/µl for each plasmid, and a ssDNA repair template (ZK071 containing the *3xflag* sequence) at 600nM. We injected the gonads of P0 wild-type hermaphrodites, selected F1 progeny that displayed the Rol phenotype, and used PCR to select animals with the desired genotype. Two independently derived strains contained the same insertion of the 22 amino acid coding region for the 3xFLAG epitope after the initial methionine codon of *pcn-1*. We named these alleles *pcn-1(am315)* and *pcn-1(am316)* (strains WU1764 and WU1765, respectively). We used a GFP-tagged balancer chromosome to maintain the strain *pcn-1(am315)/nT1g* due to the observed maternal-effect lethal phenotype.

To confirm expression of the full-length FLAG::PCN-1 product, we performed a Western blot. In brief, animals were washed from one 12cm NGM dish and rinsed 4 times with M9 buffer. Protease inhibitor (Thermo Scientific Pierce Protease Inhibitor Mini Tablets Cat# 88665) was used at 2x listed concentration in the second two washes. An equal volume of 2x lysis-and-loading buffer (100mM TrisHCl pH 6.8, 200mM DTT, 4% SDS, 0.2% Bromophenol Blue, 20% Glycerol) was added, and the samples were frozen at -80°C overnight. The samples were microwaved, boiled, sonicated in an ice bath, and boiled again. Samples (1.5, 7.5, or 15 uL) and a size reference (7uL, AccuRuler Prestained Protein Ladder LambdaBio Cat# G02101) were loaded into a pre-cast gel (BioRad Mini-PROTEAN TGX 4-20% polyacrylamide gel Cat#456-1093) in 1X Tris/ Glycine/ SDS buffer and run at 180V for ~1hour in an ice bath. Samples were transferred to activated membrane (Millipore Immobilon-P) in 1X Tris/ Glycine/ 20%Methanol buffer at 350mA for ~1hour in an ice bath. The membrane was incubated in blocking buffer (5% non-fat milk in 1X PBS + 0.5% Tween-20) for ~1 hour at room temperature with agitation. Primary mouse-anti-FLAG antibody (Sigma M2 F-1804) was diluted 1:10,000 in blocking buffer and applied overnight at 4°C with agitation. The membrane was rinsed 3x with PBSTw.

Secondary anti-mouse HRP antibody (Cell Signaling) was diluted 1:2,000 in blocking buffer and applied for ~1hr at room temperature with agitation. The membrane was rinsed 3x with PBSTw, incubated with substrate (ThermoScientific SuperSignal West Femto Maximum Sensitivity Substrate) for ~1minute, and imaged on a ChemiDoc imaging system. Protein size was estimated from conceptually translated DNA sequence using the Science Gateway Protein Molecular Weight Calculator (http://www.sciencegateway.org/tools/proteinmw.htm).

To visualize both FLAG::PCN-1 accumulation and cells in S-phase, we cultured fourth larval stage (L4) and young adult progeny of heterozygous *pcn-1(am315/+)* parent animals on EdU-labeled *E. coli* MG1693 for 30 minutes and promptly dissected (Fox *et al.* 2011). Animals were fixed with 3% paraformaldehyde for 10 minutes and post-fixed in 100% methanol at -20°C overnight. Primary mouse-anti-FLAG antibody (Sigma M2 F-1804) was diluted 1:1000 and rabbit-anti-WAPL antibody (Novus 49300002) was diluted 1:20000 in 30% goat serum and applied overnight. Secondary goat-anti-mouse-Alexa-647 antibody and secondary goat-anti-rabbit-Alexa-594 antibody (Life Technologies) were diluted 1:400 in 30% goat serum and applied for 4 hours. The Click-iT EdU Fluor 488 reaction was performed according to manufacturer instructions (ThermoFisher Cat#C10350). Animals were mounted in Vectashield + DAPI on agarose pads and imaged using a 63x/1.4NA Plan Apo oil immersion objective on a Zeiss Observer Z1 inverted microscope equipped with a Perkin-Elmer Ultraview Vox spinning disc confocal system using Volocity software. Exposure times were 150ms for EdU, 50ms for FLAG::PCN-1, and 500ms for DAPI. Images were processed with Fiji (Schindelin *et al.* 2012) and Adobe Illustrator. GFP::PCN-1 was visualized as described above, except primary rabbit-anti-GFP (gift from Swathi Arur) and secondary goat-anti-rabbit-Alexa-594 were used (Figure 1B).

To quantify fluorescence intensity, we used the region of interest ROI and Measure tools in Fiji. In brief, a cell was selected in a single plane based on DAPI channel and assigned to S-phase or gap phase based on the presence or absence of EdU. A single ROI was drawn to surround the DAPI signal, and the mean intensity of DAPI, EdU, and PCN-1 was obtained for the ROI. Background intensities of all three channels were very low and comparable, and therefore no background subtraction was performed.

Statistical analyses were performed in R (R Core Team 2013) using R studio (RStudio Team 2015) and ggplot2 (Wickham 2009). Data were compared using an ANOVA with Tukey's Honest Significant Difference post-hoc. All error bars shown in figures represent the mean +/- standard deviation.

We determined the genotype and phenotype of animals descended from P0 heterozygous *pcn-1(am315)/+* or *pcn-1(am316)/+* hermaphrodites. F1 animals were cultured individually for three to four days from egg. Each animal was observed for viability and fertility. Animals which deposited no eggs on the substrate were dissected to allow unlaid F2 eggs to develop. One to two days later, F2 progeny were examined for viability. Genotype was established by performing PCR analysis on individual F1 animals. Hermaphrodites were defined as "fertile" if they deposited one or more eggs on the agar surface that hatched and developed into larvae. Animals were defined as "sterile" if they deposited no eggs on the agar surface, or "dead eggs" if all deposited eggs failed to hatch.

Heterozygous animals were fertile and did not display obvious defects when cultured in standard laboratory conditions. The GFP-tagged balancer chromosome *nT1g* was used to track the *pcn-1* genotype in a larger number of animals. For brood size assays, P0 *pcn-1(am315)/nT1g* males were mated to *fog-2(q71)* females. The non-green F1 progeny of this cross, *pcn-*

1(am315/+); fog-2(q71/+) were synchronized at the mid-L4 stage, isolated to individual NGM dishes, and moved to fresh dishes every 24 hours. Parent animals which fled the dish or died of matricidal hatching were excluded. The F2 progeny were counted ~2 days later until the cessation of reproduction. *fog-2(q71/+)* served as the control. For survival assays (egg-to-larva and egg-to-adult), the identical crosses were performed, and F1 animals were allowed to lay eggs for several hours. These eggs were transferred to a fresh dish and counted 24 hours later, the unhatched eggs were counted to estimate the number of larvae, and the adults were counted 48 hours later.

Results

PCN-1 accumulated during all cell cycle phases in the germline progenitor zone.

PCN-1 accumulation has been monitored using an integrated transgene that encodes a GFP::PCN-1 fusion protein (Figure 2A). In *C. elegans* early embryos, PCN-1 accumulates during S-phase but not during M phase, indicating that it is regulated during the cell cycle (Brauchle *et al.* 2003; Kisielewska *et al.* 2005). Thus, we anticipated that PCN-1 would display a similar accumulation pattern in the larval and adult germline. To test this prediction, we monitored S-phase nuclei using a short, 30 minute pulse of EdU and we monitored PCN-1 expression with an anti-GFP antibody to detect the GFP::PCN-1 fusion protein (Figure 1B). The nucleotide analog EdU is used as a selective marker of DNA synthesis as it is incorporated into DNA during S-phase. In the germline, S-phase occurs only in progenitor zone cells, which include the stem cells (Figure 1A). Consistent with previous publications, approximately 50% of progenitor zone nuclei were EdU positive, indicating that these cells were in S-phase (Figure 2C)

(Crittenden *et al.* 2006; Jaramillo-Lambert *et al.* 2007; Fox *et al.* 2011). By contrast, all progenitor zone nuclei were GFP::PCN-1 positive, irrespective of their cell cycle stage (Figure 2B). Thus, about half the progenitor zone nuclei were positive for both EdU and GFP::PCN-1, indicating that cells in S-phase display nuclear accumulation of PCN-1 (Figure 2D). However, about half the progenitor zone nuclei were negative for EdU and positive for GFP::PCN-1, indicating nuclei that were not in S-phase, and presumably were in G2, M, or the short G1 phase, also accumulated PCN-1 (Figure 2D,E). It is notable that the GFP fluorescence signal in the germline displayed extremely low intensity, and we could only detect the GFP::PCN-1 fusion protein with long exposure times for GFP fluorescence in live animals or after staining with anti-GFP antibodies.

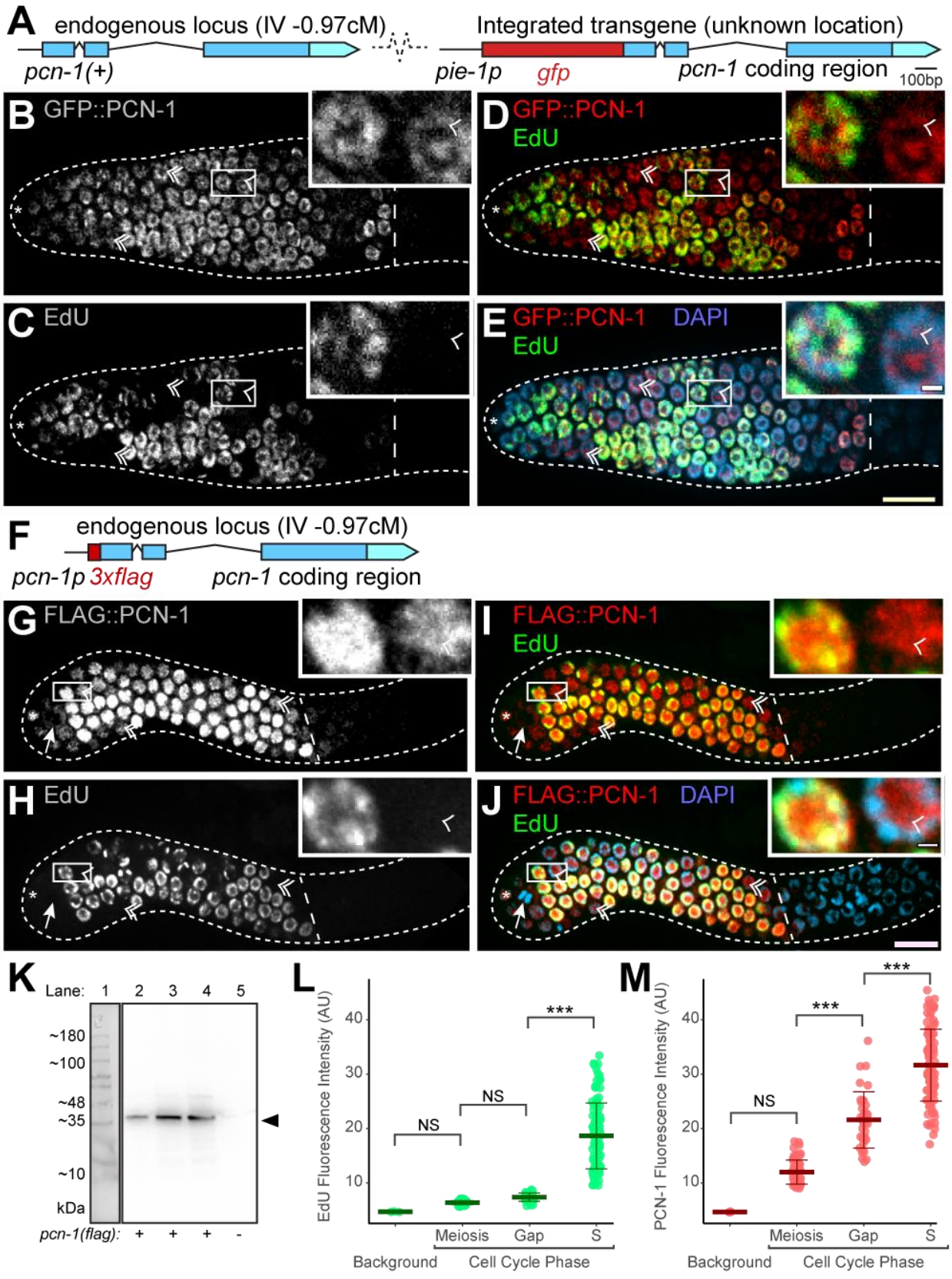
A
endogenous locus (IV -0.97cM)
Integrated transgene (unknown location)
pcn-1(+)
pie-1p
gfp
pcn-1 coding region
100bp
B GFP::PCN-1
C EdU
D GFP::PCN-1
EdU
E GFP::PCN-1 DAPI
EdU
F
endogenous locus (IV -0.97cM)
pcn-1p 3xflag
pcn-1 coding region
G FLAG::PCN-1
H EdU
I FLAG::PCN-1
EdU
J FLAG::PCN-1 DAPI
EdU
K
Lane: 1 2 3 4 5
~180
~100
~48
~35
~10
kDa
pcn-1(flag): + + + -
L
EdU Fluorescence Intensity (AU)
40
30
20
10
NS
NS
***
Meiosis
Gap
S
Background
Cell Cycle Phase
M
PCN-1 Fluorescence Intensity (AU)
40
30
20
10
NS
***
***
Meiosis
Gap
S
Background
Cell Cycle Phase

Figure 2: PCN-1 accumulated during all cell cycle phases in the germline progenitor zone.

A) A diagram of a portion of the genome of the GZ264 strain that contains the GFP::PCN-1 transgene (*isIs17*) inserted at an undefined genomic location. The *pie-1* promoter drives transcription in the germline and is fused to the coding regions of GFP (red) and PCN-1(blue). Boxes indicate exons with light shading for the 3' UTR, straight lines indicate promoters, and peaked lines indicate introns. The strain contains an intact *pcn-1* locus on chromosome IV. Scale bar is 100bp.

B-E) Confocal microscope images of a hermaphrodite gonad at the adult stage. The dotted white line outlines the gonad, and the dashed white line marks the end of the progenitor zone. Note that not all nuclei are in the focal plane. The asterisk marks the position of the distal tip cell. The inset shows an enlargement of the region outlined by a white rectangle - scale bars are in panel E. Main scale bar is 10um, inset scale bar is 1um. Single arrowheads (in inset) and double arrowheads (outside of inset) mark nuclei that were negative for EdU staining (in gap phase) and positive for GFP::PCN-1 accumulation. White or red mark GFP::PCN-1 accumulation visualized by antibody staining (B,D,E). White or green mark EdU staining visualized by click chemistry (C,D,E). Yellow indicates overlap (D). Blue marks DAPI staining for DNA (E). GFP::PCN-1 accumulated in all progenitor zone nuclei in an adult hermaphrodite, whereas only about half the nuclei were positive for EdU staining.

F) A diagram of the *pcn-1(am315)* genomic locus. The endogenous *pcn-1* promoter drives transcription and is fused to the coding regions of 3xFLAG epitope tag (red) inserted in-frame immediately after the ATG start codon to create an N-terminally tagged fusion protein expressed from the endogenous locus.

G-J) Confocal microscope images of a *pcn-1(am315)*/+ hermaphrodite gonad at the late L4 stage. The dotted white line outlines the gonad, and the dashed white line marks the end of the progenitor zone. Note that not all nuclei are in the focal plane. The asterisk marks the position of the distal tip cell. The inset shows an enlargement of the region outlined by a white rectangle – scale bars are in panel J. Main scale bar is 10um, inset scale bar is 1um. Single and double arrowheads mark nuclei that were negative for EdU staining (in gap phase) and positive for FLAG::PCN-1 accumulation. The arrow points to an anaphase nucleus. Main scale bar is 10um, inset scale bar is 1um. White or red mark FLAG::PCN-1 visualized by antibody staining (G,I,J); it accumulated in all progenitor zone nuclei. White or green mark EdU staining visualized by click chemistry (H, I, J). Yellow indicates overlap (I). Blue marks DAPI staining for DNA (J). Longer exposures of panels B and G show that all nuclei are PCN-1 positive. Longer exposures of panels D and I show that a 30 minute EdU pulse, which marks S-phase nuclei, stains about 50% of progenitor zone nuclei. Antibody staining for WAPL-1 was used to define progenitor zone cells.

K) Western blot probed with anti-FLAG antibody. Lane 1: Markers, with sizes indicated in kDa. Lanes 2, 3, and 4: 1.5ul, 7.5ul, and 15ul protein lysate from *pcn-1(am315flag)/nT1g* animals, respectively. Lane 5: 7.5ul protein lysate from wild-type animals. The Western blot shows an ~ 35kDa band specific to the lanes containing *pcn-1(am315flag)* (arrowhead on right), which corresponds well with the expected 31.75kDa size.

L,M) Quantification of fluorescence intensity of EdU (L) and FLAG::PCN-1 (M). Background values were obtained from image regions without tissue. Nuclei were selected in the DAPI channel and assigned to phases as follows: nuclei without WAPL-1 signal were assigned to meiosis (n=73), nuclei with both WAPL-1 and EdU signal were assigned to S-phase (n=104), and nuclei with WAPL-1 but without EdU signal were assigned to gap phases (n=36). ANOVA with Tukey's Honest Significant Difference post-hoc was used to compare the mean fluorescence intensity of nuclei; NS indicates $P>0.01$, * $P<0.01$, ** $P<.001$, *** $P<.0001$. The distributions of gap and S-phase EdU intensity were mutually exclusive; the FLAG::PCN-1 distributions of gap and S-phase display 74% overlap.

Two features of the transgenic strain raise the possibility that the accumulation pattern of the GFP::PCN-1 fusion protein may not accurately reflect the accumulation pattern of endogenous PCN-1; (1) fusion to the large GFP protein may affect the accumulation pattern or (2) the transgene uses the heterologous *pie-1* promoter and is integrated at a random site in the genome, not the endogenous locus (Figure 2A). To address these concerns, we used the CRISPR/Cas9 technique to edit the *C. elegans* genome. We chose the small FLAG epitope tag, reasoning that it is less likely to influence protein behavior than GFP. However, we cannot exclude the possibility that the FLAG tagged protein does not behave identically to the endogenous protein. We inserted coding sequence for three copies of the FLAG epitope tag at the N-terminus of PCN-1 into the native *pcn-1* locus (Figure 2F). Two independently derived strains with the identical insertion were generated, and we named these alleles *pcn-1(am315)* and *pcn-1(am316)*. The presence of a full-length FLAG::PCN-1 fusion protein was confirmed by performing an anti-FLAG Western blot (Figure 2K).

To monitor the expression pattern, we dissected and immunostained animals using an antibody directed against the FLAG epitope. The antibody staining was performed on the progeny of *pcn-1(am315/+)* animals, and thus included animals of three genotypes: *pcn-1(am315/am315), pcn-1(am315/+)* and *pcn-1(+/+)*. While the genotype of each individual was not determined using molecular approaches, we observed that the majority of animals showed the same pattern of FLAG::PCN-1 in the distal germline. Specifically, FLAG::PCN-1 was detected in all cells in the progenitor zone (Figure 2G). We interpreted these animals as a mixture of *pcn-1(am315/am315)* and *pcn-1(am315/+).* Thus, it is likely that *pcn-1(am315/am315)* and *pcn-1(am315/+)* animals have a similar pattern of expression. A minority of animals displayed no staining. We interpreted these animals as *pcn-1(+/+)*.

Several features of the expression pattern were notable. In metaphase and anaphase nuclei (identified by DAPI morphology), FLAG::PCN-1 signal appeared somewhat diffuse and to surround the chromatin (Figure 2G). By contrast, FLAG::PCN-1 signal in G1, S, and G2 nuclei overlapped with both chromatin and the nucleolus. Similar to the results described above with GFP::PCN-1, we detected multiple examples of nuclei in gap phase which displayed no EdU incorporation but did display nuclear FLAG::PCN-1 accumulation (Figure 2G-J). The same accumulation pattern was observed with both *pcn-1(am315)* and *pcn-1(am316)* strains. PCNA has been reported to show a punctate nuclear pattern in S-phase of mammalian cells (Leonhardt *et al.* 2000; Hahn *et al.* 2009). We did not observe punctate FLAG::PCN-1 staining; it is possible that harsh fixation conditions contribute to the lack of punctate staining.

To explore the relationship between PCN-1 expression and S-phase in detail, we quantified the intensity of FLAG::PCN-1 and EdU signal (following a 30 minute labeling) in individual distal germline nuclei (Figure 2L-M). Meiotic prophase cells that are not replicating DNA were used to establish the level of background noise. For EdU, the current gold-standard for S-phase labeling in *C. elegans*, progenitor zone nuclei either displayed very low intensity signal, similar to background, or substantial signaling; we assigned these nuclei to gap phase or S-phase, respectively. By contrast, all of the progenitor zone nuclei displayed FLAG::PCN-1 staining that was higher than background, indicating that all of these cells accumulate the protein. Thus, the presence of FLAG::PCN-1 cannot be used to reliably determine if a cell is in S-phase or gap phase. Cells in S-phase had a higher average level of FLAG::PCN-1 staining than cells in gap phase, but the distributions were highly overlapping: 71% of the true S-phase nuclei and 81% of the true gap phase nuclei (74% of total nuclei) were in the ambiguous range of

FLAG::PCN-1 intensity (Figure 2L-M). Thus, FLAG::PCN-1 appears to be continually present in nuclei, although it accumulates to higher levels during S phase.

In the *C. elegans* early embryo, GFP::PCN-1 shows nuclear accumulation only during S-phase (Brauchle *et al.* 2003; Kisielewska *et al.* 2005). A limitation of our use of FLAG::PCN-1 is that visualization cannot be performed in live embryos. Thus, our results do not establish the expression pattern of FLAG::PCN-1 in early embryos. By contrast to embryos, our results indicate that in the L4 and adult germline progenitor zone, PCN-1 accumulates throughout the cell cycle and its presence cannot be used as a reliable marker of S-phase (Figure 3). It is likely that germline PCN-1 is regulated by mechanisms other than degradation/translation and nuclear localization.

***pcn-1* was necessary for robust fertility and embryonic development.**

The GZ264 strain that contains the GFP::PCN-1 transgene (*isIs17*) and is wild-type at the *pcn-1* locus (Figure 2A) is viable and fertile. Compared to wild-type animals, this strain displayed abnormal, tortuous intestinal morphology after only 2-3 days of adulthood and a higher rate of vulval extrusion. The self-fertile brood size was not different from wild type, but the lifespan was slightly reduced (GZ264 16.6 ± 5.0 n=60; N2 20.5 ± 5.1 n=120, Log-Rank Test P=.0000019). These phenotypes could be caused by expression of the GFP::PCN-1 fusion protein, a deleterious effect of insertion of the transgene into the genome at a site of functional significance, or additional background effects.

To determine how the insertion of the sequence encoding the FLAG epitope at the *pcn-1* locus affected gene function, we analyzed heterozygous and homozygous mutant animals. To

rigorously quantify the penetrance of phenotypes, we determined the genotype and phenotype of 31 animals descended from *pcn-1(am315)/+* hermaphrodites (Table 1A). Genotype was established by performing PCR analysis on individual animals. Heterozygous animals were fertile and did not display obvious defects when cultured in standard laboratory conditions. Animals homozygous for either *pcn-1(am315)* or *pcn-1(am316)* that descended from heterozygous P0 hermaphrodites developed to adulthood and displayed sterility or maternal-effect embryonic lethality (Table 1A). These homozygous mutant animals produced few F2 homozygous embryos. Some F1 homozygous mutant hermaphrodites did not lay any embryos and displayed F2 embryos retained inside the uterus. Other F1 homozygous mutant hermaphrodites deposited a few embryos on the substrate, but these embryos failed to develop. This result was confirmed in an independent experiment (without PCR genotyping) examining 60 F1 progeny of heterozygous P0 animals; fifteen of these animals (25%) produced no viable progeny. These results indicate that both *pcn-1(am315)* and *pcn-1(am316)* are loss-of-function alleles, and *pcn-1* function is necessary to promote hermaphrodite fertility. In addition, *pcn-1* appears to have a function early in development that can be maternally rescued, since *pcn-1* homozygous mutants derived from heterozygous hermaphrodites develop to adulthood, whereas *pcn-1* homozygous mutants derived from *pcn-1* homozygous hermaphrodites displayed embryonic lethality.

To determine if the *pcn-1* mutation causes a dominant effect, we analyzed survival and fertility in heterozygous animals under standard laboratory conditions. Progeny of *pcn-1(am315/+)* heterozygous mutants displayed the same rates of egg hatching (98%) and survival to adulthood (96%) as progeny of *pcn-1(+/+)* animals (Table 1B). The self-fertile brood size of *pcn-1(am315/+)* hermaphrodites was not significantly reduced compared to *pcn-1(+/+)*

hermaphrodites (Table 1B). These results indicate that the FLAG::PCN-1 protein does not interfere with the endogenous protein function and *pcn-1(lf)* mutations are recessive for the fertility and survival phenotypes.

Table 1: Genetic analysis of *pcn-1* fertility A) Thirty-one self-progeny of heterozygous *pcn-1(am315flag)/+* hermaphrodites were analyzed by PCR of single animals to determine genotype after egg-laying was complete. Full genotypes: *pcn-1(+/+)*, *pcn-1(am315/+)*, and *pcn-1(am315/am315)*. Hermaphrodites were scored as "fertile" if they deposited one or more eggs on the agar surface that hatched and developed into larvae. Animals were scored as "sterile" if they deposited no eggs on the agar surface, or if all deposited eggs failed to hatch.
B) The percent of eggs that generate larvae and adults was determined for *pcn-1(+/+); fog-2(q71/+)* and *pcn-1(am315flag/+); fog-2(q71/+)* hermaphrodites, as described in the methods. n refers to total number of eggs analyzed. A chi-square test was used to compare the larval and adult survival. The total self-fertile brood size was determined as described in the methods. ANOVA was used to compare the brood size. mean ± s.d. n refers to total number of parental worms analyzed. NS indicates P>0.01, * P<0.01, ** P<.001, *** P<.0001.

A

	Genotype		
	pcn-1 (+/+)	*pcn-1 (flag/+)*	*pcn-1 (flag/flag)*
Fertile	7	17	0
Sterile	0	0	7

B

	Parental Genotype		
	pcn-1 (+/+)	*pcn-1 (flag/+)*	
Larval survival (%)	98.1 (n=376)	98.1 (n=324)	NS
Adult survival (%)	96.0 (n=376)	95.7 (n=324)	NS
Total Brood Size	305.4±35.5 (n=15)	332.5±35.7 (n=21)	NS

Discussion

We set out to engineer an endogenous non-feeding marker for S-phase in the *C. elegans* germline. We chose the gene PCN-1 for this purpose, as it has been used as an S-phase marker in mammals and in the *C. elegans* embryo. Both the GFP::PCN-1 transgene and our CRISPR-engineered FLAG::PCN-1 allele showed that PCN-1 localizes to the nucleus in all cells in the progenitor zone, regardless of whether the cells are in S-phase or gap phase. Therefore, PCN-1

was not a useful marker of S-phase under our conditions. The localization of PCN-1 to all nuclei in the progenitor zone was similar to the pattern of cyclin E1 (CYE-1) in the *C. elegans* germline (Fox *et al.* 2011). While this result means PCN-1 is not an S-phase marker, it reveals that the *C. elegans* germline likely regulates S-phase in an unusual way.

No previous publications have described the *pcn-1* loss-of-function phenotype. The *C. elegans* database (WormBase WS257) lists a deletion allele, *pcn-1(tm3241)* that is predicted to be a loss-of-function mutation. A strain that contains this allele displays a lethal or sterile phenotype, consistent with our findings; however, the *pcn-1(tm3241)* strain has not been backcrossed, and these phenotypes might reflect background mutations (The C. elegans Deletion Mutant Consortium 2012). We found *pcn-1(am315)* animals showed a maternal-effect embryonic lethal phenotype. While it is unclear whether *am315* is a hypomorph or null allele, our results show that *pcn-1* is necessary for fertility.

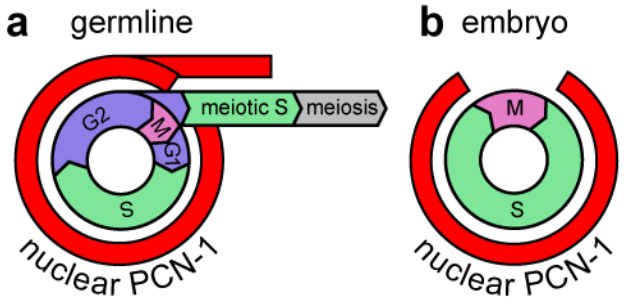

Figure 3: The adult germline and embryo show distinct patterns of PCN-1 nuclear accumulation. The inner circle represents the stages of the cell cycle; DNA replication occurs in S-phase (green), mitosis occurs in M phase (pink), and these are separated by G2 and a very short G1 phase (purple) (Fox *et al.* 2011). Germline stem cells progress to meiotic S-phase and meiosis (gray). The outer circle represents nuclear accumulation of PCN-1 (red). Germline stem cells in *C. elegans* display a more typical mitotic cell cycle with gap phases and also display constant (non-cycling) accumulation of several proteins, including PCN-1 and CYE-1, which have been reported to display cell cycle regulated accumulation in other tissues and organisms (A) (Leonardi *et al.* 1992; Fox *et al.* 2011). By contrast, early embryos in *C. elegans* display a simplified cell cycle (S,M), and PCN-1, like several other cell cycle proteins, show nuclear accumulation only during S-phase (B) (Brauchle *et al.* 2003; Kisielewska *et al.* 2005).

Conclusions

We established the nuclear accumulation pattern of PCN-1 in the larval and adult germline by analyzing FLAG::PCN-1 encoded by the native locus and GFP::PCN-1 encoded by an integrated transgene. Both fusion proteins displayed similar patterns and accumulated in all nuclei in the progenitor zone. Significantly, nuclei that were negative for EdU staining, and thus not in S-phase, displayed nuclear PCN-1 accumulation (Figure 3). Similar results were previously observed for cyclin E accumulation (CYE-1 in *C. elegans*) (Fox *et al.* 2011). These observations reinforce that mitotic cell cycle regulation in the germline stem and progenitor cells is distinct from somatic cells (Fox *et al.* 2011). The *C. elegans* proliferating cell nuclear antigen homolog *pcn-1* was necessary for robust fertility and embryonic development.

Chapter 4:

Cell Cycle Analysis in the *C. elegans* Germline

The work presented in Chapter 4 is published with the following authors:

Kocsisova Z., Mohammad A., Kornfeld K., Schedl T., **2018** Cell Cycle Analysis in the *C. Elegans* Germline with the Thymidine Analog EdU. Journal of visualized experiments: JoVE. 140: e58339–e58339.

The video component of this article can be found behind a paywall at https://www.jove.com/video/58339/

Abstract

Cell cycle analysis in eukaryotes frequently utilizes chromosome morphology, expression and/or localization of gene products required for various phases of the cell cycle, or the incorporation of nucleoside analogs. During S-phase, DNA polymerases incorporate thymidine analogs such as EdU or BrdU into chromosomal DNA, marking the cells for analysis. For *C. elegans*, the nucleoside analog EdU is fed to the worms during regular culture and is compatible with immunofluorescent techniques. The germline of *C. elegans* is a powerful model system for the studies of signaling pathways, stem cells, meiosis, and cell cycle because it is transparent, genetically facile, and meiotic prophase and cellular differentiation/gametogenesis occur in a linear assembly-like fashion. These features make EdU a great tool to study dynamic aspects of mitotically cycling cells and germline development. This protocol describes how to successfully prepare EdU bacteria, feed them to wild-type *C. elegans* hermaphrodites, dissect the hermaphrodite gonad, stain for EdU incorporation into DNA, stain with antibodies to detect various cell cycle and developmental markers, image the gonad and analyze the results. The protocol describes the variations in the method and analysis for the measurement of S-phase index, M-phase index, G2 duration, cell cycle duration, rate of meiotic entry, and rate of meiotic prophase progression. This method can be adapted to study the cell cycle or cell history in other tissues, stages, genetic backgrounds, and physiological conditions.

Introduction

In animal development, hundreds, thousands, millions, billions, or even trillions of cell divisions are required to form the adult organism. The cell cycle, the set of cellular events composed of G1 (gap), S (synthesis), G2 (gap), and M (mitosis) define the series of events that are executed each cell division. The cell cycle is dynamic and best appreciated in real time,

which can be technically difficult. The techniques presented in this protocol allow one to make the measurements of the phases and timing of the cell cycle from still images.

Labeling with nucleoside analogs such as 5-ethynyl-2'-deoxyuridine (EdU) or 5-bromo-2'-deoxyuridine (BrdU) is the gold standard to identify S-phase in the studies of cell cycle dynamics in the *Caenorhabditis elegans* (*C. elegans*) adult hermaphrodite germline (Crittenden *et al.* 2006; Fox *et al.* 2011; Fox and Schedl 2015; Seidel and Kimble 2015; Kocsisova *et al.* 2018b). Both EdU and BrdU can be used in nearly any genetic background, as they do not rely on any genetic construct. Visualizing BrdU requires harsh chemical treatment to expose the antigen for anti-BrdU antibody staining, which is often incompatible with the assessment of other cellular markers visualized by co-staining with additional antibodies. By contrast, visualizing EdU occurs by click chemistry under mild conditions and thus is compatible with antibody co-staining (Salic and Mitchison; van den Heuvel and Kipreos 2012).

The specificity of the label is clear, since nuclei only incorporate the thymidine (5-ethynyl-2’- deoxyuridine) analogs into DNA during S-phase. Visualization takes place in fixed tissue. The EdU label is invisible by itself until an azide-containing dye or fluorophore reacts covalently with the alkyne in EdU by copper-catalyzed click chemistry (ThermoFisher 2011). EdU labeling can provide immediate information on which nuclei are in S-phase, using a short pulse of labeling. EdU can also provide dynamic information, using pulse-chase or continuous labeling; for example, in a pulse-chase experiment, the label is diluted at each cell division or propagated as nondividing cells progress through development.

The *C. elegans* hermaphrodite germline is a powerful model system for the studies of signaling pathways, stem cells, meiosis, and cell cycle. The adult germline is a polarized assembly-line with stem cells found at the distal end followed by entry and progression through

meiotic prophase, coordinated with the stages of gametogenesis more proximally (**Figure 1**). At the proximal end, oocytes mature, are ovulated and fertilized, and begin embryogenesis in the uterus (Brenner 1974; Hirsh *et al.* 1976; Pazdernik and Schedl 2013). The ~20 cell-diameter long region near the distal tip cell, which includes the mitotically cycling germline stem, progenitor cells and meiotic S-phase cells but not the cells in meiotic prophase, is called the progenitor zone (Crittenden *et al.* 2006; Hansen and Schedl 2013; Pazdernik and Schedl 2013; Fox and Schedl 2015). The cell membranes provide incomplete separation between the nuclei in the distal germline, but the progenitor zone cells undergo mitotic cell cycling largely independently. The median mitotic cell cycle duration of germline progenitor zone cells in young adult hermaphrodites is ~6.5 h; G1 phase is brief or absent, and quiescence is not observed (Crittenden *et al.* 2006; Jaramillo-Lambert *et al.* 2007; Fox *et al.* 2011). Germline stem cell differentiation occurs through essentially direct differentiation and thus lacks transit-amplifying divisions (Fox and Schedl 2015). During differentiation in the pachytene stage, approximately 4 out of 5 nuclei will not form oocytes but instead undergo apoptosis, acting as nurse cells by donating their cytoplasmic contents to the developing oocyte (Gumienny *et al.* 1999; Hansen and Schedl 2013; Agarwal *et al.* 2018).

In addition to labeling cells in S-phase with nucleoside analogs, one can identify the cells in mitosis and meiosis using antibody staining. Nuclei in mitosis are immunoreactive to anti-phospho-histone H3 (Ser10) antibody (called pH3) (Hendzel *et al.* 1997; van den Heuvel and Kipreos 2012). Nuclei in meiosis are immunoreactive to anti-HIM-3 antibody (a meiotic chromosome axis protein) (Zetka *et al.*). Nuclei in the progenitor zone can be identified by the absence of HIM-3, the presence of nucleoplasmic REC-8 (Hansen *et al.* 2004b), or the presence of WAPL-1 (Crawley *et al.* 2016). WAPL-1 intensity is highest in the somatic gonad, high in the

progenitor zone, and low during early meiotic prophase. Several cell cycle measurements are possible with a few variations in the protocol: I) identify nuclei in S-phase and measure the S-phase index; II) Identify nuclei in M-phase and measure the M-phase index; III) determine whether nuclei were in mitotic or meiotic S-phase; IV) measure the duration of G2; V) measure the duration of G2+M+G1 phases; VI) measure the rate of meiotic entry; VII) estimate the rate of meiotic progression.

One can make multiple cell cycle measurements from only a few types of wet-lab experiments. The protocol below describes a 30 min pulse labeling by feeding *C. elegans* adult hermaphrodites with EdU labeled bacteria and co-labeling M-phase cells by staining with anti-pH3 antibody and progenitor zone cells by staining with anti-WAPL-1 antibody. Only changes in the duration of EdU feed (Step 2.5), type of antibodies employed (Step 5), and analyses (Step 8.3) are required for the additional measurements.

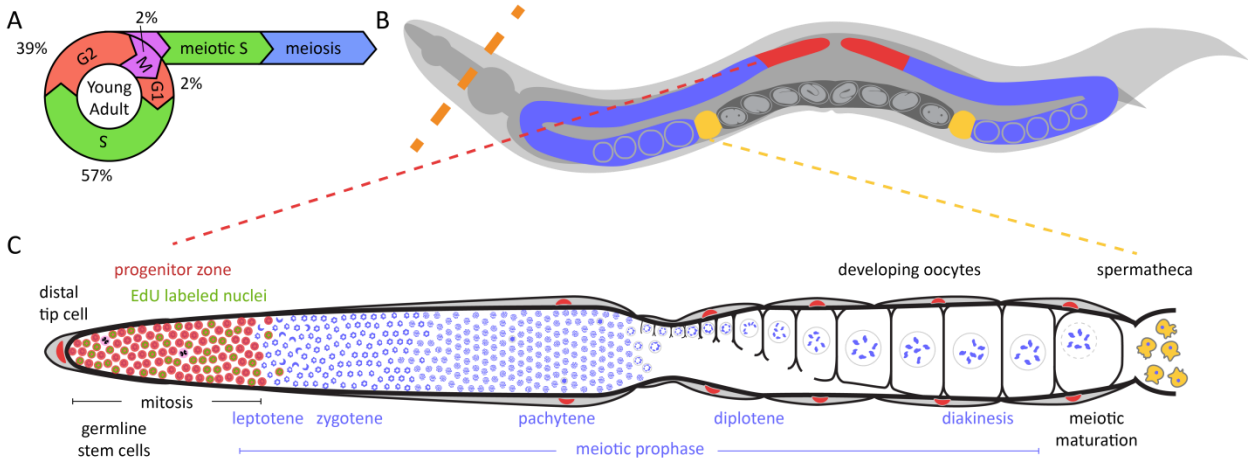

Figure 1: Diagram of *C. elegans* germline and cell cycle. (**A**) The cell cycle of germ cells in the young adult hermaphrodite germline. Numbers indicate the approximate percentage of time spent in each cell cycle stage. (**B**) *C. elegans* hermaphrodites have two U-shaped germlines (red and blue). The spermatheca is shown in yellow and the uterus with developing embryos is shown in dark gray. The dashed orange line indicates where animals are dissected to extrude the germlines. (**C**) Diagram of an unfolded *C. elegans* germline. DAPI (blue) is a DNA dye that highlights nuclear morphology. The distal progenitor zone (highlighted in red based on WAPL-1 antibody staining) contains mitotically cycling stem cells, progenitor cells and cells in meiotic S-phase (WAPL-1 also labels somatic

gonad nuclei). Cells in mitotic and meiotic S-phase label with a 30 min EdU pulse and are indicated in green. Two cells in M-phase label with pH3 antibody and are shown in black. The distal tip cell (DTC) provides the GLP-1/Notch ligand to maintain the stem cell fate of these cells. As the cells migrate away from the DTC, they exit the progenitor zone and enter meiotic prophase. Yellow cells are sperm in the spermatheca.

Protocol:

1. Preparation of EdU-labeled Bacteria

1.1. Grow a starter culture of MG1693. *Escherichia coli* (*E. coli*) strain MG1693 carries a mutation in thyA.

1.1.1. Streak out *E. coli* MG1693 from a frozen glycerol stock onto a 120 mm lysogeny broth (LB) agar Petri dish. Culture at 37 °C overnight.

1.1.2. Inoculate from two individual *E. coli* MG1693 colonies into two duplicate 4 mL tubes of liquid LB. Culture at 37 °C for ~16 h.

Note: MG1693 grows well in LB without supplemental thymine or thymidine.

1.2. Grow *E. coli* MG1693 in minimal media supplemented with EdU.

1.2.1. Autoclave a 500 mL conical flask.

1.2.2. Use sterile technique to add 5 mL of 20% glucose, 50 µL of 10 mg/mL of thiamine, 120 µL of 5 mM thymidine, 100 µL of 1 M $MgSO_4$, 200 µL of 10 mM EdU, 100 mL of M9 buffer, and 4 mL of freshly-grown overnight MG1693 culture.

Note: The final concentration of EdU is 20 µM in this culture (Fox *et al.* 2011; van den Heuvel and Kipreos 2012). This concentration leads to DNA damage and cell cycle arrest if applied to directly mammalian cells in culture (Zhao *et al.* 2013). However, only a fraction of this EdU is incorporated into the *E. coli* and thus available to *C. elegans*. There is no evidence of cell cycle arrest and no change in the size of the progenitor zone or M-phase index after EdU treatment of young adult hermaphrodites.

1.2.3. Culture overnight, but no longer than 24 h at 37 °C with shaking at 200 rpm.

1.3. Concentrate EdU-labeled *E. coli* and apply to M9 agar Petri dishes.

1.3.1. Pre-cool a tabletop centrifuge to 4 °C.

1.3.2. Use sterile technique to transfer the culture into 2-4 sterile 50 mL conical tubes.

1.3.3. Centrifuge the cultures at 3,000 x g at 4 °C for 30 min to pellet the EdU-labeled *E. coli*.

Note: Dispose of EdU-containing supernatant according to local and institutional guidelines.

1.3.4. Resuspend the pellets with 4 mL of fresh M9. Use a sterile 1 mL pipet tip or a sterile 5 mL serological pipet. Resuspending the pellets may take several minutes.

1.3.5. Use the same pipet to apply and spread ~8 drops of resuspended EdU-labeled *E. coli* MG1693 to the center of room-temperature 60 mm M9 agar Petri dishes. One batch yields ~16 dishes.

1.3.6. Allow the dishes to dry for several hours or overnight at room temperature, then seal each dish with a strip of laboratory film. Dishes can be stored at 15 °C for ~2 weeks and at 4 °C for ~2 months. Use the same batch of EdU dishes for each set of experiments.

2. Feeding EdU to *C. elegans.*

2.1. Synchronize population by timed egg lay, alkaline hypochlorite treatment followed by hatching into S-medium with cholesterol, or by picking the appropriate stage (Stiernagle 2006). Grow the animals to desired stage (here, 24 h post-L4) on Nematode Growth Medium seeded with *E. coli* OP50 at 20 °C.

Note: Prepare 50-100 animals per experiment, as some may not dissect well, and others will be lost in the process of washing and transferring.

2.2. Allow the EdU dishes to warm to 20 °C (or the temperature required for the experiment).

2.3. Wash the animals from NGM dishes using M9 into a 1.5 mL tube. Allow the animals to settle briefly by gravity or a brief spin in a microcentrifuge.

2.4. Remove the supernatant and wash the animals 1-2 times with ~1 mL of M9. Remove the supernatant.

2.5. Use a glass Pasteur pipette to transfer the animals in a tiny drop of M9 onto the center of the EdU lawn. Wait a few minutes for the liquid to be absorbed, then incubate at 20 °C for 30 min (for direct S-phase measurement) or longer (to measure history of S-phase), as needed.

Note: EdU signal is detectable in germline nuclei after as little as 15 min of EdU feeding (Fox *et al.* 2011).

2.6. Wash the worms off the EdU dish with ~2 mL of phosphate-buffered saline (PBS) into a glass dissecting dish.

3. Dissection and Fixation of *C. elegans* Germline

Note: This protocol for the dissection, fixation, and antibody staining of the *C. elegans* hermaphrodite germline is nearly identical to that published by Gervaise and Arur (2016), except that the 1 mL glass tubes can be centrifuged to speed up washing steps and a drawn-out glass Pasteur pipette can be used to remove the liquid from 1 mL glass tubes more effectively.

3.1. Wash and dissect *C. elegans* germlines.

3.1.1. Allow the animals to settle to the bottom of the dissecting dish, swirl to collect the animals in the center, and use a long Pasteur pipette to remove PBS. Wash 1-2 times with ~2 mL of PBS.

3.1.2. Add 2 mL of PBS and 4 µL of 100 mM levamisole to immobilize the animals. Swirl the dish again to collect the animals in the center of the dish.

Note: Immobilization can take between a few seconds and a few minutes. Complete immobilization is not necessary for successful dissection. Some people have better success when dissecting incompletely immobilized animals.

3.1.3. Dissect the animals with a pair of 25G 5/8" needles by cutting at the head (approximately between the two pharyngeal bulbs) or the tail. Take care not to cut the loop of the germline. Intestine and germline should "pop out" of the body cavity due to internal pressure, but remain attached. This protocol is similar to Gervaise and Arur (2016).

Note: Keep the dissection time to ~5 min, certainly no more than 15 min. Longer dissection times may result in the loss of antibody staining signal (Sudhir Nayak, personal communication) and starvation in PBS may affect the animals' physiology. Learning to dissect quickly and accurately may take some practice.

3.1.4. If needed, swirl to collect the dissected animals in the center, and use a long Pasteur pipette to remove as much PBS as possible.

3.2. Fix and dehydrate tissues

3.2.1. Add 2 mL of 3% paraformaldehyde (PFA) in PBS solution. Cover the dish loosely with laboratory film and store on a bench or in a drawer for 10 min.

Note: Thaw PFA solution in a 37 °C water bath and then cool to room temperature prior to dissecting germlines.

CAUTION: PFA solution is moderately toxic and a probable carcinogen and teratogen. Vapors emitting from paraformaldehyde solutions are flammable. Wear nitrile gloves. Dilute PFA from 16% to 3% in a chemical fume hood. When working outside of a fume hood, keep all containers covered.

3.2.2. Transfer the gonads carefully to a clean 5 mL glass centrifuge tube.

3.2.3. Add ~3 mL of PBSTw (PBS with 0.1% Tween-20) to the dish that contained the gonads

to help retrieve remaining gonads and to dilute the PFA solution.

3.2.4. Spin down in a clinical centrifuge at 870 x g for ~1 min. Younger or smaller animals require longer spin times than older or larger animals.

3.2.5. Using a long glass pipette, transfer the supernatant to unwanted material beaker for eventual discard in unwanted material bottle in the chemical hood.

3.2.6. Add 2 mL of high-grade methanol pre-chilled to -20 °C. Cover the centrifuge tube tightly with laboratory film.

Note: Use of fresh high-grade "gold label" methanol is essential for proper morphology with certain antibodies.

CAUTION: Methanol is a highly flammable liquid and vapor that is toxic if swallowed, inhaled, or allowed to contact skin. Wear gloves and appropriate personal protective equipment. Use a freezer appropriate for small volumes of flammables.

3.2.7. Store in -20 °C freezer for 1 h, even overnight or even several months.

Note: The protocol can be paused here.

4. **Rehydrate Germlines**

4.1. Fill the glass centrifuge tube to top with PBSTw to dilute the methanol and rehydrate the gonads. Spin down in a clinical centrifuge at 870 x g for ~1 min.

4.2. Using a long glass Pasteur pipette, transfer the supernatant to unwanted material beaker for eventual discard in unwanted material bottle in the chemical hood.

4.3. Wash the gonads 3 times using ~5 mL of PBSTw, spinning down in a clinical centrifuge at 870 x g for ~1 min each time. Remove the supernatant.

4.4. Rinse a small 1 mL borosilicate glass tube and a long glass Pasteur pipette with PBSTw.

4.5. Add ~700 µL of PBSTw and use the long glass Pasteur pipette to transfer the gonads to the small tube. Use a few additional drops of PBSTw to ensure that all gonads are transferred.

4.6. Spin down in a clinical centrifuge at 870 x g for ~1 min. Using a drawn-out long glass Pasteur pipette, remove as much liquid as possible without disturbing the gonads. Leave no more than 50 µL.

Note: If antibody detection is not necessary, skip to Step 6.

5. Detect Antigens with Antibodies

5.1. Dilute the primary antibodies in 30% goat serum in PBS. In the present example, anti-WAPL-1 antibody is diluted 1:2000 and anti-pH3 antibody is diluted 1:500. Centrifuge freshly thawed serum for 10 min in a microfuge at 20,000 x g at 4 °C to remove the particulates. Use the supernatant, which can be stored at 4 °C for several days. Use the appropriate serum to match the host organism of secondary antibodies (goat serum is used here). An optional blocking step may be added prior to the addition of primary antibodies.

5.2. Apply 100 µL of diluted primary antibody to each small glass tube. Incubate at room temperature for 4 h.

Note: Incubation times vary by antibody. For some antibodies, 2 h at room temperature is sufficient. Longer incubations (*e.g.*, overnight) are possible, but may increase background.

5.3. Fill the tubes to top with PBSTw and spin down in a clinical centrifuge at 870 x g for ~1 min.

5.4. Wash the gonads 3 times using ~1 mL of PBSTw. Incubate for ~5 min per wash to allow excess primary antibody to diffuse into wash. Using a drawn-out long glass Pasteur pipette, remove as much liquid as possible without disturbing the gonads. Leave no more than 50 µL.

5.5. Dilute the secondary antibodies in 30% goat serum in PBS. In the present example, goat-anti-rabbit-594 and goat-anti-mouse-647 are each diluted at 1:400.

Note: Select secondary antibodies carefully to make sure dyes are distinct from the dye in the EdU kit. In the present example, the EdU kit contained a 488 nm excitation dye.

5.6. Apply 100 µL of diluted secondary antibody to each small glass tube. Incubate in the dark at room temperature 2 h.

Note: Incubation times vary by antibody. For some secondary antibodies, 1 h at room temperature is sufficient. Longer incubations (*e.g.*, overnight) are possible, but may increase background.

5.7. Wash the gonads 3 times using ~1 mL of PBSTw. Incubate for ~5 min per wash to allow excess secondary antibody to diffuse into wash. Using a drawn-out long glass Pasteur pipette, remove as much liquid as possible without disturbing the gonads. Leave no more than 50 µL.

Note: Gonads can be stored in 100 µL of PBS after this step, if necessary, although this may reduce signal. Remove PBS prior to proceeding.

6. Perform the EdU Click Reaction to Detect EdU

Note: Performing the EdU click reaction before the antibody staining steps (perform Step 6 before Step 5) is possible, depending on the antibodies used[7]. However, the click reagents may interfere with certain antigens (*e.g.*, REC-8 antibody is sensitive to fixation and permeabilization). The order presented here yields bright antibody staining with the REC-8, WAPL-1, HIM-3, pH3, FLAG, and CYE-1 antibodies used, among others.

6.1. Prepare the click EdU cocktail (ThermoFisher 2011) fresh by adding the following to a clean 1.5 mL tube. The order of additions is important. Protect from light and maintain all reagents on ice. This recipe yields enough for one sample (100 µL); multiply the recipe as needed.

6.1.1. Add 2 mL of ultrapure water to the buffer additive. This makes 10x buffer additive, which must be diluted to 1x immediately prior to use.

6.1.2. Add 8.5 μL of 10x buffer to 76.5 μL of ultrapure water. Mix well.

6.1.3. Add 4 μL of 100 mM $CuSO_4$ (may be labeled as Component E). Mix well.

6.1.4. Add 0.25 μL of the 488 nm dye Azide. It must be thawed at room temperature, as its solvent, dimethyl sulfoxide, is solid at 4 °C. Mix well and protect from light.

6.1.5. Mix 9 μL of ultrapure water with 1 μL of the buffer additive in the cap of the tube. Pipet from the cap to add to the remaining cocktail, and mix well by pipetting up and down.

6.2. Perform the EdU click reaction.

6.2.1. Add ~100 μL of click EdU cocktail to the gonads in the small tube. Cover with laboratory film and incubate for 30-60 min at room temperature.

6.2.2. Wash once with 100 μL of reaction rinse buffer.

6.2.3. Wash the gonads 4 times using ~1 mL of PBSTw. Incubate for ~15 min per wash to allow excess EdU cocktail components to diffuse into wash. Using a drawn-out long glass Pasteur pipette, remove as much liquid as possible without disturbing the gonads. Leave no more than 50 μL.

7. Stain DNA and Prepare Slides

7.1. Add 1 drop (~25 μL) of antifade mounting medium with 4',6-diamidino-2-phenylindole (DAPI, used to visualize DNA) to the gonads. Wait a few minutes so it can settle and mix with the gonads.

Note: Alternately, a 1:1000 dilution of DAPI (from a 0.1 mg/mL stock) in PBS may be applied for 5 min, followed by 20 μL of 1,4-diazabicyclo[2.2.2]octane (DABCO) in 90% glycerol, or another antifade mounting medium.

7.2. Prepare a large 2.5% agarose pad on a standard glass microscope slide.

7.3. Use a new clean dust-free long glass Pasteur pipette to transfer the gonads to the agarose pad. Keep all liquid and gonads in the narrow bottom of the pipette to minimize the loss of gonads.

Note: Gonads stuck to small glass tube or in long glass Pasteur pipette can be "rescued" by rinsing with PBSTw, collecting the liquid in a dissecting dish, and picking individual animals onto the slide with an eyelash.

7.4. Use an eyelash (or a loop of thin hair) glued to a toothpick to distribute the gonads over the agarose pad and remove the dust particles.

7.5. Apply a rectangular glass coverslip. Lower slowly from one side to avoid air bubbles. Use a tissue to remove excess solution thus preventing the coverslip from moving freely.

Note: Choose coverslips that match to the microscope that will be used. #1 and #1.5 coverslips work well.

7.6. Allow the slides to settle and dry slightly overnight at room temperature or 4 °C. This helps to slightly flatten the gonads. Slides should be stored at 4 °C.

7.7. Optional: Seal the edges of the slide with nail polish, or another slide sealer. Sealing the corners first, then the sides, prevents the coverslip from shifting.

8. Confocal Imaging and Analysis

8.1. Image the distal gonad with a spinning disc confocal fluorescent microscope equipped with a high energy light source, plan-apochromatic objectives, and a high efficiency microscope camera. Capture the images with 1 μm or tighter spacing between z-stacks. Take note of laser power, sensitivity, and exposure time for all channels.

8.1.1. Use the following: 405 nm laser line excitation with a 485 nm (W60) emission filter for DAPI, 488 nm laser line excitation with a 527 nm (W55) emission filter for EdU, 561 nm laser line excitation with a 615 nm (W70) emission filter for WAPL-1, and a 640 nm laser line excitation with a 705 nm (W90) emission filter for pH3.

Note: Signal intensity and background intensity will vary. Likewise, the required exposure times will vary, possibly up to 10-fold.

8.2. Use the Cell Counter plug-in (De Vos 2015) in Fiji (Schindelin *et al.* 2012; Rasband 2016) to manually count each nucleus. Label each individual nucleus according to the presence and absence of pH3, EdU, and WAPL-1. Use the classes of nuclei described in **Table 1** and **Figure 2**, as these will facilitate all of the calculations outlined below.

Note: Skilled experimentalists can accurately count all nuclei in a 3D image without double-counting or missing any nuclei. Alternately, one may count every nucleus in every z-plane, and the Marks-to-Cells R script (Seidel and Kimble 2015) may be used to remove multiply-counted nuclei.

8.3. Calculate cell numbers and frequencies from the above counts depending on the type of cell cycle measurement needed. The types of nuclei are defined in **Table 1** and **Figure 2**. The calculations are summarized in **Table 2**.

8.3.1. **(variation I)** To identify the nuclei in S-phase, feed the animals EdU for 30 min. Any nuclei displaying EdU label are S-phase nuclei. To calculate, take the sum A and C nuclei, see **Table 1** and **Figure 2**.

Note: In a 30 min EdU pulse in wild-type adult hermaphrodites, all EdU labeled nuclei are co-labeled with progenitor zone markers (Fox *et al.* 2011).

8.3.2. To measure the progenitor zone, stain with a progenitor zone marker such as REC-8 or WAPL-1 antibody. The progenitor zone is defined here as all nucleoplasmic REC-8 (Hansen *et al.* 2004b) or WAPL-1 immunoreactive germline nuclei. To calculate, sum all WAPL-1 immunoreactive nuclei (A+B+C+D, see **Table 1** and **Figure 2**).

Note: WAPL-1 also labels the DTC and somatic gonad nuclei which should not be counted. Somatic nuclei are easy to identify by extremely intense WAPL-1 signal, position slightly outside the germline, and a “fried-egg” morphology of the nuclei.

8.3.3. To measure the S-phase index, perform a 30 min EdU experiment and co-label with REC-8 or WAPL-1 antibody. The S-phase index is defined as the proportion of the progenitor zone that is in S-phase. To calculate, count all S-phase nuclei, and then divide by the total number of progenitor zone nuclei (A+C / A+B+C+D, see **Table 1** and **Figure 2**).

8.3.4. **(variation II)** To identify the nuclei in M-phase, stain with pH3 antibody. Any pH3 immunoreactive nuclei are M-phase nuclei. This works regardless of the duration of the EdU feed. To calculate, take the sum of A and B nuclei, see **Table 1** and **Figure 2**.

8.3.5. To measure the M-phase index, co-label with pH3 and REC-8 or WAPL-1 antibodies. The M-phase index is defined as the proportion of the progenitor zone that is in M-phase. To calculate, count all M-phase nuclei, and then divide by the total number of progenitor zone nuclei (A+B / A+B+C+D, see **Table 1** and **Figure 2**).

8.3.6. **(variation III)** Nuclei in mitotic and meiotic S-phase both label with EdU. To tell the two populations apart, determine whether the S-phase was followed by mitosis or by meiosis. To determine whether nuclei are in mitotic or meiotic S-phase, feed EdU for 4 h and co-label for pH3 (an M-phase marker) and HIM-3 (a meiotic chromosome axis protein) by antibody staining. Record the nuclei that display both EdU and pH3 (type A, see **Table 1** and **Figure 2**) as mitotic S-phase while nuclei that display both EdU and HIM-3 (type E, see **Table 1** and **Figure 2**) as meiotic S-phase.

8.3.7. **(variation IV)** Calculate the duration of G2 phase.

Note: G2-phase separates S-phase from M-phase. Although no marker has been reported to label G2 in the *C. elegans* germline, one can calculate the duration of G2 phase by combining data from several experiments that label M-phase (at the time of dissection) and S-phase (starting at several h before dissection). A cell that displays both M-phase and S-phase markers completed G2-phase during the course of the experiment. A cell that displays only the M-phase marker and not the S-phase marker was not in S-phase during the experiment.

8.3.7.1. To calculate the duration of G2-phase, feed EdU for 2 h and co-label with pH3 antibody. Examine only nuclei that label with pH3 (these are in M-phase at the time of dissection) for the presence of EdU (these were in S-phase during the 2 h EdU label prior to dissection). Calculate the fraction of M-phase nuclei that completed G2-phase (A / A+B, see **Table 1** and **Figure 2**).

8.3.7.2. Repeat this experiment with a 3 h EdU label, and again with a 4 h EdU label (and optionally a 5 h EdU label). Plot the percent of pH3 positive nuclei that are EdU positive on the

y-axis and the duration of EdU label on the x-axis, as shown in **Figure 3A**.

8.3.7.3. Calculate the median duration of G2-phase by connecting the points on the graph and determining where the line crosses 50%, as shown in **Figure 3A**.

8.3.7.4. Calculate the maximum duration of G2-phase by connecting the points on the graph and determining where the line crosses 99%, as shown in **Figure 3A**.

8.3.8. **(variation V)** Calculate the duration of G2+M+G1.

Note: In the *C. elegans* germline, G1 phase is unusually short. Although no marker has been reported to label G1 in the *C. elegans* germline, one can estimate the sum duration of G2, M, and G1 phase, and then compare this time with the G2-phase time described above. The maximum duration of G2+M+G1 is estimated from the percentage of all progenitor zone nuclei (WAPL-1 immunoreactive) that remain EdU negative (did not undergo S-phase) after EdU labeling for several hours.

8.3.8.1. To calculate the duration of G2+M+G1, feed EdU for 2 h and co-label with REC-8 or WAPL-1 antibody. Determine the fraction of the progenitor zone that underwent S-phase during this time (A+C / A+B+C+D, see **Table 1** and **Figure 2**).

8.3.8.2. Repeat this experiment with a 3 h EdU label, and again with a 4 h EdU label (and optionally a 5 h EdU label). Plot the percent of REC-8 or WAPL-1 positive nuclei that are EdU positive on the y-axis and the duration of EdU label on the x-axis, as shown in **Figure 3B**.

8.3.8.3. Calculate the maximum duration of G2+M+G1 by connecting the points on the graph and finding where the line crosses 99%, as shown in **Figure 3B**.

Note: It is possible to perform the experiments to determine the duration of G2 and G2+M+G1 as a single set of 2, 3, 4, and 5-h EdU experiments by co-labeling with both rabbit-anti-WAPL-1 and mouse-anti-pH3 antibodies.

8.3.9. **(variation VI)** To identify the nuclei that replicated in the progenitor zone but have since entered meiosis, feed the animals EdU for 10 h and co-label with REC-8 or WAPL-1 antibodies. Any nuclei displaying EdU label were in S-phase during those 10 h. Any nuclei that

do not display nucleoplasmic REC-8 or WAPL-1 staining were in meiosis. Simply count the nuclei with EdU labeling that do not display labeling with the progenitor zone marker (E, see **Table 1**).

Note: Conversely, if gonads are stained for the meiotic prophase marker HIM-3 with anti-HIM-3 antibodies, count the number of nuclei with EdU labeling that are also positive for HIM-3.

8.3.10. To calculate the rate of meiotic entry, perform the above experiment with a 5 h, 10 h, and 15 h label of EdU. Plot the number of nuclei that entered meiosis on the y-axis and the duration of the EdU label on the x-axis, as shown in **Figure 3C**. Then use a simple linear regression to calculate the slope (nuclei entered meiosis per h) from y=mx+b.

Note: It is critical to use a linear regression to calculate the rate of meiotic entry. It would be incorrect to simply divide the number of nuclei that entered meiosis by the duration of the EdU label, because the y-intercept is not zero.

8.3.11. **(variation VII)** Measure the rate of meiotic progression.

Note: Since EdU is covalently incorporated into DNA, it can be used to track a population of cells through differentiation. The cells that underwent S-phase in the progenitor zone retain the EdU label as they enter into meiosis, progress through meiosis, and undergo oogenesis. A pulse-chase experiment with EdU can be used to measure the rate of meiotic progression.

8.3.11.1. Feed EdU-labeled bacteria to the animals for 4 h (the “pulse”). Transfer the animals to unlabeled OP50 bacteria for 48 h (the “chase”), then dissect and co-label with a progenitor zone marker such as REC-8 or WAPL-1 (or a meiotic prophase marker such as HIM-3) if desired.

8.3.11.2. When imaging, look for the position of the most proximal EdU-labeled nucleus. The rate of meiotic progression is the distance (in cell diameters from the end of the progenitor zone) traveled by the most proximal EdU labeled nucleus during the 48 h chase.

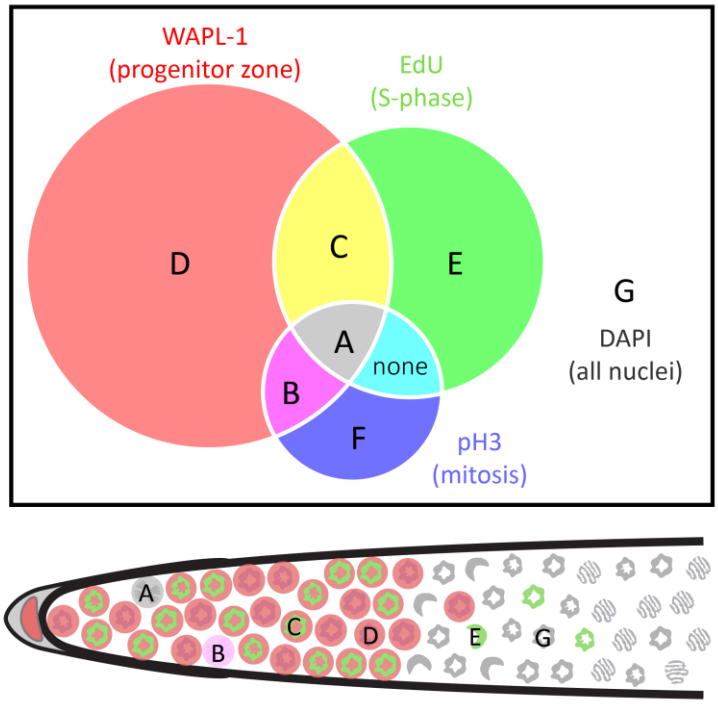

Figure 2: Venn diagram of the classes of nuclei. Nuclei are grouped by the presence and absence of three markers: WAPL-1 indicates progenitor zone cells (red), EdU indicates S-phase cells (green), and pH3 indicates M-phase cells (blue). Cell types are identified as **A-G**. Note that in wild-type young adult hermaphrodites cells of type F are not found, and cells do not co-label with EdU and pH3 outside of the (WAPL-1 positive) progenitor zone. The distal gonad diagram below indicates one example of A-E and G nuclei. See **Table 1** for more detail.

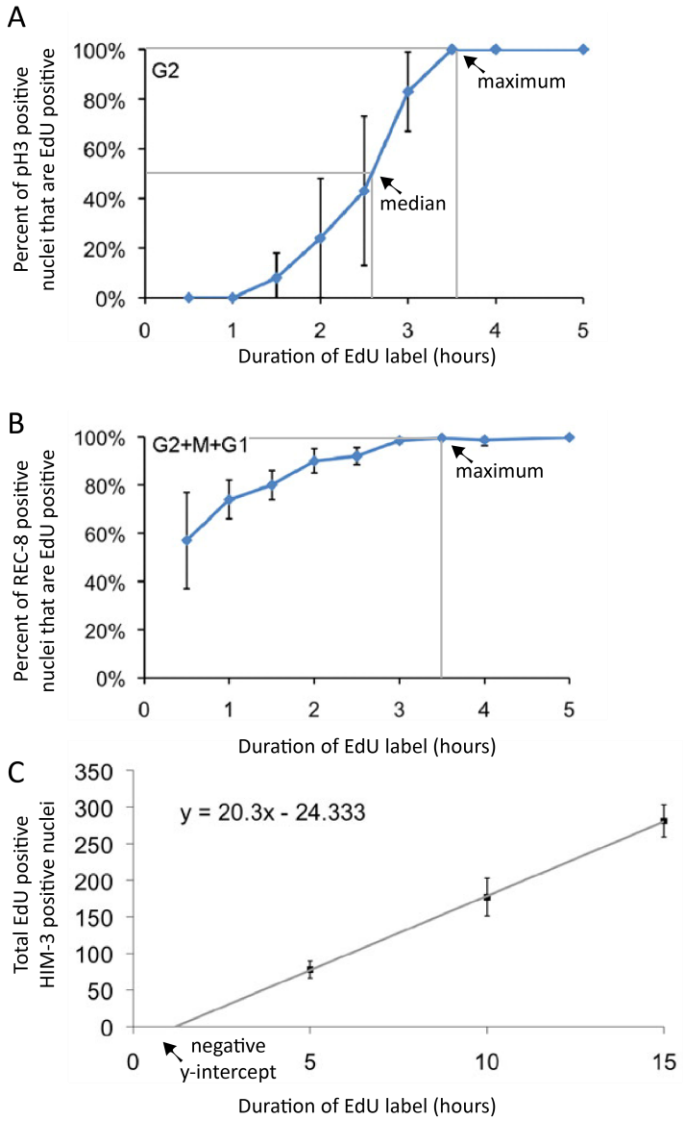

Figure 3: Graphical presentation of cell cycle duration and rate of meiotic entry experimental data. (**A**) The duration of G2 phase is interpolated from pH3 and EdU co-labeling following varied-duration EdU pulses Gray lines indicate 50th and 99th percentiles used in interpolating median and maximum G2 durations, indicated by arrows. (**B**) A cell in G2, M, or G1 phase does not incorporate EdU. Thus, the maximum duration of G2+M+G1 phase can be estimated by measuring the maximum duration of EdU label that yields EdU-negative cells. The duration of G2+M+G1 phase is interpolated from EdU and REC-8 co-labeling following varied-duration EdU pulses. Gray line indicates 99th percentile used in interpolating maximum G2+M+G1 duration, indicated by an arrow. It is not possible to interpolate the median G2+M+G1 duration. (C) The rate of meiotic entry (in nuclei per h – see **Table 2**) is calculated from the slope of the regression line. Note that since the y-intercept intercept is not zero, a regression is necessary for an accurate calculation of the rate of meiotic entry (C). . Error bars indicate standard deviation. Figures modified and reprinted with permission from Fox *et al.* (2011).

Representative Results

Since DNA synthesis is required to incorporate EdU, one can conclude that EdU-labeled nuclei underwent S-phase during the EdU-labeling time window. One may interpret the nuclei that label in a 30 min feeding with EdU labeled bacteria as nuclei in S-phase at the time of dissection. Nuclei that label in a longer continuous EdU feeding experiment may have labeled early in the time window and since left S-phase, or may have labeled in the late part of the EdU time window. EdU signal co-localizes with DAPI signal. In some nuclei, EdU signal covers all chromosomes, while in other nuclei EdU signal localizes to 1-2 bright puncta (**Figure 4**). These puncta are likely the X-chromosome, which replicates late in S-phase (Jaramillo-Lambert *et al.* 2007).

Here, the animals were fed with EdU continuously for 30 min and dissected, as described above and in **Figure 5**. One example of successful EdU staining in a young adult animal and one example of unsuccessful EdU staining in an older adult animal (see below) are shown in **Figure 4**. EdU signal from a 30 min labeling localizes to approximately half of the nuclei in the progenitor zone, defined by WAPL-1 antibody labeling but approximated by DAPI morphology (Michaelson *et al.* 2010; Luo *et al.* 2010; Qin and Hubbard 2015). S-phase index, the proportion of the progenitor zone that is EdU positive, was previously reported at 57 +/- 5% and as high as 70% in young adults (Crittenden *et al.* 2006; Fox *et al.* 2011; Seidel and Kimble 2015). M-phase index is approximately 2% - 3% (Fox *et al.* 2011; Narbonne *et al.* 2015). In continuous feeding for 4 h or longer, all nuclei in the progenitor zone label with EdU, and some nuclei that labeled in the progenitor zone have since entered meiotic prophase (Fox *et al.* 2011).

While the technique works consistently in wild-type young adult animals, a significant fraction of mated 5 day old hermaphrodites (even those containing sperm) failed to label in a 30

min EdU pulse (**Figure 4E**). However, with a 4 h EdU feeding, nearly all these animals label. Sporadic failure to label in genetic female animals with short pulses of EdU has also been reported (Cinquin *et al.* 2016). There may be other situations that result in sporadic failure to label.

One can calculate the duration of the cell cycle by performing several EdU-labeling experiments with pH3 labeling in each. The duration of G2 was estimated by analyzing the percent of nuclei in M-phase (pH3 immunoreactive) that were EdU positive during the time course (**Figure 6**). This approach gives median and maximum duration of G2 (**Figure 3A**). The median time was interpolated, showing an approximate G2 duration of 2.5 h in young adult hermaphrodites. The duration of G2+M+G1 was estimated from the percentage of all progenitor zone nuclei (WAPL-1 immunoreactive) that were EdU positive (**Figure 6**). The G2+M+G1 method provides a maximum duration measure for the combined phases (**Figure 3B**). The 99th percentile time was interpolated, showing an approximate G2+M+G1 duration of 3.4 h in young adult hermaphrodites. Data from the same experiments were used to calculate the rate of meiotic entry (nuclei per h). The rate is the slope of the linear regression of the number of nuclei that entered meiosis (EdU positive, WAPL-1 negative or HIM-3 positive) over the duration of the EdU label (**Figure 3C**). The values for wild-type 1 day old adult hermaphrodites are shown in **Table 2**.

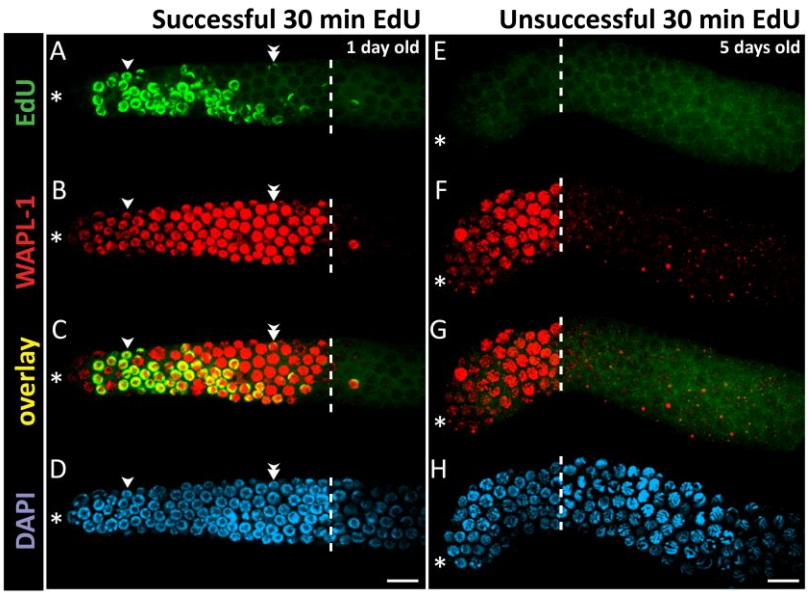

Figure 4: Example of successful and unsuccessful 30 min EdU staining. Confocal microscope images of a 1 day old (**A-D**) and a 5 day old (**E-H**) hermaphrodite gonad (not sperm depleted) after a 30 min EdU labeling experiment. The dashed white line marks the end of the progenitor zone. The asterisk marks the position of the distal tip. Green marks EdU staining visualized by click chemistry (**A**). Unsuccessful EdU labeling results in low-level background staining but no bright EdU+ nuclei (**E**). Red marks WAPL-1 immunofluorescence (**B,F**). Yellow indicates overlap (**C, G**). Blue marks DAPI staining for DNA (**D, H**). Single arrowheads indicate a nucleus with EdU staining throughout the chromatin. Double arrowheads indicate a nucleus with EdU puncta on only one pair of chromosomes. Images were obtained with a 63X objective. A 10 μm scale bar is shown (**D, H**).

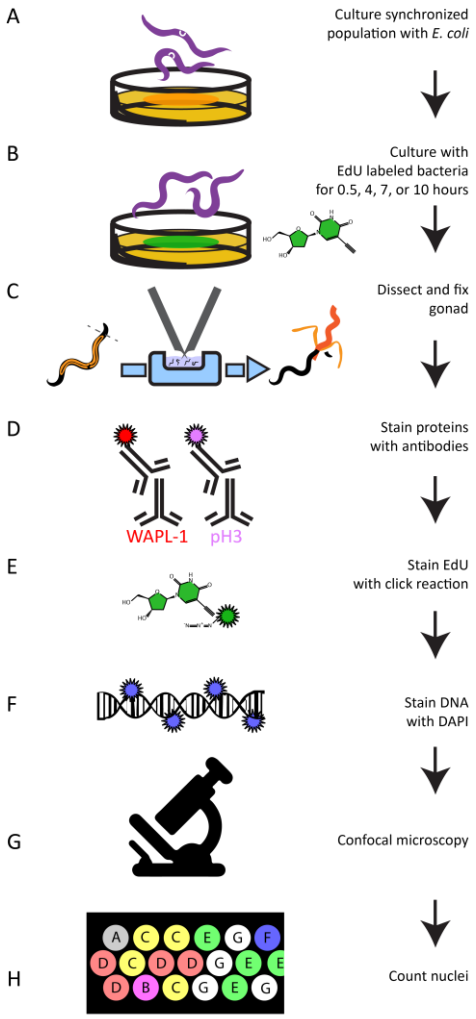

Figure 5: Experimental Workflow. A summary of the experimental protocol to grow (**A**), EdU label (**B**), dissect (**C**), antibody stain (**D**), perform the click reaction to attach a dye to EdU (**E**), stain DNA (**F**), image germlines (**G**), and quantify EdU labeled and antibody stained nuclei (**H**).

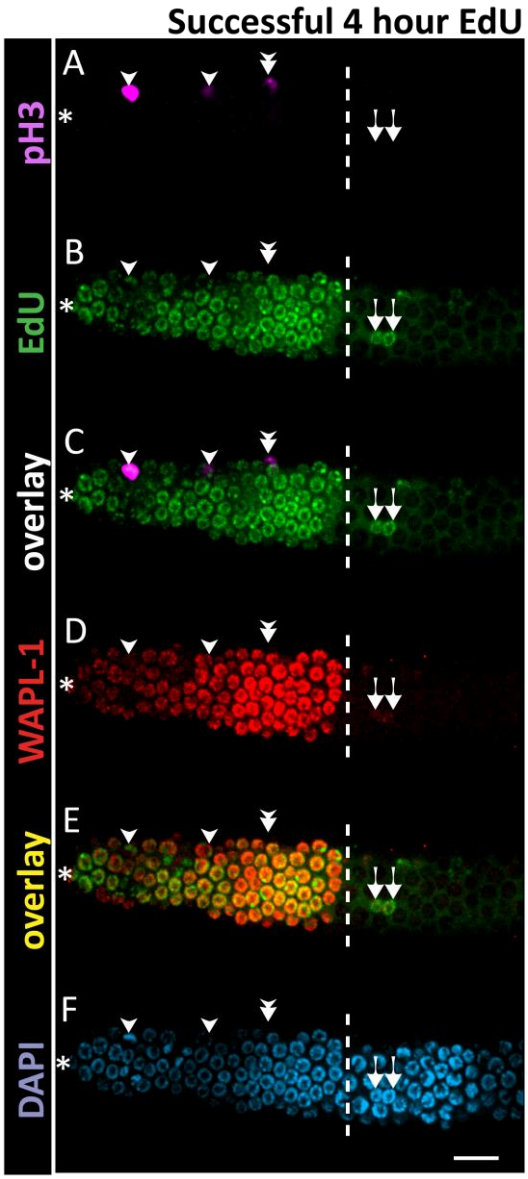

Figure 6: Example of successful 4 h EdU staining. Confocal microscope images of a 1 day old adult hermaphrodite gonad after a 4 h EdU labeling experiment. The dashed white line marks the end of the progenitor zone. The asterisk marks the position of the distal tip. Magenta marks pH3 immunofluorescence (**A, C**). Green marks EdU staining visualized by click chemistry (**B,C**). Red marks WAPL-1 immunofluorescence (**D**). Yellow indicates the overlap of EdU and WAPL-1 (**E**). Blue marks DAPI staining for DNA (**F**). Single arrowheads indicate nuclei co-labeled with EdU and pH3. Double arrowhead marks a pH3+ EdU- nucleus – a rare occurrence in a 4 h EdU labeling. Arrows mark EdU+ WAPL-1 – nuclei which have entered meiosis. Images were obtained with a 63X objective. A 10 μm scale bar is shown (**F**).

Table 1: Classes of nuclei.

Marker:	pH3	EdU*	WAPL-1 or REC-8	HIM-3	
Interpretation:	Mitosis	S-phase*	Progenitor Zone	Meiosis	
Class:					**Combined Interpretation:**
A	+	+	+	-	in M-phase, in progenitor zone, were in mitotic S-phase during EdU label (completed G2)
B	+	-	+	-	in M-phase, in progenitor zone, were not in S-phase during EdU label
C	-	+	+	-	in Interphase, in progenitor zone, were in S-phase during EdU label
D	-	-	+	-	in Interphase, in progenitor zone, were not in S-phase during EdU label
E	-	+	-	+	in meiosis, were in meiotic S-phase during EdU label (meiotic entry nuclei)
F	+	-	-	-	return to mitosis (found in some mutants) or meiotic divisions (in spermatogenesis)
G	-	-	-	+	in meiosis, were not in S-phase during EdU label
	sum total pH3 positive; all cells in M-phase	sum total EdU positive; all cells in S-phase	sum total WAPL-1 positive; all cells in progenitor zone	sum total HIM-3 positive; all cells in meiotic prophase	

*Note that 30 min and 4 h EdU experiments differ in interpretation. In longer duration EdU experiments, cells have likely progressed beyond S-phase. See Introduction and **Step 8** for duration of EdU labeling for relevant experiment.

Table 2: Cell cycle calculations.

Cell cycle part	**Operational Definition**	**Calculation***	**Value****
Progenitor Zone nuclei	all WAPL-1 (or REC-8) positive,	A+B+C+D	231 ± 23 nuclei
S-phase nuclei	nuclei EdU positive after 30 min Ed	A+C	133 ± 20 nuclei
M-phase nuclei	pH3 and WAPL-1 co-positive nuc	A+B	5.2 ± 2.3 nuclei
S-phase index	S-phase nuclei / Progenitor Zone n	A+C/ A+B+C+D	57% of cell cycle
M-phase index	M-phase nuclei / Progenitor Zone n	A+B/ A+B+C+D	2% of cell cycle
Meiotic Entry cells	EdU labeled nuclei in meiosis	E	varies by duration of EdU label
Meiotic Entry rate	Meiotic entry nuclei per h of EdU l	Slope from Figure 4C***	20.3 nuclei per h
G2 duration (median)	50% intercept from Figure4A		2.5 h
G2 duration (maximum)	99% intercept from Figure 4A		3.5 h
G2+M+G1 duration (maximum)	99% intercept from Figure 4B		3.5 h
Cell cycle duration (median)	median G2 duration / G2-index****		6.5 h
Cell cycle duration (maximum)	maximum G2 duration / G2-index****		8.1 h

*Letters represent the classes of nuclei defined in **Table 1** and **Figure 3**. Calculations are modified from Fox *et al.* (2011). **Values (± standard deviation) for wild-type hermaphrodites raised at 20 °C aged to 24 h post mid-L4 stage. ***Note that since the y-intercept intercept is not zero, a regression is necessary for an accurate calculation of the rate of meiotic entry. ****The G2-index is determined by subtracting the S-phase index, M-phase index, and approximate G1-index (2%) from 100%, as described by Fox *et al.* (2011).

Discussion

Preparation of EdU-labeled bacteria (**Step 1**) is critical for this protocol, and the first point for troubleshooting. Wild-type young adult hermaphrodites label very reliably in a 4 h EdU-pulse, making this a useful control for every new batch of EdU-labeled bacteria. Additionally, intact EdU-labeled bacteria that enter the intestine (in older animals or certain pharynx/grinder defective mutants) will label with click chemistry and appear as bright oblong puncta in the gut. An alternative technique for labeling hermaphrodites uses a "soak" in a high concentration (1 mM) of EdU (Seidel and Kimble 2015). This technique starves the animals for the duration of labeling, but provides a useful way to bypass making EdU-labeled bacteria when troubleshooting fixation and click chemistry. If an EdU "soak" experiment is successful while an EdU feed is not, then prepare fresh EdU-labeled bacteria. To reach a sufficient bacterial density while also achieving a high EdU content, one may need to adjust the concentrations of EdU and thymidine.

The main limitation of this technique for labeling of S-phase is in the need to feed EdU-labeled bacteria to animals. The animals that cannot feed (due to genotype or stage) may not be labeled with this technique. Nevertheless, nucleoside analogs are currently the only method to identify S-phase nuclei in the *C. elegans* germline, and their use does not require that any transgenes be present in the animals. Additionally, once incorporated, EdU remains in nuclei even as they exit S-phase, progress through the cell cycle, divide, or differentiate. The signal

weakens by half with every cell division. This makes EdU perfect for tracking a cell's history even through a few cell divisions.

The stability of EdU makes pulse-chase experiments straightforward; simply rinse excess EdU bacteria from the animals after the desired duration pulse is finished and transfer the animals to unlabeled bacteria. EdU remains in DNA and remains visible even after multiple cell divisions. However, the experiments are limited to a single type of S-phase label (a single pulse of EdU). Co-labeling with EdU and BrdU is possible in mammalian cells (Invitrogen 2010) but has not been reported in *C. elegans*. Co-labeling of IdU and CldU is used in mammals (Tuttle *et al.* 2010) but also has not been reported in *C. elegans*.

The main advantages of EdU labeling are that the method requires no transgenes, EdU can be fed to *C. elegans* during regular culture, the chemistry is compatible with immunofluorescent techniques, and EdU persists in DNA for a long time after feeding has stopped. These features make EdU a great tool to study many aspects of the cell cycle and germ cell dynamics.

Cell cycle and germ cell dynamics analysis with EdU can be applied to a variety of research questions. Just a few examples of further applications of this method: How do the dynamics of the cell cycle change in animals with cell cycle gene mutations? How do physiological conditions affect the cell cycle in stem cells, the rate of germ cell entry into meiotic prophase, and the rate of germ cell progression through meiotic prophase? How does the cell cycle change during larval development? How do major signaling pathway disruptions affect the cell cycle, in addition to changes in cell fate (such as ectopic proliferation)? This system can be modified to study what the cells are doing in many different conditions.

Chapter 5:

Germline aging in wild-type *C. elegans*

The work presented in Chapter 5 is published with the following authors:

Kocsisova Z., Kornfeld K., Schedl T., **2019** Rapid population-wide declines in stem cell number and activity during reproductive aging in *C. elegans.* Development 146: dev173195.

Abstract

C. elegans hermaphrodites display dramatic age-related decline of reproduction early in life while somatic functions are still robust. To understand reproductive aging, we analyzed the assembly line of oocyte production that generates fertilized eggs. Aging germlines displayed both sporadic and population-wide changes. A small fraction of aging animals displayed endomitotic oocytes in the germline and other defects. By contrast, all animals displayed age-related decreases in germline size and function. As early as day 3 of adulthood, animals displayed fewer stem cells and a slower cell cycle, which combine to substantially decrease progenitor zone output. The *C. elegans* germline is the only adult tissue that contains stem cells, allowing the analysis of stem cells in aging. To investigate the mechanism of the decrease in stem cell number, we analyzed the Notch signaling pathway. The Notch effectors LST-1 and SYGL-1 displayed age-related decreases in expression domains, suggesting a role for Notch signaling in germline aging. The results indicate that while sporadic defects account for the sterility of some animals, population-wide changes account for the overall pattern of reproductive aging.

Introduction

Aging is characterized by progressive degenerative changes of tissue structure and function that impair physiology and ultimately lead to death. A critical first step in understanding these changes is characterizing age-related changes in wild-type tissues, which constitutes the starting point for uncovering genes and pathways that modulate age-related decline. Most aging research focuses on somatic aging and lifespan. By contrast, much less is understood about aging of the reproductive system. Reproductive aging, which we define as the progressive, age-

related decline of the ability of the reproductive system to produce offspring, is important for human health, since infertility is an increasing concern for women who wait until middle age to start families. The *Caenhorbditis elegans* hermaphrodite is an important model because the ability to produce oocytes displays rapid age-related decline and ceases entirely while the animals are all still alive, moving, and feeding (Hughes *et al.* 2007). Furthermore, the *C. elegans* germline is the only adult tissue that contains stem cells, allowing study of stem cells in aging (Luo and Murphy 2011; Pazdernik and Schedl 2013). Extensive studies of reproductive function have been conducted in young adults, where germline stem cells differentiate and mature in a linear assembly line-like pattern as they progress away from the somatic distal tip cell (DTC) toward the spermatheca and uterus over the course of about two days (**Fig.1C**). The ~20 cell-diameter long region of the germline that is capped by the DTC niche is called the progenitor zone (PZ); it includes the mitotically cycling germline stem cells, progenitor cells, and meiotic S-phase cells, and is followed by stages of meiotic prophase and gametogenesis (Crittenden *et al.* 2006; Fox *et al.* 2011; Hansen and Schedl 2013; Pazdernik and Schedl 2013; Kimble and Seidel 2013). At the proximal end, oocytes mature, are ovulated and fertilized, and begin embryogenesis in the uterus (Hirsh *et al.* 1976; Pazdernik and Schedl 2013). Measures of egg laying are a convenient surrogate for measures of ovulation, because ~100% of ovulations in sperm-replete animals result in live progeny (McCarter *et al.* 1999).

While the age-related decline of reproductive output has been well-documented for many years (Garigan *et al.* 2002; Hughes *et al.* 2007, 2011; de la Guardia *et al.* 2016), it remains unclear which processes in the assembly line of oocyte production begin and sustain this decline. Previous studies have examined aging mechanisms in sperm-depleted and/or older animals (Luo *et al.* 2010; Narbonne *et al.* 2015; Qin and Hubbard 2015). To begin to understand why the

germline declines early in adult life, we applied state-of-the-art techniques to characterize the cellular and molecular changes that underlie age-related functional decline using sperm-replete animals before and during the decline in reproduction. Here, we report that aging germlines displayed both sporadic and population-wide changes. A small fraction of aging animals displayed endomitotic oocytes in the germline and a shifted DTC nucleus; longitudinal studies indicate that the sporadic endomitotic oocyte phenotype contributed to reduced progeny production, but only in a subset of aging animals. By contrast, there was a population–wide decrease in germline and PZ size during aging. The PZ mitotic cell cycle slowed, the number of germ cells entering meiosis decreased, and the rate of meiotic prophase progression decreased. The domain of expression of GLP-1/Notch signaling effectors SYGL-1 and LST-1 decreased, indicating that stem cell number declined and suggesting there was an age-related downregulation of GLP-1/Notch signaling. These population-wide changes in the distal germline began as early as day 3 of adulthood, when reproductive output was at its peak. An important theoretical issue in aging research is the role of sporadic, "stochastic' damage as a cause of age-related degenerative change versus the role of population-wide, "programmed" decline. For example, Herndon et al., (2002) reported on the heterogeneity among aging individuals and described the stochastic nature of somatic aging. Our results highlight the importance of population–wide changes in driving age-related decline of germline function and suggest that decreased number and activity of germline stem cells may be a root cause of reproductive aging.

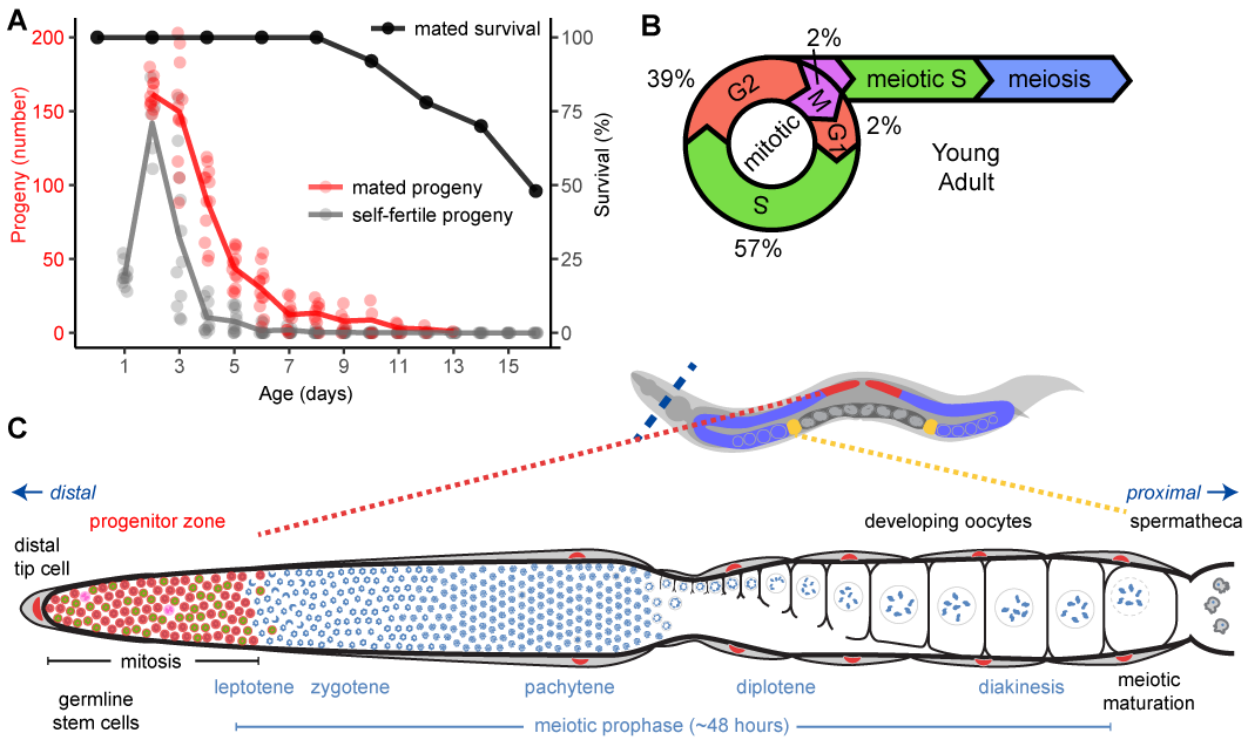

Fig.1: The female reproductive system displayed rapid age-related decline in sperm-replete *C. elegans* A) Number of progeny produced in 24 hour intervals by a wild-type self-fertile (gray) and mated (red) hermaphrodite (n=11, 12). Day 0 defined as L4 stage. Black points indicate the percent survival of wild-type mated hermaphrodites (n=54), reproduced with permission from Pickett *et al.* (2013). (See Supplemental Table 1 for statistics) **B)** Diagram of young adult germ cell mitotic cell cycle and meiotic entry. Numbers represent proportion of the cell cycle spent in each phase (Fox *et al.* (2011). **C)** Diagram shows one of two gonad arms of the young adult hermaphrodite. Cells progress from mitotic cycling to meiotic prophase to meiotic maturation before being fertilized by sperm in the spermatheca (yellow). The progenitor zone (red, defined by WAPL-1 staining) contains mitotically cycling stem cells. The DTC (nucleus in red, as are other somatic gonad cells) provides GLP-1/Notch signal to maintain the germline stem cell fate.

Results

Rapid, population-wide reproductive aging preceded somatic aging

An age-related decline in progeny production occurs in both self-fertile and mated hermaphrodites (Hughes *et al.* 2007). Wild-type hermaphrodites produced on average ~150 progeny in 24 hours at the peak of their reproductive ability on adult day 2 (**Fig.1A**). In self-fertile hermaphrodites, progeny number decreased to ~60 by day 3 (two-fold decrease), to ~8 by

day 5 (twenty-fold decrease), and was negligible after that. This rapid decline was due to sperm depletion, complicating interpretation of these data relative to reproductive aging. To monitor reproductive aging without the confounding variable of sperm depletion (Angeles-Albores *et al.* 2017), we analyzed mated hermaphrodites. Mating for 24 hours beginning at the L4 stage provides sufficient sperm to avoid sperm depletion, evidenced by production of male progeny until the cessation of reproduction and no increase in brood size after re-mating at day 5 (Ward and Carrel 1979; Hughes *et al.* 2007; Pickett *et al.* 2013; Cinquin *et al.* 2016). The presence of sperm was confirmed by immunostaining for major sperm protein when possible, and sperm-depleted animals were excluded from analyses. In mated hermaphrodites, progeny number is increased and the reproductive span is extended compared to self-fertile animals. Nevertheless, progeny production declines to ~40 by day 5 (four-fold decrease) and to ~12 by day 7 (fourteen-fold decrease) due to aging of the reproductive tract, consistent with previous findings (Hughes *et al.* 2007). In contrast to the rapid decline of progeny production, the decline of survival probability was slower; 100% of mated hermaphrodites were alive at day 10 and half remained alive until day 16 (**Fig.1A**). Thus, the age-related decline of progeny production occurs in animals with relatively healthy somatic tissue.

Endomitotic oocytes were a sporadic, low frequency, age-related defect that negatively affected reproduction

To investigate the basis for reproductive aging in mated hermaphrodites, we analyzed the morphology of dissected germlines in day 1, 3 and 5 adults. The ability to withstand dissection is unlikely to affect these comparisons, because gonads dissect reliably at these ages. DAPI staining was used to analyze nuclear morphology, and WAPL-1 antibody staining was used to

measure the size of the PZ and the position of the DTC and somatic gonad nuclei (**Fig.S1**). Some abnormalities were observed at such a low frequency (<2% of germlines) that they could not be effectively studied with our sample size. These included premature meiotic entry of all PZ cells (Glp phenotype), short and narrow PZ, enlarged PZ nuclei, ectopic proliferation, and gaps and oocyte-like formations in the middle of the pachytene region (**Fig.S2**). Two abnormalities were observed at a low but consistent frequency that supported statistical analysis: the presence of endomitotic oocytes and a shifted DTC nucleus.

Endomitotic oocytes within the proximal gonad arm result from miscoordination of meiotic maturation and ovulation and can be visualized with DAPI staining (**Fig.2D**). Mutations of at least 21 genes are known to result in endomitotic oocytes (Iwasaki *et al.* 1996; McCarter *et al.* 1997; Greenstein 2005; "Wormbase WS260" 2017). Endomitotic oocytes can negatively affect reproduction, since several endomitotic oocytes in a gonad block productive maturation and ovulation. In mated hermaphrodites, endomitotic oocytes were extremely rare in day 1 adults. There was an age-related increase in frequency; about 5% of day 3 adults displayed single endomitotic oocytes, usually in only one gonad arm, positioned distal to the spermatheca and not in the uterus (**Fig.2A**). At least 9% of germlines of day 5 adults displayed endomitotic oocytes, and affected animals typically displayed multiple endomitotic oocytes with large nuclei, often in both gonad arms.

To investigate the model that endomitotic oocytes cause an age-related decrease in progeny production, we performed a longitudinal analysis. Progeny production by mated wild-type hermaphrodites is quite variable in the 24 hours between days 4 and 5, averaging 32 +/- 18 and ranging from 0 to 108 (**Fig.2B**). We measured progeny production in this interval for 186 hermaphrodites, then sacrificed the animals and measured endomitotic oocytes. The

subpopulation with the lowest progeny production exhibited significantly more endomitotic germlines than the other subpopulations (**Fig.2C**). There was no significant correlation between the least-fertile subpopulation and distal germline phenotypes (**Fig.S3E,F**). The strong correlation between the presence of endomitotic oocytes and low progeny production suggests these two processes are causally linked.

The somatic DTC caps the end of the germline and intercalates between the distal germ cells. The DTC provides the niche for the germline stem cells by expressing LAG-2 (delta ligand) that is received by GLP-1 (Notch receptor) on the germline stem cells (Kimble and Ward 1988; Pepper *et al.* 2003; Greenwald and Kovall 2013; Pazdernik and Schedl 2013; Kimble and Seidel 2013). To monitor age-related changes, we determined the position of the DTC nucleus relative to the distal end of the germline (**Fig.2E**). In day 1 adults, the DTC nucleus was always positioned within 3 cell diameters (c.d.) of the end of the germline. Day 3 and 5 adults displayed a shift of 5 c.d. or more in 7% and 17% of germlines, respectively (**Fig.2F,G;Fig.S3B**). To analyze the functional consequences of the shifted DTC, we used a longitudinal approach to determine the correlation with progeny production between days 4 and 5. Although the least-fertile subpopulation displayed a higher extent of shifted DTC nucleus, the trend was not statistically significant with this sample size (**Fig.S3E**). Additionally, the shifted DTC nucleus and endomitotic oocyte phenotypes were not correlated (**Fig.2H,I; Fig.S3C,D**). These results document an age-related increase in the frequency of a shifted DTC but do not rigorously establish the functional consequences of this anatomical change, and it is possible that it does not negatively influence reproduction.

If endomitotic oocytes or shifted DTC nuclei are caused by systemic factors, then the two gonad arms of an individual are predicted to display similar behavior. By contrast, if these

abnormalities result from anatomically local causes, then the two gonad arms in an individual are predicted to behave independently. To investigate these possibilities, we took advantage of the subset of animals in which both germlines were visible after dissection and compared within-pair variation to between-pair variation using an intraclass correlation analysis. There was no significant correlation in the degree of DTC nucleus shift within a pair of germlines in the same animal (**Fig.S3G-I**). Thus, the shifted DTC nucleus appears to result from local rather than systemic conditions. By contrast, if one gonad arm displayed endomitotic oocytes, then the other arm was also more likely to display this defect, indicating there may be systemic conditions that promote this defect (**Fig.S3A**).

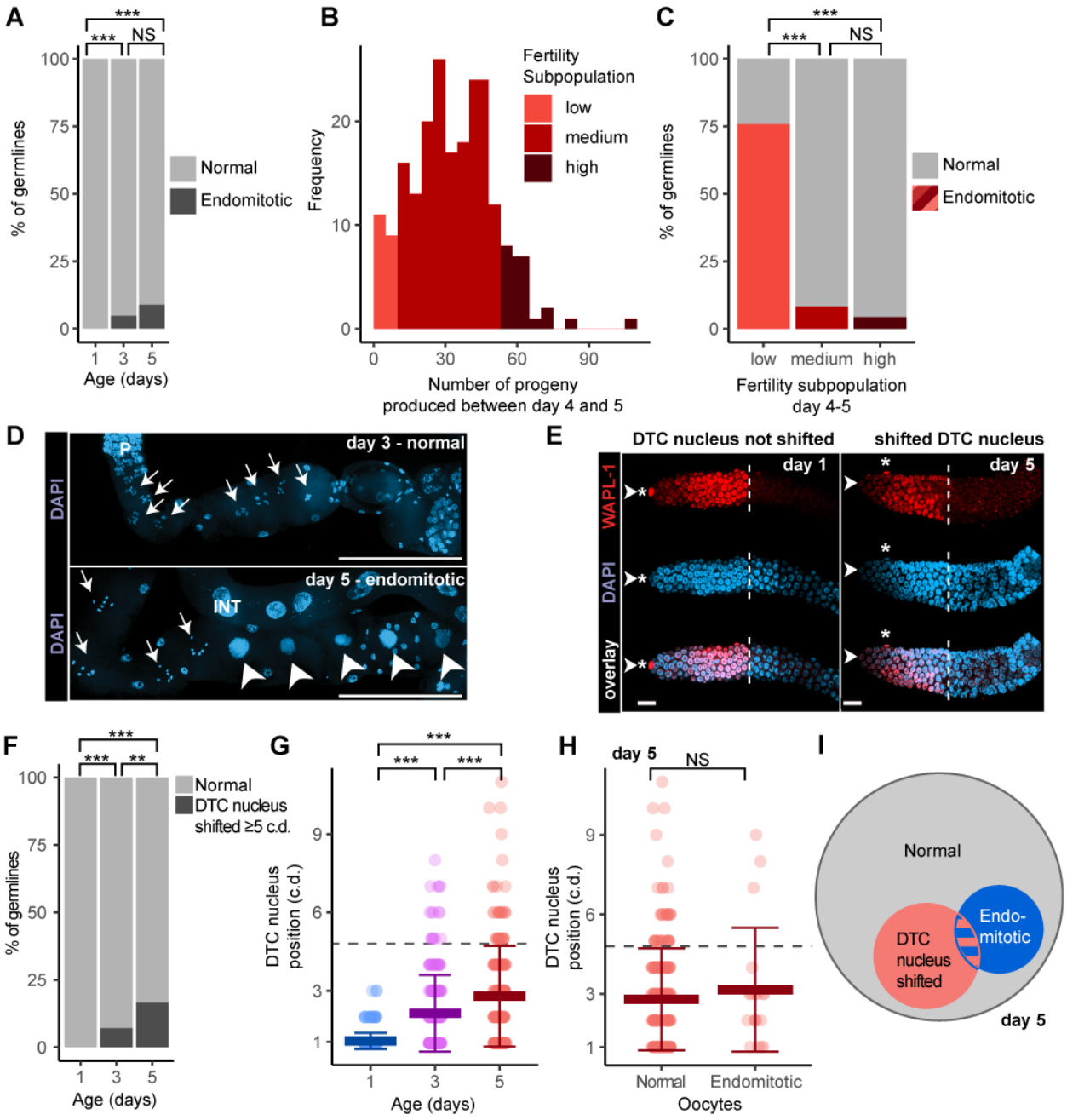

Fig.2: Endomitotic oocytes and a shifted DTC nucleus occurred at a low frequency. A) Day 1, 3 and 5 mated wild-type hermaphrodites were analyzed for endomitotic oocytes in dissected germlines. Gray indicates no detectable endomitotic oocytes (normal), and black indicates one or more endomitotic oocytes. PC test. **B)** Longitudinal experiment - bars represent number of mated hermaphrodites (frequency) that produced the indicated number of progeny between days 4 and 5. We defined three fertility subpopulations: low (bottom 10%), medium (middle 80%), and high (top 10%). **C)** Proportion of endomitotic germlines at day 5 in fertility subpopulations. **D)** Representative fluorescence micrographs of normal diakinesis oocytes (arrows) in a day 3 adult (top) and endomitotic oocytes (arrowheads) in a day 5 adult (bottom), with DNA stained by DAPI. P, pachytene. INT, intestine. Scale bar = 100 µm. **E)** Representative fluorescence micrographs of day 1 and 5 adult germlines stained for WAPL-1 (red, row 1), DAPI (blue, row 2), and WAPL-1+DAPI (row 3). Arrowhead indicates the distal tip of

the gonad, asterisk indicates the position of the DTC nucleus. The DTC nucleus is at cell diameter position 1 (left) and 5 (right). Dashed lines indicate the boundary of WAPL-1-positive cells. Scale bar=10μm.
F,G) DTC nucleus position was determined by counting the number of c.d. from the gonad tip in day 1, 3, and 5 mated hermaphrodites. **F)** gray indicates DTC nucleus was ≤4 c.d. (normal), black indicates the DTC nucleus was ≥5 c.d. (shifted) from the tip. PC test. **G)** each data point indicates position of one DTC nucleus. Position 1 means DTC nucleus is at the distal tip. KW test. Dashed line represents cutoff for panel **F**. **H)** We categorized day 5 adult mated hermaphrodite germlines as non-endomitotic (normal) or endomitotic, and each data point indicates the position of one DTC nucleus. KW test. **I)** Venn diagram, proportion of day 5 mated hermaphrodite germlines showing endomitotic nuclei (blue), shifted DTC nucleus (red), both (blue/red) or neither (gray). (See Supplemental Table 2 for statistics; NS indicates P>0.05, * P<0.05, ** P<.001, *** P<.0001.)

Population-wide, age-related decline in the size of the germline and progenitor zone

The majority of day 5 adults displayed neither endomitotic oocytes nor a shifted DTC nucleus, yet all these animals produced far fewer progeny than young adults. To explain the population-wide decline in progeny production, we searched for age-related changes in the germline that affect all animals. To measure germline size, we counted the number of cell diameters from the distal tip to the loop (distal portion of the germline) or the distance in micrometers from the distal tip to the spermatheca (entire germline). Both measurements revealed a significant decrease in overall size at days 3 and 5 (**Fig.3B,C**). The size of the PZ measured in cell diameters or total number of cells displayed a significant and progressive decrease (**Fig.3A,D,E**). The age-related changes identified in this cross sectional analysis appear to affect essentially the entire population, albeit within a normal distribution (**Fig.3B-F**).

If the decreased size of the PZ is caused by systemic factors, then a similar decrease is predicted to occur in both gonad arms of an individual. Indeed, a significant within-pair correlation of PZ size in day 3 and 5 adults was observed (**Fig.S4A-C**). The low relative variance within pairs of day 3 and 5 germlines is consistent with an age-related systemic process that affects both gonad arms in an individual animal.

To investigate the relationship between the DTC nucleus position and the size of the PZ, we analyzed the correlation between these features. Overall, the position of the DTC nucleus did not explain the decrease in the size of the PZ, indicating these two age-related changes do not share a common cause (**Fig.S4D-F**). Day 3 hermaphrodites that were self-fertile or mated to males displayed similar distal germline sizes and extents of the PZ, indicating male exposure did not cause these age-related changes (**Fig.S5**).

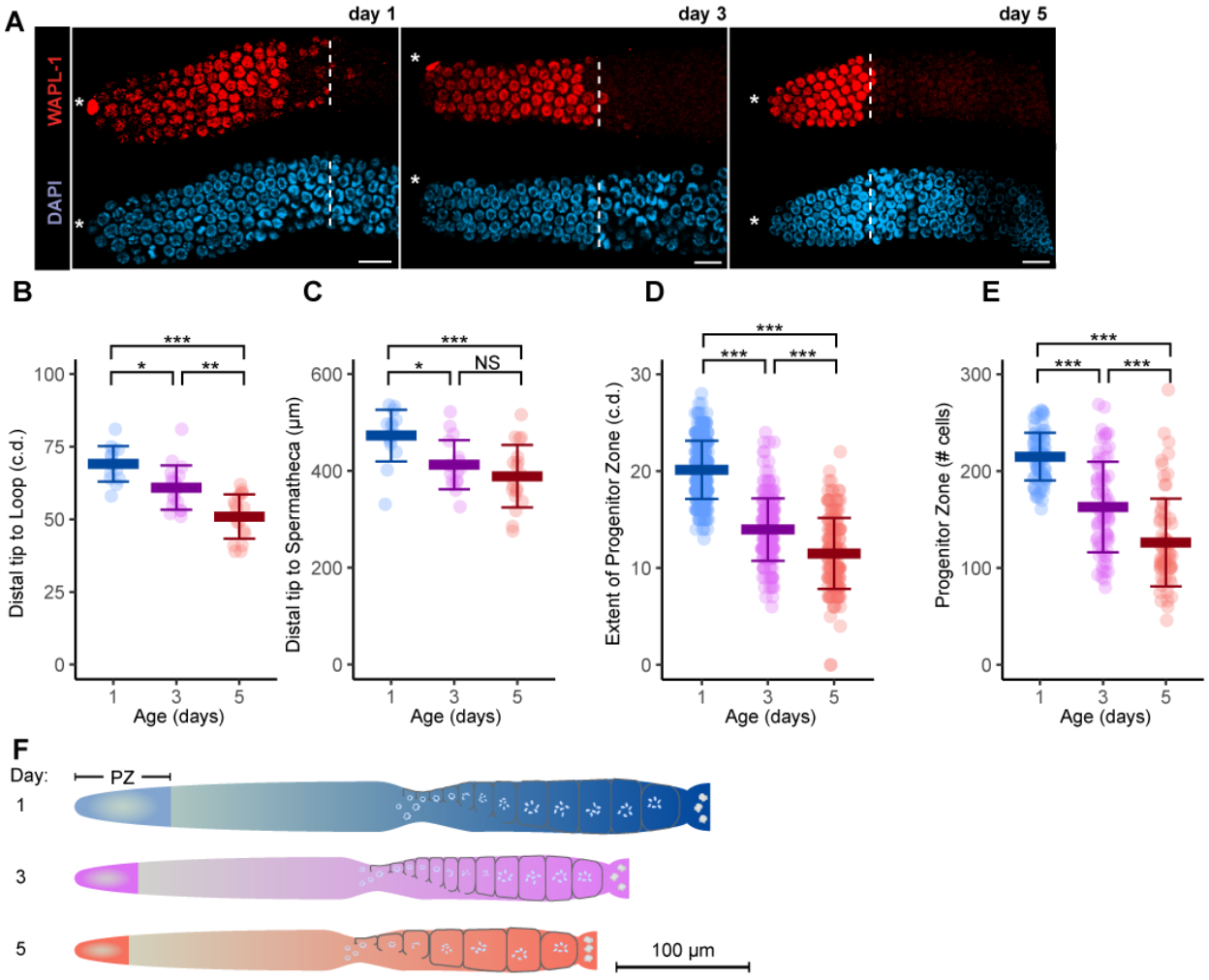

Fig.3: Population-wide, age-related decreases in the size of the germline and progenitor zone. A) Representative fluorescence micrographs of one germline from day 1, 3 and 5 adults stained for WAPL-1 (top, red) and DAPI (bottom, blue). Asterisks, DTC nucleus position; white dashed line, proximal boundary of WAPL-1-positive cells. Scale bar=10µm. **B,C)** Each data point is length from the distal tip to the loop (in cell diameters, c.d.)

(**B**) or spermatheca (in micrometers, used due to unequal size of cells in proximal region) (**C**) in mated hermaphrodites at adult days 1, 3 or 5. KW test. **D)** Each data point is length of the PZ (in c.d.), defined by WAPL-1 antibody staining and measured from the distal tip to the last row where at least half of the cells were WAPL-1-positive. KW test. **E)** Each data point is the total number of PZ cells, defined as WAPL-1-positive. KW test. (See Supplemental Table 3 for statistics) **F)** Diagram of the size of the entire germline and PZ in day 1, 3, and 5 adults.

The duration of the mitotic cell cycle displayed population-wide, age-related increase.

The reduction in size of the PZ may be the result of a decrease in the frequency of cell division and/or the size of the stem cell pool. To analyze the cell cycle, we measured multiple parameters that make it possible to calculate the overall duration of the cell cycle and the proportion of each phase (**Fig.1B,S1**). In day 1 adult hermaphrodites, the mitotic cell cycle takes 6.5-8 hours, germ cells do not undergo transit-amplifying divisions (Fox and Schedl 2015), and quiescent cells are not observed (Crittenden *et al.* 2006). The cell cycle consists of the phases S, G2, and M, since the G1-phase is short or absent (Fox *et al.* 2011). To investigate age-related changes in the cell cycle, we measured the mean and maximum duration of the cell cycle in day 1, 3 and 5 adults.

To estimate the durations of cell cycle phases, we fed animals EdU continuously for 0.5, 4, 7, or 10 hours and dissected them immediately. A significant fraction of day 5 animals failed to label following a 0.5 hour EdU feed; the alternative method of soaking in EdU gave a similar result (see Methods; **Fig.S6**). Cinquin et al., (2016) reported a similar phenomenon. Some day 5 animals may have reduced ability to absorb and transport EdU. These animals were not informative about cell cycle duration and were excluded from data analysis.

The duration of G2 was estimated by analyzing the percent of cells in M-phase (pH3 immunoreactive) that were EdU-positive; these cells must have been in S-phase during the EdU pulse and then proceeded through G2 and entered M-phase at the time of dissection (**Fig.4A,B**).

No M-phase cells were EdU-positive after a 0.5-hour pulse, indicating G2 was always more than 0.5 hours, whereas all M-phase cells were EdU-positive after a 10-hour pulse, indicating G2 was always less than 10 hours. Using all four data points, we estimated the median G2 duration as ~2.5, ~4.5 and ~4.9 hours in day 1, 3, and 5 animals, respectively. Thus, there was a significant ~100% increase in the duration of G2 between days 1 and 3.

The duration of G2+M+G1 was estimated from the percentage of all PZ cells (WAPL-1-immunoreactive) that were EdU-negative (**Fig.4C,D**). About 40% of cells were EdU-negative following a 0.5 hour pulse, indicating these cells were in G2+M+G1 during the entire pulse, whereas no cells were EdU-negative following a 10 hour pulse, indicating G2+M+G1 was always less than 10 hours. These data were used to calculate maximum duration of these three phases, and the 90th percentile duration was determined by interpolation. We estimated the 90th percentile G2+M+G1 duration as ~3.4, ~7.6, and ~7.4 hours in day 1, 3, and 5 animals, respectively. Thus, there was a significant ~100% increase in the duration of G2+M+G1 between days 1 and 3.

In principle, there are two explanations for the age-related increase in median and maximum cell cycle durations across the population of PZ cells at day 3: 1) in all cells the duration of all phases of the cell cycle increased proportionately or 2) in some cells one phase of the cell cycle increased disproportionately, similar to cell cycle arrest that occurs during germline starvation, sperm depletion, and during *Drosophila* germline aging (Angelo and Van Gilst 2009; Narbonne *et al.* 2015; Kao *et al.* 2015; Seidel and Kimble 2015). To distinguish these possibilities, we determined the fraction of cells in M-phase using anti-pH3 antibody (M-phase index, **Fig.4F, S7A,B,D**) and the fraction of cells in S-phase using a 0.5 hour pulse of EdU (S-phase index, **Fig 4E,G, S7C,E**). The M-phase index was approximately 2.5% in day 1, 3 and 5

animals, indicating there is not an age-related change in the fraction of cells in M-phase. Similarly, the S-phase index did not display an age-related change but was approximately 57% in day 1, 3 and 5 animals. These results indicate that adult germline stem cells do not become quiescent, at least up to day 3 of adulthood. These results indicate there is an age-related increase in cell cycle duration in all cells, whereas there is no age-related change in the proportion of cells in each cell cycle phase (**Fig.4H**).

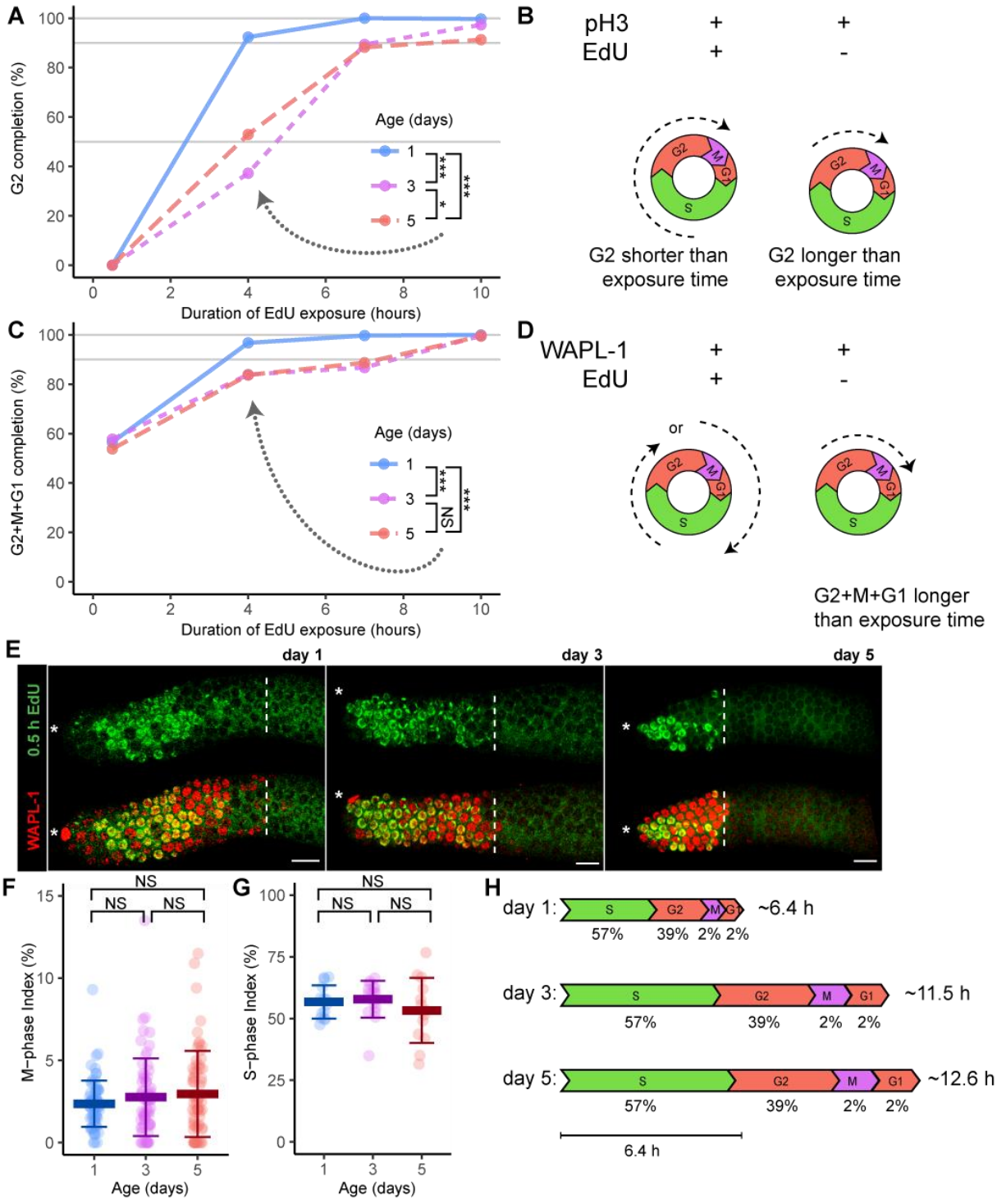

Fig.4: Population-wide, age-related increase in the duration of the cell cycle. Mated hermaphrodites at day 1 (blue), 3 (purple) or 5 (red) were exposed to EdU for 0.5, 4, 7, or 10 hours, and germlines were dissected and stained with anti-pH3 antibody, anti-WAPL-1 antibody, and/or EdU click chemistry. **(A)** Percent G2 completion was defined as the number of cells that were both pH3-positive (indicative of M-phase) and EdU-positive (indicative of cell in S-phase sometime during EdU exposure), divided by the total number of pH3-positive cells. These data were used to estimate the median time taken to complete G2-phase (n=1655 cells, 366 germlines). Gray horizontal lines

indicate the 50th, 90th, and 100th percentiles. A PC test was used to compare the 4 hour time point (dotted arrow). **B,D)** Dashed arrows in diagrams illustrate inferred cell cycle stage at the beginning (S or G2) and end (M, G1 or S) of the experiment. **C)** Percent G2+M+G1 completion was defined as the number of cells that were both WAPL-1-positive (interpreted as being in the PZ) and EdU-positive, divided by the total number of WAPL-1-positive cells. These data were used to estimate the maximum time taken to complete G2+M+G1 phase (n=193 animals, 31958 cells). Gray horizontal lines indicate the 90th and 100th percentiles. A PC test was used to compare the 4 hour time point. **E)** Representative fluorescence micrographs of one germline from adults exposed to EdU for 0.5 hours and stained for EdU (green, row 1), and EdU and WAPL-1 (red, yellow overlap, row 2). Asterisk, DTC nucleus position; white dashed line, proximal boundary of WAPL-1-positive cells. Scale bar=10μm. **F)** Each data point indicates the M-phase index (number of cells that were pH3-positive divided by the number of PZ WAPL-1-positive cells). **G)** Each data point indicates the S-phase index (number of EdU-positive cells divided by the number of PZ WAPL-1-positive cells) of adults following an EdU exposure of 0.5 hours. KW test. (See Supplemental Table 4 for statistics) **H)** Scale diagrams illustrate the inferred duration of each cell cycle phase, values below indicate percent, and values at right indicate total duration. Scale bar=6.4 hours.

The rate of meiotic entry, a measure of the output of the progenitor zone, displayed population-wide, age-related decline.

A critical factor in germline function is the rate at which cells exit the PZ and enter meiosis. We predicted the output of the PZ would decrease in day 3 and 5 adults as a functional consequence of a slower cell cycle and a smaller stem cell pool (see below). To measure the rate of meiotic entry, we exposed animals to EdU for 4, 7, or 10 hours and counted the number of EdU-positive cells in the meiotic region, defined as cells that displayed EdU signal but no WAPL-1 signal. These cells must have resided in the PZ at the beginning of the experiment to become EdU labeled and then entered the meiotic region by the end of the experiment to become WAPL-1-negative (**Fig.5A**).

The rate of meiotic entry was calculated as the slope of the regression using three data points (**Fig.5B**). Day 1 animals displayed 19.3 cells per hour entering meiosis, consistent with previous reports (Fox *et al.* 2011). Day 3 and 5 animals displayed a much lower rate, only ~4 and ~2 cells per hour entering meiosis, respectively. There was no significant correlation between the size of the PZ and the number of cells that entered meiosis in day 1, 3 and 5 animals (**Fig.S8**).

Thus, the rate of meiotic entry displayed a dramatic age-related decrease of ~78% by day 3 and over 91% by day 5 (**Fig.5C**).

A large proportion of germ cells that enter meiosis in the adult function as nurse cells that provide essential constituents to growing oocytes but do not become oocytes, as they undergo apoptosis in late pachytene (Gumienny *et al.* 1999; Wolke *et al.* 2007). We estimate that 84% of day 1 cells that enter meiosis become nurse cells, similar to other estimates (see Methods; Agarwal et al., 2018). The number of nurse cells did not change significantly at day 3 (79%) and day 5 (85%).

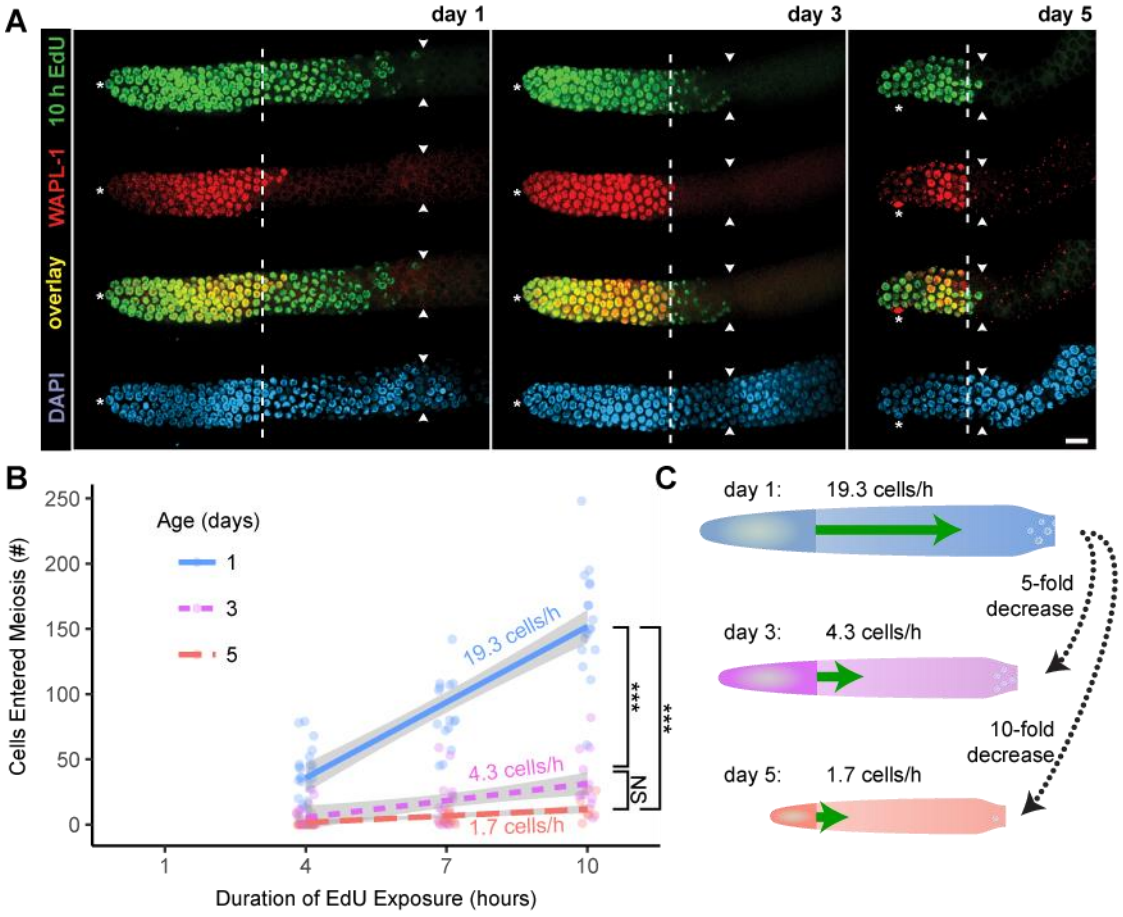

Fig.5: Population wide, age-related decrease in the rate of meiotic entry Mated hermaphrodites at day 1 (blue), 3 (purple), or 5 (red) were exposed to EdU for 4, 7, or 10 hours, and germlines were dissected and stained with anti-WAPL-1 antibody and EdU click chemistry. **A)** Representative fluorescence micrographs of one germline from day 1, 3 and 5 adults exposed to EdU for 10 hours and stained for EdU (green, row 1), WAPL-1 (red, row 2), EdU+WAPL-1 (overlay, row 3) and DAPI (blue, row 4). Asterisk, DTC nucleus position; white dashed line,

proximal boundary of WAPL-1-positive cells; and white arrowheads, proximal boundary of EdU-positive cells. Scale bar=10μm. **B)** The rate of meiotic entry (cells/hour) was calculated from the slope of the linear regression of the number of cells that entered meiosis (EdU-positive, WAPL-1-negative) versus the duration of the EdU exposure. Gray range indicates 95% confidence interval on linear regression. KW test compared the number of cells entered meiosis in 10 hours. (See Supplemental Table 5 for statistics) **C)** Diagram of day 1, 3, and 5 germlines highlighting the age-related decrease in the rate of meiotic entry (green arrows).

The assembly-line-like progression from the progenitor zone to oocytes displayed population-wide, age-related decline.

The rate at which cells progress through meiotic prophase is an important aspect of germline function. To determine how this value changes during aging, we used an EdU pulse-chase technique similar to that reported by Jaramillo-Lambert *et al.* (2007). The "pulse" consisted of 4 hours feeding with EdU labeled bacteria, which marks the majority of PZ cells. The "chase" consisted of transferring animals to unlabeled bacteria for 48 hours, followed immediately by dissection. Cells labeled with EdU during the "pulse" retain this label during the "chase" as they progress through meiotic prophase and gametogenesis (**Fig.6A**). Thus, the most proximal labeled cells provide a measure of the distance travelled from the PZ in 48 hours. Because the distance is measured during a two-day interval, the rate is an average during days 1-3, 3-5, or 5-7. We analyzed the length of the germline, length of the PZ, and the position of the most-proximal cell of the population of EdU labeled cells (**Fig.6C, Fig.S9A-C**). In addition, the meiotic prophase substage (mid-pachytene, late pachytene, diplotene, or diakinesis) of the most proximal EdU positive cell was determined (**Fig.6D, S9D,E**).

The rate of progression through meiotic prophase decreased in day 3 and 5 compared to day 1. Starting with day 1 adults, after 48 hours the most proximal cell progressed ~52 c.d. (**Fig.6C**). It was most commonly in diplotene, with some in late pachytene and some in diakinesis (**Fig.6D, S9D,E**). Day 3 animals displayed significantly less movement and maturity

after 48 hours. The most proximal cell progressed ~31 c.d., despite the entire germline decreasing in size, and was most commonly in late pachytene (**Fig.6C,D, S9D,E**). Day 5 adults were not significantly different compared to day 3 adults. Thus, the rate that cells move through meiotic prophase during days 3-5 was dramatically slower than the rate during days 1-3 (**Fig.6E**).

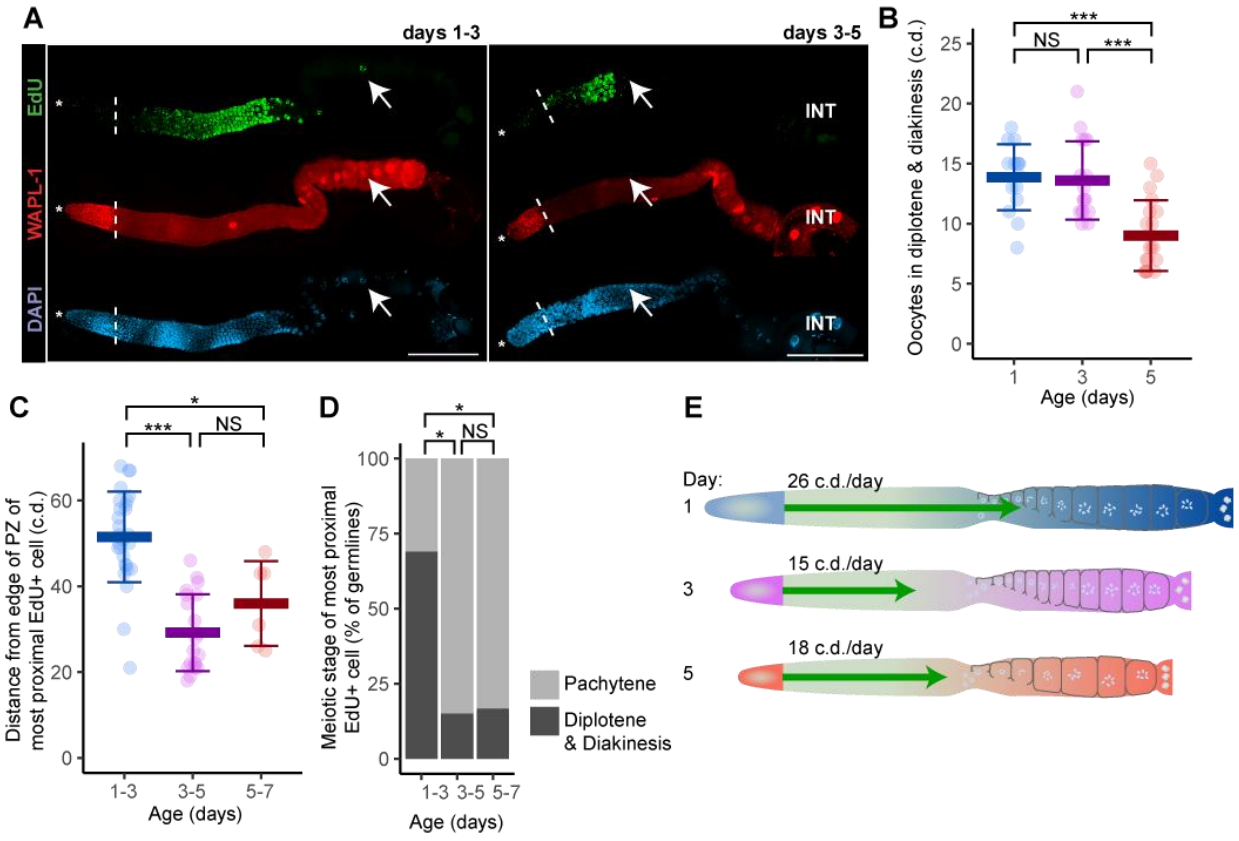

Fig.6: Population-wide, age-related decrease in the rate of meiotic progression Mated hermaphrodites at days 1, 3 or 5 were fed EdU labeled bacteria for 4 hours ("pulse") to label all cells that underwent S-phase and then fed unlabeled bacteria for 48 hours ("chase") to determine the extent of movement. Because the distance is measured during a two-day interval, the rate is an average of the rate during days 1-3, 3-5, or 5-7. **A)** Representative fluorescence micrographs of one germline labeled at day 1 and 3 and analyzed after 48 hours by staining for EdU (green, row 1), WAPL-1 (red, row 2), and DAPI (blue, row 3). Asterisk, DTC nucleus position; white dashed line, proximal boundary of WAPL-1-positive cells; white arrows, proximal boundary of EdU-positive cells; and INT, intestine. Scale bar=100µm. **B)** Each data point represents the number of cell diameters of diplotene and diakinesis oocytes in the proximal assembly-line in mated hermaphrodites at adult days 1, 3 or 5. KW test. **C)** In each germline, the most proximal EdU-positive cell was identified, and each data point indicates its distance in c.d. from the proximal edge of the PZ. Because the most proximal EdU-positive cell was presumably near the proximal end of the PZ at the beginning of the experiment, this value estimates the distance moved during 48 hours. KW test. **D)** In each germline, the most proximal EdU-positive cell was categorized as pachytene or diplotene/diakinesis. PC test.

(See Supplemental Table 6 for statistics) **E)** Diagram of day 1, 3, and 5 germlines highlighting the age-related decrease in the rate of meiotic progression (green arrows).

Age-related changes in the distal germline have a delayed effect on progeny production.

Our results document that the distal gonad displays striking age-related declines by day 3, but at this time progeny production is still at or near its peak. We reasoned that the changes in the distal gonad would have a delayed effect on progeny production that might not be apparent until about 2.5 days later, given the time necessary for germ cells to transit through the germline (**Fig.6**). Thus, progeny deposited into the environment at day 3 result from PZ cells on day 1 that transitioned into developing oocytes in the proximal arm of the germline. This model predicts that the number of developing oocytes would remain unchanged between days 1 and 3 but would decrease by day 5. To test this hypothesis, we counted the number of oocytes in diplotene and diakinesis in dissected DAPI-stained germlines. The number of oocytes was ~14 at days 1 and 3, but decreased significantly to ~9 at day 5 (**Fig.6B**). Thus, the effect on progeny production caused by the slowing cell cycle and shrinking size of the PZ at day 3 only appears about 2 days later.

A population-wide, age-related decline in stem cell number and the domain of Notch signaling

Our results document dramatic changes in the number and behavior of the PZ cells by days 3 and 5. To further investigate the mechanisms that promote these changes, we took a candidate approach by analyzing the Notch signaling pathway. The DTC expresses LAG-2 (Delta), which interacts with GLP-1(Notch) receptor on germ cells. Following GLP-1 cleavage, the intracellular domain translocates to the nucleus and interacts with LAG-1 to activate the

transcription of Notch effector genes (Kimble and Ward 1988; Pepper *et al.* 2003; Greenwald and Kovall 2013; Pazdernik and Schedl 2013; Kershner *et al.* 2014; Lee *et al.* 2016; Shin *et al.* 2017). Notch signaling is critical for the stem cell fate, since withdrawal of Notch signaling results in entry into meiosis. We hypothesized that an age-related decrease in GLP-1/Notch signaling contributes to age-related changes in stem cell fate specification. Two direct transcriptional targets of GLP-1 are the *sygl-1* and *lst-1* genes, which are redundantly necessary and each sufficient to promote germline stem cell fate and block differentiation (Kershner *et al.* 2014; Lee *et al.* 2016). To analyze *sygl-1* and *lst-1* expression, we engineered the FLAG epitope tag into the endogenous loci so that these genes express FLAG::SYGL-1 and LST-1::FLAG, respectively (**Fig.7A,E**).

To investigate whether the number of germline stem cells decreases with age, we used FLAG::SYGL-1. We interpret the SYGL-1 expression zone to approximate the stem cell pool, as genetic analysis indicates SYGL-1 is sufficient for the stem cell fate (Shin *et al.* 2017). Dissected germlines of day 1 adults displayed expression of FLAG::SYGL-1 in the cytoplasm of the most distal ~10 cell diameters of the germline; the FLAG::SYGL-1 region encompassed 81 +/- 14 cells. (**Fig.7B-D, S10C**). Day 3 adults displayed a significant ~1.4-fold decrease in the number of FLAG::SYGL-1 cells, and day 5 adults displayed a significant ~2-fold decrease (**Fig.7C,I**). The expression zone measured in cell diameters displayed a similar age-related decline (**Fig.7D**). Thus, the extent of SYGL-1 expression displayed age-related decline by day 3, indicating there is an age-related decline in the number of germline stem cells.

To investigate whether changes in GLP-1/Notch signaling are responsible for the age-related decrease in the size of the PZ, we used LST-1::FLAG. Dissected germlines of day 1 adults stained with anti-FLAG antibody displayed expression of LST-1::FLAG in the cytoplasm

of the most distal ~5 cell diameters (**Fig.7F-H, S10A**), which corresponded well with the localization of *lst-1* pre-mRNA introns, and thus the region of Notch-mediated transcription (Lee *et al.* 2016). Consistent with this interpretation, when the DTC nucleus was shifted, the domain of LST-1::FLAG displayed a corresponding shift (**Fig.S10B**). The LST-1::FLAG region encompassed 38 +/-10 cells at day 1 (**Fig.7G**). Day 3 adults displayed a significant ~1.4-fold decrease in the number of LST-1::FLAG cells, and day 5 adults displayed a further significant ~2.2-fold decrease (**Fig.7G,I**). The expression zone measured in cell diameters displayed a similar age-related decline (**Fig.7H**). Thus, the extent of LST-1 expression displayed age-related decline by day 3, indicating there is an age-related decline in the GLP-1/Notch signaling system that maintains germline stem cells.

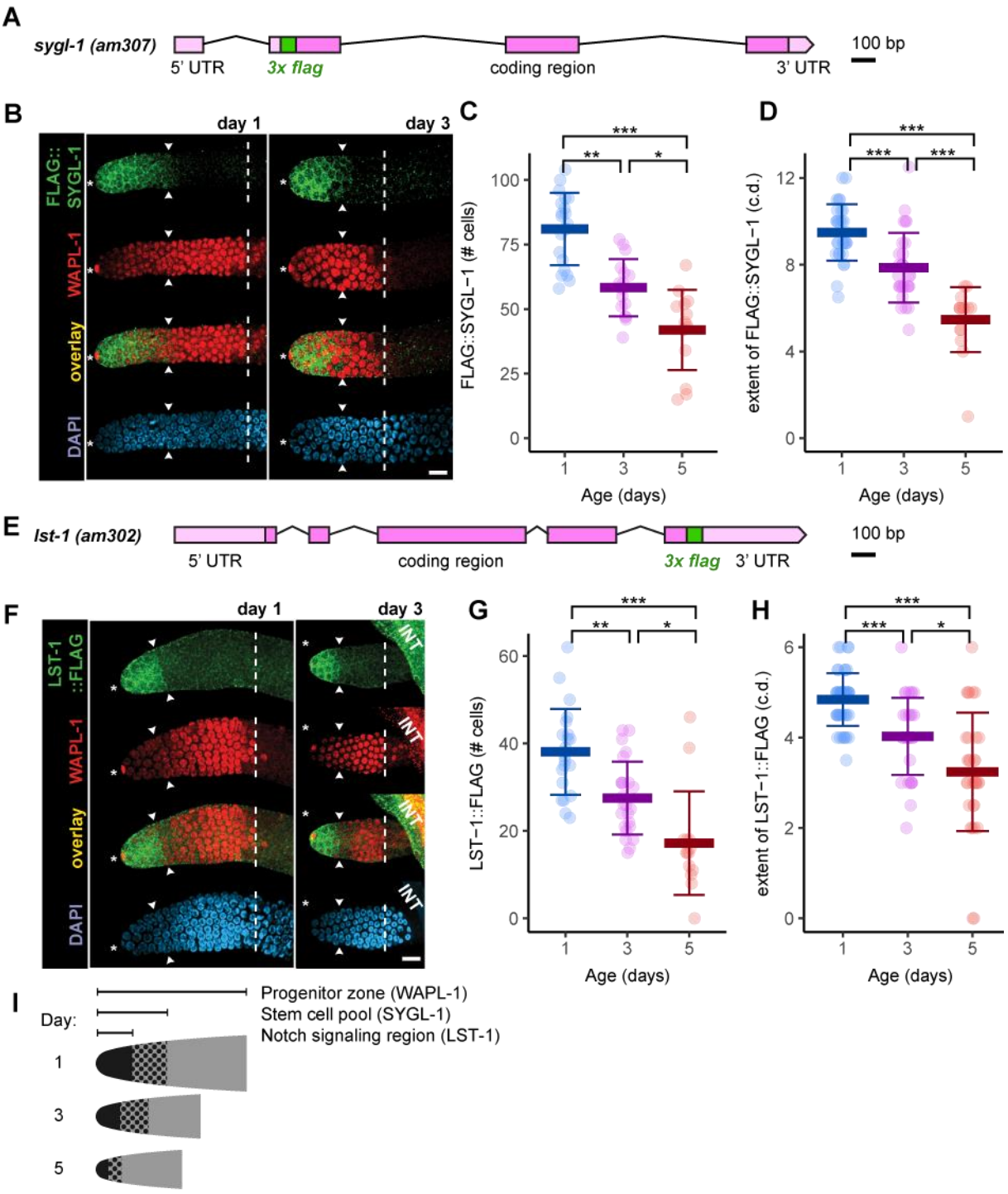

Fig.7: Population-wide, age-related decrease in the stem cell pool and GLP-1 (Notch) signaling. Mated *sygl-1(am307)* and *lst-1(am302)* hermaphrodites expressing FLAG::SYGL-1 or LST-1::FLAG fusion proteins, respectively, were stained with anti-FLAG antibody. **A,E)** Diagram of the *sygl-1(am307)* and *lst-1(am302)* genomic loci. DNA encoding 3xFLAG epitopes was inserted in-frame using CRISPR/Cas9 genome editing, resulting in an N-terminally (**A**, *sygl-1*) or a C-terminally (**E**, *lst-1*) tagged fusion protein expressed from the endogenous locus.

B, F) Representative fluorescence micrographs of one germline from day 1 and 3 adults stained for FLAG::SYGL-1 (**B**) or LST-1::FLAG (**F**) (green, row 1), WAPL-1 (red, row 2), FLAG+WAPL-1 (overlay, row 3) and DAPI (blue, row 4). Asterisks, DTC nuclear position; white arrowheads, proximal boundary of FLAG staining; white dashed lines, boundary of WAPL-1-positive cells; and INT, intestine. Scale bar=10μm. **C,D,G,H)** Data points indicate the number of expressing cells (**C**,**G**) or the extent of these cells (c.d.) (**D**,**H**). KW test. (See Supplemental Table 7 for statistics) **I)** Diagram of the size decrease in the PZ, stem cell pool, and Notch signaling region.

Discussion

Sporadic changes contributed to age-related reproductive decline in a subset of animals, but population-wide changes accounted for reproductive aging in the majority of animals.

An important issue in understanding the biology of aging is distinguishing the roles of "stochastic" versus "deterministic" changes. Experimental data can be used to categorize changes as low-frequency (sporadic) versus high-frequency (pervasive, population-wide). The next layer of interpretation suggests that low-frequency or sporadic changes have a mechanism that is stochastic, probabilistic, or unpredictable. In aging studies, the cause of such changes is inferred to be entropy, an energetic environment that damages biological systems in unpredictable ways that cause degeneration. By contrast, high-frequency or population-wide changes are inferred to have a mechanism that is programmed, deterministic, or predictable, which arises from genetic programs, such as those that control development.

Here we documented both low-frequency, sporadic changes as well as high-frequency, population-wide changes. Some defects occurred so infrequently that we could not quantify them, whereas the appearance of endomitotic oocytes in the proximal germline and a shifted DTC nucleus could be quantified; by day 5, ~9% and ~17% of germlines displayed endomitotic oocytes and a shifted DTC nucleus, respectively. There was no correlation between the appearance of these two defects in individual animals, indicating that they do not share a common cause. A longitudinal study indicated that the presence of endomitotic oocytes reduced

progeny production, consistent with previous studies of mutant strains that display high levels of endomitotic oocytes and are subfertile or sterile (Iwasaki *et al.* 1996; McCarter *et al.* 1997; Greenstein 2005; "Wormbase WS260" 2017). These results suggest that low-frequency, sporadic defects account for age-related decrease in progeny production in a subset of animals (**Fig.8C**). Similar to these results, sporadic defects of mispositioned niche cells and ectopic germ cell proliferation were reported in a subset of middle-aged *Drosophila* ovaries (Kao *et al.* 2015).

A variety of high-frequency, population-wide changes were observed by analyzing the stem cell pool and mitotic cell cycle. Striking declines in germline function were observed very early in life, at day 3 of adulthood when each animal was still producing >100 progeny per day, including a 25% decrease in PZ cell number, a 1.4-fold decrease in stem cell number, a doubling of the cell cycle duration, and a 5-fold decrease in the rate of meiotic entry. Due to the assembly-line organization of the germline, these declines in distal germline function were manifested at day 5, contributing at least in part to the 4-fold decrease in progeny production (**Fig.8A,B**). Further distal germline declines on day 5 were manifested as decreased progeny production on day 7 and beyond. These age-related changes appeared to occur in all animals, and thus were quite different from the low-frequency changes. These studies suggest that population-wide changes are the predominant cause of the age-related decline in progeny production (**Fig 8C**). Furthermore, we found a significant correlation between gonad arms in the decrease in PZ size, indicating that there is an age-related systemic change, likely cell non-autonomous, that results in a functional decline in both germlines.

Previous studies of *C. elegans* aging in the distal germline focused on sperm-depleted and/or older animals. The progenitor zone shrinks with age, and mating enhances this phenotype through promoting qin; TGF-β and insulin signaling pathways accelerate these changes (Luo *et*

al. 2010; Narbonne *et al.* 2015; Qin and Hubbard 2015). By contrast, we examined sperm-replete animals prior to and during the rapid decrease in reproductive output using mated hermaphrodites. Male exposure might have multiple effects on hermaphrodites, including male pheromones, seminal fluid, and physical trauma (Maures *et al.* 2014; Shi and Murphy 2014), and we cannot formally separate these possible effects from sperm transfer. However, self-fertile and mated day 3 hermaphrodites displayed no difference in the size of the progenitor zone, suggesting that the age-related decline in progenitor zone size was not caused by male exposure.

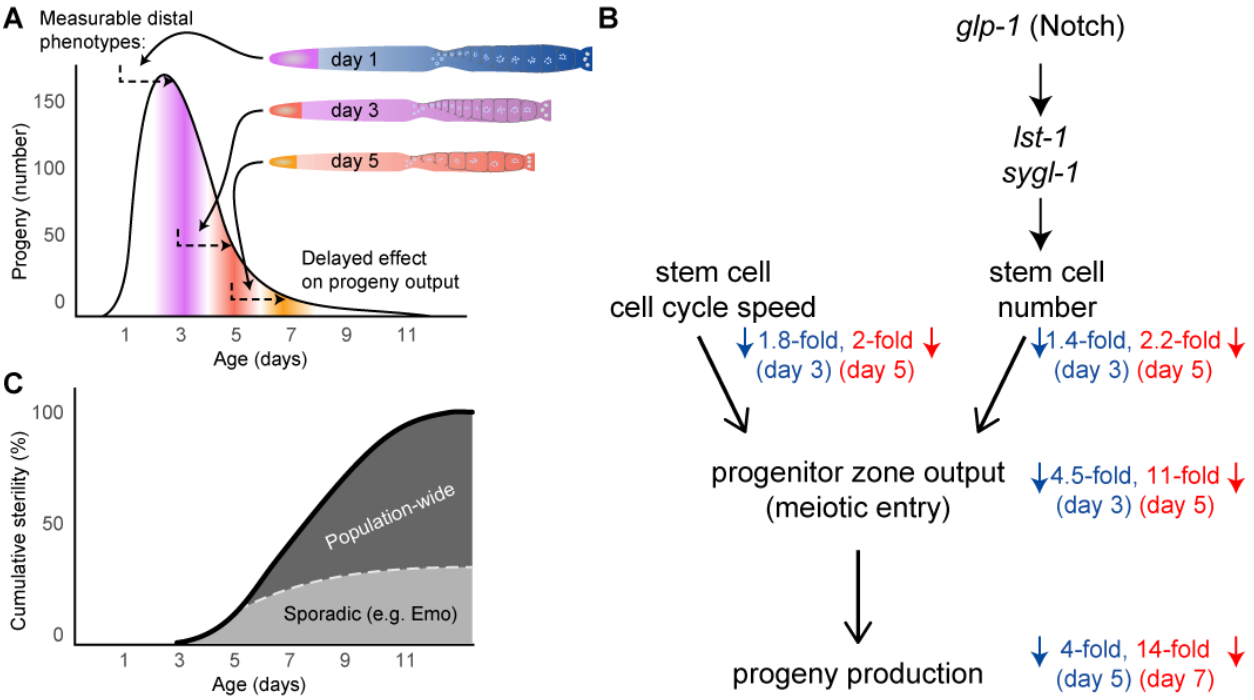

Fig.8: Model of age-related changes that drive reproductive decline in sperm-replete *C. elegans*. A) Diagrams of day 1, 3, and 5 germlines are shown with a typical wild-type progeny production curve (like in **Fig.1A**) to illustrate that PZ cells take two or more days to become oocytes and be laid as eggs. Thus, age-related changes in the PZ of day 3 and 5 adults affect egg laying on days 5 and 7, respectively. **B)** A model relating *glp-1* (Notch) activity and cell cycle dynamics to progeny production. Filled arrows indicate molecular pathway, line arrows indicate cell events from distal (top) to proximal (bottom). Blue and red numbers indicate fold-declines in function between peak and days 3, 5, and 7. **C)** The cumulative sterility of a population results from age-related changes that are both sporadic and population-wide. The dotted line indicates a projection of the relative contribution of sporadic defects (e.g. endomitotic oocytes) as a cause of sterility. Population-wide declines in stem cell number and activity contribute to the quantitative decline in progeny production in all animals and are the cause of sterility in a fraction of the population.

Age-related changes in Notch signaling and mitotic cell cycling were associated with reproductive decline

GLP-1/Notch signaling is necessary for the germline stem cell fate (Austin and Kimble 1987). Based on our observation that the size of the PZ declined with age, we hypothesized that the extent of GLP-1/Notch signaling declines with age, leading to a decrease in germline stem cell number. We measured the extent of expression of two GLP-1/Notch effectors, *sygl-1* and *lst-1*; these genes are direct transcriptional targets of the GLP-1/Notch intracellular domain transcription complex and are redundantly necessary and singly sufficient for the stem cell fate (Kershner *et al.* 2014; Lee *et al.* 2016). Expression of SYGL-1 encompassed ~81 distal-most cells in day 1 adults, decreasing by ~1.4-fold at day 3. As SYGL-1 expression is sufficient for the stem cell fate, the number of SYGL-1 expressing cells provides a measure of stem cell number (Shin *et al.* 2017). LST-1 expression was more limited, in the 38 distal-most cells in day 1 adults, decreasing ~1.4-fold at day 3. Interestingly, single molecule fluorescent *in situ* hybridization showed that the transcription of introns for both *lst-1* and *sygl-1* extends only ~5 cell diameters from the DTC (Lee *et al.* 2016), which closely matches the region of LST-1 accumulation, but is significantly shorter than that of SYGL-1 accumulation, consistent with posttranscriptional mechanisms functioning in extending SYGL-1 expression (Shin *et al.* 2017). We suggest that LST-1 is a more direct readout of the amount of GLP-1/Notch signaling and thus propose that GLP-1/Notch signaling decreases in day 3 and 5 adults. This proposal is consistent with the age-dependent enhancement of the premature meiotic entry phenotype in a weak *glp-1* loss-of-function mutant (Qin and Hubbard 2015). One way to test the hypothesis that

the age-related decline in Notch signaling is a cause of reproductive aging is to analyze mutant strains with altered Notch signaling. Chromosomal mutations that increase *glp-1* activity and transgenic constructs that increase *sygl-1* activity have been reported (Pepper *et al.* 2003; Shin *et al.* 2017), and if these manipulations delay reproductive aging it would provide direct support for our hypothesis.

The mitotic cell cycle duration doubled by day 3 of adulthood, with the proportions of the cell cycle phases unchanged and no cell cycle quiescence. Similarly, there is a slowing of cell cycle duration in *Drosophila* female germline aging (Kao *et al.* 2015). The doubling of cell cycle duration is not due to a decrease in GLP-1/Notch signaling, as cell cycle duration is unaffected in weak *glp-1* loss-of-function mutants that decrease stem cell number (Fox and Schedl 2015; Lee *et al.* 2016). In contrast to aging in day 3 mated adults, starvation at various life cycle stages (L1, L2 and mid-L4) results in germline quiecence, with a G2 cell cycle arrest (Fukuyama *et al.* 2006; Baugh 2013; Narbonne *et al.* 2015; Seidel and Kimble 2015). Likewise, PZ quiescence in the absence of sperm also appears to be in G2-phase (Narbonne *et al.* 2015; Qin and Hubbard 2015). Thus, the mechanisms affecting cell cycle changes during aging in mated hermaphrodites appear to be distinct from those described to occur during starvation and the absence of sperm. The doubling of cell cycle duration and the decrease in stem cell number (GLP-1/Notch signaling) provide an informed point to further define the systemic molecular mechanisms that account for the rapid, population-wide changes in the distal germline.

The evolutionary biology of reproductive aging

Detailed measurements of reproductive aging raise the intriguing question: what selective forces during evolution sculpted the progeny production curve so that it displays such a dramatic

decline early in life? Two long-standing theories are based on the premise that an organism achieves reproductive success by generating as many progeny as possible. According to this logic reproductive aging is a deleterious trait because it decreases progeny production. Medawar (1952) proposed that extrinsic mortality creates a "shadow of selection" that gradually prevents natural selection from favoring animals with a longer reproductive span. Williams (1957) proposed that selection for high levels of early reproduction causes a decline of late reproduction as a result of antagonistically pleiotropic genes. By contrast, the optimal progeny number theory proposed by Hughes et al. (2007) is based on the premise that an organism achieves reproductive success by generating an optimal number of progeny – not too few and not too many. According to this logic, reproductive aging is an adaptive trait that contributes to sculpting the progeny production curve to achieve the optimal number. It is apparent that reproductive success is not as simple as the number of F1 progeny generated by the P0 parent – a more sophisticated perspective is the number of F1 progeny that mature to be reproductive adults and generate F2 progeny. The extension of this logic is that reproductive success must be judged based on an organism's long-term contribution to the gene pool measured after innumerable generations. Thus, reproductive success is related to long-term population dynamics. Individuals are part of populations that exist in ecological niches with finite resources. If the population exceeds the carrying capacity of the ecological niche, then there will be widespread deprivation and population instability characterized by cycles of boom and bust. Thus, reproductive success is fostered by individual reproductive patterns that promote stable population dynamics. By limiting progeny production, reproductive aging may be a cause of reproductive restraint that promotes the optimal progeny number and leads to adaptive population dynamics.

The results presented here do not directly test evolutionary theories, but they relate to these theories in two important ways. First, we demonstrated that reproductive aging in *C. elegans* is primarily caused by population-wide changes in stem cell number and activity and only rarely caused by sporadic defects such as endomitotic oocytes. This pattern is suggestive of an evolved genetic program that controls the decline of reproduction, consistent with a prediction of the optimal progeny number theory. Second, our results document a very early decline in germline function, long before comparable declines in somatic function. This pattern suggests that during evolution somatic tissues were selected to be durable during the rise and fall of reproductive function, so that somatic aging does not limit reproduction. We speculate that this pattern facilitates selection to accelerate or delay reproductive aging as a way to manipulate progeny number, since somatic function is not the limiting factor. An important test of these evolutionary theories will be to experimentally determine how reproductive aging influences population dynamics over many generations. To this end we are developing a laboratory ecosystem to measure population dynamics and a simulation model to determine how the progeny production curve and reproductive aging affect population dynamics.

Materials and Methods

Strains and General Methods

C. elegans strains were cultured at 20°C on 6 cm Petri dishes containing nematode growth media (NGM) agar and a lawn of *E. coli* strain OP50 unless otherwise noted. The wild-type *C. elegans* strain and parent of edited strains was Bristol N2 (Brenner 1974). Mated, wild-type N2 hermaphrodites were used except: unmated self-fertile N2 hermaphrodite data (**Fig.1A,S5**) and mated hermaphrodites with the genotype *lst-1(am302)* and *sgyl-1(am307)* in which the endogenous loci encode the FLAG epitope (**Fig.7,S10**).

Males of the strain CB4855 ("Mr. Vigorous") were used to mate hermaphrodites because these males display a higher mating ability – they also deposit a copulatory plug after mating (Hodgkin and Doniach 1997). Strains were obtained from the CGC unless otherwise noted.

Animals were synchronized by picking fourth-stage larvae (L4), defined as day 0, from populations that had not experienced starvation for a minimum of three generations. For mating experiments, 30-50 L4 hermaphrodites were cultured on a dish with 30-50 young adult males (at a 1:1 ratio) for 24 hours, then the hermaphrodites were removed from the males. The presence of copulatory plugs on many of the hermaphrodites confirmed a high frequency of mating in the population; however, hermaphrodites without a copulatory plug were not excluded from the experiment. Hermaphrodites were moved to fresh NGM+*E. coli* OP50 dishes daily until they reached the desired age.

To measure progeny production of mated hermaphrodites, we placed 30 L4, wild-type hermaphrodites and 30 young adult, CB4855 males on a Petri dish with abundant food for 24 hours. After 24 hours (adult day 1), we placed each mated hermaphrodite on an individual dish, transferred the animal to a fresh dish daily, and two days later scored the number of live progeny

produced daily. This method provides accurate and precise measurements of daily progeny production, consistent with previous findings (Hughes *et al.* 2007). Because animals were mated in groups, we did not obtain progeny counts for the first 24 hours for the mated animals in **Fig.1A**. To measure progeny production of self-fertile hermaphrodites, we placed each L4 hermaphrodite on an individual dish, transferred the animal to a fresh dish daily, and two days later scored the number of live progeny on the dish.

Previous studies showed that exposure to a high concentration of males or male pheromone reduced longevity and caused shrinking of hermaphrodites (Maures *et al.* 2014; Shi and Murphy 2014). The damage appears to be caused by functional sperm,but not seminal fluid (Shi and Murphy 2014). In the experiments described here, male exposure was limited to the minimum required for sperm transfer. Under these conditions, day 3 adults that were mated and self-fertile displayed a similar size of the distal germline or extent of the PZ (**Fig.S5**); at day 3 most of the unmated hermaphrodites are still self-fertile, and thus the PZ has not become quiescent due to the absence of sperm (Narbonne *et al.* 2015; Qin and Hubbard 2015). Previous work in our labs showed no effect of brief mating on the longevity of hermaphrodites (Pickett *et al.* 2013).

Generating alleles encoding the FLAG epitope using CRISPR/Cas9

To visualize the localization of LST-1 and SYGL-1, we engineered alleles that encode the FLAG epitope (C-terminal *lst-1(am302[lst-1::flag])*, in which all 6 predicted LST-1 isoforms are fused to FLAG, and N-terminal *sygl-1(am307[flag::sygl-1])*. Generally, the co-CRISPR approach was used to edit genomic loci (Arribere *et al.* 2014). Guides and repair templates were designed in ApE (Davis 2016) (**Table 1**). Oligonucleotides and gblocks were purchased from

IDT. gblocks were amplified by PCR, purified using an Invitrogen PCR cleanup kit, concentrated using ethanol precipitation, and then resuspended in Tris-EDTA buffer. Guide oligonucleotides were ligated into Mike Nonet's derivative of pDR274 (previously digested with BsaI-HF and purified on a Quiagen column) to generate guide RNA expression plasmids, which were transformed into competent DH5-alpha cells. Plasmids were purified using a Quiagen miniprep column according to manufacturer's instructions, including the extra PB wash, and resuspended in Tris-EDTA buffer. All new plasmids were confirmed by sequencing.

Injection mixes were diluted into water and contained Cas9-expressing pDD162 (gift of Mike Nonet) at 50ng/ul, *dpy-10* guide plasmid (pMN3153) at 20ng/ul, *dpy-10(cn64)* repair oligonucleotide AFZF827 at 500nM, our gene-of-interest guide plasmids at 40ng/ul for each plasmid, a ssDNA repair template at 600nM or a dsDNA repair template at between 50ng/ul and 500ng/ul. Approximately 30 young adult P0 animals were injected in one or both gonads and recovered in recovery buffer (5mm HEPES pH 7.2, 3 mM CaCl2, 3 mM MgCl2, 66 mM NaCl, 2.4 mM KCl, 4% Glucose (w/v)) on NGM dishes.

Young adult F1 hermaphrodites were screened for the Rol or Dpy phenotype, and mutant animals were picked singly or in groups of up to 8 to fresh NGM dishes and allowed to produce progeny overnight. Next, animals were picked into 10ul of 1X PCR buffer containing 0.1 mg/mL Proteinase K, incubated at 65 °C for 60 minutes and then at 95 °C for 30 minutes to inactivate Proteinase K. Using primers that hybridize outside of the homology template, PCR was used to detect insertions of 66nt (New England Biological). The young adult F2 progeny of homozygous or heterozygous edited F1 animals were picked to individual dishes and genotyped in a similar manner. The DNA sequence of the PCR product from homozygous edited F2 progeny was

determined to confirm the in-frame insertion of DNA encoding the FLAG epitope. Strains were outcrossed to N2, resulting in WU1756 and WU1770 for *lst-1* and *sygl-1*, respectively.

To address the possibility that insertion of DNA encoding the epitome tag disrupted the activity of the *lst-1* or *sygl-1* gene, we performed a functional test. Neither *lst-1(null)* nor *sygl-1(null)* single mutants display a visible phenotype, whereas *lst-1(null);sygl-1(null)* double mutants (or double RNAi knockdowns) display a sterile phenotype. We used RNAi to knock down the expression of *sygl-1* in *lst-1(am302)* animals or *lst-1* in *sygl-1(am307)* animals. We did not observe a sterile phenotype in either case, indicating that these alleles retain gene activity.

Table 1: CRISPR/Cas9 plasmids and oligonucleotides specific to this study

Locus	Corresponding Plasmid	Oligo name	Sequence	Notes
lst-1	pZK07	ZK034	TTTGGAAGAACATTTGAAGGGGG	g4
	pZK07	ZK035	AAACCCCCCTTCAAATGTTCTTC	g4
	pZK13	ZK073	TTTGTTGCTCAACTCGATCGTGC	g16
	pZK13	ZK074	AAACGCACGATCGAGTTGAGCAA	g16
	NA	ZK038	AAAAATCTTCTCAAATTATTATTATTTCAG ATGTCCCCGTTTATGGTTCGCTCAATTGGA CCGAGCAGGTTCAGAGATGGTGGAGCAGA TGGGACACGCTCGAAATGTTCCAGTCGACT ACAAAGACCATGACGGTGATTATAAAGAT CATGATATCGATTACAAGGATGACGATGA CAAGTAAGCAATAAAATTGGTTTAAATAT CAATTAATTTATATTTTACGACCCGCTTGA ATAGTTCTTCTTGTTTTACACTATCATCCAA AAAAATGCGGTTC	gblock
	NA	ZK039	AAAAATCTTCTCAAATTATTATTATTTCAG A	amplify gblock
	NA	ZK040	GAACCGCATTTTTTTGGATG	amplify gblock
	NA	ZK028	CACTTTATGATATGCAAGGACGAG	geno-typing
	NA	ZK029	CAAAAGAGCACATGGATATACAGC	geno-typing
sygl-1	pZK15	ZK041	TTTGGACGTCAGAGACGATGAGG	g1
	pZK15	ZK042	AAACCCTCATCGTCTCTGACGTC	g1
	pZK17	ZK043	TTTGTGGAATGGCATTATGCACG	g5

	pZK17	ZK044	AAACCGTGCATAATGCCATTCCA	g5
	pZK20	ZK045	TTTGAACTCTACATGGATCACCG	g6
	pZK20	ZK046	AAACCGGTGATCCATGTAGAGTT	g6
	NA	ZK049	TTCAGCGATCATCGAACCATTGTCATCACG CCACGTGCATAATGGACTACAAAGACCAT GACGGTGATTATAAAGATCATGATATCGA TTACAAGGATGACGATGACAAGCCATTCC ATTATCCAAAATTATATATGGACCATCGCG GAAACATGTCTACGTCTTCGTCTCTGACGT CATCGACAACCGCCACGTCATCA	repair oligo
	NA	ZK047	ATCTACCCGCCGATTTTCTAAT	geno-typing
	NA	ZK048	ATCTCCAAGTGTTGCACATAACC	geno-typing

EdU labeling experiments

To make EdU dishes, we seeded M9 agar dishes (Stiernagle 2006) with concentrated *E. coli* MG1693 Thy- which had been grown for 24 hours at 37C with shaking in minimal media containing 20uM 5-ethynyl-2'-deoxyuridine (EdU, Invitrogen). The culture consisted of 100mL M9, 4ml overnight LB-grown MG1693 *E. coli*, 5ml 20% glucose, 50ul 1.25mg/ml thiamine, 1.2ml 0.5mM thymidine, 100ul 1M MgSO4, 200ul 10mM EdU (Fox *et al.* 2011).

Appropriately mated and aged animals were either washed with phosphate buffered saline (PBS) or picked to EdU dishes and incubated for the appropriate time: 0.5, 4, 7, or 10 hours. Cells with any amount of EdU signal overlapping with DAPI staining were scored as EdU-positive. We defined S-phase index as the proportion of all progenitor zone cells (WAPL-1-positive) that were also EdU-positive. For the full detailed protocol, see Kocsisova et al. (2018a)

In day 5 hermaphrodites, a subpopulation displayed robust EdU labeling and a subpopulation displayed a complete lack of EdU labeling (**Fig.S6A-C**). When fed EdU for 0.5 hours, 85% of day 5 animals showed no EdU-positive cells. In the remaining 15% of animals,

the average S-phase index was 53% (range 31.5 - 76.7% of cells), which is not significantly different than the S-phase index for day 1 or 3 hermaphrodites (**Fig.4G**). In 29 of 33 day 5 animals fed EdU for 0.5 hours where both germlines were visible, either both germlines displayed EdU incorporation or both germlines displayed no EdU incorporation (intraclass correlation coefficient = 0.75, $p<0.0001$). In the remaining 4 of 33 day 5 animals, two germlines were discordant for EdU labeling (**Fig.S6D**). Soaking day 5 animals in a solution of 500 μM EdU in M9, as described in Furuta et al., (2018), also resulted in a subpopulation that completely lacked EdU labeling. As the duration of EdU feeding increased, so did the proportion of animals showing labeling. When day 5 animals were fed EdU for 4 hours, 81% of animals displayed EdU-positive cells (range 48.1% to 94.4% of cells). Our observation that older animals frequently displayed no EdU incorporation following a short duration of EdU exposure but only infrequently displayed this following a longer duration of EdU exposure is similar to findings reported by Cinquin et al., (2016).

We observed that both EdU-positive and EdU-negative animals displayed EdU labeled bacteria in the intestinal lumen, indicating that both groups of animals successfully ingested EdU labeled bacteria. One possible explanation for animals that do not incorporate EdU is that some day 5 hermaphrodites are inefficient in intestinal absorption of EdU, transport of EdU to the germline, and/or incorporation of EdU into DNA. Alternatively, some day 5 hermaphrodites may be susceptible to trauma following transfer from one dish to another, resulting in a temporary block in EdU incorporation. Alternatively, in some day 5 hermaphrodites all progenitor zone cells may be arrested in a cell cycle phase other than S-phase. In this case, the arrest appears to be transient, because we observed (a) scattered M-phase cells in germlines that lacked EdU labeling, indicating that in these germlines most cells were in a Gap-phase or arrested while

others were in M-phase, (b) longer durations of EdU exposure resulted in a significantly higher proportion of EdU labeled animals, and (c) in EdU pulse-chase experiments, the distal germline did not contain cells with intense EdU labeling, indicating that all stem cells underwent several cell divisions during the 48 hour chase. To our knowledge, there is no method to unambiguously identify S-phase cells in the *C. elegans* germline without feeding or injecting nucleotide analogs (van den Heuvel and Kipreos 2012; Kocsisova *et al.* 2018a; b).

Dissection and Immunohistochemistry

The dissection and staining protocol follows the batch method (Francis *et al.* 1995), where all dissected tissues were incubated within small glass tubes rather than on a slide. Animals were washed with phosphate-buffered saline (PBS) into a dissecting watchglass (Carolina Biological Item # 742300), immobilized with Levamisole (final concentration 200uM), and dissected with a pair of 25G 5/8" needles (PrecisionGlide from BD) by cutting at the pharynx and/or at the tail. Dissected gonads were fixed in 2 mL 3% paraformaldehyde (PFA) (10 mL 16% PFA, EM Grade, Electron Microscopy Sciences, Hatfield, PA Catalog No 15710) phosphate-buffered solution for 10 minutes at room temperature and then post-fixed with 2 mL 100% methanol (Gold-label from Fisher) at -20C for 1 hour or longer (up to several days).

In the past there were discrepancies in the literature possibly due to different analysis methods in very old worms: in situ analysis versus dissected gonads. To circumvent this issue, we performed dissections at time points when these discrepancies are less likely to be a problem.

Fixed gonads were rehydrated and washed three times in PBS + 0.1% Tween-20 (PBSTw), then incubated in 100ul of primary antibody at room temperature for 4-24 hours, washed 3 times in PBSTw, and incubated in 100ul of secondary antibody at room temperature or

4C for 2-24 hours. Antibodies were diluted in 30% goat serum (Gibco C16210-072) in PBS. Primary antibodies used were: rabbit-anti-WAPL-1 (Novus Biologicals Cat#49300002, Lot G3048-179A02) (1:2000), mouse-anti-MSP (Major Sperm Protein) (Miller *et al.* 2001) (1:2000), mouse-anti-pH3 (Millipore clone 3H10 Cat#05-806, Lot#2680533) (1:500), mouse-anti-FLAG (SIGMA M2, purified in-house) (1:1000). Secondary antibodies were: goat-anti-mouse IgG-conjugated Alexa Fluor 488/594/647, goat-anti-rabbit IgG-conjugated Alexa Fluor 488/594/647 (Invitrogen).

Following antibody staining, gonads were washed 3 times in PBSTw. An EdU Click-iT reaction was performed according to manufacturer's instructions (Invitrogen C10350), using 100ul reagent for a 30 minute incubation, followed by a quick wash in manufacturer-supplied rinse buffer and four ~15 minute washes in PBSTw. Stained gonads were resuspended in 1 drop of Vectashield containing 4',6-Diamidino-2-Phenylindole Dihydrochloride (DAPI) (Vector Laboratories H-1200), applied to a large pre-made agarose pad on a glass slide, and covered with a 22 mm x 40 mm #1 cover glass. The slide was allowed to settle overnight at room temperature, sealed with clear nail polish, and stored at 4 °C as needed. Images were acquired within 72 hours when possible.

Confocal Imaging

Images were collected using a Zeiss Plan Apo 63X 1.4 oil-immersion objective lens on a PerkinElmer Ultraview Vox spinning disc confocal system on a Zeiss Observer Z1 microscope using Volocity software. Approximately twenty 1 μm z-slice images were acquired for each gonad. Images were exported as hyperstack .tif files for further analysis.

Image analysis

Images were stitched either in Volocity or using the Image J plugins for pairwise stitching and Grid/Collection of sequential images (Preibisch *et al.* 2009). Images were rotated, cropped, arranged, and annotated in Illustrator (Adobe).

Cells were manually counted in each z-slice where they occurred. The person performing counts was not blinded to experimental groups, because the differences were generally obvious to an experienced observer. Counts of cells were performed in Fiji/ImageJ (Schindelin *et al.* 2012) using the Cell Counter plug-in (De Vos 2015; Rasband 2016). To remove multiply-counted cells, a modified version of the R-script Marks-to-Cells was used (Seidel and Kimble 2015). This script improved the precision of cell counts in the germline.

Nuclear morphology: DAPI staining was used to assess meiotic prophase stages, nuclear counts, row counts and progression of gametogenesis. Endomitotic oocytes in the proximal gonad arm, distal to the spermatheca, were recognized as large DAPI stained blobs. Endomitotic oocytes are known to result from failure to coordinate meiotic maturation of diakinesis stage oocytes with ovulation, resulting in the unfertilized mature oocytes that are mitotic cell cycling without cytokinesis because of the absence of the sperm derived centriole (Iwasaki *et al.* 1996; McCarter *et al.* 1997; Greenstein 2005). This is distinct from endomitotic oocytes in the uterus, which naturally occur in older unmated hermaphrodites that have exhausted their self-sperm. In this case the most proximal oocyte undergoes low-frequency spontaneous maturation and ovulation, but because there is no sperm in the spermatheca the matured but unfertilized oocyte begins endomitotic cycling (McCarter *et al.* 1999). Endomitotic oocytes were identified from dissected germlines; as the proximal germline was not always visible, this raises the possibility that the frequency was under-estimated.

Distal tip cell nucleus: The DTC nucleus was identified by its position at the exterior of the distal gonad and bright WAPL-1 staining. When analyzing the shift of the DTC nucleus, we chose a stringent cutoff of 5 c.d., because of a concern that a DTC nucleus might shift by one or two c.d. due to physical forces during dissection and staining. We did analyze our data with the cutoff set to 2 c.d., and even with this broad definition of "shifted" DTC nucleus, the majority of germlines were "normal".

Progenitor zone: The PZ has been previously called the mitotic zone or the proliferative zone. We employed staining with the cohesin chaperone WAPL-1 to measure the size of the PZ (Mohammad *et al.* 2018). In mated hermaphrodites, the total number of PZ cells was 215 +/- 25 in day 1 adults, and it decreased to 163 +/- 47 in day 3 animals, and to 126 +/- 45 in day 5 animals. A similar number of PZ cells, ~230, was found for day 1 unmated hermaphrodites using a combination of the nucleoplasmic REC-8 staining PZ marker and the meiotic prophase marker HIM-3 (Hansen *et al.* 2004a; Fox *et al.* 2011; Fox and Schedl 2015). Other studies of unmated day 1 hermaphrodites used the crescent-shaped DAPI morphology of leptotene cells to approximate the proximal boundary of the PZ and found that the PZ contains ~214 (Korta *et al.* 2012), ~205 (Roy *et al.* 2016), or ~225 cells (Seidel and Kimble 2015). Our day 1 PZ cell numbers for mated hermaphrodites are thus similar to PZ cell numbers for unmated day 1 hermaphrodites reported in other studies; therefore, mating did not have a significant effect on PZ cell numbers at day 1. Prior studies of changes in PZ cell number during aging with unmated hermaphrodites report the following: Hubbard and colleagues found ~250 PZ cells in day 1 adults, ~156 by day 3, ~100 by day 6, ~50 by day 12 (Killian and Hubbard 2005; Qin and Hubbard 2015); Murphy and colleagues reported a decrease in PZ cell number from ~220 at day 2 to ~150 at day 6 in unmated hermaphrodites (Luo *et al.* 2010); and Kimble and colleagues

reported that PZ cell number remained unchanged up to day 6 of adulthood (day 1 ~243, day 2 ~227, day 3 ~214) (Crittenden *et al.* 2006). In mated hermaphrodites, Shi and Murphy (2014) found a decrease in the number of PZ cells with age, from ~150 in day 1 to ~100 in day 2 through day 4. However, under the conditions employed the mated hermaphrodites displayed damage to the soma (body size shrinkage), which was not the case with the conditions employed in the experiments described here. The Hubbard and Narbonne groups reported that starting at day 3 and older, when unmated hermaphrodites have become sperm depleted (or in younger adult genetic females), the absence of sperm, and thus flux through the germline, results in mitotic cell cycle arrest of PZ cells, likely in G2 phase (Narbonne *et al.* 2015; Qin and Hubbard 2015). One interpretation of this finding is that the mitotic cell cycle quiescence of the PZ in the absence of sperm is a physiological mechanism of preserving the germline during aging, in anticipation of subsequent mating. To avoid this preservation mechanism in our studies of germline aging, we always used mated hermaphrodites.

M-phase cells and the presence of sperm: Cells in M-phase were detected by staining with mouse anti-phospho-histone 3 (pH3) antibody, while sperm were identified by staining with mouse anti-MSP (Major Sperm Protein) antibody. In these co-staininig experiments, M-phase cells and sperm were distinguished by (1) position in the germline and (2) DAPI morphology; M-phase cells were in the PZ at the distal end of the germline, while sperm were in the spermatheca at the proximal end of the gonad. Stages of M-phase (prophase, metaphase & anaphase) were analyzed in cells detected with pH3 antibody; minimal differences were observed between day 1, 3 and 5 (**Fig.S7**).

SYGL-1 and LST-1: The length in cell diameters and the number of cells in the PZ that contain cytoplasmic SYGL-1 and LST-1 were assessed with anti-FLAG antibody staining using

strains in which CRISPR genome editing was employed to insert DNA encoding a 3xFLAG epitope into the endogenous locus. In day 1 animals, we observed staining similar to that reported by Shin et al. (2017). However, we note that at day 3 and 5, the length of the SYGL-1 staining region could be similar to the length of the PZ, as assessed by WAPL-1 staining (i.e. only a few WAPL-1-positive, SYGL-1 negative cells were observed).

Germline stem cell differentiation occurs through essentially direct differentiation and thus lacks transit-amplifying divisions; following loss of GLP-1 Notch signaling, germ cells complete their ongoing mitotic cell cycle and then begin meiotic S-phase (Fox and Schedl 2015). SYGL-1 activity is sufficient for the stem cell fate (Kershner *et al.* 2014; Lee *et al.* 2016; Shin *et al.* 2017). However, it is unknown if all cells that are expressing endogenous levels of SYGL-1 are stem cells. There is a noticeable gradient of SYGL-1 staining between the highly-expressing distal-most and lowly-expressing proximal-most cells, raising the possibility that the level of SYGL-1 in the proximal-most cells is not sufficient to promote the stem cell fate and inhibit the meiotic fate. Additionally, Spike et al. (2018) have shown that RNA binding proteins LIN-41 and GLD-1 are post-translationally inactivated prior to their degradation; similarly, proximal SYGL-1 may be inactivated prior to degradation. Thus, while the extent of SYGL-1 accumulation provides a readout that is correlated with stem cell identity, detectable SYGL-1 accumulation cannot currently be used to define the number of stem cells.

Meiotic entry and nurse cells: Most cells that exit the progenitor zone and enter meiosis in an adult hermaphrodite do not become oocytes. Instead, these cells function as nurse cells and undergo apoptosis. We calculated the nurse cell proportion following the method outlined in Agarwal et al. (2018). We compared the output of the progenitor zone on days 1, 3, and 5 (**Fig.5B, Supplemental Table 5**) to the number of embryos (and therefore oocytes) produced on

days 3, 5, and 7, then divided by 2 to account for two gonads per animal (**Fig.1A, Supplemental Table 1**). The two-day difference was used to account for the time required for a cell to progress through meiotic prophase (**Fig.S9, Supplemental Table S9**). We defined the nurse cell proportion as 1-(0.5 * # oocytes per hour / # cells entered meiosis per hour in one gonad).

Statistical Analysis

Statistical analyses were performed in R (R Core Team 2013) using R studio (RStudio Team 2015) and the following packages: ggplot2 (Wickham 2009), svglite, plyr, gridExtra, grid, lattice, multcomp, car, broom, psych, FSA, fifer. Individual measurements and script used to analyze them are provided in Supplemental Tables and files. Depending on the type of variable, the following tests were performed and are indicated in the text and Figure legends with the relevant test name abbreviation. KW test: for continuous measurement variables, the Kruskal-Wallis Rank-sum test was used with a Dunn post-hoc and p-values adjusted with the Benjamini-Hochberg FDR method. Data were also compared using an ANOVA with a Tukey post-hoc test. PC test: for categorical measurement variables, the Pearson's Chi-squared test of independence was used with post-hoc p-values adjusted with the False Discovery Rate method. PIC test: to test for linear relationships between variables, we used the Pearson's *inter*class correlation. ICC test: used for *intra*class correlations to compare the pooled variance between pairs of germlines from one animal and pooled variance within pairs (Shrout and Fleiss 1979). Boolean variables were treated as TRUE = 1, FALSE = 0 for purposes of correlation analysis. All error bars shown in figures represent the mean +/- standard deviation. NS indicates P>0.05, * P<0.05, ** P<.001, *** P<.0001.

All data were subjected to consistent exclusion criteria. Animals that displayed evidence of matricidal hatching or sperm depletion (as indicated by lack of Major Sperm Protein immunofluorescence) were excluded from all analyses. Animals that displayed sporadic phenotypes such as endomitotic oocytes, a shifted DTC nucleus, or failure to exhibit any EdU staining are reported, but were excluded from further analyses. Exact statistical methods and exclusion criteria are provided in the supplemental R script.

Chapter 6:

Germline aging in *Caenorhabditis* and mutants of *C. elegans*

The work presented in Chapter 6 is in preparation for submission with the following authors:

Kocsisova Z., Bagatelas, E.*, Santiago, J.*, Hanyue, C.L.*, Mosley, M., Egan, B.E., Schneider, D.L., Baer, C., Schedl T.,‡ Kornfeld K.‡

*,‡ These authors contributed equally.

Mid-life reproductive improvement results from loss-of-function in nutrient sensing and gain-of-function in Notch signaling in *C. elegans*

Introduction:

Successful reproduction is the ultimate goal of an organism. Therefore the age-related decline of reproductive function is likely to be critical for the evolution of aging. From a single fertilized egg, the *C. elegans* hermaphrodite develops its entire soma and both arms of its reproductive tract and begins laying eggs at ~65 hours at 20°C (Byerly *et al.* 1976). At the peak of reproduction, oocytes are ovulated every ~23 min (McCarter *et al.* 1999), resulting in an average of ~150 progeny per day. Even when sperm are not limiting, reproduction ceases relatively early in life: at 20°C on standard nematode growth medium seeded with live *E. coli* OP50, in wild-type hermaphrodites with excess sperm from mating to males, the reproductive span is 8.8 ± 1.8 days and the lifespan is 15.6 ± 3.3 days (Pickett *et al.* 2013). Further, progeny production declines from a peak of ~150 progeny per day on adult day 2 to ~40 progeny per day on adult day 5 and to ~12 progeny per day on adult day 7, while the animals are all still alive, moving, and feeding (Kocsisova *et al.* 2019). This suggests that the age-related decline in reproductive function may not be caused primarily by a decline in somatic functions that maintain survival.

In nematodes, somatic aging has been studied far more than reproductive aging, and reproductive aging has been studied nearly exclusively in *C. elegans*. When Hughes et al. (2007) tested whether the use of the reproductive tract contributes to its degeneration with age, they used a *C. elegans* germline feminization mutant to be able to study aging in females, yet in a hermaphroditic species. The interpretation of this finding – that early progeny production does not appear to carry a cost to late progeny production – has led to discussions about theories of aging which invoke tradeoffs. However, the experiments carry the usual caveats of pleiotropies

of mutations and the difficulty of placing *fog-2* animals into an evolutionary context (Hughes *et al.* 2007). *C. elegans* is a great system for comparative studies. The genus *Caenorhabditis* contains 63 species. At least three of these are hermaphroditic (*C. elegans, C. briggsae,* and *C. tropicalis*) while the remaining species exhibit the ancestral gonochoristic (male and female) reproductive strategy (e.g. *C. brenneri*, *C. remanei*, and *C. angaria*) (Kiontke *et al.* 2011). In order to generalize conclusions about reproductive aging in nematodes, we examined the pattern of reproductive aging in two gonochoristic species, *C. brenneri* and *C. remanei*.

Previous studies of reproductive aging focused on late-life fertility (the tail of reproduction). While nearly 100% of wild-type hermaphrodites regain fertility when mated on adult day 8, only 50% do so when mated on day 10, and none regain fertility when mated on day 15 (Mendenhall et al. 2011). Progeny production, when analyzed as the number of progeny produced on each day of life, is a quantitative phenotype. It is possible to analyze it as a discrete phenotype: fertile versus sterile (Luo *et al.* 2009; Wang *et al.* 2014). However, this process essentially equates an animal producing 1 egg per day to an animal producing 150 eggs per day, and some studies examined the sum of progeny produced on and after day 10 in mated hermaphrodites (Hughes *et al.* 2007, 2011) or on and after day 11 in self-fertile hermaphrodites (Gems *et al.* 1998). However, the most striking decline in reproduction occurs much earlier, at approximately day 5 of adulthood, when mated wild-type *C. elegans* produce only ~40 progeny – a quarter of peak reproduction. We reasoned that interesting age-related changes in the germline occur a day or two before this decrease in progeny production. Here, we measured the daily progeny production of mated hermaphrodites. We categorized reproduction into three periods: **early (days 1-4), mid-life (days 5-7), and late** (day 8+).

Many age-related changes in the morphology and cellular function of the germline have been described (reviewed in Chapter 2). Recently, we described the **molecular and cellular changes** that underlie the functional decline in egg production, with the rationale that identifying changes in the germline which correlate with the decline in progeny production would lead us to identify the causes of the decline in reproduction (Kocsisova *et al.* 2019). Here we build on that study of wild-type reproductive aging by examining germline aging in three *C. elegans* mutants previously published to extend reproduction. We also present the results of a candidate-based screen for increased progeny production in *C. elegans* mutants previously published to extend lifespan.

In Kocsisova et al., (2019) we present the model that the age-related slowing of the stem cell cycle and decline in stem cell number cause reproductive aging. Two predictions follow from this model: 1) that increasing the number of stem cells and/or the rate of the stem cell cycle will reduce the rate of reproductive decline and 2) that mutations which extend reproductive span also delay the age-related declines in the germline. Here, we tested both of these predictions.

In this study, we identify a pattern of progeny production we call mid-life reproductive improvement. We found that that increasing the accumulation of a Notch effector is sufficient to increase mid-life reproduction and that long-reproductive mutants display a slower decline in meiotic entry, compared to wild-type. These results are consistent with the model we presented in (Kocsisova *et al.* 2019). In addition, we identified mutants that extend lifespan without compromising early progeny production and other mutants that increase reproductive ability without extending lifespan. These results indicate that while reproductive function and somatic lifespan are inter-linked, they are also separable.

Results:

I. Early reproductive decline is conserved in the genus *Caenorhabditis*

We measured the lifespan and progeny production of females of wild-type *C. brenneri* and *C. remanei*, as well as *fog-2* mutant (feminized) *C. elegans*. All females were continuously mated to conspecific males, as described in the methods. We noticed that in *C. brenneri* all males except one nearly always fled the Petri dish within 24 hours, when three males were placed with one female on each Petri dish. All three species experienced a peak of reproduction at days 2-3 of adulthood, followed by a decline in reproduction (**Figure 1**). Very few progeny were produced after day 8 (**Table S1**). In contrast, survival of animals was above 75% until day 10 (**Figure 1**). In mated females from both gonochoristic and androdioecious species in the genus *Caenorhabditis*, a decline in reproductive function occurred several days before animals began to die.

Several strains of gonochoristic species exhibited high levels of sterility and embryonic lethality, whereas *C. elegans* N2 embryonic lethality was 1.2% (n=171). *C. remanei* SB146 was initially relatively healthy, with a brood size average of 389 ± 273, but deteriorated within a few generations from receipt from the *Caenorhabditis* Genetics Center. In these experiments SB146 displayed very high levels of embryonic lethality, ~75% (n=319). *C. brenneri* CB5161 was very sickly with a brood average 15.2 ± 32.7, with half of the animals fully sterile. The average lifespan was 14.5 ± 6.1 days and embryonic lethality was higher than 90%. It is likely this is due to balanced lethal or sterile recessive polymorphisms, identified in genome sequencing (Eric Haag, personal communication). *C. brenneri* VX02253 displayed high levels of embryonic lethality ~55% (n=807). Even accounting for animals with delayed development, lethality was ~20% (n=515) when animals were scored after 4 hours, and many progeny which hatched late

remained arrested in the L1 stage. Broods from individual hermaphrodites showed a range of lethality ranging from 8% to 55%. Whereas protandrous species such as *C. elegans* are well-suited for laboratory culture of small populations, gonochoristic species such as *C. remanei* and *C. brenneri* experience a severe inbreeding depression that poses a challenge to laboratory studies of aging.

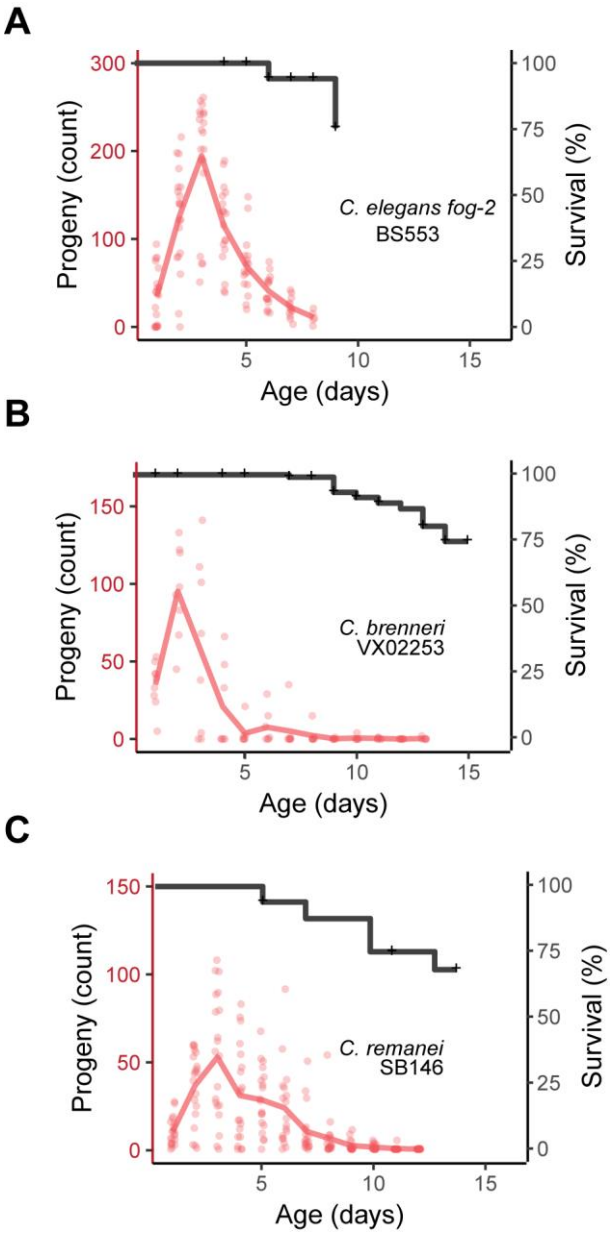

Figure 1: Early reproductive decline is conserved in the genus *Caenorhabditis*
The daily progeny production of mated females is plotted in red. The daily survival of mated females is plotted in black. Vertical marks on survival plots indicate animals were censored due to matricidal hatching or crawling off the dish. A) *C. elegans fog-2(oz40)*. B) *C. brenneri* strain BS553. C) *C. remanei* strain SB146.

II. Mutations in nutrient sensing pathways extend reproduction

Several mutants have been reported to extend reproduction in sperm-replete hermaphrodites. The number of progeny produced after day 10 is significantly higher in *daf-2(e1370), eat-2(ad465),* and in *phm-2(am117)* animals than in wild-type animals (Hughes *et al.* 2007, 2011; Kumar *et al.* 2019). We **confirmed** that *daf-2(e1370)* and *eat-2(ad465)* produced significantly more progeny on and after day 8 of life (61±28 and 65±32, respectively) than wild-type (11±11) (**Figure 2A,B,F**). *phm-2(am117)* animals produced more progeny on and after day 8 (26±26) than wild-type, but the difference was not significant at this sample size; only 4 mated wild-type animals avoided death by matricidal hatching by day 8 of life (**Figure 2F**). We also noted that the early brood size and total brood size of all three mutants was significantly smaller than wild-type (**Figure 2D**).

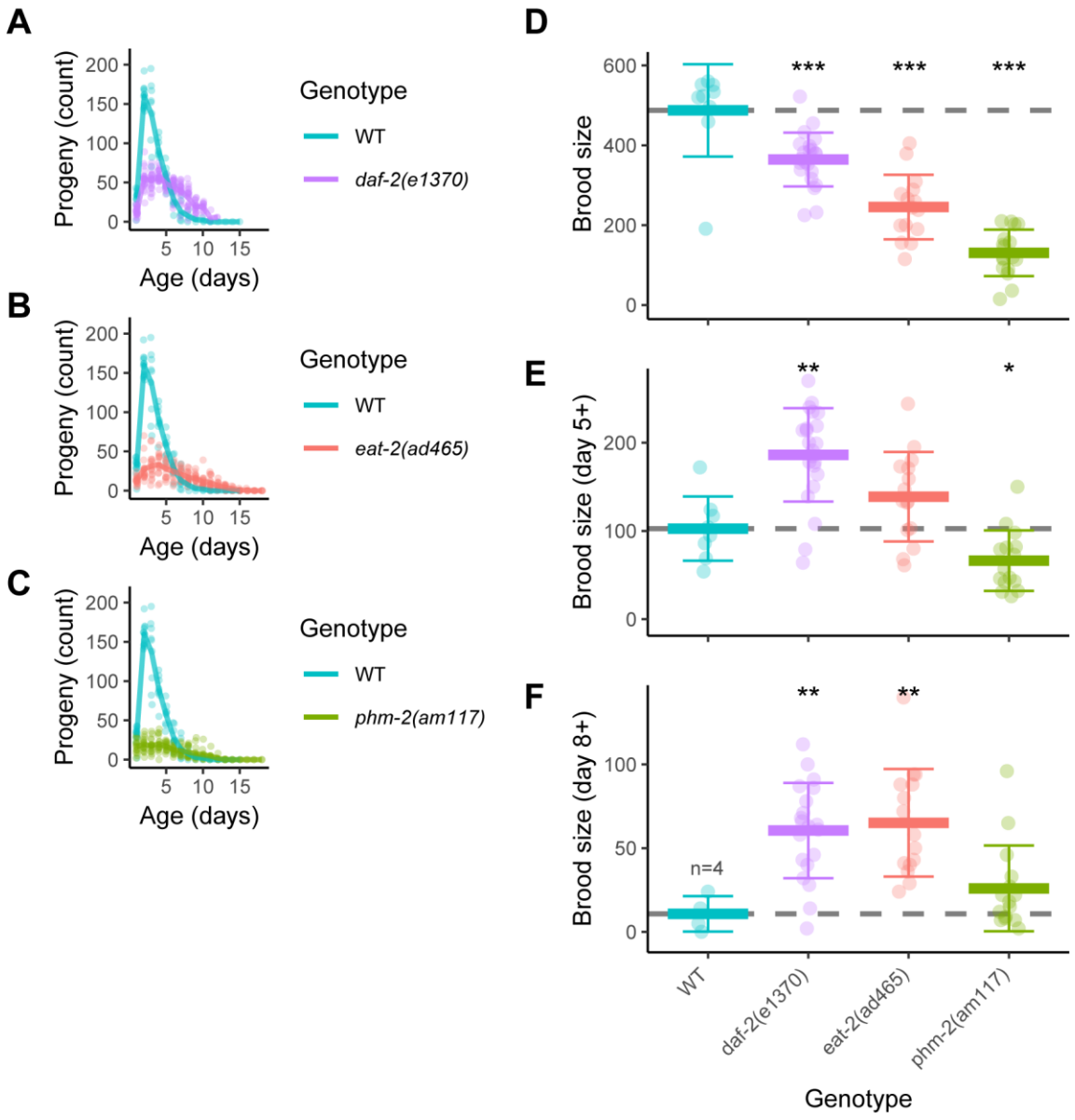

Figure 2: Mutations in nutrient sensing pathways extend reproduction
Mated *daf-2(e1370)*, *eat-2(ad465)*, and *phm-2(am117)* hermaphrodites have been reported to increase reproduction on and after day 10 of adulthood (Hughes 2005; Hughes *et al.* 2007, 2011; Kumar *et al.* 2019). Here, we confirm these findings and analyze the daily progeny production of these mutants using the statistical methods which will be used in the remainder of this study. The daily progeny production of mated wild-type and mutant hermaphrodites is shown in A-C. The total brood size is plotted in D. The "mid-life" brood size (on and after day 5) is plotted in E. The "late-life" brood size (on and after day 8) is plotted in F. Data are represented as mean ± SD. To aid comparisons, dashed gray lines indicate the mean of wild-type.* indicates P<0.05, ** P<.001, *** P<.0001.

To investigate whether additional mutants extend reproduction, and whether any mutants extend reproduction without decreasing early reproduction, we performed a candidate-based

screen. We mated L4 hermaphrodites to males for 24 hours and then measured the daily progeny production. In some experiments, only the late progeny production (day 8 and beyond) was measured for convenience. We hypothesized that mutations in genes known to affect lifespan or nutrient sensing were likely to extend reproduction, and tested 26 strains.

We tested whether additional alleles in the insulin signaling pathway increase late reproduction in mated hermaphrodites. We found no significant difference in the number of progeny produced on or after day 8 in *daf-2(e1368)* (28±13), *age-1(hx546)* (11±7), or *age-1(am88)* (23±18) compared to wild-type (23±22, **Table S2**). The total mated brood size of *daf-2(e1368)* (424±71) was significantly smaller than wild-type (485±121). Hughes (2005) reported that neither *daf-2(m41)* nor *age-1(hx546)* increased late reproduction (1.3±0.7 and 0.5±0.2 progeny after day 9, respectively) compared to wild-type (1.8±0.5). Thus, *daf-2(e1370)* remains the unique allele in the insulin signaling pathway to increase late reproduction in mated hermaphrodites.

Previous reports and personal communication suggested that *sma-2(e502)* and *dbl-1(nk3)* in the TGFB pathway and the *crh-1(tz2)* CREB homolog may increase late reproduction in mated hermaphrodites (Kauffman *et al.* 2010; Luo *et al.* 2010; Templeman *et al.* 2018). We found no significant difference in the number of progeny produced by mated mutant hermaphrodites on or after day 8 compared to wild-type. The total mated brood size of *sma-2(e502)* (183±84) and *crh-1(tz2)* (350±86) was significantly smaller than wild-type (485±121). Thus, while *sma-2* animals exhibit a delay in age-related sterility (Luo *et al.* 2010), they do not produce more progeny on or after day 8 than wild-type, and they exhibit a decrease in early reproduction, similar to other long-lived mutants.

Recently, Cinquin et al. (2016) reported that the DNA damage response pathway may also be implicated in reproductive aging, because (when fed HB101 bacteria) mated *hus-1(op241[reduction-of-function])* hermaphrodites produce more progeny on and after day 4 than mated wild-type hermaphrodites, while producing the same number of progeny on days 1-3 and resulting in a significantly larger brood size than wild-type. Since bacterial diet affects daily progeny production (Wang *et al.* 2014; Sowa *et al.* 2015), we measured the daily progeny production of *hus-1(op241)* on both HB101 bacteria and in standard culture with OP50 (**Table S3**). When fed HB101, we detected no significant difference in the number of progeny produced on days 1-4, 5+, or 8+. We also detected no significant difference between the total mated brood size of *hus-1(op241)* compared to wild-type (785±171 and 728±226, respectively; P=0.529). When fed HB101, mated wild-type hermaphrodites produced a similar number of total progeny as when fed OP50 (728±226 and 637±172, respectively; P=0.16). When fed OP50, the brood size of mated *hus-1(op241)* hermaphrodites was not significantly different from mated wild-type hermaphrodites in either of two biological replicates (Replicate 1: *hus-1* 557±119; wt 556±139; P=1; Replicate 2: *hus-1* 682±191; wt 637±172; P=0.28). When fed OP50, the number of progeny produced on and after day 8 by mated *hus-1(op241)* hermaphrodites was not significantly different from mated wild-type hermaphrodites in one of two biological replicates (Replicate 1: *hus-1* 10±15; wt 13±16; P=0.37; Replicate 2: *hus-1* 2±3; wt 0±0; P=0.036). Thus, it is not clear whether *hus-1(op241)* results in increased late reproduction on OP50. However, the total brood size of mated *hus-1(op241)* hermaphrodites is not different from wild-type on either OP50 or HB101.

Next, we tested whether the long-lived mutants in the serotonin and mTOR signaling pathways, *tph-1(mg280)* and *raga-1(ok386)*, increased late reproduction in mated

hermaphrodites (Templeman and Murphy 2018). We noted that the *raga-1(ok386)* strain exhibited a surprisingly low rate of death by matricidal hatching in mated animals: only 32%. While neither strain exhibited increased late reproduction, the total mated brood size of *tph-1* (445±126) was no different than wild-type (485±121; P=0.36). This is striking, because most, if not all, long-lived mutants in which mated reproduction has been reported to date (i.e. *daf-2, age-1, clk-1, isp-1, raga-1, sma-2*) exhibit decreased early reproduction and/or decreased mated brood size (Hughes et al., 2007, 2011; Kumar et al., 2019, this study).

Because two mutants in an immune-system-dietary-restriction pathway and one mutant in the insulin signaling pathway resulted in increased progeny production after day 8 and after day 10, we hypothesized that nutrient sensing may play a role in reproductive aging. We interpreted the reproductive extension in *eat-2* and *phm-2* to be due to dietary restriction, and the decrease in early progeny production to be due to bacterial colonization and nutrient deficiency. We predicted that these two variables could be separated in animals with a defect in nutrient sensing without an accompanying nutrient deficiency. To this end, we tested multiple mutants that affect chemosensation, some of which also extend lifespan: *che-3(e1124), che-3(p801), che-3(am162), odr-10(ky225), osm-3(p802), osm-3(am172), osm-3(am177), osm-5(p813), tax-4(p678)* (**Table 1, S2**) (Apfeld and Kenyon 1999; Lans and Jansen 2007; Collins *et al.* 2008a; Mair *et al.* 2011). We found that most of these produced no more progeny on average on and after day 8 (range: 10-24) than wild-type (range: 16-24). However, in one replicate, *che-3(p801)* produced 36±16 progeny, which was significantly more than wild-type (22±15, P=0.0139).

Next, we tested whether *che-3(p801)* animals also exhibit decreased early progeny production compared to wild-type. To our surprise, we found that the brood size of c*he-3(p801)* (555±82) was not significantly different from wild-type (485±121, P=0.0712). In this replicate,

the number of progeny produced on and after day 8 by *che-3(p801)* (24±14) was not significantly higher than wild-type (16±9) (P=0.1122). However, when examining the daily progeny production, we noticed an increase in progeny produced in mid-life, around day 5. The number of progeny produced on and after day 5 by *che-3(p801)* (170±54) was significantly higher than wild-type (102±41) (P=0.0002). Taken together, these results show a different type of reproductive extension than that exhibited by *daf-2(e1370), eat-2(ad465),* and *phm-2(am117).* Mated *che-3(p801)* hermaphrodites produce wild-type levels of progeny on days 1-4, significantly exceed wild-type levels on days 5-7, and may or may not exceed wild-type levels on day 8 and beyond. Most importantly, these mutants outperform wild-type animals in middle and old age without any associated decrease in progeny production in young animals. Thus, *che-3(p801)* was sufficient to increase mid-life progeny production without decreasing peak progeny production. It is plausible that additional mutations in the chemosensory pathway may exhibit a similar pattern of increased mid-life progeny production.

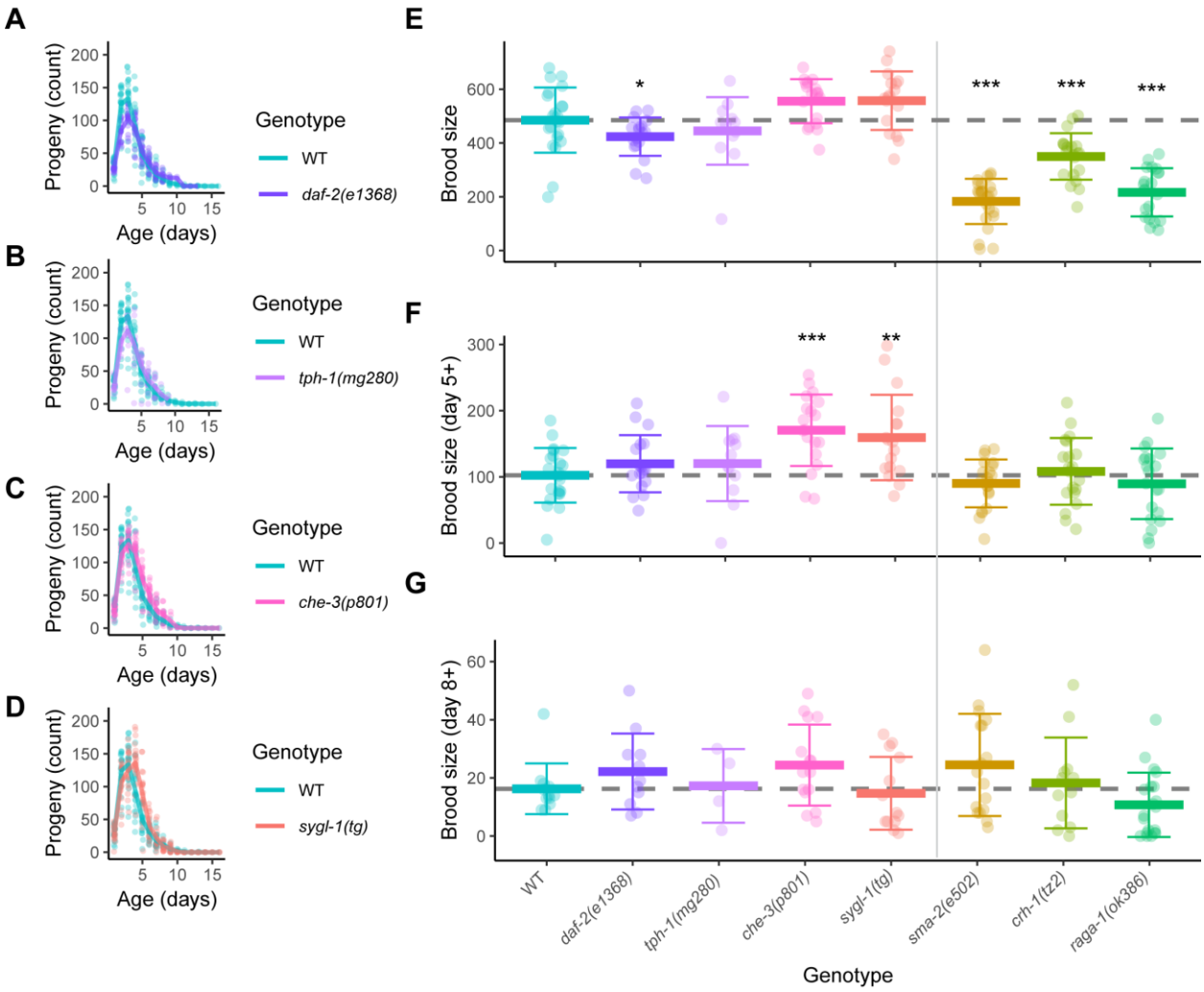

Figure 3: Mutations in nutrient sensing pathways and Notch pathway de-repression are sufficient to extend reproduction

We performed a candidate-based screen to investigate whether additional mutants extend reproduction, and whether any mutants extend reproduction without decreasing early reproduction. The daily progeny production of mated wild-type and mutant hermaphrodites is shown in A-D. The total brood size is plotted in E. The "mid-life" brood size (on and after day 5) is plotted in F. The "late-life" brood size (on and after day 8) is plotted in G. The daily progeny production curves of *sma-2*, c*rh-1*, and *raga-1* are available in **Figure S#**. Data are represented as mean ± SD. To aid comparisons, dashed gray lines indicate the mean of wild-type.* indicates P<0.05, ** P<.001, *** P<.0001.

III. Notch pathway de-repression is sufficient to extend reproduction

We recently reported an age-related decline in stem cell number and in the domain of Notch signaling (Kocsisova *et al.* 2019). The observed correlation between decreased progeny

production, decreased progenitor zone output, decreased number of progenitor cells, a slower cell cycle, and a decreased number of cells expressing two Notch pathway effectors (and presumed stem cell markers), *lst-1* and *sygl-1*, leads to an intriguing hypothesis: that the decrease in Notch pathway signaling causes the decrease in stem cells, progenitor cells, progenitor zone output, and progeny production. This hypothesis leads to the prediction that increasing the activity of the Notch pathway could lead to increased progeny production. We tested this hypothesis using a partial gain-of-function allele of the Notch receptor, *glp-1(ar202)*, and a transgenic strain which results in the de-repression of the Notch effector, *sygl-1* (Pepper *et al.* 2003; Shin *et al.* 2017).

Experiments with *glp-1(ar202)* were performed at the permissive temperature 15 °C, because at the restrictive temperature 20 °C the Notch gain-of-function results in over-proliferation of stem cells and the tumorous (Tum) phenotype in *glp-1(ar202)* hermaphrodites. Even at 15 °C, *glp-1(ar202)* hermaphrodites exhibit a larger progenitor zone, indicative of a partial gain-of-function (Pepper *et al.* 2003).

The total brood size and the early brood size (day 1-4) of mated *glp-1(ar202)* hermaphrodites was significantly lower (approximately one-half) than that of mated wild-type hermaphrodites in two biological replicates (**Table S2**). The late brood size of mated *glp-1(ar202)* hermaphrodites, whether measured on and after day 5 or on and after day 8, was smaller than that of mated wild-type hermaphrodites in two biological replicates (**Table S2**). Thus, the partial gain-of-function in the Notch receptor was not sufficient to increase the number of progeny produced in mid-life or late-life.

Shin et al. (2017) reported that the Notch effector *sygl-1* is downregulated through its 3' untranslated region and generated a transgene, *qSi150*, in which the 3'UTR of *sygl-1* is replaced

by the 3'UTR of *tbb-2*. We call this strain *sygl-1(tg)*. In young adult *sygl-1(tg)* hermaphrodites, the region of *sygl-1* protein accumulation is larger than in animals with the wild-type 3'UTR.

To test whether de-repression of *sygl-1* is sufficient to increase mid-life and/or late-life progeny production, we measured the daily progeny production of *sygl-1(tg)*. Mated *sygl-1(tg)* hermaphrodites produced 159±65 progeny on and after day 5, which was significantly more than wild-type (102±41; P=0.006). This result was confirmed in a second biological replicate (P<0.0001). While mated *sygl-1(tg)* hermaphrodites produced significantly more progeny on and after day 5 and produced slightly more progeny on and after day 8 in one biological replicate, the difference was not statistically significant (P=0.058) and was not confirmed in the second biological replicate.

In these studies hermaphrodites occasionally failed to mate, allowing us to measure self-fertile reproduction. We noticed that the self-fertile brood size of *sygl-1(tg)* hermaphrodites was significantly higher in both biological replicates (262±41 and 306±23 self-progeny in wild-type; 382±47 and 476±91 self-progeny in *sygl-1(tg)*; P=0.0025 and 0.013, respectively, **Figure S#, Table S2**). Because self-fertile brood size is usually determined by the number of sperm produced during development, this result suggests that *sygl-1(tg)* hermaphrodites produce more self-sperm than wild-type, a phenotype known as partial masculinization of the germline (Mog).

Next, we tested whether mated *sygl-1(tg)* hermaphrodites also exhibit decreased early progeny production compared to wild-type. Similar to our findings with c*he-3(p801)* and *tph-1(mg280)*, the total brood size of mated *sygl-1(tg)* hermaphrodites (557±109) was not significantly different from wild-type (485±121, P=0.0673). In a second biological replicate, the total brood size of mated *sygl-1(tg)* hermaphrodites was actually significantly larger than that of mated wild-type hermaphrodites (P<0.0001) (**Table S2**). Thus, increased Notch signaling,

achieved by de-repression of *sygl-1*, was sufficient to increase mid-life progeny production without decreasing peak progeny production.

All strains tested in this study, except for *sygl-1(tg)*, have been reported to extend lifespan compared to wild-type hermaphrodites. We measured the lifespan of unmated *sygl-1(tg)* hermaphrodites' it was not significantly different from wild-type (WT: 12.46 days; *sygl-1(tg)* 11.89 days; log-rank test P=0.7343). Unlike the strains previously reported to increase late-life reproduction, *sygl-1(tg)* did not exhibit an extension of lifespan (**Figure S#**).

IV. Germline stem cell function is extended in long-reproductive mutants

In Kocsisova et al., (2019) we described molecular and cellular age-related changes in the wild-type germline and gonad. In brief, the decline in progeny production is preceded by decreased meiotic entry from the progenitor zone, a slower stem cell cycle, a decreased stem cell pool, and decreased Notch signaling. We hypothesized that the age-related changes which correlate with decreased progeny production are causal. If this hypothesis is valid, we predict that mutations which delay reproductive aging (increase mid-life and late-life progeny production) will also delay the decline in germline phenotypes reported in Kocsisova et al., (2019).

We used the same techniques and protocols as in Kocsisova et al., (2019) to measure various germline phenotypes in 1, 3, 5, and 7 day old wild-type, *daf-2(e1370)*, *eat-2(ad465)*, and *phm-2(am117)* mated hermaphrodites. We measured the number of oocytes, presence of endomitotic oocytes, meiotic entry, progenitor zone size, position of the distal tip cell nucleus, number of oocytes, and extent of accumulation of two Notch effector proteins: SYGL-1 and LST-1. These results are reported in **Figure S#** and **Table S4**.

To measure meiotic entry, we fed the nucleoside analog EdU for 10 hours to appropriately mated and aged animals, then dissected, fixed, stained, and imaged the germline. We counted the number of rows of cells which exhibited EdU signal. Rather than measuring the exact rate of meiotic entry, which requires combining data from multiple durations of EdU feeding, we measured the number of rows of cells with EdU signal in a single 10 hour EdU pulse. We compared the meiotic entry of *daf-2(e1370)*, *eat-2(ad465)*, and *phm-2(am117)* mated hermaphrodites to wild-type mated hermaphrodites of the same age.

Wild-type hermaphrodites experienced a decline in meiotic entry from 18.1±3.3 c.d. at day 1, to 6.0±3.5 c.d. at day 3, to 3.5±2.8 at day 5 (**Figure 4**). Germline deterioration by day 7 in wild-type hermaphrodites was so severe, that it was not possible to measure meiotic entry in most animals. The single individual that avoided sperm depletion, matricidal hatching, development of endomitotic oocytes, severe shifts in the distal tip cell nucleus, and other sporadic defects, exhibited EdU signal only in the progenitor zone; no cells entered meiosis during the measured 10 hour interval.

The meiotic entry of *daf-2(e1370)*, *eat-2(ad465)*, and *phm-2(am117)* mated hermaphrodites at day 1 (9.4±1.9 c.d., 4.9±2.0 c.d., and 6.7±2.6 c.d., respectively) was significantly lower than that of wild-type mated hermaphrodites (18.1±3.3 c.d.). This result was not surprising, as the peak progeny production of these three mutants is significantly lower than in wild-type (**Figure 2**), and the progenitor zone is significantly narrower and/or shorter in young adult *daf-2(e1370)* and *eat-2(ad465)* (Brenner and Schedl 2016).

While all three mutant strains exhibited a lower level of meiotic entry at the start of adulthood, we anticipated that meiotic entry would decrease in all three mutant strains and result

in complete loss of meiotic entry at either a) an earlier age than in wild-type, b) the same age as wild-type, or c) a later age than wild-type, depending on the rate of decline (slope).

If the decline in meiotic entry causes the decline in progeny production, and given that all three mutant strains exhibit increased late-life progeny production (**Figure 2**), we predicted that meiotic entry could decline at a slower rate (slope) and result in a delay in the loss of meiotic entry (x-intercept). As can be seen in Figure 4, the slope of the decline is lower in all three mutant strains compared to wild-type.

At day 7, mated hermaphrodites of all three mutant strains appeared much healthier and younger, subjectively. Objectively, all three exhibited measurable meiotic entry (7.2±3.9 c.d. in *daf-2(e1370)*, 3.2±2.6 c.d. in *eat-2(ad465)*, and 2.9±2.5 c.d. in *phm-2(am117)*) at day 7 when wild-type had deteriorated to an extent where measuring meiotic entry was not possible (**Figure 4**).

In particular, *daf-2(e1370)* exhibited significantly higher meiotic entry at day 3 (10.2±2.8 c.d; $P<0.000001$) and day 5 (6.9±2.4 c.d.; $P=0.002$) compared to wild-type (6.0±3.5 c.d. at day 3; 3.5±2.8 c.d. at day 5). In fact, the meiotic entry of day 7 *daf-2(e1370)* (7.2±3.9 c.d.) was significantly higher than that of day 5 wild-type (3.5±2.8 c.d.; $P=0.001$).

Taken together, we found that mutations which increase the number of progeny produced in late life also increase the meiotic entry from the progenitor zone. These results are consistent with the hypothesis that the age-related decrease in progenitor function leads to a decrease in meiotic entry and causes the age-related decrease in progeny production.

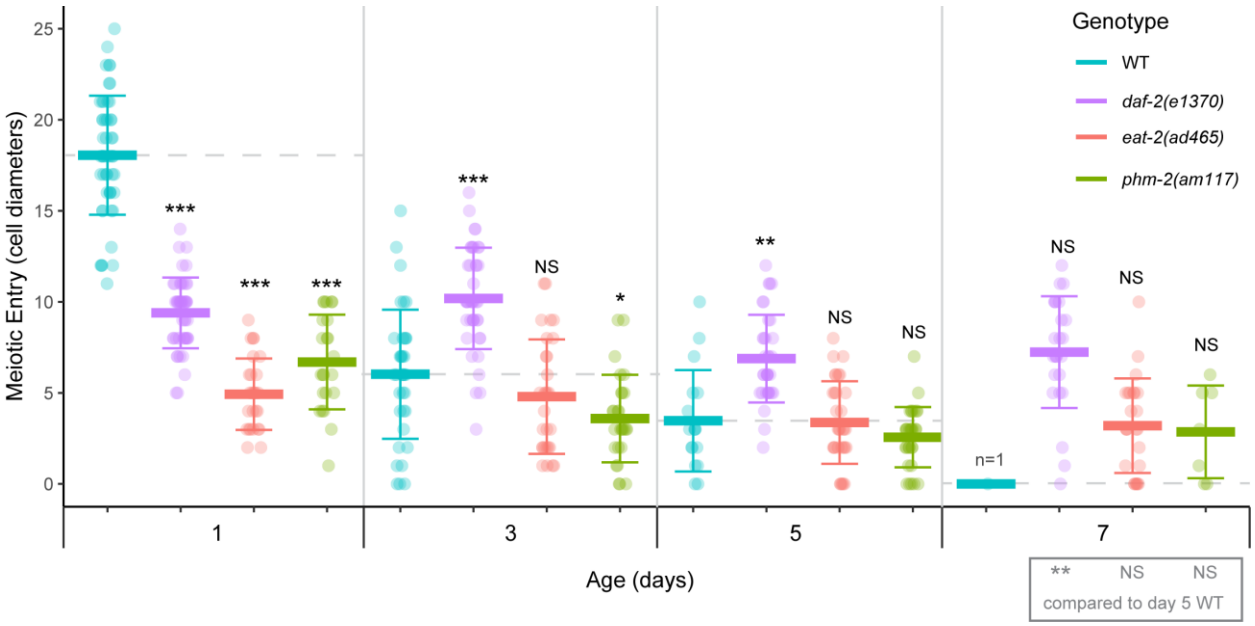

Figure 4: Meiotic entry, one measure of germline stem cell function, is extended in long-reproductive mutants We quantified the extent of EdU signal, in cell diameters, following a 10 hour EdU labeling feeding. Data are represented as mean ± SD. To aid comparisons, dashed gray lines indicate the mean of wild-type. NS indicates P>0.05, * P<0.05, ** P<.001, *** P<.0001. Statistical comparisons were made between mutant and wild-type animals of the same age, with the exception of comparisons displayed in the gray box underneath, which were made between day 7 mutant and day 5 wild-type animals.

Discussion:

I. Post-reproductive lifespan is a feature of both protandrous and gonochoristic *Caenorhabditids*.

The majority of studies in *Caenorhabditis* focus on a single exceptional species: *C. elegans*. Many of the remaining studies use *C. briggsae*, another exceptional species. While *C. elegans* and *C. briggsae* (and also *C. tropicalis*) are protandrous hermaphrodites, which makes them convenient for laboratory genetic studies, this feature also makes them the exceptions in their genus, which is dominated by gonochoristic species (Kiontke *et al.* 2011). While it is unlikely that protandry would have led to fundamental changes in serotonin signaling in the pharynx or insulin signaling in the intestine, we cannot assume the evolution of a radically

different mode of reproduction did not affect reproductive aging. Some of the genes regulating the development of protandry, such as *fog-2* in *C. elegans*, are new and unique to the species. Also, the near-lack of males, small size of self-sperm, radically different ascaroside signaling, and, most-importantly, frequency of sperm-depletion created very different evolutionary pressure on the aging reproductive tract. For these reasons, we examined reproductive aging in two gonochoristic species: *C. brenneri* and *C. remanei*.

Studies of gonochoristic species are inherently more difficult due to inbreeding depression. Strains suitable for laboratory study can be generated through careful mating protocols to achieve a relatively inbred strain (i.e. VX02253) which harbors only few deleterious, sterile, and lethal alleles. Alternatively, strains can be used within a few generations of isolation from the wild and mating pairs which are sterile or near-sterile removed from the analysis as outliers.

A decline in reproductive function occurred several days before mated females began to die of old age in the gonochoristic species *C. brenneri* and *C. remanei*. This is the same pattern as was previously reported (and confirmed here) in both wild-type protandrous and feminized *C. elegans* (Hughes *et al.* 2007), indicating that a post-reproductive lifespan is not likely to be a consequence of an evolutionary history of sperm depletion. This result is consistent with recent findings in another gonochoristic species, the sister species to *C. elegans*: *C. inopinata* (prior to the 2017 announcement at the International Worm Meeting referred to as *C. sp. 34.*) which was isolated from figs and fig wasps (Kanzaki *et al.* 2018; Woodruff and Phillips 2018). *C. inopinata* produce the majority of progeny at days 2-3 of adulthood, few progeny at days 5-7, and are nearly sterile thereafter, while survival remains over 75% until ~day 15 of adulthood (Woodruff *et al.* 2019). In order to better describe the patterns of reproductive and somatic aging across the

genus *Caenorhabditis*, additional studies of species including *C. angaria*, as distant from *C. elegans* as birds are from humans (Kiontke and Fitch 2005; Mortazavi *et al.* 2010) would be helpful.

Examining reproductive aging in more typical gonochoristic species is important to discussions about the evolution of reproductive aging. Aging varies across the tree of life (Jones *et al.* 2014), yet in almost all species that age, reproduction fails earlier in life than somatic functions (Mitteldorf and Goodnight 2013). Researchers have hypothesized that the evolution of sperm-limitation as a consequence of protandrous hermaphroditism could have led to the emergence of a post-reproductive lifespan and an adaptive death (Lohr *et al.* 2019). This hypothesis is inconsistent with results presented in this study and in Woodruff et al. (2019).

II. Mutations which delay reproductive aging also delay decline in germline stem cell function.

In Kocsisova et al. (2019) we described molecular and cellular age-related changes in the wild-type germline and gonad. To this end, we measured the same phenotypes as Kocsisova et al. (2019) in three mutants previously reported to extend reproductive span and increase the number of progeny produced in late-life: *daf-2(e1370)*, *eat-2(ad465)*, and *phm-2(am117)*.

We found that while the germline of these three mutant animals starts out smaller and meiotic entry is lower than in wild-type, the slope of decline is more gradual than in wild-type. At days 5 and 7 the mutant animals appear more youthful than wild-type at days 5 and 7. This effect is most pronounced in *daf-2(e1370)*. Overall, the pattern of meiotic entry over age in all three mutants and in wild-type resembled the pattern of progeny production over age. While it remains possible that another cause exists, these results are consistent with the hypothesis that an

age-related decrease in progenitor function leads to a decrease in meiotic entry and causes the age-related decrease in progeny production.

III. Defects in nutrient sensing lead to mid-life reproductive improvement

Dozens of mutations have been reported to extend lifespan and delay somatic aging, but only a handful which delay reproductive aging. Over a decade ago, Hughes et al. (2007) reported the daily progeny production of long-lived mutants known at that time, finding that some, *daf-2(e1370) and eat-2(ad465)*, increase late-life progeny production while others, including *clk-1(qm30)* and *isp-1(qm150)*, do not. Since then, two reverse-genetic studies reported extended reproductive span in mated hermaphrodites: in the TGFβ pathway by *sma-2(e502)* (Luo *et al.* 2010) and in the sodium homeostasis pathway by RNAi-mediated knockdown of *nhx-2* and *sgk-1*(Wang *et al.* 2014). While the daily progeny production of mated hermaphrodites from these two studies has not been reported, both *nhx-2(RNAi)* and *sgk-1(RNAi)* result in decreased self-progeny production during the first 2-3 days of adulthood, compared to wild-type (Wang *et al.* 2014). Further, it is not clear whether mutations in *nhx-2* and *sgk-1*also result in reproductive span extension or whether *E. coli* HT115 is necessary for the phenotype (Meng C. Wang, personal communication). A forward-genetic screen for extended reproduction by mated hermaphrodites identified that *phm-2(am117)* increased the number of progeny produced on and after day 10 of adulthood and extended lifespan (Hughes *et al.* 2011; Kumar *et al.* 2019). The mechanism of lifespan extension and increased late-life progeny production in both *eat-2(ad465)* and *phm-2(am117)* includes an immune and behavioral response which leads to dietary restriction (Kumar *et al.* 2019). We continued searching for mutations that increase late-life

progeny production (here defined as progeny produced on and after day 8) in sperm-replete (mated) conditions using a candidate-based approach.

Unlike *daf-2(e1370), eat-2(ad465),* and *phm-2(am117)* (**Figure 2**), most long-lived candidate mutations did not result in significantly increased progeny production on and after day 8. Several candidates were chosen because they affect the insulin signaling pathway, including several alleles of *age-1* and *daf-2*. The numerous mutations in *daf-2* have been described in an allelic series and sorted into two classes: Class I alleles, including *e1368* and *m41*, affect certain extracellular regions of the receptor while Class II alleles, including *e1370*, are pleiotropic and affect either the ligand binding pocket or the tyrosine kinase domain. Class I and Class II alleles differ in movement, fecundity, and aging phenotypes (Gems *et al.* 1998; Arantes-Oliviera *et al.* 2002; Patel *et al.* 2008; Ewald *et al.* 2015; Podshivalova *et al.* 2017). Of the insulin signaling pathway mutants tested in this study and by Hughes (2005) (*daf-2(e1368), daf-2(m41), age-1(am88),* and *age-1(hx546)*), only *daf-2(e1370)* extended reproduction and significantly increased progeny production on and after day 8. This result suggests that the *e1370* allele creates levels of insulin signaling that are "just-right" to delay reproductive aging without hindering development. However, *daf-2(e1370)* did significantly decrease early reproduction (Hughes, 2005; Hughes et al., 2007; this study)

While reproductive span studies focus on the last few progeny produced by asking whether an animal is entirely sterile or still slightly fertile, we asked whether older, yet still fertile animals produce more progeny than wild-type. It appears that a day 8 cutoff was too stringent and did not offer the optimal signal-to-noise ratio. Therefore, we measured the daily progeny production of several candidate mutants. This approach led us to identify a reproductive

pattern distinct from both wild-type and from late-life reproductive improvement seen in *daf-2(e1370), eat-2(ad465),* and *phm-2(am117)* – mid-life reproductive improvement (**Figure 5**).

This pattern of increased progeny production on days 5, 6, and 7 was exhibited by *che-3(p801)*. This mutant was also unusual because it exhibited wild-type levels of progeny production on days 1-4. The lifespan extension of *che-3(p801)* occurs due to defective chemosensation because of defects in the amphid neurons (Apfeld and Kenyon 1999; Collins *et al.* 2008a). We interpret the pattern of progeny production in *che-3(p801)* to be a result of a perception of nutrient deficiency without any associated nutritional deficiency or immune defect that likely result in decreased peak progeny production in *eat-2(ad465)* and *phm-2(am117)*.

Previously reported long-lived mutants displayed decreased early peak progeny production and a decreased brood size in mated hermaphrodites (Hughes *et al.* 2007, 2011; Wang *et al.* 2014; Kumar *et al.* 2019). While *che-3(p801)* is long-lived (Collins *et al.* 2008a), this mutant displays no decrease in early or peak progeny production. Likewise, *tph-1(mg280)* is a long-lived mutant which exhibited no significant reduction in total mated brood size. These results suggest that it is possible for a mutation to extend life without reducing the total brood size.

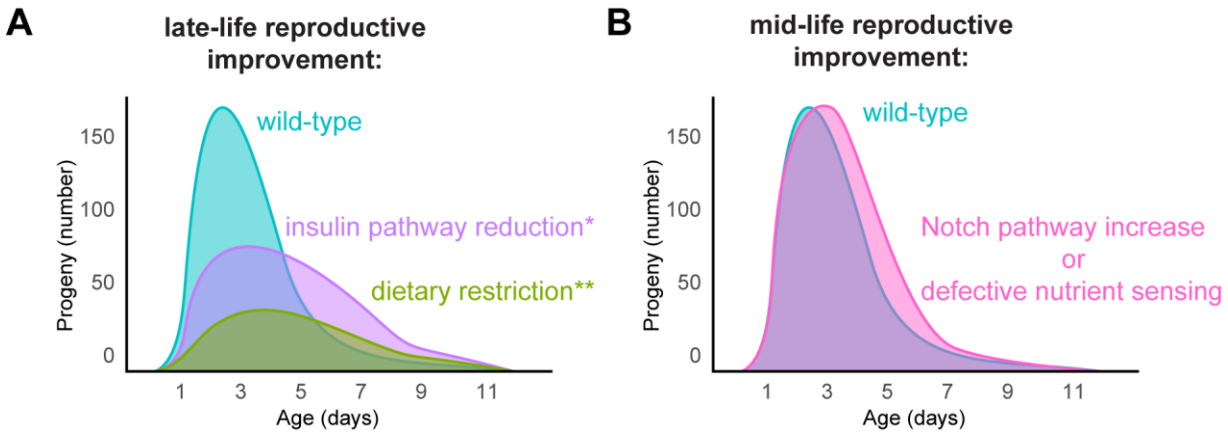

Figure 5: Mid-life reproductive improvement results from loss-of-function in nutrient sensing or gain-of-function in Notch signaling.
A) The model summarizes the pattern of daily progeny production in mated *daf-2(e1370), eat-2(ad465),* and *phm-2(am117)* hermaphrodites which display late-life reproductive improvement, as reported by Hughes et al., (2007) and replicated in this study. Note the decrease in peak progeny production. *Only very specific reduction in the insulin pathway in *daf-2(e1370)* result in this pattern of progeny production, as reported by Hughes (2005) and this study. **dietary restriction in *eat-2(ad465)* and in *phm-2(am117)* is complicated by an immune and behavioral response to pathogenesis of *E. coli* OP50 (Kumar *et al.* 2019). B) The model summarizes the pattern of daily progeny production in mated *che-3(p801)* and *sygl-1(tg)* hermaphrodites, which display mid-life reproductive improvement. Note that peak progeny production is not different from wild-type.

IV. Increased Notch signaling leads to mid-life reproductive improvement

The hypothesis presented in Kocsisova et al., (2019) was that the age-related slowing of the stem cell cycle and decline in stem cell number cause reproductive aging. Another prediction of this hypothesis is that increasing the number of stem cells and/or the rate of the stem cell cycle will reduce the rate of reproductive decline. It is unclear what molecular pathway regulates the rate of the stem cell cycle. On the other hand, Notch signaling affects stem cell number without affecting the rate of the stem cell cycle (Fox and Schedl 2015). We set out to test whether increasing the level of Notch signaling, and thus increasing the number of stem cells without affecting the rate of the stem cell cycle, would be sufficient to increase progeny production.

A partial gain-of-function allele, *glp-1(ar202)* did not increase progeny production at any point in life. A transgenic strain, JK5500, in which 3'UTR-mediated repression of the Notch effector *sygl-1* is interrupted, displays a larger stem cell pool (Shin *et al.* 2017). Here, we report that *sygl-1(tg)* is sufficient for increased progeny production in mid-life (days 5-7), similar to *che-3(p801)*. Unlike previously reported mutants, which increased late-life reproduction and decreased peak reproduction, *sygl-1(tg)* exhibited wild-type levels of reproduction on days 1-4. To our surprise, and unlike *che-3(p801),* this long-reproductive strain was not long-lived. The

finding that this manipulation that increases Notch effector (*sygl-1*) activity also increased mid/late-life reproduction provides support for the hypothesis that the age-related decline in Notch signaling is a cause of reproductive aging.

Conclusions

In this study, we identify mid-life reproductive improvement, the pattern of increased progeny production on days 5-7 of adulthood in *che-3(p801)* and *sygl-1(tg),* and find that certain mutants extend lifespan without compromising early progeny production and that other mutants increase reproductive ability without extending lifespan. These results show that while reproductive function and somatic lifespan are inter-linked, they are also separable. The discovery of new patterns of reproduction in a small candidate-based screen (<30 mutants examined on adult days 8-16, with <10 examined during their entire reproductive period) suggests that future candidate-based studies may lead to additional discoveries about reproductive aging. The identification of mid-life reproductive improvement emphasizes the need to measure daily progeny production during the entire reproductive period.

The result that long-reproductive mutants, particularly *daf-2(e1370)*, reduce the rate of decline of meiotic entry and germ cell phenotypes strengthens the argument that these age-related changes are causal, as proposed in (Kocsisova *et al.* 2019). The model that together the cell cycle rate and the number of stem cells lead to progenitor zone shrinking, slower meiotic entry, slower meiotic progression, and finally to decreased progeny production was strengthened by the finding that increasing the levels of Notch effectors in *sygl-1(tg)* was sufficient to increase mid-life reproduction. If additional manipulations that increase Notch signaling and/or *sygl-1* activity also delay reproductive aging it would provide additional support for the hypothesis that

the age-related decline in Notch signaling is a cause of reproductive aging. Future studies that measure germline function in *che-3(p801), sygl-1(tg),* and any additional mutants with increased reproduction will also test the hypothesis that decline in germline function is a cause of reproductive aging.

An important difference between nematode and mammalian female germline development is that while mammalian female germline stem cells appear to cease dividing by mitosis before birth, nematode germline stem cell divisions continue into adulthood. The results presented here apply to *Caenorhabditis* nematodes and do not examine human or mammalian reproductive aging. Nevertheless, an analogy to human female reproductive aging may be illustrative: rather than looking for ways to help a few women have babies in their early 60s (reproductive span extension), we looked for ways to help women be able to have babies in their early 50s (late-life reproductive increase) or 40s (mid-life reproductive increase), without compromising fertility in 20s and 30s. We found that in *C. elegans* it is possible to increase mid-life reproduction without compromising early/peak reproduction.

Materials and Methods:

Strains and General Methods

C. elegans strains were cultured at 20°C on 6 cm Petri dishes containing nematode growth media (NGM) agar and a lawn of *E. coli* strain OP50 unless otherwise noted. The wild-type *C. elegans* strain and parent of edited strains was Bristol N2 (Brenner 1974). Males of the strain CB4855 ("Mr. Vigorous") were used to generate mated hermaphrodites because they display a higher mating ability; they also deposit a copulatory plug after mating (Hodgkin and Doniach 1997). Strains were obtained from the CGC unless otherwise noted. Animals were

synchronized by picking fourth-stage larvae (L4), defined as day 0, from populations that had not experienced starvation for a minimum of three generations.

To obtain populations of mated middle-aged hermaphrodites, 30-50 L4 hermaphrodites were cultured on a dish with 30-50 young adult males (at a 1:1 ratio) for 24 hours, then the hermaphrodites were removed from the males. The presence of copulatory plugs on many of the hermaphrodites confirmed a high frequency of mating in the population; however, hermaphrodites without a copulatory plug were not excluded from the experiment. Hermaphrodites were moved to fresh NGM+OP50 dishes daily until they reached the desired age.

Table 1: Strains used in this study.

Strain	Gene	Allele	Reference
N2	wt	wt	(Brenner 1974)
TJ1052	*age-1*	*hx546*	
WU710	*age-1*	*am88*	
CB1124	*che-3*	*e1124*	
PR801	*che-3*	*p801*	
WU1026	*che-3*	*am162*	
YT17	*crh-1*	*tz2*	
CB1370	*daf-2*	*e1370*	
DR1572	*daf-2*	*e1368*	
NU3	*dbl-1*	*nk3*	
DA465	*eat-2*	*ad465*	
BS553	*fog-2*	*oz40*	
BS3164	*glp-1*	*ar202*	
DG2389	*glp-1*	*bn18*	
WS2277	*hus-1*	*op241*	
CX3410	*odr-10*	*ky225*	(Hahm *et al.* 2015)
PR802	*osm-3*	*p802*	
WU1024	*osm-3*	*am172*	
WU968	*osm-3*	*am177*	
PR813	*osm-5*	*p813*	

WU1686	*phm-2*	*am117*	(Hughes *et al.* 2011; Kumar *et al.* 2019)
VC222	*raga-1*	*ok386*	
CB502	*sma-2*	*e502*	
JK5500	*sygl-1*	*transgene**	(Shin *et al.* 2017)
PR678	*tax-4*	*p678*	
WT5434	*tph-1*	*mg280*	(Sze *et al.* 2000)
Strain	**Species**	**Note**	**Reference**
CB4855	elegans	wild isolate "Mr. Vigorous" deposit copulatory plug	(Hodgkin and Doniach 1997)
PX439	remanei remanei	sterile/sickly	
VX02253	brenneri	Provided by Charles Baer	
PS1010	angaria	sterile/sickly	
CB5161	brenneri	sterile/sickly	
VT733	remanei vulgaris	sterile/sickly	
SB146	remanei remanei	sterile/sickly	

*Full genotype: *sygl-1(q828null), mut-16(unknown) I; unc-119(ed3lf); qSi150[psygl-1::3xflag::sygl-1::tbb-2 3'utr; Cbr-unc-119(+)] II;*

Progeny Production

To measure progeny production of mated hermaphrodites, we placed 1 L4 hermaphrodite of the appropriate genotype and 3 young adult, CB4855 males on an individual Petri dish with abundant food for 24 hours. After 24 hours, we removed the males and placed each mated hermaphrodite on a fresh dish. We transferred the parent animal to a fresh dish daily. We incubated the previous dish for 2 days at room temperature (19-23 °C) for two days in order to allow progeny to develop to adulthood, then scored the presence/absence of male progeny and the number of progeny produced. Progeny which desiccated on the edge of the dish were included in the analysis. For convenience, progeny plates were sometimes refrigerated at 4 °C to arrest reproduction prior to counting. This method provides accurate and precise measurements of daily progeny production, consistent with previous findings (Hughes *et al.* 2007).

To measure late progeny production, parent generation animals were mated in batches of 30-50 and transferred to fresh NGM+OP50 dishes in batches, as described in the general methods section above. After 7 days, individual hermaphrodites were moved to fresh NGM+OP50 dishes daily, and progeny were counted after 2 days. In some experiments, 50 μL of 10mg/mL palmitic acid dissolved in ethanol were applied to the rim of the dish to reduce fleeing.

In experiments with *C. elegans*, *C. remanei*, and *C. brenneri*, conspecific males were used.

Lifespan of JK5500

Studies of lifespan were begun on day zero by placing ~60 L4 stage hermaphrodites on a Petri dish. Hermaphrodites were transferred to a fresh Petri dish daily during the reproductive period (approximately the first ten days) to eliminate self-progeny and every 2-3 days thereafter. Each hermaphrodite was examined daily using a dissecting microscope for survival, determined by spontaneous movement or movement in response to prodding with a platinum wire. Dead worms that displayed matricidal hatching, vulval extrusion, or desiccation due to crawling off the agar were excluded from the data analysis. Data is aggregated from 2 simultaneous biological replicates starting with 60 worms each. Mean lifespan and the log-rank test were calculated using OASIS 2 (Han *et al.* 2016).

Embryonic viability

Individual young adult hermaphrodites were placed on a dish and allowed to deposit eggs. After several hours, the eggs were picked to a fresh dish and arranged in a line next to the lawn of *E. coli* OP50. After 16 hours, the line was observed and any unhatched eggs were

counted. After 48 hours, the line was observed again and eggs which still had not hatched were counted.

EdU labeling experiments

To make EdU dishes, we seeded M9 agar dishes (Stiernagle 2006) with concentrated *E. coli* MG1693 Thy- which had been grown for 24 hours at 37C with shaking in minimal media containing 20uM 5-ethynyl-2'-deoxyuridine (EdU, Invitrogen). The culture consisted of 100mL M9, 4ml overnight LB-grown MG1693 *E. coli*, 5ml 20% glucose, 50ul 1.25mg/ml thiamine, 1.2ml 0.5mM thymidine, 100ul 1M MgSO4, 200ul 10mM EdU (Fox *et al.* 2011).

Appropriately mated and aged animals were either washed with phosphate buffered saline (PBS) or picked to EdU dishes and incubated for the appropriate time: 0.5, 4, 7, or 10 hours, then dissected and processed as detailed in the following section. Nuclei with any amount of EdU signal overlapping with DAPI staining were scored as EdU-positive. For the full detailed protocol, see Kocsisova et al. (2018).

Dissection and Immunohistochemistry

The dissection and staining protocol follows the batch method (Francis *et al.* 1995), where all dissected tissues were incubated within small glass tubes rather than on a slide. Animals were washed with phosphate-buffered saline (PBS) into a dissecting watchglass (Carolina Biological Item # 742300), immobilized with Levamisole (final concentration 200uM), and dissected with a pair of 25G 5/8” needles (PrecisionGlide from BD) by cutting at the pharynx and/or at the tail. Dissected gonads were fixed in 2 mL 3% paraformaldehyde (PFA) (10 mL 16% PFA, EM Grade, Electron Microscopy Sciences, Hatfield, PA Catalog No 15710)

phosphate-buffered solution for 10 minutes at room temperature and then post-fixed with 2 mL 100% methanol (Gold-label from Fisher) at -20C for 1 hour or longer (up to several days).

Fixed gonads were rehydrated and washed three times in PBS + 0.1% Tween-20 (PBSTw), then incubated in 100ul of primary antibody at room temperature for 4-24 hours, washed 3 times in PBSTw, and incubated in 100ul of secondary antibody at room temperature or 4C for 2-24 hours. Antibodies were diluted in 30% goat serum (Gibco C16210-072) in PBS. Primary antibodies used were: rabbit-anti-WAPL-1 (Novus Biologicals Cat#49300002, Lot G3048-179A02) (1:2000), mouse-anti-MSP (Major Sperm Protein) (Miller *et al.* 2001) (1:2000), mouse-anti-pH3 (Millipore clone 3H10 Cat#05-806, Lot#2680533) (1:500), mouse-anti-FLAG (SIGMA M2) (1:1000). Secondary antibodies were: goat-anti-mouse IgG-conjugated Alexa Fluor 488/594/647, goat-anti-rabbit IgG-conjugated Alexa Fluor 488/594/647 (Invitrogen).

Following antibody staining, gonads were washed 3 times in PBSTw. An EdU Click-iT reaction was performed according to manufacturer's instructions (Invitrogen C10350), using 100ul reagent for a 30 minute incubation, followed by a quick wash in manufacturer-supplied rinse buffer and four ~15 minute washes in PBSTw. Stained gonads were resuspended in 1 drop of Vectashield containing 4',6-Diamidino-2-Phenylindole Dihydrochloride (DAPI) (Vector Laboratories H-1200), applied to a large pre-made agarose pad on a glass slide, and covered with a 22 mm x 40 mm #1 cover glass. The slide was allowed to settle overnight at room temperature, sealed with clear nail polish, and stored at 4 °C as needed. Images were acquired within 72 hours when possible.

Confocal Imaging

Images were collected using a Zeiss Plan Apo 63X 1.4 oil-immersion objective lens on a PerkinElmer Ultraview Vox spinning disc confocal system on a Zeiss Observer Z1 microscope using Volocity software. Approximately twenty 1 μm z-slice images were acquired for each gonad. Images were exported as hyperstack .tif files for further analysis.

Image analysis

Images were stitched either in Volocity or using the Image J plugins for pairwise stitching and Grid/Collection of sequential images (Preibisch *et al.* 2009). Images were rotated, cropped, arranged, and annotated in Illustrator (Adobe).

Nuclei were manually counted in each z-slice where they occurred. The person performing counts was not blinded to experimental groups, because the differences were generally obvious to an experienced observer. Counts of nuclei were performed in Fiji/ImageJ (Schindelin *et al.* 2012) using the Cell Counter plug-in (De Vos 2015; Rasband 2016). To remove multiply-counted nuclei, a modified version of the R-script Marks-to-Cells was used (Seidel and Kimble 2015). This script improved the precision of cell counts in the germline.

Nuclear morphology: DAPI staining was used to assess meiotic prophase stages, nuclear counts, row counts and progression of gametogenesis. Endomitotic oocytes in the proximal gonad arm, distal to the spermatheca, were recognized as large DAPI stained blobs. Endomitotic oocytes are known to result from failure to coordinate meiotic maturation of diakinesis stage oocytes with ovulation, resulting in the unfertilized mature oocytes that are mitotic cell cycling without cytokinesis because of the absence of the sperm derived centriole (Iwasaki *et al.* 1996; McCarter *et al.* 1997; Greenstein 2005). This is distinct from endomitotic oocytes in the uterus, which naturally occur in older unmated hermaphrodites that have exhausted their self-sperm. In

this case the most proximal oocyte undergoes low frequency spontaneous maturation and ovulation, but because there is no sperm in the spermatheca the matured but unfertilized oocyte begins endomitotic cycling (McCarter *et al.* 1999). Endomitotic oocytes were identified from dissected germlines; as the proximal germline was not always visible, this raises the possibility that the frequency was under-estimated.

Progenitor zone: The PZ has been previously called the mitotic zone or the proliferative zone. We employed staining with the cohesin chaperone WAPL-1 to measure the size of the PZ (Mohammad *et al.* 2018; Kocsisova *et al.* 2019). Other studies of unmated day 1 hermaphrodites used the crescent-shaped DAPI morphology of leptotene nuclei to approximate the proximal boundary of the PZ (Crittenden *et al.* 2006; Roy *et al.* 2016).

SYGL-1 and LST-1: The length in c.d. and the number of cells in the PZ that contain cytoplasmic SYGL-1 and LST-1 was assessed with anti-FLAG antibody staining using strains where CRISPR genome editing was employed to insert a 3xFLAG epitope onto the endogenous gene product (Shin *et al.* 2017; Kocsisova *et al.* 2019).

Statistical Analysis

Statistical analyses were performed in R (R Core Team 2013) using R studio (RStudio Team 2015) and the following packages: ggplot2 (Wickham 2009), svglite, plyr, and tidyR. Individual measurements and script used to analyze them are provided in supplemental tables and files. Depending on the type of variable, the following tests were performed. For continuous measurement variables, the Kruskal-Wallis Rank-sum test was used with a Dunn post-hoc and p-values adjusted with the Benjamini-Hochberg FDR method. Data were also compared using an ANOVA with a Tukey post-hoc test. Brood sizes were compared using pairwise t-tests. For

categorical measurement variables, the Pearson's Chi-squared test of independence was used with post-hoc p-values adjusted with the False Discovery Rate method. Statistical comparisons were made between mutant and wild-type animals of the same age, with the exception noted in the supplemental tables and figure legends. In the text all data are represented as mean ± SD. All error bars shown in figures represent the mean +/- standard deviation. NS indicates $P>0.05$, * $P<0.05$, ** $P<.001$, *** $P<.0001$.

All data were subjected to consistent exclusion criteria. Animals that displayed evidence of matricidal hatching or sperm depletion (as indicated by lack of male progeny or lack of Major Sperm Protein immunofluorescence) were excluded from all analyses unless otherwise noted. Animals that displayed sporadic phenotypes such as endomitotic oocytes, a shifted distal tip cell, or failure to exhibit any EdU staining were excluded from analyses. Animals which fled the plate are excluded from the brood size calculations. Animals that died by matricidal hatching are included in the brood size calculations. For this reason, it is possible that brood sizes are slight under-estimates. Matricidal hatching was very common, and excluding these animals would have biased the dataset. Exact statistical methods and exclusion criteria are provided in the supplemental R script.

Chapter 7:

Future directions

The results reported in the preceding chapters provide tools to analyze the cell cycle and aging germline, a detailed description of stochastic and pervasive age-related changes in the germline, and several leads regarding molecular mechanisms of reproductive aging. The results also raise new questions and open several avenues for future research. Besides the future directions already discussed in each chapter, below are five approaches to continue the study of the molecular and cellular basis of reproductive aging, including approaches to identify additional genetic and pharmacological interventions to increase late-life progeny production and approaches to dissect the Notch signaling pathway to determine the role of the *lag-2* ligand in the DTC during age-related decline.

Identify mutations that extend reproduction in a candidate genetic screen

Mutations in many genes extend lifespan, and some of these mutations also delay the onset of age-related changes (Collins *et al.* 2008b; Son *et al.* 2018). In contrast, mutations in only a few genes are published to extend reproduction in sperm-replete hermaphrodites. In Hughes *et al.* (2007, 2011) and Kumar *et al.* (2019), the Kornfeld lab reported that specific mutations in *daf-2, eat-2, phm-2* robustly extend reproduction in sperm-replete hermaphrodites. Mutations in *sma-2, hus-1,* and *egl-1* have also been reported to extend reproductive span (Andux and Ellis 2008; Luo *et al.* 2010; Cinquin *et al.* 2016). In addition, Wang *et al.* (2014) searched for genes involved in reproductive aging using RNAi-mediated knockdown. However, few labs study reproductive aging, and even fewer do so in sperm-replete (mated) animals. We hypothesize that additional mutations extend reproduction and increase mid-life and/or late-life progeny production. As detailed in Chapter 6, the discovery of new patterns of reproduction in a small candidate-based screen (<30 mutants examined on adult days 8-16, with <10 examined during

their entire reproductive period) suggests that future candidate-based screens focused on days 5-16 may lead to additional discoveries about reproductive aging.

Current literature about reproductive and somatic aging suggests several candidate genes for this screen. RNAi-mediated knockdown of the *Drosophila* Indy homolog *nac-2* resulted in extended lifespan and smaller body size (Fei *et al.* 2004), two phenotypes also displayed by *phm-2(am117)* and *eat-2(ad465)* (Hughes *et al.* 2007, 2011; Kumar *et al.* 2019). It is plausible that *nac-2(lf)* may increase mid-life or late-life reproduction (Hughes 2005). RNAi-mediated knockdown of *nhx-2* and *sgk-1* extended reproductive span and increased late progeny production (Wang *et al.* 2014). Thus, *nhx-2(lf)* and *sgk-1(lf)* are also reasonable candidates for this screen. Kumar *et al.* (2016) reported that RNAi-mediated knockdown of *acn-1* extended lifespan yet did not strongly affect self-fertile reproduction or self-fertile brood size. Unpublished data from the Kornfeld lab found that while *acn-1(lf)* resulted in larval lethality, *acn-1(lf/+)* extended lifespan. It is plausible that RNAi-mediated knockdown of *acn-1* or *acn-1(lf/+)* may extend reproductive span and increase late-life progeny production in sperm-replete hermaphrodites. The genes identified in these studies represent several distinct pathways. However, loss-of-function mutations of genes targeted by RNAi-mediated knockdown do not always show the same phenotypes, perhaps because the level of gene function in the mutant may not match the level after RNAi-mediated knockdown, or because RNAi methods typically employ a different strain of *E. coli* (HT115).

Additional candidates for this screen are genes in nutrient sensing pathways. Dietary restriction mutants extend reproductive span, but experience reduced peak reproduction due to the associated nutritional deficiency and/or immune defect (Hughes *et al.* 2007, 2011; Kumar *et al.* 2019). We hypothesize that perception of nutrient deficiency without actual nutritional

deficiency may result in extended reproductive span, increased late-life and mid-life progeny production, and unchanged peak progeny production. As detailed in Chapter 6, *che-3(p801)* displayed increased mid-life progeny production, and unchanged peak progeny production. The effect of *che-3(p801)* one late-life progeny production was variable, and this allele was chosen from a longer list of candidates because it increased late-life progeny production in the first replicate. Two other alleles of this gene, *che-3(e1124)* and *che-3(am162),* and several alleles of other genes in chemosensory, osmosensory, and other sensory pathways, *odr-10(ky225), osm-3(p802), osm-3(am172), osm-3(am177), osm-5(p813), tax-4(p678),* had no effect on late progeny production in a single biological replicate, but their effect on peak and mid-life progeny production was not tested.

GLP-1/Notch signaling plays a critical role in promoting the stem cell fate. In Chapter 5 we document an age-related decline in the expression domain of the direct GLP-1/Notch target genes *lst-1* and *sygl-1*. We hypothesize that age-related reductions in GLP-1/Notch signaling contribute to age-related decreases in the number or function of germ-line stem cells and predict that increasing GLP-1/Notch signaling in adulthood will increase mid-life and late-life progeny production. In chapter 6, we report that the temperature-sensitive *glp-1(ar202)* weak gain-of-function allele does not extend reproductive span. However, a transgenic strain, *sygl-1(tg)* that stabilizes the *sygl-1* mRNA due to an altered 3' UTR, did increase mid-life progeny production. However, this strain has a relatively complex genotype, since it contains the *qSi150* transgene as well as a loss-of-function *sygl-1* mutation, *sygl-1(q828lf)*, and the genotype at the *mut-16* and *unc-119* loci are unknown. To address the possibility that this loss-of-function mutation contributes to the phenotype, it would be necessary to analyze the *sygl-1(q828lf)* strain or to separate the *sygl-1(q828lf)* mutation from the *qSi150* transgene to determine how these two

perturbations of the *sygl-1* gene behave in isolation. An alternate approach would be to use CRISPR/Cas9 to edit the 3' UTR to achieve de-repression and increased translation from the native *sygl-1* locus. If these manipulations also delay reproductive aging it would provide direct support for our hypothesis.

Test whether adult-only knockdown of *daf-2* delays reproductive aging

Prior to the results outlined in Chapter 6, every published mutation that extended reproductive span and increased late progeny production (including *daf-2*) also decreased peak progeny production. However, the affected genes are necessary for proper larval development of the germline (pleiotropy). We hypothesize that we it may be able to extend reproductive span and increase mid-life and/or late-life progeny production without decreasing peak progeny production by initiating knockdown of *daf-2* in the adult.

Dillin *et al.* (2002) report that adult-only RNAi-mediated knockdown of *daf-2* (using the Kenyon lab's cDNA-based *daf-2* RNAi plasmid in HT115 bacteria) is sufficient to extend lifespan. In addition, they found that while lifelong RNAi-mediated knockdown delayed the onset of reproduction, initiating knockdown at L4 resulted in the same pattern of self-fertile reproduction as the control treatment. This study, however, did not test sperm-replete reproduction.

While data on *daf-2(e1368)* and *daf-2(m41)* reproductive aging appear to be discouraging, Templeman *et al.* (2018) report that RNAi-mediated knockdown of *daf-2* does extend reproductive span in sperm-replete hermaphrodites. While it is not perfectly clear from the methods, this experiment was probably performed using life-long feeding of the Kenyon

lab's cDNA-based *daf-2* RNAi plasmid in HT115 bacteria (Templeman *et al.* 2018). The study did not report daily progeny production, only sterility versus fertility.

In order to make possible comparisons to the majority of sperm-replete reproductive aging experiments, which were performed using standard *C. elegans* culture methods including live *E. coli* OP50, it may be necessary to confirm lifespan and reproductive span extension using RNAi-mediated knockdown of *daf-2* in standard (*E. coli* OP50) culture. Recently, Xiao *et al.* (2015) developed a method to perform RNAi-mediated knockdown on a diet of *E. coli* OP50.

The recently developed auxin-inducible degradation (AID) system (Zhang *et al.* 2015) provides an alternative approach to RNAi-mediated knockdown of *daf-2*. In fact, the Mair laboratory has already engineered a strain for auxin-inducible degradation of *daf-2*. CRISPR technology was used to edit the endogenous locus to encode DAF-2 protein fused to the 44 amino acid Degron and a fluorescent reporter, likely GFP. An intergrated TIR1 transgene under the control of a ubiquitous promoter (*eft-3*) and tagged with mRuby was crossed into this strain. When the strain containing *peft-3::TIR1::mRuby* and *daf-2::gfp::degron* is exposed to auxin, *daf-2* is rapidly degraded (William B. Mair, personal communication). Auxin at the relevant concentration does not affect brood size, which makes the AID system well-suited to studies of the reproductive system (Zhang *et al.* 2015)

Whether by RNAi-mediated knockdown or using the auxin-inducible degradation system, this experiment will test whether adult-only reduction of *daf-2* function extends reproductive span and increases late-life progeny production (and total brood size) without decreasing peak progeny production. The theory of antagonistic pleiotropy explains aging as a result of late-life detrimental effects of genes which function to promote development and peak fertility. Separating these antagonistically pleiotropic effects of *daf-2* will have implications for

evolutionary theories of aging. If downregulation of *daf-2* in adulthood is sufficient to increase late-life reproduction without decreasing early reproduction, this result raises the question of why *daf-2* is not downregulated during adulthood in wild-type animals. One explanation could be that adult *daf-2* functions in a process we do not observe under laboratory culture conditions. Another explanation could be that force of selection decreases after the onset of reproduction, and thus the high level of *daf-2* function was not selected against.

Test whether FDA-approved drugs delay age-related changes in the germline

Pharmaceuticals offer an orthogonal approach to modulate aging, and may provide a more direct route to finding interventions to delay aging in humans. Many pharmaceuticals have been reported to extend lifespan, and some of these pharmaceuticals also delay the onset of age-related changes. In contrast, only ethosuximide (2 mg/ml) and trimethadione (4 mg/ml) are published to extend reproduction in sperm-replete hermaphrodites (Hughes 2005; Hughes *et al.* 2007). It is likely that additional pharmaceuticals also delay reproductive aging.

Since the measurement of daily progeny production is labor intensive, candidate drugs should be selected carefully or automation employed to increase the throughput of this candidate-based pharmaceutical screen. For example, since ethosuximide treatment inhibits chemosensory perception and delays reproductive aging without decreasing early progeny production, additional pharmaceuticals predicted to inhibit chemosensory perception may yield delayed reproductive aging. Alternately, treatments such as captopril, which extends lifespan without significantly reducing self-fertile brood size (Kumar *et al.* 2016), may also delay reproductive aging in sperm-replete hermaphrodites. Additional caveats of pharmaceutical screens include finding the relevant dosage, timing, and determining whether any observed effect

occurs due to a direct effect on *C. elegans*, as opposed to affecting the metabolism of the *E. coli* OP50 which *C. elegans* eat.

Studying pharmaceuticals in conjunction with mutations may provide avenues to explore the cellular and molecular mechanisms of delayed reproductive aging, especially in instances where the molecular target of a drug is known, or where a particular drug's dosage can mimic partial loss-of-function of a gene.

Analyze germline function in genetic and pharmacological interventions that extend reproduction

In Chapter 5, we described the role of sporadic versus population–wide changes and the role of stem cell number versus the duration of the cell cycle. In Chapter 6, we began exploring how mutations that extend reproductive span affect the progenitor zone and meiotic entry. We also identified two new genetic factors that increase mid-life progeny production. We hypothesize that the reported age-related changes, which correlate with an age-related decrease in progeny production, in fact cause the age-related decrease in progeny production. A prediction of this hypothesis is that mutations and drug treatments which delay reproductive aging also delay the decline in germline phenotypes. Future experiments may use these newly developed assays to evaluate the effects of *che-3(p801)*, *sygl-1(tg)*, 2 mg/ml ethosuximide, 4 mg/ml trimethadione, and any newly discovered mutations and pharmaceuticals that increase mid-life and late-life progeny production.

Characterize the expression and function of the LAG-2 ligand in reproductive aging.

The distal tip cell expresses the Notch ligand *lag-2* (homolog of delta), thereby signaling to germline stem cells. We documented an age-related decline in Notch target gene expression in stem cells, but it is unknown if changes in expression of *lag-2* contribute to reproductive aging. To elucidate the role of *lag-2*, future experiments will analyze expression and function to test the hypothesis that Notch ligand plays a role in age-related reproductive decline in sperm-replete hermaphrodites.

To rigorously monitor LAG-2 expression in the DTC over time, the same approaches can be used that were described in Chapter 5 for LST-2 and SYGL-1, including quantification of a large number of germlines and multiple biological replicates. In addition, it is possible that the distal tip cell morphology affects Notch signaling. Future experiments could employ a strain containing the single copy *lag-2p::myrGFP* reporter (Byrd *et al.* 2014) to monitor the morphology of the distal tip cell body, plexus, and long external processes. If *lag-2* expression displays an age-related decline, then it is a candidate to cause the degenerative change. Preliminary data from Hughes (2005) suggest that this is the case in unmated hermaphrodites; with age LAG-2::GFP expression appeared in the proximal gonad, was lost in one or both DTCs, or appeared in various locations in the body as if the DTCs had migrated away from the center of the body. However, this pattern has not been explored in sperm-replete hermaphrodites or using fluorescent or epitope-tagged alleles at the native locus, which may be less pleiotropic than a transgenic *lag-2p::GFP* reporter. An age-related decline in *lag-2* expression would suggest a role in reproductive aging; by contrast, stable expression over time would indicate that age-related changes occur downstream of ligand expression.

If the expression of LAG-2 decreases with age, it is plausible that the decrease in LAG-2 causes the decrease in SYGL-1 and the associated decrease in progeny production. A longitudinal study can be used to determine the correlation between early progeny production (days 1-5), which is predictive of both reproductive span and life, and LAG-2 expression level on day 5. If low levels of progeny production positively correlate with low levels of *lag-2* expression, then it will indicate that the decline of ligand expression may be functionally significant.

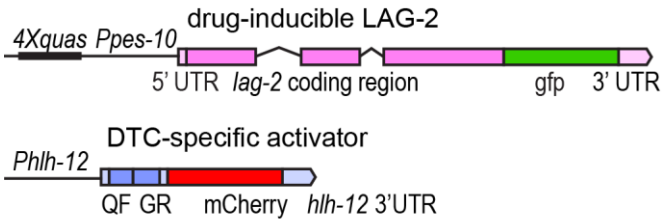

Figure 1: Diagram of proposed drug-inducible, tissue-specific LAG-1 over-expression

To analyze the function of *lag-2*, future experiments could examine the effect of conditionally increasing expression of *lag-2 i*n the distal tip cell. This could be achieved using the Q-system (Monsalve *et al.* 2019) by generating an integrated transgene containing *lag-2* (*4Xquas::Ppes-10::lag-2::gfp*) under the control of the distal-tip-cell-specific, dexamethasone-inducible Q system (*Phlh-12::QF::GR::linker::mCherry*). After exposing animals to dexamethasone continuously or transferring animals to dexamethasone only during adulthood, one could measure progeny production, the size of the progenitor zone, the rate of meiotic entry, and the extent of the Notch effectors, LST-1 and SYGL-1. If *lag-2* overexpression is sufficient to extend progeny production, delay changes in stem cell and progenitor cell number, and delay age-related decline of expression of Notch target genes *lst-1* and *sygl-1*, then it will provide strong support for the hypothesis that age-related decline in stem cells is mediated at the level of

ligand expression. By contrast, if *lag-2* overexpression is not sufficient to extend Notch target gene expression, it will indicate that the age-related change occurs downstream of the ligand. This would provide important new insights into germline aging.

References

Adachi H., Fujiwara Y., Ishii N., 1998 Effects of Oxygen on Protein Carbonyl and Aging in Caenorhabditis elegans Mutants With Long (age-1) and Short (mev-1) Life Spans. Journal of Gerontology: BIOLOGICAL SCIENCES **53**: 24–244.

Agarwal I., Farnow C., Jiang J., Kim K. S., Leet D. E., Solomon R. Z., Hale V. A., Goutte C., 2018 HOP-1 presenilin deficiency causes a late-onset notch signaling phenotype that affects adult germline function in caenorhabditis elegans. Genetics **208**: 745–762.

Aitlhadj L., Stürzenbaum S. R., 2010 The use of FUdR can cause prolonged longevity in mutant nematodes. Mechanisms of Ageing and Development **131**: 364–365.

Amrit F. R. G., Ratnappan R., Keith S. A., Ghazi A., 2014 The C. elegans lifespan assay toolkit. Methods **68**: 465–475.

Amrit F. R. G., Steenkiste E. M., Ratnappan R., Chen S. W., McClendon T. B., Kostka D., Yanowitz J., Olsen C. P., Ghazi A., 2016 DAF-16 and TCER-1 Facilitate Adaptation to Germline Loss by Restoring Lipid Homeostasis and Repressing Reproductive Physiology in C. elegans. PLoS Genetics **12**.

Andux S., Ellis R. E., 2008 Apoptosis maintains oocyte quality in aging Caenorhabditis elegans females. PLoS Genetics **4**.

Angeles-Albores D., Leighton D. H. W., Tsou T., Khaw T. H., Antoshechkin I., Sternberg P. W., 2017 The Caenorhabditis elegans Female State: Decoupling the Transcriptomic Effects of Aging and Sperm-Status. G3: Genes, Genomes, Genetics **7**: 2969–2977.

Angelo G., Gilst M. R. Van, 2009 Starvation Protects Germline Stem Cells and Extends Reproductive Longevity in C. elegans. Science **326**: 954–958.

Apfeld J., Kenyon C., 1999 Regulation of lifespan by sensory perception in Caenorhabditis elegans. Nature **402**: 804–809.

Arantes-Oliviera N., Apfeld J., Dillin A., Kenyon C., 2002 Regulation of Life-Span by germ - line stem cells in Caenorhabditis elegans. Science **295**: 502–505.

Arribere J. A., Bell R. T., Fu B. X. H., Artiles K. L., Hartman P. S., Fire A. Z., 2014 Efficient marker-free recovery of custom genetic modifications with CRISPR/Cas9 in Caenorhabditis elegans. Genetics **198**: 837–846.

Austin J., Kimble J., 1987 glp-1 is required in the germ line for regulation of the decision between mitosis and meiosis in C. elegans. Cell **51**: 589–599.

Avery L., Thomas J. H., 1997 Feeding and defecation. C. elegans II **33**: 679–716.

Avery L., Shtonda B. B., 2003 Food transport in the C. elegans pharynx. The Journal of experimental biology **206**: 2441–2457.

Baker G. T., Sprott R. L., 1988 Biomarkers of aging. Experimental Gerontology **23**: 223–239.

Balaban R. S., Nemoto S., Finkel T., 2005 Mitochondria, Oxidants, and Aging. Cell **120**: 483–495.

Bansal A., Zhu L. J., Yen K., Tissenbaum H. A., 2015 Uncoupling lifespan and healthspan in Caenorhabditis elegans longevity mutants. Proc Natl Acad Sci U S A **112**: E277-86.

Baugh L. R., 2013 To grow or not to grow: Nutritional control of development during Caenorhabditis elegans L1 Arrest. Genetics **194**: 539–555.

Beck C. D. O., Rankin C. H., 1993 Effects of aging on habituation in the nematode Caenorhabditis elegans. Behavioural Processes **28**: 145–163.

Ben-Zvi A., Miller E. A., Morimoto R. I., 2009 Collapse of proteostasis represents an early molecular event in Caenorhabditis elegans aging. Proceedings of the National Academy of Sciences **106**: 14914–14919.

Bolanowski M. A., Russell R. L., Jacobson L. A., 1981 Quantitative measures of aging in the nematode Caenorhabditis elegans. I. Population and longitudinal studies of two behavioral parameters. Mechanisms of Ageing and Development **15**: 279–295.

Bolanowski M. A., Jacobson L. A., Russell R. L., 1983 Quantitative measures of aging in the nematode caenorhabditis elegans: II. Lysosomal hydrolases as markers of senescence. Mechanisms of Ageing and Development **21**: 295–319.

Bonduriansky R., Brassil C. E., 2002 Rapid and costly ageing in wild male flies. Nature **420**: 377.

Braeckman B. P., Houthoofd K., Vreese A. De, Vanfleteren J. R., 2002a Assaying metabolic activity in ageing Caenorhabditis elegans. Mechanisms of Ageing and Development **123**: 105–119.

Braeckman B. P., Houthoofd K., Brys K., Lenaerts I., Vreese A. De, Eygen S. Van, Raes H., Vanfleteren J. R., 2002b No reduction of energy metabolism in Clk mutants. Mechanisms of Ageing and Development **123**: 1447–1456.

Braeckman B. P., Houthoofd K., Vanfleteren J. R., 2002c Assessing metabolic activity in aging Caenorhabditis elegans: concepts and controversies. Aging Cell **1**: 82–88.

Brauchle M., Baumer K., Gönczy P., 2003 Differential activation of the DNA replication checkpoint contributes to asynchrony of cell division in C. elegans embryos. Current Biology **13**: 819–827.

Brenner S., 1974 The genetics of Caenorhabditis elegans. Genetics **77**: 71–94.

Brenner J. L., Schedl T., 2016 Germline stem cell differentiation entails regional control of cell fate regulator GLD-1 in Caenorhabditis elegans. Genetics **202**: 1085–1103.

Brooks K. K., Liang B., Watts J. L., 2009 The Influence of Bacterial Diet on Fat Storage in C. elegans. PLOS ONE **4**: e7545.

Brys K., Castelein N., Matthijssens F., Vanfleteren J. R., Braeckman B. P., 2010 Disruption of insulin signalling preserves bioenergetic competence of mitochondria in ageing Caenorhabditis elegans. BMC Biology **8**.

Burns D. M. F., Harper J. M., Lynne A. M., 2017 Age Does Not Affect the Induction of Mortality by the Foodborne Pathogen Salmonella enterica in Caenorhabditis elegans.

Byerly L., Cassada R. C., Russell R. L., 1976 The life cycle of the nematode Caenorhabditis elegans: I. Wild-type growth and reproduction. Developmental Biology **51**: 23–33.

Byrd D. T., Knobel K., Affeldt K., Crittenden S. L., Kimble J., 2014 A DTC niche plexus surrounds the germline stem cell pool in Caenorhabditis elegans. PLoS ONE **9**.

Chang J. T., Kumsta C., Hellman A. B., Adams L. M., Hansen M., 2017 Spatiotemporal regulation of autophagy during Caenorhabditis elegans aging. eLife **6**: 1–23.

Chatterjee I., Ibanez-Ventoso C., Vijay P., Singaravelu G., Baldi C., Bair J., Ng S., Smolyanskaya A., Driscoll M., Singson A., 2013 Dramatic fertility decline in aging C. elegans males is associated with mating execution deficits rather than diminished sperm quality. Experimental Gerontology **48**: 1156–1166.

Chen D., Thomas E. L., Kapahi P., 2009 HIF-1 modulates dietary restriction-mediated lifespan extension via IRE-1 in Caenorhabditis elegans. PLoS Genet **5**: e1000486.

Cherkasova V., Ayyadevara S., Egilmez N., Reis R. S., 2000 Diverse Caenorhabditis elegans genes that are upregulated in dauer larvae also show elevated transcript levels in long-lived, aged, or starved adults. Journal of Molecular Biology **300**: 433–448.

Chow D. K., Glenn C. F., Johnston J. L., Goldberg I. G., Wolkow C. A., 2006 Sarcopenia in the Caenorhabditis elegans pharynx correlates with muscle contraction rate over lifespan. Experimental Gerontology **41**: 252–260.

Churgin M. A., Jung S. K., Yu C. C., Chen X., Raizen D. M., Fang-Yen C., 2017 Longitudinal imaging of caenorhabditis elegans in a microfabricated device reveals variation in behavioral decline during aging. eLife **6**.

Cinquin A., Chiang M., Paz A., Hallman S., Yuan O., Vysniauskaite I., Fowlkes C. C., Cinquin O., 2016 Intermittent Stem Cell Cycling Balances Self-Renewal and Senescence of the C. elegans Germ Line. PLoS Genetics **12**: e1005985.

Coburn C., Allman E., Mahanti P., Benedetto A., Cabreiro F., Pincus Z., Matthijssens F., Araiz C., Mandel A., Vlachos M., Edwards S.-A., Fischer G., Davidson A., Pryor R. E., Stevens A., Slack F. J., Tavernarakis N., Braeckman B. P., Schroeder F. C., Nehrke K., Gems D., 2013 Anthranilate Fluorescence Marks a Calcium-Propagated Necrotic Wave That Promotes Organismal Death in C. elegans. PLOS Biology **11**: e1001613-.

Collins J. J., Evason K., Pickett C. L., Schneider D. L., Kornfeld K., 2008a The anticonvulsant ethosuximide disrupts sensory function to extend C. elegans lifespan. PLoS Genet **4**: e1000230.

Collins J. J., Huang C., Hughes S., Kornfeld K., 2008b The measurement and analysis of age-related changes in Caenorhabditis elegans. WormBook : the online review of C. elegans biology: 1–21.

Copes N., Edwards C., Chaput D., Saifee M., Barjuca I., Nelson D., Paraggio A., Saad P., Lipps D., Stevens S. M., Bradshaw P. C., 2015 Metabolome and proteome changes with aging in Caenorhabditis elegans. Experimental Gerontology **72**: 67–84.

Cournil A., Kirkwood T., 2001 If you would live long, choose your parents well. Trends in Genetics **17**: 233–235.

Crawley O., Barroso C., Testori S., Ferrandiz N., Silva N., Castellano-Pozo M., Jaso-Tamame A. L., Martinez-Perez E., 2016 Cohesin-interacting protein WAPL-1 regulates meiotic chromosome structure and cohesion by antagonizing specific cohesin complexes. eLife **5**: 1–26.

Crittenden S. L., Leonhard K. A., Byrd D. T., Kimble J., 2006 Cellular analyses of the mitotic region in the Caenorhabditis elegans adult germ line. Molecular biology of the cell **17**: 3051–61.

Croll N. A., Smith J. M., Zuckerman B. M., 1977 The aging process of the nematode Caenorhabditis elegans in bacterial and axenic culture. Experimental Aging Research **3**: 175–189.

Dambroise E., Monnier L., Ruisheng L., Aguilaniu H., Joly J.-S., Tricoire H., Rera M., 2016 Two phases of aging separated by the Smurf transition as a public path to death. Scientific Reports **6**: 23523.

Darr D., Fridovich I., 1995 Adaptation to oxidative stress in young, but not in mature or old, caenorhabditis elegans. Free Radical Biology and Medicine **18**: 195–201.

David D. C., Ollikainen N., Trinidad J. C., Cary M. P., Burlingame A. L., Kenyon C., 2010 Widespread protein aggregation as an inherent part of aging in C. elegans. PLoS Biology **8**: 47–48.

Davies S. K., Bundy J. G., Leroi A. M., 2015 Metabolic youth in middle age: Predicting aging in Caenorhabditis elegans using metabolomics. Journal of Proteome Research **14**: 4603–4609.

Davis B. 0, Anderson G. L., Dusenbery D. B., 1982 Total Luminescence Spectroscopy of Fluorescence Changes during Aging in Caenorhabditis elegans? Biochemistry **21**: 4089–4095.

Davis M. W., 2016 A Plasmid Editor (ApE).

Dillin A., Crawford D. K., Kenyon C., 2002 Timing Requirements for Insulin/IGF-1 Signaling in C. elegans. Science **298**: 830–834.

Epstein J., Himmelhoch S., Gershon D., 1972 Studies on ageing in nematodes III. Electronmicroscopical studies on age-associated cellular damage. Mechanisms of Ageing and Development **1**: 245–255.

Ewald C. Y., Landis J. N., Porter Abate J., Murphy C. T., Blackwell T. K., 2015 Dauer-independent insulin/IGF-1-signalling implicates collagen remodelling in longevity. Nature **519**: 97–101.

Ezcurra M., Benedetto A., Sornda T., Gilliat A. F., Au C., Zhang Q., Schelt S. van, Petrache A. L., Wang H., la Guardia Y. de, Bar-Nun S., Tyler E., Wakelam M. J., Gems D., 2018 C. elegans Eats Its Own Intestine to Make Yolk Leading to Multiple Senescent Pathologies. Current Biology **28**: 2544-2556.e5.

Fabian T. J., Johnson T. E., 1995a Total RNA, rRNA and poly(A)+ RNA abundances during aging in Caenorhabditis elegans. Mechanisms of Ageing and Development **83**: 155–170.

Fabian T. J., Johnson T. E., 1995b Identification genes that are differentially expressed during aging in Caenorhabditis elegans. The journals of gerontology. Series A, Biological sciences and medical sciences **50**: B245-53.

Fei Y.-J., Liu J.-C., Inoue K., Zhuang L., Miyake K., Miyauchi S., Ganapathy V., 2004 *Relevance of NAC-2, an Na +-coupled citrate transporter, to life span, body size and fat content in Caenorhabditis elegans*.

Felkai S., Ewbank J. J., Lemieux J., Labbé J. C., Brown G. G., Hekimi S., Andersson S., Avery L., Bolanowski M., Russell R., Jacobson L., Brown G., Beattie D., Croll N., Smith J., Zuckerman B., Ewbank J., Barnes T., Lakowski B., Lussier M., Bussey H., Hekimi S., Felton J., Michaelis S., Wright A., Fire A., Xu S., Montgomery M., Kostas S., Driver S., Mello C., Hagen T., Yowe D., Bartholomew J., Wehr C., Do K., Park J., Ames B., Harman D., Hekimi S., Lakowski B., Barnes T., Ewbank J., Ishii N., Fujii M., Hartman P., Tsuda M., Yasuda K., Senoomatsuda N., Yanase S., Ayusawa D., Suzuki K., Johnson L., Walsh M., Bockus B., Chen L., Jonassen T., Marbois B., Kim L., Chin A., Xia Y., Lusis A., Clarke C., Jonassen T., Proft M., Randez-Gil F., Schultz J., Marbois B., Entian K., Clarke C., Labbé J., Hekimi S., Rokeach L., Lakowski B., Hekimi S., Lakowski B., Hekimi S., Linnane A., Marzuki S., Ozawa T., Tanaka M., Marbois B., Clarke C., Mello C., Fire A., Mello C., Kramer J., Stinchcomb D., Ambros V., Miquel J., Murfitt R., Vogel K., Sanadi D., Poyton R., McEwen J., Shigenaga M., Hagen T., Ames B., Wong A., Boutis P., Hekimi S., 1999 CLK-1 controls respiration, behavior and aging in the nematode Caenorhabditis elegans. The EMBO journal **18**: 1783–92.

Fletcher M., Kim D. H., 2017 Age-Dependent Neuroendocrine Signaling from Sensory Neurons Modulates the Effect of Dietary Restriction on Longevity of Caenorhabditis elegans (K Ashrafi, Ed.). PLOS Genetics **13**: 1–15.

Fox P. M., Vought V. E., Hanazawa M., Lee M.-H. H., Maine E. M., Schedl T., 2011 Cyclin E and CDK-2 regulate proliferative cell fate and cell cycle progression in the C. elegans germline. Development **138**: 2223–2234.

Fox P. M., Schedl T., 2015 Analysis of Germline Stem Cell Differentiation Following Loss of GLP-1 Notch Activity in Caenorhabditis elegans. Genetics **201**: 167–184.

Francis R., Barton M. K., Kimble J., Schedl T., 1995 gld-1, a tumor suppressor gene required for oocyte development in Caenorhabditis elegans. Genetics **139**: 579–606.

Friedman D. B., Johnson T. E., 1988 A mutation in the age-1 gene in Caenorhabditis elegans lengthens life and reduces hermaphrodite fertility. Genetics **118**: 75–86.

Fukuyama M., Rougvie A. E., Rothman J. H., 2006 C. elegans DAF-18/PTEN mediates nutrient-dependent arrest of cell cycle and growth in the germline. Current biology : CB **16**: 773–9.

Furuta T., Joo H.-J., #1 K. A. T., Chen S.-Y., Arur S., Trimmer K. A., Chen S.-Y., Arur S., 2018 No Title. Development (Cambridge, England) **145**: dev.161042.

Galand P., Degraef C., 1989 Cyclin/PCNA immunostaining as an alternative to tritiated thymidine pulse labelling for marking S phase cells in paraffin sections from animal and human tissues. Cell Proliferation **22**: 383–392.

Gao A. W., Chatzispyrou I. A., Kamble R., Liu Y. J., Herzog K., Smith R. L., Lenthe H. Van, Vervaart M. A. T., Cruchten A. Van, Luyf A. C., Kampen A. Van, Pras-Raves M. L., Vaz F. M., Houtkooper R. H., 2017 A sensitive mass spectrometry platform identifies metabolic changes of life history traits in C. elegans. Scientific Reports **7**: 1–14.

Garigan D., Hsu A. L., Fraser A. G., Kamath R. S., Abringet J., Kenyon C., 2002 Genetic analysis of tissue aging in Caenorhabditis elegans: A role for heat-shock factor and bacterial proliferation. Genetics **161**: 1101–1112.

Garsin D. A., Villanueva J. M., Begun J., Kim D. H., Sifri C. D., Calderwood S. B., Ruvkun G., Ausubel F. M., 2003 Long-Lived C. elegans daf-2 Mutants Are Resistant to Bacterial Pathogens. Science **300**: 1921 LP – 1921.

Gems D., Sutton A. J., Sundermeyer M. L., Albert P. S., King K. V., Edgley M. L., Larsen P. L., Riddle D. L., 1998 Two pleiotropic classes of daf-2 mutation affect larval arrest, adult behavior, reproduction and longevity in Caenorhabditis elegans. Genetics **150**: 129–155.

Gems D., Riddle D. L., 2000 Genetic, behavioral and environmental determinants of male longevity in Caenorhabditis elegans. Genetics **154**: 1597–1610.

Gershon D., 1970 *STUDIES ON AGING IN NEMATODES I. THE NEMATODE AS A MODEL ORGANISM FOR AGING RESEARCH*. Pergamon Press.

Gerstbrein B., Stamatas G., Kollias N., Driscoll M., 2005 In vivo spectrofluorimetry reveals endogenous biomarkers that report healthspan and dietary restriction in Caenorhabditis elegans. Aging Cell **4**: 127–137.

Gervaise A. L., Arur S., 2016 Spatial and Temporal Analysis of Active ERK in the C. elegans Germline. Journal of Visualized Experiments: e54901–e54901.

Glenn C. F., Chow D. K., David L., Cooke C. A., Gami M. S., Iser W. B., Hanselman K. B., Goldberg I. G., Wolkow C. A., 2004 Behavioral Deficits During Early Stages of Aging in Caenorhabditis elegans Result From Locomotory Deficits Possibly Linked to Muscle Frailty. The Journals of Gerontology Series A: Biological Sciences and Medical Sciences **59**: 1251–1260.

Golden T. R., Melov S., 2004 Microarray analysis of gene expression with age in individual nematodes. Aging Cell **3**: 111–124.

Golden T. R., Melov S., 2007 Gene expression changes associated with aging in C. elegans (The C. elegans Research Community, Ed.). WormBook: 1–12.

Golden T. R., Beckman K. B., Lee A. H. J., Dudek N., Hubbard A., Samper E., Melov S., 2007 Dramatic age-related changes in nuclear and genome copy number in the nematode Caenorhabditis elegans. Aging Cell **6**: 179–188.

Goudeau J., Aguilaniu H., 2010 Carbonylated proteins are eliminated during reproduction in C. elegans. Aging Cell **9**: 991–1003.

Greenstein D., 2005 Control of oocyte meiotic maturation and fertilization (The C. elegans Research Community, Ed.). WormBook: 1–12.

Greenwald I., Kovall R., 2013 Notch signaling: genetics and structure. In: The C. elegans Research Community (Ed.), *WormBook*,, p. 1.10.2.

Greer E. L., Dowlatshahi D., Banko M. R., Villen J., Hoang K., Blanchard D., Gygi S. P., Brunet A., 2007 An AMPK-FOXO Pathway Mediates Longevity Induced by a Novel Method of Dietary Restriction in C. elegans. Current Biology **17**: 1646–1656.

Gruber J., Ng L. F., Fong S., Wong Y. T., Koh S. A., Chen C.-B., Shui G., Cheong W. F., Schaffer S., Wenk M. R., Halliwell B., 2011 Mitochondrial Changes in Ageing Caenorhabditis elegans – What Do We Learn from Superoxide Dismutase Knockouts? (VN Uversky, Ed.). PLoS ONE **6**: e19444.

Gumienny T. L., Lambie E., Hartwieg E., Horvitz H. R., Hengartner M. O., 1999 Genetic control of programmed cell death in the Caenorhabditis elegans hermaphrodite germline. Development (Cambridge, England) **126**: 1011–1022.

Hahm J.-H., Kim S., DiLoreto R., Shi C., Lee S.-J. V., Murphy C. T., Nam H. G., 2015 C. elegans maximum velocity correlates with healthspan and is maintained in worms with an insulin receptor mutation. Nature communications **6**: 8919.

Hahn A. T., Jones J. T., Meyer T., 2009 Quantitative analysis of cell cycle phase durations and PC12 differentiation using fluorescent biosensors. Cell Cycle **8**: 1044–1052.

Haithcock E., Dayani Y., Neufeld E., Zahand A. J., Feinstein N., Mattout A., Gruenbaum Y., Liu J., 2005 Age-related changes of nuclear architecture in Caenorhabditis elegans. Proceedings of the National Academy of Sciences **102**: 16690–16695.

Han S. K., Lee D., Lee H., Kim D., Son H. G., Yang J.-S., Lee S.-J. V., Kim S., Han S. K., Lee D., Lee H., Kim D., Son H. G., Yang J.-S., Lee S.-J. V., Kim S., 2016 OASIS 2: online application for survival analysis 2 with features for the analysis of maximal lifespan and healthspan in aging research. Oncotarget **7**: 56147–56152.

Hansen D., Wilson-Berry L., Dang T., Schedl T., 2004a Control of the proliferation versus meiotic development decision in the C. elegans germline through regulation of GLD-1

protein accumulation. Development **131**: 93–104.

Hansen D., Hubbard E. J. A., Schedl T., 2004b Multi-pathway control of the proliferation versus meiotic development decision in the Caenorhabditis elegans germline. Developmental Biology **268**: 342–357.

Hansen M., Taubert S., Crawford D., Libina N., Lee S. J., Kenyon C., 2007 Lifespan extension by conditions that inhibit translation in Caenorhabditis elegans. Aging Cell **6**: 95–110.

Hansen D., Schedl T., 2013 Stem Cell Proliferation Versus Meiotic Fate Decision in Caenorhabditis elegans. In: *Germ Cell Development in C. elegans, Advances in Experimental Medicine and Biology*,, pp. 71–99.

Heintz C., Doktor T. K., Lanjuin A., Escoubas C., Zhang Y., Weir H. J., Dutta S., Silva-Garcia C. G., Bruun G. H., Morantte I., Hoxhaj G., Manning B. D., Andresen B. S., Mair W. B., 2017 Splicing factor 1 modulates dietary restriction and TORC1 pathway longevity in C. elegans. Nature **541**: 102–106.

Hendzel M. J., Wei Y., Mancini M. A., Hooser A. Van, Ranalli T., Brinkley B. R., Bazett-Jones D. P., Allis C. D., 1997 Mitosis-specific phosphorylation of histone H3 initiates primarily within pericentromeric heterochromatin during G2 and spreads in an ordered fashion coincident with mitotic chromosome condensation. Chromosoma **106**: 348–360.

Herndon L. A., Schmeissner P. J., Dudaronek J. M., Brown P. A., Listner K. M., Sakano Y., Paupard M. C., Hall D. H., Driscoll M., 2002 Stochastic and genetic factors influence tissue-specific decline in ageing C. elegans. Nature **419**: 808–814.

Heuvel S. van den, Kipreos E. T., 2012 C. elegans Cell Cycle Analysis. Methods in Cell Biology **107**: 265–294.

Hibshman J. D., Hung A., Baugh L. R., 2016 Maternal Diet and Insulin-Like Signaling Control Intergenerational Plasticity of Progeny Size and Starvation Resistance (K Ashrafi, Ed.). PLOS Genetics **12**: e1006396.

Hirsh D., Oppenheim D., Klass M., 1976 Development of the reproductive system of Caenorhabditis elegans. Developmental Biology **49**: 200–219.

Hodgkin J., Barnes T. M., 1991 More is not better: brood size and population growth in a self-fertilizing nematode. Proc R Soc Lond B Biol Sci **246**: 19–24.

Hodgkin J., Doniach T., 1997 Natural variation and copulatory plug formation in Caenorhabditis elegans. Genetics **146**: 149–164.

Hoffman J. M., Lyu Y., Pletcher S. D., Promislow D. E. L., 2017 Proteomics and metabolomics in ageing research: from biomarkers to systems biology. Essays In Biochemistry **61**: 379–388.

Hosokawa H., Ishii N., Ishida H., Ichimori K., Nakazawa H., Suzuki K., 1994 Rapid accumulation of fluorescent material with aging in an oxygen-sensitive mutant mev-1 of Caenorhabditis elegans. Mechanisms of Ageing and Development **74**: 161–170.

Hosono R., 1978 Age dependent changes in the behavior of Caenorhabditis elegans on attraction to Escherichia coli. Experimental Gerontology **13**: 31–36.

Hosono R., Sato Y., Aizawa S.-I., Mitsui Y., 1980 Age-dependent changes in mobility and separation of the nematode Caenorhabditis elegans. Experimental Gerontology **15**: 285–289.

Hosono R., Nishimoto S., Kuno S., 1989 Alterations of life span in the nematode Caenorhabditis elegans under monoxenic culture conditions. Experimental Gerontology **24**: 251–264.

Hsu A.-L. L., Feng Z., Hsieh M.-Y. Y., Xu X. Z. S., 2009 Identification by machine vision of the rate of motor activity decline as a lifespan predictor in C. elegans. Neurobiology of Aging **30**: 1498–503.

Huang C., Xiong C., Kornfeld K., 2004 Measurements of Age-Related Changes of Physiological Processes That Predict Lifespan of Caenorhabditis elegans. Proceedings of the National Academy of Sciences of the United States of America **101**: 8084–8089.

Hughes S. E., 2005 Reproductive Aging in Caenorhabditis elegans.

Hughes S. E., Evason K., Xiong C., Kornfeld K., 2007 Genetic and pharmacological factors that influence reproductive aging in nematodes. PLoS Genet **3**: e25.

Hughes S. E., Huang C., Kornfeld K., 2011 Identification of mutations that delay somatic or reproductive aging of Caenorhabditis elegans. Genetics **189**: 341–356.

Hulme S. E., Shevkoplyas S. S., McGuigan A. P., Apfeld J., Fontana W., Whitesides G. M., 2010 Lifespan-on-a-chip: microfluidic chambers for performing lifelong observation of C. elegans. Lab Chip **10**: 589–597.

Ibáñez-Ventoso C., Yang M., Guo S., Robins H., Padgett R. W., Driscoll M., 2006 Modulated microRNA expression during adult lifespan in Caenorhabditis elegans. Aging Cell **5**: 235–246.

Ikeda T., Yasui C., Hoshino K., Arikawa K., Nishikawa Y., 2007 Influence of Lactic Acid Bacteria on Longevity of Caenorhabditis elegans and Host Defense against Salmonella enterica Serovar Enteritidis. Applied and Environmental Microbiology **73**: 6404 LP – 6409.

Invitrogen, 2010 EdU (5-ethynyl-2'-deoxyuridine). : 1–7.

Iwasaki K., McCarter J., Francis R., Schedl T., 1996 emo-1, a Caenorhabditis elegans Sec61p gamma homologue, is required for oocyte development and ovulation. J Cell Biol **134**: 699–714.

Jaramillo-Lambert A., Ellefson M., Villeneuve A. M., Engebrecht J., 2007 Differential timing of S phases, X chromosome replication, and meiotic prophase in the C. elegans germ line. Developmental Biology **308**: 206–221.

Jemielity S., Chapuisat M., Parker J. D., Keller L., 2005 Long live the queen: Studying aging in

social insects. Age **27**: 241–248.

Johnson T. E., 1987 Aging can be genetically dissected into component processes using long-lived lines of Caenorhabditis elegans. Proc Natl Acad Sci U S A **84**: 3777–3781.

Johnston J., Iser W. B., Chow D. K., Goldberg I. G., Wolkow C. A., 2008 Quantitative image analysis reveals distinct structural transitions during aging in Caenorhabditis elegans tissues. PLoS One **3**: e2821.

Jones O. R., Scheuerlein A., Salguero-Gómez R., Camarda C. G., Schaible R., Casper B. B., Dahlgren J. P., Ehrlén J., García M. B., Menges E. S., Quintana-Ascencio P. F., Caswell H., Baudisch A., Vaupel J. W., 2014 Diversity of ageing across the tree of life. Nature **505**: 169–73.

Jung T., Bader N., Grune T., 2007 Lipofuscin: Formation, distribution, and metabolic consequences. Annals of the New York Academy of Sciences **1119**: 97–111.

Kaeberlein T. L., Smith E. D., Tsuchiya M., Welton K. L., Thomas J. H., Fields S., Kennedy B. K., Kaeberlein M., 2006 Lifespan extension in Caenorhabditis elegans by complete removal of food. Aging Cell **5**: 487–494.

Kamath R. S., Martinez-Campos M., Zipperlen P., Fraser A. G., Ahringer J., 2000 Effectiveness of specific RNA-mediated interference through ingested double-stranded RNA in Caenorhabditis elegans. Genome Biology **2**: research0002.1.

Kamath R. S., Fraser A. G., Dong Y., Poulin G., Durbin R., Gotta M., Kanapin A., Bot N. Le, Moreno S., Sohrmann M., Welchman D. P., Zipperlen P., Ahringer J., 2003 Systematic functional analysis of the Caenorhabditis elegans genome using RNAi. Nature **421**: 231–237.

Kamili F., Lu H., 2018 Annual Review of Analytical Chemistry Recent Advances and Trends in Microfluidic Platforms for C. elegans Biological Assays.

Kanzaki N., Tsai I. J., Tanaka R., Hunt V. L., Liu D., Tsuyama K., Maeda Y., Namai S., Kumagai R., Tracey A., Holroyd N., Doyle S. R., Woodruff G. C., Murase K., Kitazume H., Chai C., Akagi A., Panda O., Ke H.-M., Schroeder F. C., Wang J., Berriman M., Sternberg P. W., Sugimoto A., Kikuchi T., 2018 Biology and genome of a newly discovered sibling species of Caenorhabditis elegans. Nature Communications **9**: 3216.

Kao S.-H. H., Tseng C.-Y. Y., Wan C.-L. L., Su Y.-H. H., Hsieh C.-C. C., Pi H., Hsu H.-J. J., 2015 Aging and insulin signaling differentially control normal and tumorous germline stem cells. Aging Cell **14**: 25–34.

Kaplan E. L., Meier P., 1958 *Nonparametric Estimation from Incomplete Observations*.

Kato M., Chen X., Inukai S., Zhao H., Slack F. J., 2011 Age-associated changes in expression of small, noncoding RNAs, including microRNAs, in C. elegans. Rna **17**: 1804–1820.

Kato M., Hamazaki Y., Sun S., Nishikawa Y., Kage-Nakadai E., 2018 Clostridium butyricum MIYAIRI 588 Increases the Lifespan and Multiple-Stress Resistance of Caenorhabditis

elegans. Nutrients **10**.

Kauffman A. L., Ashraf J. M., Corces-Zimmerman M. R., Landis J. N., Murphy C. T., 2010 Insulin signaling and dietary restriction differentially influence the decline of learning and memory with age (J Dubnau, Ed.). PLoS Biol **8**: e1000372.

Kenyon C., Chang J., Gensch E., Rudner A., Tabtiang R., 1993 A C. elegans mutant that lives twice as long as wild type. Nature **366**: 461–464.

Kershner A. M., Shin H., Hansen T. J., Kimble J., 2014 Discovery of two GLP-1/Notch target genes that account for the role of GLP-1/Notch signaling in stem cell maintenance. Proceedings of the National Academy of Sciences of the United States of America **111**: 3739–44.

Killian D. J., Hubbard E. J. A., 2005 Caenorhabditis elegans germline patterning requires coordinated development of the somatic gonadal sheath and the germ line. Developmental Biology **279**: 322–335.

Kim D. H., 2013 Bacteria and the Aging and Longevity of Caenorhabditis elegans. Annual Review of Genetics **47**: 233–246.

Kimble J., Ward S., 1988 Germ-line Development and Fertilization. Cold Spring Harbor Monograph Archive **17**: 191–213.

Kimble J., Seidel H. S., 2013 C . elegans germline stem cells and their niche. In: *StemBook*, Harvard Stem Cell Institute, pp. 1–12.

Kiontke K., Fitch D. H. a, 2005 The phylogenetic relationships of Caenorhabditis and other rhabditids. WormBook : the online review of C. elegans biology: 1–11.

Kiontke K., Sudhaus W., Giblin-Davis R., 2011 Description of Caenorhabditis angaria n. sp. (Nematoda: Rhabditidae), an associate of sugarcane and palm weevils (Coleoptera: Curculionidae). Nematology **13**: 61–78.

Kirkwood T. B., Holliday R., 1979 The evolution of ageing and longevity. Proceedings of the Royal Society of London. Series B, Biological sciences **205**: 531–46.

Kirkwood T. B. L., Austad S. N., 2000 Why do we age? Nature **408**: 233–238.

Kirkwood T. B. L., Melov S., 2011 On the programmed/non-programmed nature of ageing within the life history. Current Biology **21**: R701–R707.

Kisielewska J., Lu P., Whitaker M., 2005 GFP-PCNA as an S-phase marker in embryos during the first and subsequent cell cycles. Biology of the Cell **97**: 221–229.

Klass M. R., 1977 Aging in the nematode Caenorhabditis elegans: Major biological and environmental factors influencing life span. Mechanisms of Ageing and Development **6**: 413–429.

Klass M., Nguyen P. N., Dechavigny A., 1983 Age-correlated changes in the DNA template in

the nematode Caenorhabditis elegans. Mechanisms of Ageing and Development **22**: 253–263.

Kocsisova Z., Mohammad A., Kornfeld K., Schedl T., 2018a Cell Cycle Analysis in the C. Elegans Germline with the Thymidine Analog EdU. Journal of visualized experiments : JoVE. **140**: e58339–e58339.

Kocsisova Z., Kornfeld K., Schedl T., 2018b Cell cycle accumulation of the proliferating cell nuclear antigen PCN-1 transitions from continuous in the adult germline to intermittent in the early embryo of C. elegans. BMC Developmental Biology **18**: 1–12.

Kocsisova Z., Kornfeld K., Schedl T., 2019 Rapid population-wide declines in stem cell number and activity during reproductive aging in C. elegans. Development **146**: dev173195.

Korta D. Z., Tuck S., Hubbard E. J. A., 2012 S6K links cell fate, cell cycle and nutrient response in C. elegans germline stem/progenitor cells. Journal of Cell Science **125**: 859–870.

Kumar S., Dietrich N., Kornfeld K., Kim S. K., 2016 Angiotensin Converting Enzyme (ACE) Inhibitor Extends Caenorhabditis elegans Life Span. PLoS Genet **12**: e1005866.

Kumar S., Egan B. M., Kocsisova Z., Schneider D. L., Murphy J. T., Diwan A., Kornfeld K., 2019 Lifespan Extension in C. elegans Caused by Bacterial Colonization of the Intestine and Subsequent Activation of an Innate Immune Response. Developmental Cell **49**: 100-117.e6.

Kurz C. L., Ewbank J. J., 2003 Caenorhabditis elegans: an emerging genetic model for the study of innate immunity. Nature Reviews Genetics **4**: 380–390.

la Guardia Y. de, Gilliat A. F., Hellberg J., Rennert P., 2016 Run-on of germline apoptosis promotes gonad senescence in C . elegans. Oncotarget **7**: 39082–96.

Labbadia J., Morimoto R. I., 2015 Repression of the Heat Shock Response Is a Programmed Event at the Onset of Reproduction. Molecular Cell **59**: 639–650.

Labrousse A., Chauvet S., Couillault C., Léopold Kurz C., Ewbank J. J., 2000 Caenorhabditis elegans is a model host for Salmonella typhimurium. Current Biology **10**: 1543–1545.

Lakowski B., Hekimi S., 1998 The genetics of caloric restriction in Caenorhabditis elegans. Proceedings of the National Academy of Sciences of the United States of America **95**: 13091–13096.

Lans H., Jansen G., 2007 Multiple sensory G proteins in the olfactory, gustatory and nociceptive neurons modulate longevity in Caenorhabditis elegans. Developmental Biology **303**: 474–482.

Laws T. R., Harding S. V, Smith M. P., Atkins T. P., Titball R. W., 2006 Age influences resistance of Caenorhabditis elegans to killing by pathogenic bacteria. FEMS Microbiology Letters **234**: 281–287.

Lee G. D., Wilson M. A., Zhu M., Wolkow C. A., Cabo R. De, Ingram D. K., Zou S., 2006

Dietary deprivation extends lifespan in Caenorhabditis elegans. Aging Cell **5**: 515–524.

Lee C., Sorensen E. B., Lynch T. R., Kimble J., Parrish S., Timmons L., Plasterk R., Fire A., Singh A., Raj A., Rossant J., Lee C., Sorensen E. B., Lynch T. R., Kimble J., 2016 *C. elegans* GLP-1/Notch activates transcription in a probability gradient across the germline stem cell pool. eLife **5**: 269–282.

Leiser S. F., Begun A., Kaeberlein M., 2011 HIF-1 modulates longevity and healthspan in a temperature-dependent manner. Aging Cell **10**: 318–326.

Leiser S. F., Jafari G., Primitivo M., Sutphin G. L., Dong J., Leonard A., Fletcher M., Kaeberlein M., 2016 Age-associated vulval integrity is an important marker of nematode healthspan. AGE **38**: 419–431.

Leonardi E., Girlando S., Serio G., Mauri F. A., Perrone G., Scampini S., Palma D., Barbareschi M., 1992 PCNA and Ki67 expression in breast carcinoma: Correlations with clinical and biological variables. J Clin Pathol **45**: 416–419.

Leonhardt H., Rahn H.-P., Weinzierl P., Sporbert A., Cremer T., Zink D., Cardoso M. C., 2000 Dynamics of DNA Replication Factories in Living Cells. The Journal of Cell Biology **149**.

Li G., Gong J., Liu J. J. J., Liu J. J. J., Li H., Hsu A.-L., Liu J. J. J., Xu X. Z. S., 2019 Genetic and pharmacological interventions in the aging motor nervous system slow motor aging and extend life span in *C. elegans*. Science Advances **5**: eaau5041.

Liu J. J., Zhang B., Lei H., Feng Z., Liu J. J., Hsu A.-L., Xu X. Z. S., 2013 Functional aging in the nervous system contributes to age-dependent motor activity decline in C. elegans. Cell metabolism **18**: 392–402.

Lohr J. N., Galimov E. R., Gems D., 2019 *Does senescence promote fitness in Caenorhabditis elegans by causing death?* Elsevier.

Lucanic M., Plummer W. T., Chen E., Harke J., Foulger A. C., Onken B., Coleman-Hulbert A. L., Dumas K. J., Guo S., Johnson E., Bhaumik D., Xue J., Crist A. B., Presley M. P., Harinath G., Sedore C. A., Chamoli M., Kamat S., Chen M. K., Angeli S., Chang C., Willis J. H., Edgar D., Royal M. A., Chao E. A., Patel S., Garrett T., Ibanez-Ventoso C., Hope J., Kish J. L., Guo M., Lithgow G. J., Driscoll M., Phillips P. C., 2017 Impact of genetic background and experimental reproducibility on identifying chemical compounds with robust longevity effects. Nature Communications **8**: 14256.

Luckinbill L. S., Clare M. J., 1985 Selection for life span in Drosophila melanogaster. Heredity **55**: 9–18.

Lund J., Tedesco P., Duke K., Wang J., Kim S. K., Johnson T. E., 2002 *Transcriptional Profile of Aging in C. elegans are part of an insulin-related signaling pathway are in*.

Luo S., Shaw W. M., Ashraf J., Murphy C. T., 2009 TGF-B Sma/Mab signaling mutations uncouple reproductive aging from somatic aging (SK Kim, Ed.). PLoS Genetics **5**: e1000789.

Luo S., Kleemann G. A., Ashraf J. M., Shaw W. M., Murphy C. T., 2010 TGF-beta and insulin signaling regulate reproductive aging via oocyte and germline quality maintenance. Cell **143**: 299–312.

Luo S., Murphy C. T., 2011 Caenorhabditis elegans reproductive aging: Regulation and underlying mechanisms. Genesis **49**: 53–65.

Macneil L. T., Watson E., Arda H. E., Zhu L. J., Walhout A. J. M., 2013 Diet-Induced Developmental Acceleration Independent of TOR and Insulin in C. elegans. Cell **153**: 240–252.

Maier W., Adilov B., Regenass M., Alcedo J., 2010 A Neuromedin U Receptor Acts with the Sensory System to Modulate Food Type-Dependent Effects on C. elegans Lifespan. PLOS Biology **8**: e1000376.

Mair W., Morantte I., Rodrigues A. P. C., Manning G., Montminy M., Shaw R. J., Dillin A., 2011 Lifespan extension induced by AMPK and calcineurin is mediated by CRTC-1 and CREB. Nature **470**: 404–408.

Mari M., Filippidis G., Palikaras K., Petanidou B., Fotakis C., Tavernarakis N., 2015 Imaging ectopic fat deposition in caenorhabditis elegans muscles using nonlinear microscopy. Microscopy Research and Technique **78**: 523–528.

Mari M., Palikaras K., Filippidis G., Pasparaki A., Tavernarakis N., Petanidou B., Mari M., Petanidou B., Pasparaki A., Filippidis G., Tavernarakis N., 2016 Ectopic fat deposition contributes to age-associated pathology in Caenorhabditis elegans . Journal of Lipid Research **58**: 72–80.

Maures T. J., Booth L. N., Benayoun B. A., Izrayelit Y., Schroeder F. C., Brunet A., 2014 Males shorten the life span of C. elegans hermaphrodites via secreted compounds. Science **343**: 541–544.

McCarter J., Bartlett B., Dang T., Schedl T., 1997 Soma-germ cell interactions in Caenorhabditis elegans: multiple events of hermaphrodite germline development require the somatic sheath and spermathecal lineages. Dev Biol **181**: 121–143.

McCarter J., Bartlett B., Dang T., Schedl T., 1999 On the Control of Oocyte Meiotic Maturation and Ovulation in Caenorhabditis elegans. Developmental Biology **205**: 111–128.

McGee M. D., Weber D., Day N., Vitelli C., Crippen D., Herndon L. A., Hall D. H., Melov S., 2011 Loss of intestinal nuclei and intestinal integrity in aging C. elegans. Aging Cell **10**: 699–710.

Medawar P. B., 1952 *An unsolved problem of biology*. Lewis, London.

Meier R., Ruttkies C., Treutler H., Neumann S., 2017 Bioinformatics can boost metabolomics research. Journal of Biotechnology **261**: 137–141.

Melov S., Lithgow G. J., Fischer D. R., Tedesco P. M., Johnson T. E., 1995 Increased frequency of deletions in the mitochondrial genome with age of *Caenorhabditis elegans*. Nucleic

Acids Research **23**: 1419–1425.

Mendenhall A. R., Wu D., Park S. K., Cypser J. R., Tedesco P. M., Link C. D., Phillips P. C., Johnson T. E., 2011 Genetic dissection of late-life fertility in Caenorhabditis elegans. Journals of Gerontology - Series A Biological Sciences and Medical Sciences **66**: 842–854.

Meyer J. N., Boyd W. A., Azzam G. A., Haugen A. C., Freedman J. H., Houten B. Van, 2007 Decline of nucleotide excision repair capacity in aging Caenorhabditis elegans. Genome Biology **8**.

Michaelson D., Korta D. Z., Capua Y., Hubbard E. J. A., 2010 Insulin signaling promotes germline proliferation in C. elegans. Development **137**: 671–680.

Miller M. A., Nguyen V. Q., Lee M. H., Kosinski M., Schedl T., Caprioli R. M., Greenstein D., 2001 A sperm cytoskeletal protein that signals oocyte meiotic maturation and ovulation. Science (New York, N.Y.) **291**: 2144–2147.

Mitteldorf J. J., Goodnight C., 2013 Post Reproductive Life Span and Demographic Stability. Biochemistry (Moscow) **78**: 1293–1305.

Miyachi K., Fritzler M. J., Tan E. M., 1978 Autoantibody to a Nuclear Antigen in Proliferating Cells. The Journal of Immunology **121**: 2228–2234.

Mohammad A., Broek K. Vanden, Wang C., Daryabeigi A., Jantsch V., Hansen D., Schedl T., 2018 Initiation of Meiotic Development Is Controlled by Three Post-transcriptional Pathways in Caenorhabditis elegans. Genetics **209**: 1197–1224.

Moldovan G. L., Pfander B., Jentsch S., 2007 PCNA, the Maestro of the Replication Fork. Cell **129**: 665–679.

Monsalve G. C., Yamamoto K. R., Ward J. D., 2019 A new tool for inducible gene expression in caenorhabditis elegans. Genetics **211**: 419–430.

Morsci N. S., Hall D. H., Driscoll M., Sheng Z.-H., 2016 Age-Related Phasic Patterns of Mitochondrial Maintenance in Adult Caenorhabditis elegans Neurons. The Journal of Neuroscience **36**: 1373.

Mortazavi A., Schwarz E. M., Williams B., Schaeffer L., Antoshechkin I., Wold B. J., Sternberg P. W., 2010 Scaffolding a Caenorhabditis nematode genome with RNA-seq. Genome Research **20**: 1740–1747.

Murakami H., Bessinger K., Hellmann J., Murakami S., 2005 Aging-dependent and -independent modulation of associative learning behavior by insulin/insulin-like growth factor-1 signal in Caenorhabditis elegans. J Neurosci **25**: 10894–10904.

Muschiol D., Schroeder F., Traunspurger W., 2009 Life cycle and population growth rate of Caenorhabditis elegans studied by a new method. BMC Ecology **9**: 14.

Narayan V., Ly T., Pourkarimi E., Murillo A. B., Gartner A., Lamond A. I., Kenyon C., 2016 Deep Proteome Analysis Identifies Age-Related Processes in C. elegans. Cell Systems **3**:

144–159.

Narbonne P., Maddox P. S., Labbe J.-C., 2015 daf-18/PTEN locally antagonizes insulin signalling to couple germline stem cell proliferation to oocyte needs in C. elegans. Development: 4230–4241.

Newell Stamper B. L., Cypser J. R., Kechris K., Kitzenberg D. A., Tedesco P. M., Johnson T. E., 2018 Movement decline across lifespan of Caenorhabditis elegans mutants in the insulin/insulin-like signaling pathway. Aging Cell **17**: e12704.

Palikaras K., Mari M., Petanidou B., Pasparaki A., Filippidis G., Tavernarakis N., 2016 Ectopic fat deposition contributes to age-associated pathology in Caenorhabditis elegans. Journal of lipid research: jlr.M069385.

Pan C.-L., Peng C.-Y., Chen C.-H., McIntire S., 2011 Genetic analysis of age-dependent defects of the Caenorhabditis elegans touch receptor neurons. Proceedings of the National Academy of Sciences **108**: 9274–9279.

Patel D. S., Garza-Garcia A., Nanji M., McElwee J. J., Ackerman D., Driscoll P. C., Gems D., 2008 Clustering of genetically defined allele classes in the Caenorhabditis elegans DAF-2 insulin/IGF-1 receptor. Genetics **178**: 931–46.

Pazdernik N., Schedl T., 2013 Introduction to Germ Cell Development in Caenorhabditis elegans. In: *Germ Cell Development in C. elegans, Advances in Experimental Medicine and Biology*,, pp. 1–16.

Pepper A. S. R. S.-R., Killian D. J., Hubbard E. J. A., 2003 Genetic Analysis of Caenorhabditis elegans glp-1 Mutants Suggests Receptor Interaction or Competition. Genetics **163**: 115–132.

Petrascheck M., Miller D. L., 2017 Computational Analysis of Lifespan Experiment Reproducibility . Frontiers in Genetics **8**: 92.

Pickett C. L., Kornfeld K., 2013 Age-related degeneration of the egg-laying system promotes matricidal hatching in Caenorhabditis elegans. Aging Cell **12**: 544–553.

Pickett C. L., Dietrich N., Chen J., Xiong C., Kornfeld K., 2013 Mated progeny production is a biomarker of aging in Caenorhabditis elegans. G3 (Bethesda) **3**: 2219–2232.

Pincus Z., Slack F. J., 2010 Developmental biomarkers of aging in Caenorhabditis elegans. Developmental Dynamics **239**: 1306–1314.

Pincus Z., Smith-Vikos T., Slack F. J., 2011 MicroRNA predictors of longevity in caenorhabditis elegans. PLoS Genetics **7**.

Pincus Z., Mazer T. C., Slack F. J., 2016 Autofluorescence as a measure of senescence in C. elegans: look to red, not blue or green. Aging **8**: 889–898.

Pletcher S. D., Khazaeli A. A., Curtsinger J. W., 2000 *Why Do Life Spans Differ? Partitioning Mean Longevity Differences in Terms of Age-Specific Mortality Parameters*.

Podshivalova K., Kerr R. A., Kenyon C., 2017 How a Mutation that Slows Aging Can Also Disproportionately Extend End-of-Life Decrepitude. Cell Reports **19**: 441–450.

Pontoizeau C., Mouchiroud L., Molin L., Mergoud-Dit-Lamarche A., Dalliere N., Toulhoat P., Elena-Herrmann B., Solari F., 2014 Metabolomics analysis uncovers that dietary restriction buffers metabolic changes associated with aging in Caenorhabditis elegans. J Proteome Res **13**: 2910–2919.

Porta E. A., 2002 Pigments in Aging : An Overview. New York **687**: 217–23.

Portal-Celhay C., Bradley E. R., Blaser M. J., 2012 Control of intestinal bacterial proliferation in regulation of lifespan in Caenorhabditis elegans. BMC Microbiology **12**: 49.

Preibisch S., Saalfeld S., Tomancak P., 2009 Globally optimal stitching of tiled 3D microscopic image acquisitions. Bioinformatics (Oxford, England) **25**: 1463–5.

Pu M., Ni Z., Wang M., Wang X., Wood J. G., Helfand S. L., Yu H., Lee S. S., 2015 Trimethylation of Lys36 on H3 restricts gene expression change during aging and impacts life span. Genes and Development **29**: 718–731.

Pu M., Wang M., Wang W., Velayudhan S. S., Lee S. S., 2018 Unique patterns of trimethylation of histone H3 lysine 4 are prone to changes during aging in Caenorhabditis elegans somatic cells. PLoS Genetics **14**: 1–26.

Qin Z., Hubbard E. J. A., 2015 Non-autonomous DAF-16/FOXO activity antagonizes age-related loss of C. elegans germline stem/progenitor cells. Nature communications **6**: 7107.

R Core Team, 2013 R: A Language and Environment for Statistical Computing. : http://www.r-project.org/.

Raamsdonk J. M. van, Hekimi S., 2011 FUdR causes a twofold increase in the lifespan of the mitochondrial mutant gas-1. Mechanisms of Ageing and Development **132**: 519–521.

Rangaraju S., Solis G. M., Thompson R. C., Gomez-Amaro R. L., Kurian L., Encalada S. E., Niculescu A. B., Salomon D. R., Petrascheck M., 2015 Suppression of transcriptional drift extends C. Elegans lifespan by postponing the onset of mortality. eLife **4**: 1–39.

Rasband W. ., 2016 ImageJ. : http://imagej.nih.gov/ij/.

Regmi S. G., Rolland S. G., Conradt B., 2014 Age-dependent changes in mitochondrial morphology and volume are not predictors of lifespan. Aging **6**: 118–130.

Reis-Rodrigues P., Czerwieniec G., Peters T. W., Evani U. S., Alavez S., Gaman E. A., Vantipalli M., Mooney S. D., Gibson B. W., Lithgow G. J., Hughes R. E., 2012 Proteomic analysis of age-dependent changes in protein solubility identifies genes that modulate lifespan. Aging Cell **11**: 120–127.

Restif C., Ibáñez-Ventoso C., Vora M. M., Guo S., Metaxas D., Driscoll M., 2014 CeleST: Computer Vision Software for Quantitative Analysis of C. elegans Swim Behavior Reveals Novel Features of Locomotion (A Prlic, Ed.). PLoS Computational Biology **10**: e1003702.

Riesen M., Feyst I., Rattanavirotkul N., Ezcurra M., Tullet J. M. A., Papatheodorou I., Ziehm M., Au C., Gilliat A. F., Hellberg J., Thornton J. M., Gems D., 2014 MDL-1, a growth- and tumor-suppressor, slows aging and prevents germline hyperplasia and hypertrophy in C. elegans. Aging **6**: 98–117.

Robertson O. H., 1961 Prolongation of the life span of konkanee salmon (Oncorhynchus nerka kennerlyi) by castration before beginning of gonad development. Proceedings of the National Academy of Sciences **47**: 609–621.

Robertson O. H., Wexler B. C., 1962 Histological changes in the organs and tissues of senile castrated kokanee salmon (Oncorhynchus nerka kennerlyi). General and Comparative Endocrinology **2**: 458–472.

Rodriguez N., Murdoch S., Bergmann S., Virk B., Casanueva O., Novère N. Le, Pearce J., Mains A., Hastings J., 2019 Multi-Omics and Genome-Scale Modeling Reveal a Metabolic Shift During C. elegans Aging. Frontiers in Molecular Biosciences **6**: 1–18.

Rogina B., Reenan R. a, Nilsen S. P., Helfand S. L., 2000 Extended life-span conferred by cotransporter gene mutations in Drosophila. Science (New York, N.Y.) **290**: 2137–2140.

Rose M. R., 1984 Laboratory Evolution of Postponed Senescence in Drosophila melanogaster. Evolution **38**: 1004–1010.

Rousakis A., Vlanti A., Borbolis F., Roumelioti F., Kapetanou M., Syntichaki P., 2014 Diverse Functions of mRNA Metabolism Factors in Stress Defense and Aging of Caenorhabditis elegans (DL Kontoyiannis, Ed.). PLoS ONE **9**: e103365.

Roy D., Michaelson D., Hochman T., Santella A., Bao Z., Goldberg J. D., Hubbard E. J. A., 2016 Cell cycle features of C. elegans germline stem/progenitor cells vary temporally and spatially. Developmental Biology **409**: 261–271.

RStudio Team, 2015 RStudio: Integrated Development Environment for R. : www.rstudio.com/.

Russell J. C., Burnaevskiy N., Ma B., Mailig M. A., Faust F., Crane M., Kaeberlein M., Mendenhall A., 2017 Electrophysiological Measures of Aging Pharynx Function in C. elegans Reveal Enhanced Organ Functionality in Older, Long-lived Mutants. The Journals of Gerontology: Series A.

Salic A., Mitchison T. J., A chemical method for fast and sensitive detection of DNA synthesis in vivo.

Sánchez-Blanco A., Kim S. K., 2011 Variable pathogenicity determines individual lifespan in Caenorhabditis elegans. PLoS genetics **7**: e1002047–e1002047.

Sánchez-Blanco A., Rodríguez-Matellán A., González-Paramás A., González-Manzano S., Kim S. K., Mollinedo F., 2016 Dietary and microbiome factors determine longevity in Caenorhabditis elegans. Aging **8**: 1513–1539.

Schindelin J., Arganda-Carreras I., Frise E., Kaynig V., Longair M., Pietzsch T., Preibisch S., Rueden C., Saalfeld S., Schmid B., Tinevez J.-Y., White D. J., Hartenstein V., Eliceiri K.,

Tomancak P., Cardona A., 2012 Fiji: an open-source platform for biological-image analysis. Nature Methods **9**: 676–682.

Schisa J. A., Pitt J. N., Priess J. R., 2001 Analysis of RNA associated with P granules in germ cells of C. elegans adults. Development (Cambridge, England) **128**: 1287–1298.

Seidel H. S., Kimble J., 2015 Cell-cycle quiescence maintains Caenorhabditis elegans germline stem cells independent of GLP-1/Notch. eLife **4**: e10832.

Shamir L., Wolkow C. A., Goldberg I. G., 2009 Quantitative measurement of aging using image texture entropy. Bioinformatics (Oxford, England) **25**: 3060–3.

Shaw W. M., Luo S., Landis J., Ashraf J., Murphy C. T., 2007 The C. elegans TGF-?? Dauer Pathway Regulates Longevity via Insulin Signaling. Current Biology **17**: 1635–1645.

Shemesh N., Shai N., Ben-Zvi A., 2013 Germline stem cell arrest inhibits the collapse of somatic proteostasis early in Caenorhabditis elegans adulthood. Aging Cell **12**: 814–822.

Shi C., Murphy C. T., 2014 Mating induces shrinking and death in Caenorhabditis mothers. Science (New York, N.Y.) **343**: 536–40.

Shi C., Runnels A. M., Murphy C. T., 2017 Mating and male pheromone kill Caenorhabditis males through distinct mechanisms. eLife **6**.

Shin H., Haupt K. A., Kershner A. M., Kroll-Conner P., Wickens M., Kimble J., 2017 SYGL-1 and LST-1 link niche signaling to PUF RNA repression for stem cell maintenance in Caenorhabditis elegans (D Greenstein, Ed.). PLOS Genetics **13**: e1007121.

Shrout P. E., Fleiss J. L., 1979 Intraclass Correlations: Uses in Assessing Rater Reliability. Psychological Bulletin **86**: 420–428.

Sifri C. D., Begun J., Ausubel F. M., Calderwood S. B., 2003 Caenorhabditis elegans as a Model Host for Staphylococcus aureus Pathogenesis. Infection and Immunity **71**: 2208 LP – 2217.

Simpson V. J., Johnson T. E., Hammen R. F., 1986 Caenorhabditis elegans DNA does not contain 5-methylcytosine at any time during development or aging. Nucleic Acids Research **14**: 6711–6719.

Solis G. M., Petrascheck M., 2011 Measuring Caenorhabditis elegans life span in 96 well microtiter plates. Journal of visualized experiments : JoVE.

Son H. G., Altintas O., Eun |, Kim J. E., Kwon S., Seung-Jae |, Lee V., 2018 Age-dependent changes and biomarkers of aging in Caenorhabditis elegans.

Soukas A. A., Kane E. A., Carr C. E., Melo J. A., Ruvkun G., 2009 Rictor/TORC2 regulates fat metabolism, feeding, growth, and life span in Caenorhabditis elegans. Genes & development **23**: 496–511.

Sowa J. N., Mutlu A. S., Xia F., Wang M. C., 2015 Olfaction Modulates Reproductive Plasticity

through Neuroendocrine Signaling in Caenorhabditis elegans. Current Biology **25**: 2284–2289.

Spike C. A., Huelgas-Morales G., Tsukamoto T., Greenstein D., 2018 Multiple Mechanisms Inactivate the LIN-41 RNA-Binding Protein To Ensure a Robust Oocyte-to-Embryo Transition in Caenorhabditis elegans. Genetics **210**: 1011–1037.

Steinkraus K. A., Smith E. D., Davis C., Carr D., Pendergrass W. R., Sutphin G. L., Kennedy B. K., Kaeberlein M., 2008 Dietary restriction suppresses proteotoxicity and enhances longevity by an hsf-1-dependent mechanism in Caenorhabditis elegans. Aging Cell **7**: 394–404.

Stewart E. J., Madden R., Paul G., Taddei F., 2005 Aging and death in an organism that reproduces by morphologically symmetric division. PLoS Biology **3**: 0295–0300.

Stiernagle T., 2006 Maintenance of C. elegans. WormBook: 1–11.

Stroustrup N., Ulmschneider B. E., Nash Z. M., López-Moyado I. F., Apfeld J., Fontana W., 2013 The Caenorhabditis elegans Lifespan Machine. Nature Methods **10**: 665–670.

Stroustrup N., Anthony W. E., Nash Z. M., Gowda V., Gomez A., López-Moyado I. F., Apfeld J., Fontana W., 2016 The temporal scaling of Caenorhabditis elegans ageing. Nature **530**: 103–107.

Sze J. Y., Victor M., Loer C., Shi Y., Ruvkun G., 2000 Food and metabolic signalling defects in a Caenorhabditis elegans serotonin-synthesis mutant. Nature **403**: 560–564.

Szewczyk N. J., Udranszky I. a, Kozak E., Sunga J., Kim S. K., Jacobson L. a, Conley C. a, 2006 Delayed development and lifespan extension as features of metabolic lifestyle alteration in C. elegans under dietary restriction. The Journal of experimental biology **209**: 4129–39.

Tan M. W., Mahajan-Miklos S., Ausubel F. M., 1999 Killing of Caenorhabditis elegans by Pseudomonas aeruginosa used to model mammalian bacterial pathogenesis. Proceedings of the National Academy of Sciences of the United States of America **96**: 715–20.

Tank E. M. H., Rodgers K. E., Kenyon C., 2011 Spontaneous Age-Related Neurite Branching in Caenorhabditis elegans The Journal of Neuroscience **31**: 9279.

Taylor R. C., Dillin A., 2011 Aging as an event of proteostasis collapse. Cold Spring Harbor perspectives in biology **3**: a004440.

Taylor R. C., Dillin A., 2013 XBP-1 Is a Cell-Nonautonomous Regulator of Stress Resistance and Longevity. Cell **153**: 1435–1447.

Taylor P. H., Cinquin A., Cinquin O., 2016 Quantification of in vivo progenitor mutation accrual with ultra-low error rate and minimal input DNA using SIP-HAVA-seq. Genome Research: 1600–1611.

Templeman N. M., Murphy C. T., 2018 Regulation of reproduction and longevity by nutrient-sensing pathways. The Journal of cell biology **217**: 93–106.

Templeman N. M., Luo S., Kaletsky R., Shi C., Ashraf J., Keyes W., Correspondence C. T. M., Murphy C. T., 2018 Insulin Signaling Regulates Oocyte Quality Maintenance with Age via Cathepsin B Activity. Current Biology **28**: 753-760.e4.

The C. elegans Deletion Mutant Consortium, 2012 Large-Scale Screening for Targeted Knockouts in the Caenorhabditis elegans Genome. G3 Genes|Genomes|Genetics Genes|Genomes|Genetics **2**: 1415–1425.

ThermoFisher, 2011 *Click-iT EdU Imaging Kits*.

Thomas J. H., 1990 Genetic analysis of defecation in Caenorhabditis elegans. Genetics **124**: 855–872.

Tiku V., Jain C., Raz Y., Nakamura S., Heestand B., Liu W., Späth M., Suchiman H. E. D., Müller R. U., Slagboom P. E., Partridge L., Antebi A., 2016 Small nucleoli are a cellular hallmark of longevity. Nature Communications **8**.

Timbers T. A., Giles A. C., Ardiel E. L., Kerr R. A., Rankin C. H., 2013 Intensity discrimination deficits cause habituation changes in middle-aged Caenorhabditis elegans. Neurobiology of Aging **34**: 621–631.

Timmons L., Fire A., 1998 Specific interference by ingested dsRNA. Nature **395**: 854.

Toth M. L., Melentijevic I., Shah L., Bhatia A., Lu K., Talwar A., Naji H., Ibanez-Ventoso C., Ghose P., Jevince A., Xue J., Herndon L. A., Bhanot G., Rongo C., Hall D. H., Driscoll M., 2012 Neurite Sprouting and Synapse Deterioration in the Aging Caenorhabditis elegans Nervous System. The Journal of Neuroscience **32**: 8778.

Tserevelakis G. J., Megalou E. V., Filippidis G., Petanidou B., Fotakis C., Tavernarakis N., 2014 Label-free imaging of lipid depositions in C. elegans using third-harmonic generation microscopy. PLoS ONE **9**.

Tuttle A. H., Rankin M. M., Teta M., Sartori D. J., Stein G. M., Kim G. J., Virgilio C., Granger A., Zhou D., Long S. H., Schiffman A. B., Kushner J. A., 2010 Immunofluorescent Detection of Two Thymidine Analogues (CldU and IdU) in Primary Tissue. Journal of Visualized Experiments: e2166–e2166.

Vanfleteren J. R., Braeckman B. P., Roelens I., Vreese A. De, 1998 Age-specific Modulation of Light Production Potential, and Alkaline Phosphatase and Protein Tyrosine Kinase Activities in Various Age Mutants of Caenorhabditis elegans. The Journals of Gerontology Series A: Biological Sciences and Medical Sciences **53A**: B380–B390.

Voorhies W. A. Van, Ward S., 1999 Genetic and environmental conditions that increase longevity in Caenorhabditis elegans decrease metabolic rate. Proceedings of the National Academy of Sciences of the United States of America **96**: 11399–403.

Vos K. De, 2015 Cell Counter Plugin. : https://imagej.nih.gov/ij/plugins/cell-counter.htm.

Walker G. A., White T. M., McColl G., Jenkins N. L., Babich S., Candido E. P. M., Johnson T. E., Lithgow G. J., 2001 Heat Shock Protein Accumulation Is Upregulated in a Long-Lived

Mutant of Caenorhabditis elegans. The Journals of Gerontology Series A: Biological Sciences and Medical Sciences **56**: B281–B287.

Walker G., Houthoofd K., Vanfleteren J. R., Gems D., 2005 Dietary restriction in C. elegans: From rate-of-living effects to nutrient sensing pathways. Mechanisms of Ageing and Development **126**: 929–937.

Walther D. M., Kasturi P., Zheng M., Pinkert S., Vecchi G., Ciryam P., Morimoto R. I., Dobson C. M., Vendruscolo M., Mann M., Hartl F. U., 2015 Widespread proteome remodeling and aggregation in aging C. elegans. Cell **161**: 919–932.

Wan Q.-L., Shi X., Liu J., Ding A.-J., Pu Y.-Z., Li Z., Wu G.-S., Luo H.-R., 2017 Metabolomic signature associated with reproduction-regulated aging in <i>Caenorhabditis elegans</i> Aging.

Wang M. C., Oakley H. D., Carr C. E., Sowa J. N., Ruvkun G., 2014 Gene Pathways That Delay Caenorhabditis elegans Reproductive Senescence (GS Barsh, Ed.). PLoS Genetics **10**: e1004752.

Wang H., Zhao Y., Ezcurra M., Benedetto A., Gilliat A. F., Hellberg J., Ren Z., Galimov E. R., Athigapanich T., Girstmair J., Telford M. J., Dolphin C. T., Zhang Z., Gems D., 2018 A parthenogenetic quasi-program causes teratoma-like tumors during aging in wild-type C. elegans. npj Aging and Mechanisms of Disease **4**: 6.

Ward S., Carrel J. S., 1979 Fertilization and Sperm Competition in the Nematode Caenorhabditis elegans. Developmental Biology **73**: 304–321.

Wickham H., 2009 *ggplot2: Elegant Graphics for Data Analysis*. Springer-Verlag, New York.

Williams G. C., 1957 Plieotropy, natural selection, and the evolution of senescence. Evolution **11**: 398–411.

Wolke U., Jezuit E. a, Priess J. R., 2007 Actin-dependent cytoplasmic streaming in C. elegans oogenesis. Development (Cambridge, England) **134**: 2227–2236.

Wolkow C. A., 2006 Identifying factors that promote functional aging in Caenorhabditis elegans.

Woodruff G. C., Phillips P. C., 2018 Field studies reveal a close relative of C. elegans thrives in the fresh figs of Ficus septica and disperses on its Ceratosolen pollinating wasps. BMC Ecology **18**: 26.

Woodruff G. C., Johnson E., Phillips P. C., 2019 A large close relative of C. elegans is slow-developing but not long-lived. BMC Evolutionary Biology **19**: 74.

Wormbase WS260, 2017

Xiao R., Chun L., Ronan E. A., Friedman D. I., Liu J., Xu X. Z. S., 2015 RNAi Interrogation of Dietary Modulation of Development, Metabolism, Behavior, and Aging in C. elegans. Cell reports **11**: 1123–33.

Yanase S., Suda H., Yasuda K., Ishii N., 2017 Impaired p53/CEP-1 is associated with lifespan extension through an age-related imbalance in the energy metabolism of C. elegans. Genes to Cells **22**: 1004–1010.

Yang J.-S., Nam H. G. H.-J., Seo M., Han S. K., Choi Y., Nam H. G. H.-J., Lee S.-J., Kim S., 2011 OASIS: Online Application for the Survival Analysis of Lifespan Assays Performed in Aging Research (E Scalas, Ed.). PLoS ONE **6**: e23525.

Yasuda K., Ishii T., Suda H., Akatsuka A., Hartman P. S., Goto S., Miyazawa M., Ishii N., 2006 Age-related changes of mitochondrial structure and function in Caenorhabditis elegans. Mechanisms of Ageing and Development **127**: 763–770.

Youngman M. J., Rogers Z. N., Kim D. H., 2011 A decline in p38 MAPK signaling underlies immunosenescence in caenorhabditis elegans. PLoS Genetics **7**.

Yuan Y., Hakimi P., Kao C., Kao A., Liu R., Janocha A., Boyd-Tressler A., Hang X., Alhoraibi H., Slater E., Xia K., Cao P., Shue Q., Ching T. T., Hsu A. L., Erzurum S. C., Dubyak G. R., Berger N. A., Hanson R. W., Feng Z., 2016 Reciprocal changes in phosphoenolpyruvate carboxykinase and pyruvate kinase with age are a determinant of aging in Caenorhabditis elegans. Journal of Biological Chemistry **291**: 1307–1319.

Zetka M. C., Kawasaki I., Strome S., Mü Ller F., Synapsis and chiasma formation in Caenorhabditis elegans require HIM-3, a meiotic chromosome core component that functions in chromosome segregation.

Zhang M., Poplawski M., Yen K., Cheng H., Bloss E., Zhu X., Patel H., Mobbs C. V, 2009 Role of CBP and SATB-1 in aging, dietary restriction, and insulin-like signaling. PLoS Biol **7**: e1000245.

Zhang L., Ward J. D., Cheng Z., Dernburg A. F., 2015 The auxin-inducible degradation (AID) system enables versatile conditional protein depletion in C. elegans. Development **142**: 4374–4384.

Zhang W. B., Sinha D. B., Pittman W. E., Hvatum E., Stroustrup N., Pincus Z., 2016 Extended Twilight among Isogenic C. elegans Causes a Disproportionate Scaling between Lifespan and Health. Cell Systems **3**: 333–345.

Zhao H., Halicka H. D., Li J., Biela E., Berniak K., Dobrucki J., Darzynkiewicz Z., 2013 DNA damage signaling, impairment of cell cycle progression, and apoptosis triggered by 5-ethynyl-2′-deoxyuridine incorporated into DNA. Cytometry Part A **83**: 979–988.

Zhao Y., Gilliat A. F., Ziehm M., Turmaine M., Wang H., Ezcurra M., Yang C., Phillips G., Mcbay D., Zhang W. B., Partridge L., Pincus Z., Gems D., 2017 Two forms of death in ageing Caenorhabditis elegans. Nature Communications **8**: 15458.

Appendix

Appendix 1: Publication List

ACADEMIC PUBLICATIONS

Kocsisova Z, Bagatelas E, Santiago J, Hanyue CL, Mosley M, Egan BE, Schneider DL, Baer C, Schedl T, Kornfeld K. Pathways that delay germline aging in *C. elegans*. *(in preparation)*

Kocsisova Z, Egan B, Scharf A, Andersen X, Kornfeld K. Aging and Healthspan Analysis in *C. elegans*. (*invited review for Wormbook*)

Kocsisova Z, Kornfeld K, Schedl T. (**2019**) Rapid population-wide declines in stem cell number and activity during reproductive aging in *C. elegans.* Development (Cambridge, England) 146: dev173195.

Kumar, S., Egan, B. M., **Kocsisova, Z**., Schneider, D. L., Murphy, J. T., Diwan, A., & Kornfeld, K. (**2019**). Lifespan extension in *C. elegans* caused by bacterial colonization of the intestine and subsequent activation of an innate immune response. Developmental cell, 49(1), 100-117.

Kocsisova Z, Mohammad A, Kornfeld K, Schedl T. (**2018**) Cell cycle analysis in the *C. elegans* germline with the thymidine analog EdU. Journal of visualized experiments: JoVE. 140, e58339–e58339.

Kocsisova, Z., Kornfeld, K., & Schedl, T. (**2018**). Cell cycle accumulation of the proliferating cell nuclear antigen PCN-1 transitions from continuous in the adult germline to intermittent in the early embryo of *C. elegans.* BMC Developmental Biology, 18(1), 12.

Warnhoff K, Roh HC, **Kocsisova Z**, Tan CH, Morrison A, Croswell D, Schneider DL, Kornfeld K. (**2017**) The Nuclear Receptor HIZR-1 Uses Zinc as a Ligand to Mediate Homeostasis in Response to High Zinc. PLoS Biol 15(1): e2000094.

Leung, W., ... Stamm, J., ...**Kocsisova, Z**. ... Elgin, S.C.R. (**2017**). Retrotransposons are the major contributors to the expansion of the *Drosophila ananassae* Muller F element. G3: Genes, Genomes, Genetics, 7(8), 2439-2460.

Leung, W., ... Stamm, J., ...**Kocsisova, Z**. ... Elgin, S.C.R. (**2015**). *Drosophila* Muller F Elements Maintain a Distinct Set of Genomic Properties Over 40 Million Years of Evolution. G3: Genes| Genomes| Genetics, 5(5), 719-740.

Kumar, S., **Kocsisova, Z**., & Kornfeld, K. (**2014**). Keep on Laying Eggs Mama, RNAi My Reproductive Aging Blues Away. PLoS genetics, 10(12), e1004808.

OTHER PUBLICATIONS

Kocsisova, Z. (2019). High Hopes for Medical Cannabis. *The Ampersand*. https://artsci.wustl.edu/ampersand/high-hopes-medical-cannabis

Kocsisova, Z. (**2018**). Preparing for the Competition. *The Ampersand.* https://artsci.wustl.edu/ampersand/preparing-competition

Kocsisova, Z. (**2018**). A new species in Forest Park. *The Ampersand.* https://artsci.wustl.edu/ampersand/new-species-forest-park

Kocsisova, Z. (**2018**). NSF Fellowship encourages graduate students to go beyond research. *The Ampersand.* artsci.wustl.edu/ampersand/graduate-students-go-beyond-research

Kocsisova, Z. (**2018**). Thinking outside the lab. *The Ampersand.* https://artsci.wustl.edu/ampersand/thinking-outside-lab

Amy Hereford, Dan Berg, **Zuzana Kocsisova**, *et al*. (**2018**) *Dogtown Ecovillage Green Book.* CreateSpace Independent Publishing, St. Louis.

MEETINGS

***C. elegans* International Meeting**, Los Angeles, CA (2019). Presented "Rapid, population-wide decline in germline stem cell number and activity during reproductive aging in *C. elegans*" (Talk)

Germ Cells, Cold Spring Harbor Labs, NY (2018). Presented "Reproductive Aging in *Caenorhabditis* nematodes" (Talk)

Mechanisms of Aging, Cold Spring Harbor Labs, NY (2018). Presented "Reproductive Aging in *Caenorhabditis* nematodes" (Poster)

***C. elegans* International Meeting**, Los Angeles, CA (2017). Presented "Reproductive and germline aging in *C. elegans*" (Poster)

Germ Cells, Cold Spring Harbor Labs, NY (2016). Presented "Reproductive Aging in *Caenorhabditis* nematodes" (Poster)

Mechanisms of Aging, Cold Spring Harbor Labs, NY (2016). Presented "Reproductive Aging in *Caenorhabditis* nematodes" (Poster)

***C. elegans* International Meeting**, Los Angeles, CA (2015). Presented "Monitoring S-phase in aging wild type and mutant *C. elegans* germlines using EdU labeling and a GFP::PCNA transgene" (Poster)

The Ellison Medical Foundation Colloquium on the Biology of Aging (2014). Attended as part of the Molecular Biology of Aging course at Marine Biological Laboratory in Woods Hole, MA

Appendix 2: Supplemental data for Chapter 5

Supplemental tables, scripts, and figures are available as .csv, .R, and .pdf files (respectively) at http://dev.biologists.org/lookup/doi/10.1242/dev.173195.supplemental

Supplemental Table 1: Data for Figure 1: The female reproductive system displayed rapid age-related decline in sperm-replete *C. elegans*

[1] Adult days. L4 stage = day 0.

[2] Mean value rounded to whole number. View data in spreadsheet for decimal values.

[3] Standard deviation.

[4] Number of animals in experiment producing one or more viable egg during a 24-hour period. Some animals died of matricidal hatching or vulval extrusion and were censored from the experiment.

[5] Number of animals in experiment producing no viable eggs during a 24-hour period, that were alive with no evidence of internal hatching of embryos or vulval extrusion.

[6] Progeny production on a given day, divided by peak progeny production on day 2, expressed as percent.

[7] Sample size (number of P0 "mother" animals).

[8] ND = Not determined, as animals were mated in groups on day 1.

Figure and Panel											
1A	Age (days)[1]	Mean number mated progeny[2]	s.d.[3]	% of peak[6]	n (animals)[7]	Number repro-ductive animals[4]	Number sterile animals[5]	Mean self-fertile progeny[2]	s.d[3]	% of peak[6]	n (animals)[7]
	0					12	0				
	1	ND[8]	ND[8]	ND[8]	12	12	0	39	8	27%	11
	2	162	10	100%	12	12	0	142	24	100%	11
	3	150	35	93%	12	12	0	64	51	45%	11
	4	89	25	55%	12	12	0	10	10	7%	11
	5	44	12	27%	12	12	0	8	8	6%	11
	6	30	15	18%	12	12	0	1	3	1%	11
	7	12	9	8%	10	9	1	2	4	1%	11
	8	13	7	8%	9	8	1	0	1	0%	11
	9	8	7	5%	6	5	1	0	1	0%	11
	10	9	11	5%	4	2	2	0	0	0%	11
	11	3	4	2%	4	2	2	0	1	0%	9
	12	3	4	2%	2	1	1	0	0	0%	7
	13	1	NA	1%	1	1	0	0	0	0%	7
	14							0	0	0%	7
	15							0	0	0%	7
	16							0	0	0%	6

Supplemental Table 2: Data for Figure 2: Endomitotic oocytes and a shifted DTC nucleus occurred at a low frequency

[1] Summary of values, mean, standard deviation, and sample size (n). Sample size is expressed as the number of animals or germlines, as indicated. Mean and standard deviations rounded to whole number or one decimal. View data in spreadsheet for decimal values.

[2] Global comparisons were used to test overall differences between all groups.
[3] Post-hoc comparisons were used for pairwise tests and to correct for multiple comparisons (familywise error).
[4] Both parametric tests, which assume the data are normally distributed, and non-parametric tests were performed for all comparisons.

Figure and Panel																					
2A	Summary of Values[1]			Global Comparison[2]			Post-hoc pairwise comparisons[3]														
	Age (days)	Endomitotic germlines (% germlines)	n (germlines)	Pearson's Chi-squared	P-value		Pairwise Comparison	Adjusted P-value													
	1	0.0%	304	27.137	0.00000128	***	1 vs 3	0.0001	***												
	3	4.9%	247				1 vs 5	<0.00001	***												
	5	8.9%	270				3 vs 5	0.0841	ns												
2B	Summary of Values[1]																				
	Age (days)	Subpopulation	Mated progeny (mean)	s.d.	n (animals)																
	5	low	5	3	20																
	5	medium	31	11	146																
	5	high	63	13	20																
2C	Summary of Values[1]				Global Comparison[2]			Post-hoc pairwise													
	Age (days)	Subpopulation	Endomitotic germlines (% germlines)	n (germlines)	Pearson's Chi-squared	P-value		Pairwise Comparison	Adjusted P-value												
	5	low	75.9%	29	39.3	<0.0000001	***	low vs med	<0.0000001	***											
	5	medium	8.3%	24				low vs high	<0.0000001	***											
	5	high	4.3%	23				med vs high	1.0000	ns											
2F	Summary of Values[1]			Global Comparison[2]			Post-hoc pairwise comparisons[3]														
	Age (days)	Shifted DTC nuclei (%	n (germlines)	Pearson's Chi-squared	P-value		Pairwise Comparison	Adjusted P-value													
	1	0.0%	290	52.4	<0.0000001	***	1 vs 3	<0.0000001	***												
	3	7.2%	222				1 vs 5	<0.0000001	***												
	5	16.7%	228				3 vs 5	0.0022	**												
2G	Summary of Values[1]				Parametric Global Comparison[2,4]			Post-hoc pairwise comparisons[3,4]			Non-parametric Global Comparison[2,4]			Post-hoc pairwise comparisons[3,4]							
	Age (days)	mean DTC nucleus position (c.d.)	s.d.	n (germlines)	ANOVA F-value	P-value		Pairwise Comparison	Tukey post-hoc Adjusted P-value		Kruskal-Wallis Chi-squared	P-value		Pairwise Comparison	Dunn post-hoc Adjusted P-value						
	1	1.08	0.31	290	106.4	< 2.2e-16	***	1 vs 3	<0.0000001	***	218.45	< 2.2e-16	***	1 vs 3	1.733078e-24	***					
	3	2.14	1.47	222				1 vs 5	<0.0000001	***				1 vs 5	2.146941e-44	***					
	5	2.79	1.93	228				3 vs 5	1.1e-06	***				3 vs 5	4.699616e-04	***					
2H	Summary of Values[1]				Parametric Global Comparison[2,4]			Non-parametric Global Comparison[2,4]													
	Oocytes	mean DTC nucleus position (c.d.)	s.d.	n (germlines)	ANOVA F-value	P-value		Kruskal-Wallis Chi-squared	P-value												
	Normal	2.8	1.9	228	0.6059	0.4371	ns	0.29482	0.5871	ns											
	Endomitot	3.2	2.3	19																	

Supplemental Table 3: Data for Figure 3: Population-wide, age-related decreases in the size of the germline and progenitor zone

[1] Summary of values, mean, standard deviation, and sample size (n). Sample size is expressed as the number of animals or germlines, as indicated. Mean and standard deviations rounded to whole number or one decimal. View data in spreadsheet for decimal values.
[2] Global comparisons were used to test overall differences between all groups.
[3] Post-hoc comparisons were used for pairwise tests and to correct for multiple comparisons (familywise error).
[4] Both parametric tests, which assume the data are normally distributed, and non-parametric tests were performed for all comparisons.

Figure and Panel																	
3B	Summary of Values[1]					Parametric Global Comparison[2,4]			Post-hoc pairwise comparisons[3,4]			Non-parametric Global Comparison[2,4]			Post-hoc pairwise comparisons[3,4]		
	Age (days)	mean length DT to loop (c.d.)	s.d.	n (germlines)	Decrease from day 1	ANOVA F-value	P-value		Pairwise Comparison	Tukey post-hoc Adjusted P-value		Kruskal-Wallis Chi-squared	P-value		Pairwise Comparison	Dunn post-hoc Adjusted P-value	
	1	69	6	14		25.169	3.712e-08	***	1 vs 3	0.0073402	**	26.738	1.563e-06	***	1 vs 3	1.084482e-02	*
	3	61	8	18	11.85%				1 vs 5	<0.0000001	***				1 vs 5	7.673677e-07	***
	5	51	8	18	26.24%				3 vs 5	0.0004353	***				3 vs 5	8.012675e-03	**
3C	Summary of Values[1]					Parametric Global Comparison[2,4]			Post-hoc pairwise comparisons[3,4]			Non-parametric Global Comparison[2,4]			Post-hoc pairwise comparisons[3,4]		
	Age (days)	mean length DT to spermatheca (um)	s.d.	n (germlines)	Decrease from day 1	ANOVA F-value	P-value		Pairwise Comparison	Tukey post-hoc Adjusted P-value		Kruskal-Wallis Chi-squared			Pairwise Comparison	Dunn post-hoc Adjusted P-value	
	1	473	53	15		9.4718	0.000341	***	1 vs 3	0.0119830	*	14.069	0.0008811	***	1 vs 3	0.0112382010	*
	3	413	51	17	12.75%				1 vs 5	0.0002572	***				1 vs 5	0.0007493357	***
	5	389	64	19	17.79%				3 vs 5	0.4267655	NS				3 vs 5	0.3412788086	NS
3D	Summary of Values[1]					Parametric Global Comparison[2,4]			Post-hoc pairwise comparisons[3,4]			Non-parametric Global Comparison[2,4]			Post-hoc pairwise comparisons[3,4]		
	Age (days)	mean length Progenitor Zone (c.d.)	s.d.	n (germlines)	Decrease from day 1	ANOVA F-value	P-value		Pairwise Comparison	Tukey post-hoc Adjusted P-value		Kruskal-Wallis Chi-squared	P-value		Pairwise Comparison	Dunn post-hoc Adjusted P-value	
	1	20	3	293		439.83	< 2.2e-16	***	1 vs 3	<0.0000001	***	399.73	< 2.2e-16	***	1 vs 3	1.354422e-47	***
	3	14	3	206	30.63%				1 vs 5	<0.0000001	***				1 vs 5	2.492722e-74	***
	5	12	4	168	42.90%				3 vs 5	<0.0000001	***				3 vs 5	1.453504e-05	***
3E	Summary of Values[1]					Parametric Global Comparison[2,4]			Post-hoc pairwise comparisons[3,4]			Non-parametric Global Comparison[2,4]			Post-hoc pairwise comparisons[3,4]		
	Age (days)	mean number progenitor	s.d.	n (germlines)	Decrease from day 1	ANOVA F-value	P-value		Pairwise Comparison	Tukey post-hoc Adjusted P-value		Kruskal-Wallis Chi-squared	P-value		Pairwise Comparison	Dunn post-hoc Adjusted P-value	
	1	215	25	81		96.181	< 2.2e-16	***	1 vs 3	<0.0000001	***	103.56	< 2.2e-16	***	1 vs 3	1.145758e-09	***
	3	163	47	75	24.22%				1 vs 5	<0.0000001	***				1 vs 5	2.653290e-23	***
	5	126	45	71	41.25%				3 vs 5	<0.0000002	***				3 vs 5	8.965058e-05	***

3F	Summary of Values[1]									
	Age (days)	mean DTC nucleus position	mean length Progenitor Zone (c.d.)	mean length Progenitor Zone (um)	mean distance DT to end of pachytene (c.d.)	mean distance DT to end of pachytene (um)	mean distance DT to loop (c.d.)	mean distance DT to loop (um)	mean distance DT to spermatheca (c.d.)	mean distance DT to spermatheca (um)
	1	1.0	21	72	62	239	69	301	76	473
	3	2.2	13	47	53	223	61	293	66	413
	5	2.4	10	40	50	221	51	233	59	389

Supplemental Table 4: Data for Figure 4: An age-related increase in the duration of the cell cycle

[1] Summary of values, mean, standard deviation, and sample size (n). Sample size is expressed as the number of animals or germlines, as indicated. Mean and standard deviations rounded to whole number or one decimal. View data in spreadsheet for decimal values.

[2] Global comparisons were used to test overall differences between all groups.

[3] Post-hoc comparisons were used for pairwise tests and to correct for multiple comparisons (familywise error).

[4] Both parametric tests, which assume the data are normally distributed, and non-parametric tests were performed for all comparisons.

Figure and Panel

4A

Summary of Values[1]

Age (days)	Duration of EdU exposure (hours)	pH3 positive, EdU positive cells	pH3 positive, EdU negative cells	co-labeling (% of pH3 positive cells)	n (cells)	n (germlines)
1	0.5	0	63	0%	63	9
3	0.5	0	15	0%	15	8
5	0.5	0	43	0%	43	28
1	4	375	31	92%	406	77
3	4	54	91	37%	145	28
5	4	63	56	53%	119	29
1	7	77	0	100%	77	22
3	7	42	5	89%	47	19
5	7	30	4	88%	34	11
1	10	337	1	100%	338	64
3	10	291	8	97%	299	46
5	10	63	6	91%	69	25
					total = 1655	total = 366

G2 duration

Summary of Values			Global Comparison[2] of 4 hour timepoint:			Post-hoc pairwise comparisons[3]		
Age (days)	Median (50th percentile interpolation)	Maximum (90th percentile interpolation)	Pearson's Chi-squared	P-value		Pairwise Comparison	Adjusted P-value	
1	2.5	4	197.55	< 2.2e-16	***	1 vs 3	0.0000	***
3	4.5	7				1 vs 5	0.0000	***
5	4.9	7				3 vs 5	0.0128	*

4C

Summary of Values[1]

Age (days)	Duration of EdU exposure (hours)	WAPL-1 positive, EdU positive cells	WAPL-1 positive, EdU negative cells	co-labeling (% of WAPL-1 positive cells)	n (cells)	n (germlines)
1	0.5	1739	1337	57%	3076	14
3	0.5	1960	1434	58%	3394	17
5	0.5	856	735	54%	1591	13
1	4	5128	173	97%	5301	24
3	4	1173	225	84%	1398	11
5	4	3157	614	84%	3771	29
1	7	2977	9	100%	2986	15
3	7	2143	327	87%	2470	19
5	7	927	118	89%	1045	11
1	10	3867	2	100%	3869	18
3	10	2134	8	100%	2142	13
5	10	910	5	99%	915	9
					total = 31958	total = 193

G2+M+G1 duration

Summary of values		Global Comparison[2] of 4 hour timepoint:			Post-hoc pairwise comparisons[3]		
Age (days)	Maximum (90th percentile interpolation)	Pearson's Chi-squared	P-value		Pairwise Comparison	Adjusted P-value	
1	3.4	504.08	< 2.2e-16	***	1 vs 3	0.0000	***
3	7.6				1 vs 5	0.0000	***
5	7.4				3 vs 5	0.8987	ns

4F	Summary of Values[1]				Parametric Global Comparison[2,4]			Post-hoc pairwise comparisons[3,4]			Non-parametric Global Comparison[2,4]			Post-hoc pairwise comparisons[3,4]		
	Age (days)	mean M-phase Index	s.d.	n (germlines)	ANOVA F-value	P-value		Pairwise Comparison	Tukey post-hoc Adjusted P-value		Kruskal-Wallis Chi-squared	P-value		Pairwise Comparison	Dunn post-hoc Adjusted P-value	
	1	2.36	1.41	76	1.3943	0.2504	ns	1 vs 3	0.5184277	ns	0.61132	0.7366	ns	1 vs 3	0.8694857	ns
	3	2.76	2.36	66				1 vs 5	0.2376242	ns				1 vs 5	1.0000000	ns
	5	2.96	2.61	65				3 vs 5	0.8633569	ns				3 vs 5	0.8512768	ns

4G	Summary of Values[1]				Parametric Global Comparison[2,4]			Post-hoc pairwise comparisons[3,4]			Non-parametric Global Comparison[2,4]			Post-hoc pairwise comparisons[3,4]		
	Age (days)	mean S-phase Index	s.d.	n (germlines)	ANOVA F-value	P-value		Pairwise Comparison	Tukey post-hoc Adjusted P-value		Kruskal-Wallis Chi-squared	P-value		Pairwise Comparison	Dunn post-hoc Adjusted P-value	
	1	56.72	6.73	14	0.9269	0.4039	ns	1 vs 3	0.9428753	ns	1.5129	0.4693	ns	1 vs 3	0.8119074	ns
	3	57.82	7.51	17				1 vs 5	0.6022773	ns				1 vs 5	0.5472124	ns
	5	53.25	13.19	13				3 vs 5	0.3869973	ns				3 vs 5	0.6587128	ns

4H	Summary of Values[1]					
	Age (days)	Calculated duration of S (h)	Median durati	Calculated duration of M (h)	Calculated duration of G1 (h)	Calculation of one cell
		*based on 57%	*from 5A	*based on 2%	*based on 2%	*based on G2 phase
	1	3.7	2.5	0.1	0.1	6.4
	3	6.6	4.5	0.2	0.2	11.5
	5	7.2	4.9	0.3	0.3	12.6

Supplemental Table 5: Data for Figure 5: Age-related decrease in the rate of meiotic entry

[1] Summary of values, mean, standard deviation, and sample size (n). Sample size is expressed as the number of animals or germlines, as indicated. Mean and standard deviations rounded to whole number or one decimal. View data in spreadsheet for decimal values.

[2] Global comparisons were used to test overall differences between all groups.

[3] Post-hoc comparisons were used for pairwise tests and to correct for multiple comparisons (familywise error).

[4] Both parametric tests, which assume the data are normally distributed, and non-parametric tests were performed for all comparisons.

Figure and Panel														
5B	Summary of Values[1]													
	Age (days)	Duration of EdU exposure (hours)	mean WAPL-1 negative, EdU positive cells	s.d.	n (cells)	n (germlines)								
	1	4	38	20	919	24								
	3	4	8	9	91	11								
	5	4	2	4	56	29								
	1	7	86	27	1283	15								
	3	7	15	17	284	19								
	5	7	5	4	51	11								
	1	10	155	40	2793	18								
	3	10	34	21	439	13								
	5	10	13	9	117	9								
					total = 6033	total = 149								
	Global Parametric Comparison[2] of 10 hour timepoint:			Post-hoc pairwise comparisons[3,4]			Non-parametric Global Comparison[2,4]			Post-hoc pairwise comparisons[3,4]		
	ANOVA F-value	P-value		Pairwise Comparison	Tukey post-hoc Adjusted P-value		Kruskal-Wallis Chi-squared	P-value		Pairwise Comparison	Dunn post-hoc Adjusted P-value	
	95.609	2.411e-15	***	1 vs 3	0.000000	***	30.898	1.952e-07	***	1 vs 3	1.140513e-04	***
				1 vs 5	0.000000	***				1 vs 5	1.016512e-06	***
				3 vs 5	0.254375	ns				3 vs 5	1.386366e-01	ns
	Linear Regression:											
	Age (days)	Slope (cells / h)	s.e. of slope	Decrease from day 1	Intercept (cells)	s.e. of intercept	Adjusted R^2	F-statistic	P-value			
	1	19.337	1.512		-41.619	10.819	**0.7438**	163.6	< 2.2e-16	***		
	3	4.324	1.163	22.4%	-11.943	8.703	**0.2338**	13.82	0.0006	***		
	5	1.7029	0.3103	8.8%	-5.2638	1.9338	**0.3776**	30.12	1.59E-06	***		

Supplemental Table 6: Data for Figure 6: Age-related decrease in the rate of meiotic progression

[1] Summary of values, mean, standard deviation, and sample size (n). Sample size is expressed as the number of animals or germlines, as indicated. Mean and standard deviations rounded to whole number or one decimal. View data in spreadsheet for decimal values.

[2] Global comparisons were used to test overall differences between all groups.

[3] Post-hoc comparisons were used for pairwise tests and to correct for multiple comparisons (familywise error).

[4] Both parametric tests, which assume the data are normally distributed, and non-parametric tests were performed for all comparisons.

Figure and Panel																		
6B	Summary of Values[1]					Parametric Global Comparison[2,4]			Post-hoc pairwise comparisons[3,4]			Non-parametric Global Comparison[2,4]			Post-hoc pairwise comparisons[3,4]		
	Age (days)	mean oocyte count	s.d.	n (germlines)	Fold decrease	ANOVA F-value	P-value		Pairwise Comparison	Tukey post-hoc Adjusted P-value		Kruskal-Wallis Chi-squared	P-value		Pairwise Comparison	Dunn post-hoc Adjusted P-value	
	1	13.87	2.75	15		14.787	9.923e-06	***	1 vs 3	0.9628850	ns	18.843	8.096e-0	***	1 vs 3	0.5839319448	ns
	3	13.59	3.26	17	1.020491				1 vs 5	0.0000657	***				1 vs 5	0.0002777538	***
	5	9.00	2.94	19	1.540741				3 vs 5	0.0000964	***				3 vs 5	0.0008002545	***
6C	Summary of Values[1]					Parametric Global Comparison[2,4]			Post-hoc pairwise comparisons[3,4]			Non-parametric Global Comparison[2,4]			Post-hoc pairwise comparisons[3,4]		
	Age (days)	mean distance of most proximal EdU+ nucleus from edge of PZ (c.d.)	s.d.	n (germlines)	Fold decrease	ANOVA F-value	P-value		Pairwise Comparison	Tukey post-hoc Adjusted P-value		Kruskal-Wallis Chi-squared	P-value	***	Pairwise Comparison	Dunn post-hoc Adjusted P-value	***
	1	51.52	10.55	29		30.989	1.376e-09	***	1 vs 3	0.0000000	***	31.139	1.731e-07		1 vs 3	1.223073e-07	*
	3	29.20	8.95	20	1.764289				1 vs 5	0.0028673	**				1 vs 5	2.274812e-02	ns
	5	36.00	9.88	6	1.431034				3 vs 5	0.3131732	ns				3 vs 5	2.771452e-01	
6D	Summary of Values[1] of Meiotic stage of most proximal EdU+ nucleus						Global Comparison[2]			Post-hoc pairwise comparisons[3]							
	Age (days)	Pachytene (count)	Diplotene & Diakinesis (count)	n (germlines)	Mid Pachytene (%)	Diakinesis (%)	Pearson's Chi-squared	P-value		Pairwise Comparison	Adjusted P-value						
	1	9	20	29	31.03%	68.97%	23.767	0.0005	***	1 vs 3	0.001	*					
	3	17	3	20	85.00%	15.00%				1 vs 5	.0416	*					
	5	5	1	6	83.33%	16.67%				3 vs 5	1.000	ns					

Supplemental Table 7: Data for Figure 7: Population-wide age-related decrease in the stem cell pool and GLP-1 (Notch) signaling

[1] Summary of values, mean, standard deviation, and sample size (n). Sample size is expressed as the number of animals or germlines, as indicated. Mean and standard deviations rounded to whole number or one decimal. View data in spreadsheet for decimal values.

[2] Global comparisons were used to test overall differences between all groups.

[3] Post-hoc comparisons were used for pairwise tests and to correct for multiple comparisons (familywise error).

[4] Both parametric tests, which assume the data are normally distributed, and non-parametric tests were performed for all comparisons.

Figure and Panel																	
7C	Summary of Values[1]					Parametric Global Comparison[2,4]			Post-hoc pairwise comparisons[3,4]			Non-parametric Global Comparison[2,4]			Post-hoc pairwise comparisons[3,4]		
	Age (days)	mean FLAG::SYGL−1 (cells)	s.d.	n (germlines)	Decrease from day 1	ANOVA F-value	P-value		Pairwise Comparison	Tukey post-hoc Adjusted P-value		Kruskal-Wallis Chi-squared	P-value		Pairwise Comparison	Dunn post-hoc Adjusted P-value	
	1	81.0	14.0	20		35.132	4.666e-10	***	1 vs 3	0.0000279	***	30.652	2.208e-07	***	1 vs 3	1.099951e-03	**
	3	58.3	11.1	16	28.01%				1 vs 5	0.0000000	***				1 vs 5	1.888737e-07	***
	5	41.9	15.6	14	48.24%				3 vs 5	0.0053783	**				3 vs 5	3.972201e-02	*
7D	Summary of Values[1]					Parametric Global Comparison[2,4]			Post-hoc pairwise comparisons[3,4]			Non-parametric Global Comparison[2,4]			Post-hoc pairwise comparisons[3,4]		
	Age (days)	mean FLAG::SYGL−1 (cell diameters)	s.d.	n (germlines)	Decrease from day 1	ANOVA F-value	P-value		Pairwise Comparison	Tukey post-hoc Adjusted P-value		Kruskal-Wallis Chi-squared	P-value		Pairwise Comparison	Dunn post-hoc Adjusted P-value	
	1	9.5	1.3	30		37.779	6.703e-12	***	1 vs 3	0.0001925	***	40.413	1.677e-09	***	1 vs 3	7.091695e-04	***
	3	7.9	1.6	29	17.10%				1 vs 5	0.0000000	***				1 vs 5	9.499694e-10	***
	5	5.5	1.5	15	42.36%				3 vs 5	0.0000071	***				3 vs 5	7.463996e-04	***
7G	Summary of Values[1]					Parametric Global Comparison[2,4]			Post-hoc pairwise comparisons[3,4]			Non-parametric Global Comparison[2,4]			Post-hoc pairwise comparisons[3,4]		
	Age (days)	mean LST−1::FLAG (cells)	s.d.	n (germlines)	Decrease from day 1	ANOVA F-value	P-value		Pairwise Comparison	Tukey post-hoc Adjusted P-value		Kruskal-Wallis Chi-squared	P-value		Pairwise Comparison	Dunn post-hoc Adjusted P-value	
	1	38.1	9.8	22		20.003	2.622e-07	***	1 vs 3	0.0015156	**	24.512	4.757e-06	***	1 vs 3	8.044253e-03	**
	3	27.5	8.3	24	27.80%				1 vs 5	0.0000002	***				1 vs 5	2.744426e-06	***
	5	17.2	11.8	14	54.81%				3 vs 5	0.0076200	**				3 vs 5	1.087033e-02	*
7H	Summary of Values[1]					Parametric Global Comparison[2,4]			Post-hoc pairwise comparisons[3,4]			Non-parametric Global Comparison[2,4]			Post-hoc pairwise comparisons[3,4]		
	Age (days)	mean LST−1::FLAG (cell diameters)	s.d.	n (germlines)	Decrease from day 1	ANOVA F-value	P-value		Pairwise Comparison	Tukey post-hoc Adjusted P-value		Kruskal-Wallis Chi-squared	P-value		Pairwise Comparison	Dunn post-hoc Adjusted P-value	
	1	4.8	0.6	48		29.895	3.947e-11	***	1 vs 3	0.0004116	***	40.784	1.393e-09	***	1 vs 3	1.439823e-04	***
	3	4.0	0.9	34	16.81%				1 vs 5	0.0000000	***				1 vs 5	1.560086e-09	***
	5	3.2	1.3	33	33.06%				3 vs 5	0.0019541	**				3 vs 5	2.989472e-02	*

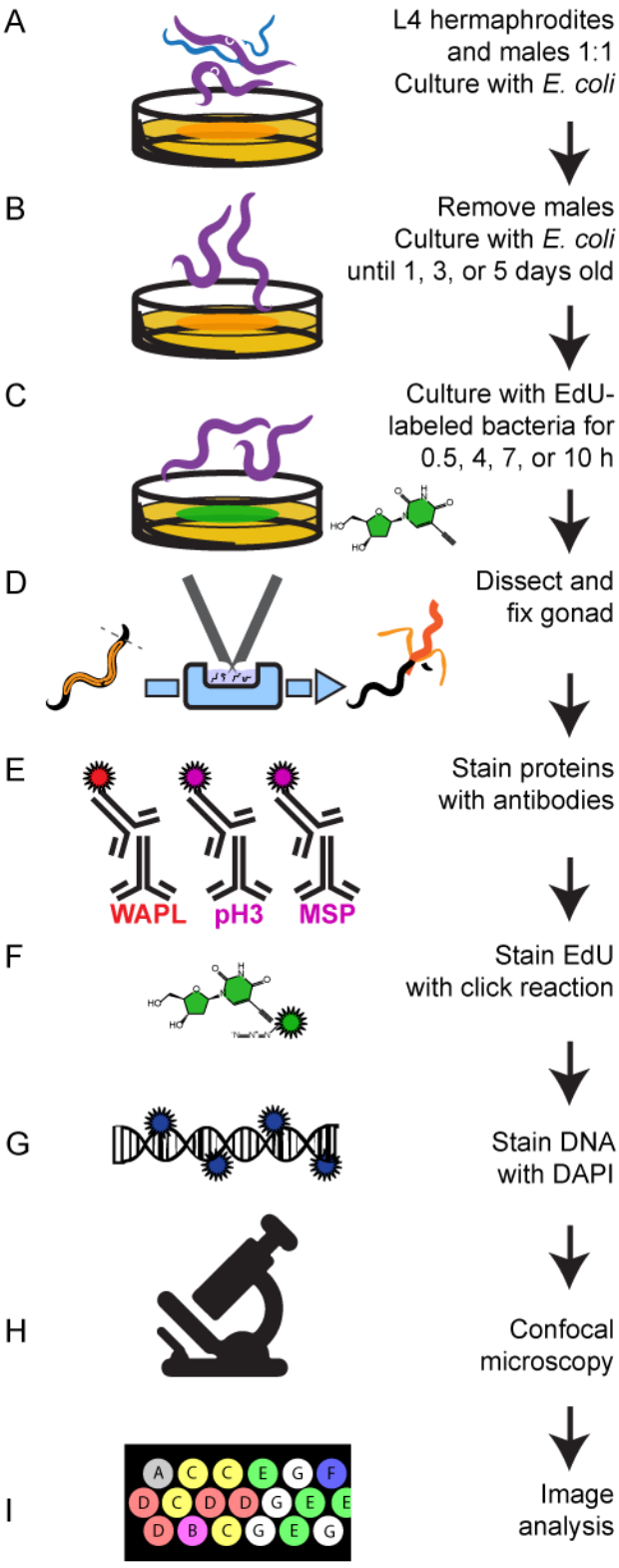

Supplemental Figure 1: Experimental Workflow. Experimental workflow used to assay the relationship between S-phase (EdU labeling), M-phase (pH3 antibody staining), progenitor zone cells, as well as the somatic gonadal

DTC and sheath cell nuclei (WAPL-1 antibody staining), sperm presence (Major Sperm Protein antibody staining), and DNA morphology of each individual *C. elegans* germline. Hermaphrodites were mated to males **(A)**, cultured to the appropriate age **(B)**, EdU labeled by feeding **(C)**, dissected **(D)**, and stained with antibodies **(E)**. A click reaction was used to attach a dye to EdU **(F)**, DNA was stained with DAPI **(G)**, and germlines were imaged on a spinning disc confocal microscope **(H)** and analyzed in FIJI **(I)**. Diagram modified with permission from Kocsisova et al. (2018a).

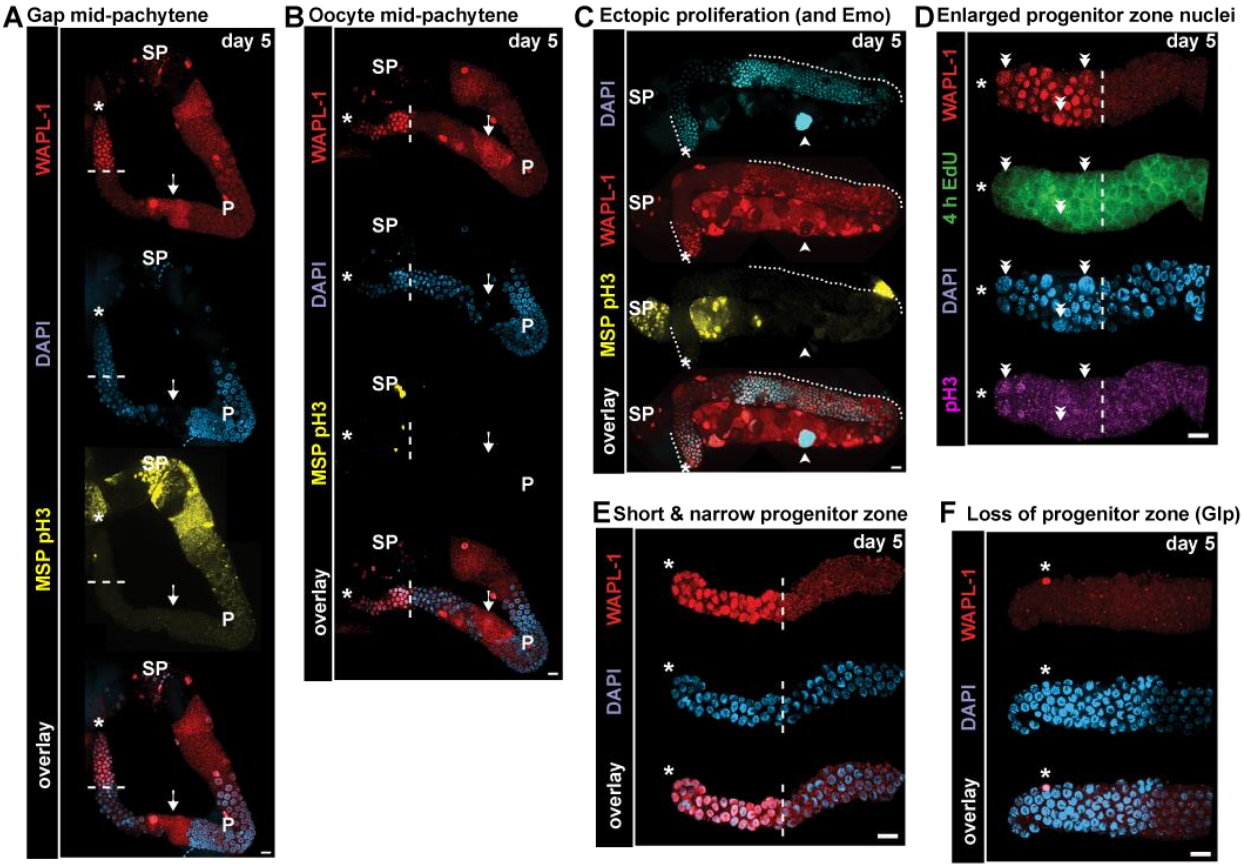

Supplemental Figure 2: Very low frequency germline defects displayed by day 5 mated hermaphrodites. Representative confocal fluorescence micrographs of germlines displaying defects observed at very low frequency in mated day 5 wild-type hermaphrodites. Germlines were stained for WAPL-1 (red), DAPI (blue), MSP (Major Sperm Protein) and pH3 (both yellow), EdU (green), pH3 (violet), or a combination of markers (overlay). Asterisk indicates the position of the DTC nucleus, and white dashed line indicates the proximal boundary of WAPL-1-positive cells. P indicates pachytene region. SP indicates sperm in spermatheca. Scale bar = 10 μm **(A)** Arrow points to a gap in the middle of the pachytene region that lacks germ cell nuclei. **(B)** Arrow points to oocyte-like formations in the middle of the pachytene region. **(C)** Ectopic proliferation indicated by two WAPL-1-positive regions, one at the normal distal position and another more proximal, highlighted by dotted white lines; this germline also contained an endomitotic oocyte in the proximal germline, indicated with an arrowhead. **(D)** Double arrowheads indicate enlarged progenitor zone nuclei, suggestive of a mitotic cell cycle abnormality. **(E)** A germline that displayed an unusually short and narrow progenitor zone. **(F)** Apparent premature meiotic entry (Glp) phenotype, as the distal germline lacks WAPL-1-positive cells; note that DTC nucleus (asterisk) is displaced 7 c.d. from the distal end and may be nonfunctional.

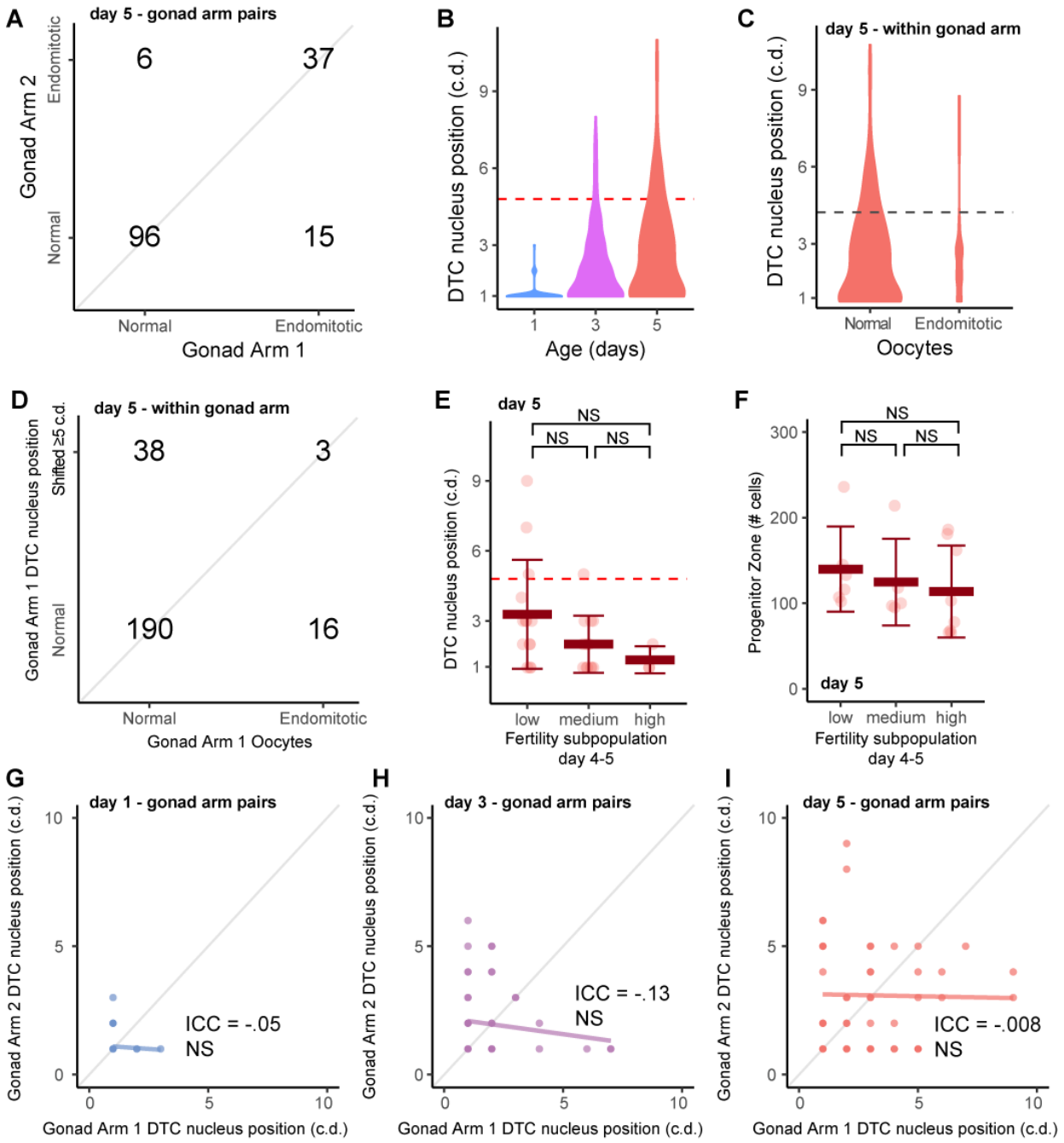

Supplemental Figure 3: Endomitotic oocytes and a shifted DTC nucleus occurred at a low frequency. A) To investigate co-occurrence of endomitotic oocytes in the two gonad arms in day 5 adults, we took advantage of a subset of animals in which both gonad arms were visible after dissection by comparing within-pair variation to between-pair variation using an intraclass correlation analysis. 96 animals displayed two normal germlines, 37 animals displayed two Emo germlines, and 21 animals displayed discordant germlines. There was a significant intraclass correlation (intraclass correlation coefficient = 0.68, P<.0000001). This result indicates the existence of a systemic process that uncouples oocyte meiotic maturation from ovulation, leading to the generation of endomitotic oocytes in both gonad arms in a small number of animals. **B)** Violin plots show the distribution of the position of the DTC nucleus (in cell diameters, c.d.) in day 1, 3 and 5 mated hermaphrodites. The same data are displayed in

Fig.2G. The DTC nucleus was identified by its position at the exterior of the distal gonad and bright WAPL-1 staining, and its position was determined by counting the number of cell diameters from the tip of the gonad. **C)** Violin plots show the distribution of the position of the DTC nucleus in day 5 mated hermaphrodites in germlines with and without endomitotic oocytes. The same data are displayed in **Fig.2H**. **D)** To investigate co-occurrence of endomitotic oocytes and a shifted DTC nucleus, we categorized day 5 mated wild-type hermaphrodites as (i) not displaying endomitotic nuclei (normal) or displaying endomitotic nuclei, and (ii) not displaying a shifted DTC nucleus (<5 c.d., defined as normal) or displaying a shifted DTC nucleus (≥5 c.d., defined as shifted). 190 animals displayed two normal germlines, 3 animals displayed an Emo germline and a shifted DTC nucleus, and 54 animals displayed discordant germlines. There was not a significant relationship between endomitotic oocytes and shift of the DTC nucleus (Pearson's Chi-squared $P>0.99$), indicating one systemic process does not cause both defects. **E)** Each data point indicates the position of one DTC nucleus in the three fertility subpopulations of day 5 animals defined in **Fig.2B** (n=14, 13, 3). Bars represent the average, and whiskers represent the standard deviation. Position 1 means the DTC nucleus is at the distal tip. Dashed line represents cutoff for a nucleus to be designated as "shifted". Comparison by Kruskal-Wallis test. The position of the DTC nucleus at day 5 did not correlate with the number of progeny produced between day 4 and 5. **F)** Each data point indicates the size of the progenitor zone measured as total number of cells in the three fertility subpopulations of day 5 animals defined in **Fig.2B**. Bars represent the average, and whiskers represent the standard deviation. Comparison by Kruskal-Wallis test. The size of the progenitor zone at day 5 did not correlate with the number of progeny produced between day 4 and 5. **E,F)** We hypothesize that an effect of the shifted DTC nucleus and progenitor zone size on progeny production would be delayed by 2-3 days, as cells in the distal germline require 2-3 days to progress through meiosis, mature, be ovulated, fertilized, and deposited. Thus, the absence of a correlation was expected, and does not rule out the possibility that changes in distal germline morphology affect progeny production on later days that could not be measured in this experiment. **G-I)** To investigate correlation of the DTC nucleus position in the two gonad arms in day 1, 3, and 5 adults, we took advantage of a subset of animals in which both gonad arms were visible after dissection by comparing the within-pair variation to the between-pair variation using an intraclass correlation analysis. There was no significant correlation in the degree of DTC nucleus shift within a pair of germlines in the same animal. Thus, the shifted DTC nucleus appears to result from local rather than systemic conditions. NS indicates $P>0.05$, * $P<0.05$, ** $P<.001$, *** $P<.0001$. (See Supplemental Table S3 for statistics)

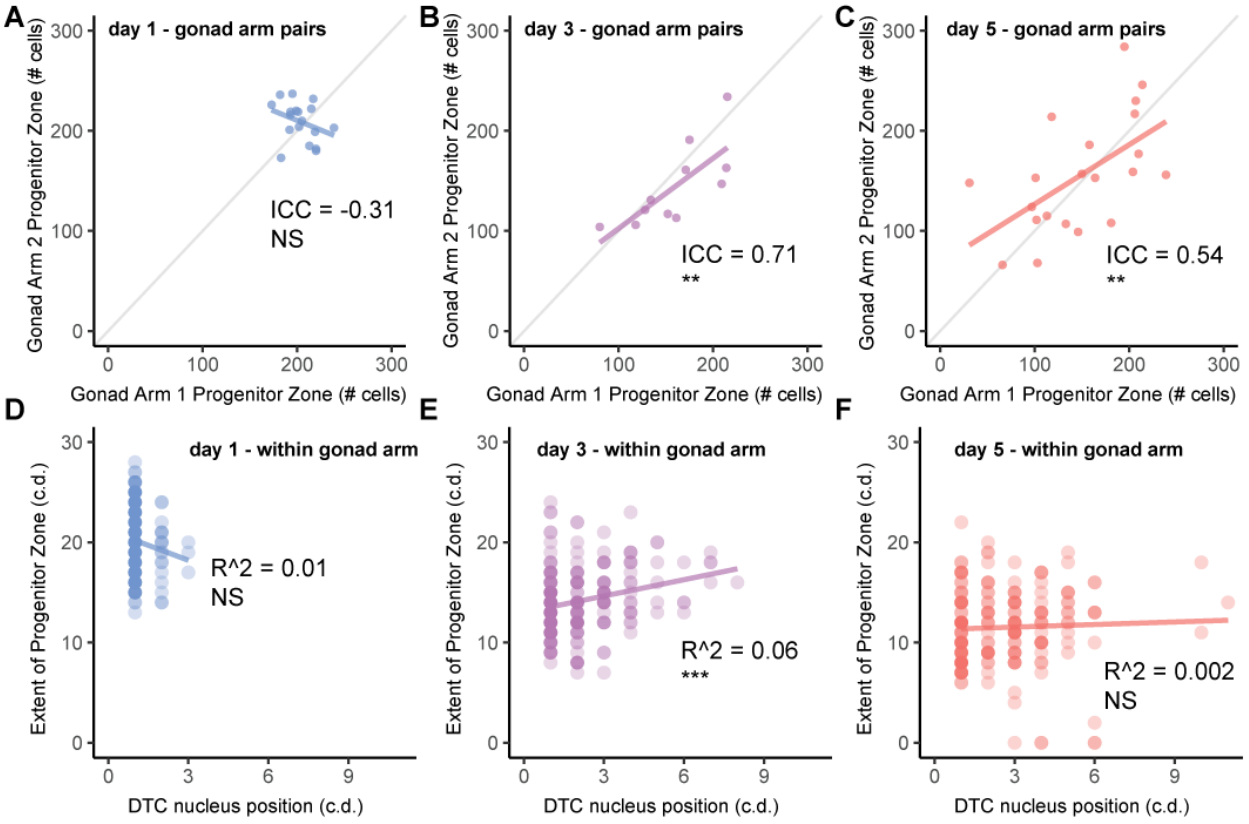

Supplemental Figure 4: Correlational analysis of distal phenotypes A-C) To investigate the relationship between the progenitor zone size in the two gonad arms in day 1, 3, and 5 adults, we took advantage of a subset of animals in which both germlines were visible after dissection by comparing the within-pair variation to the between-pair variation using an intraclass correlation analysis. Each data point indicates total number of progenitor zone cells in the two gonad arms of one animal. The line is a best fit, and statistical comparisons are shown. These data indicate that the age-related decrease in progenitor size appears to be result from systemic conditions. **D-F)** To investigate the relationship between the DTC nucleus position and the progenitor zone size in individual animals, we measured both values in the same gonad arm. Data points represent the two values expressed in cell diameters. There was no significant correlation in the degree of DTC nucleus shift and the extent of the progenitor zone in day 1 and 5 animals, and a slight positive correlation in day 3 animals. NS indicates P>0.05, * P<0.05, ** P<.001, *** P<.0001. (See Supplemental Table S4 for statistics)

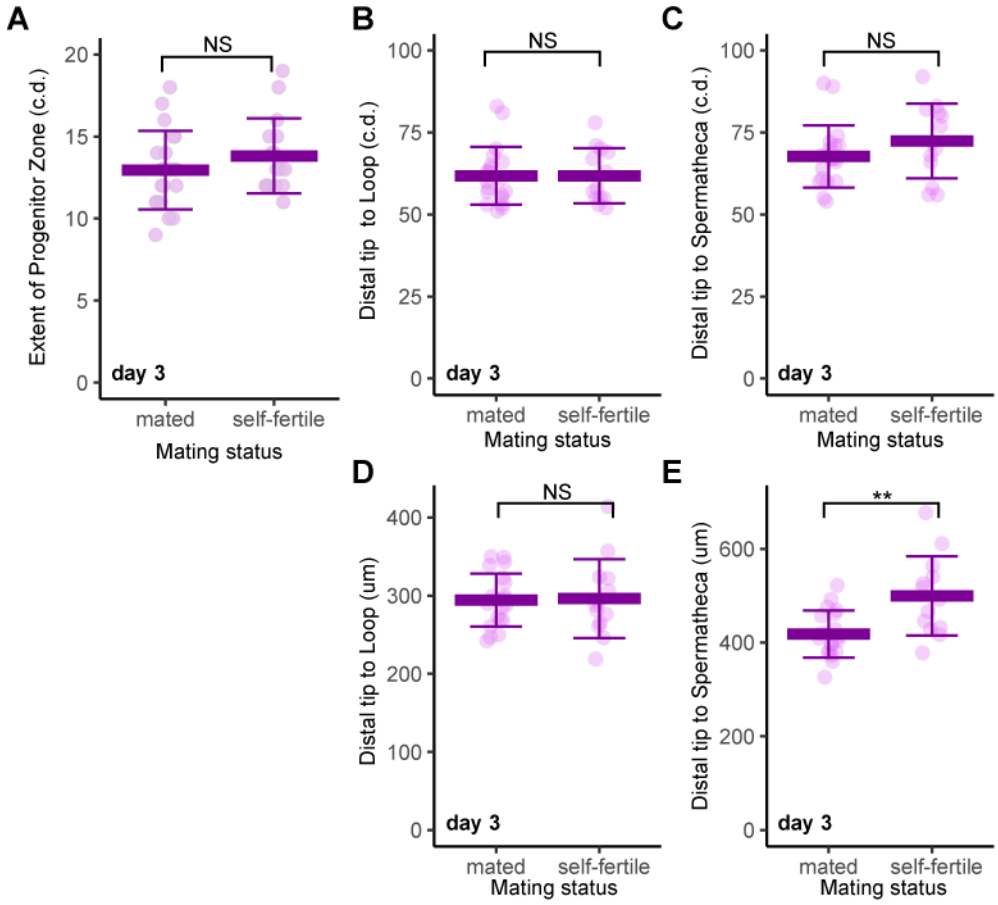

Supplemental Figure 5: Evaluation of the effect of male mating on hermaphrodite germline size To determine how mating influences the size of the germline, we analyzed day 3 adults that were self-fertile or mated to males for 24 hours. There was no significant difference in the length (measured in cell diameters) of the progenitor zone **(A)**, the distal germline **(B)**, or the entire germline **(C)** comparing self-fertile and mated animals. When the distal germline **(D)** or the entire germline **(E)** were measured using micrometers as the unit, the distal germline displayed no significant difference, whereas the entire germline was significantly longer in self-fertile animals. The likely reason for this difference is that some self-fertile hermaphrodites were sperm-depleted at day 3, resulting in diakinesis arrested oocytes that were stacked-up in the proximal germline, which extends the length of the tissue. NS indicates P>0.05, * P<0.05, ** P<.001, *** P<.0001. (See Supplemental Table S5 for statistics)

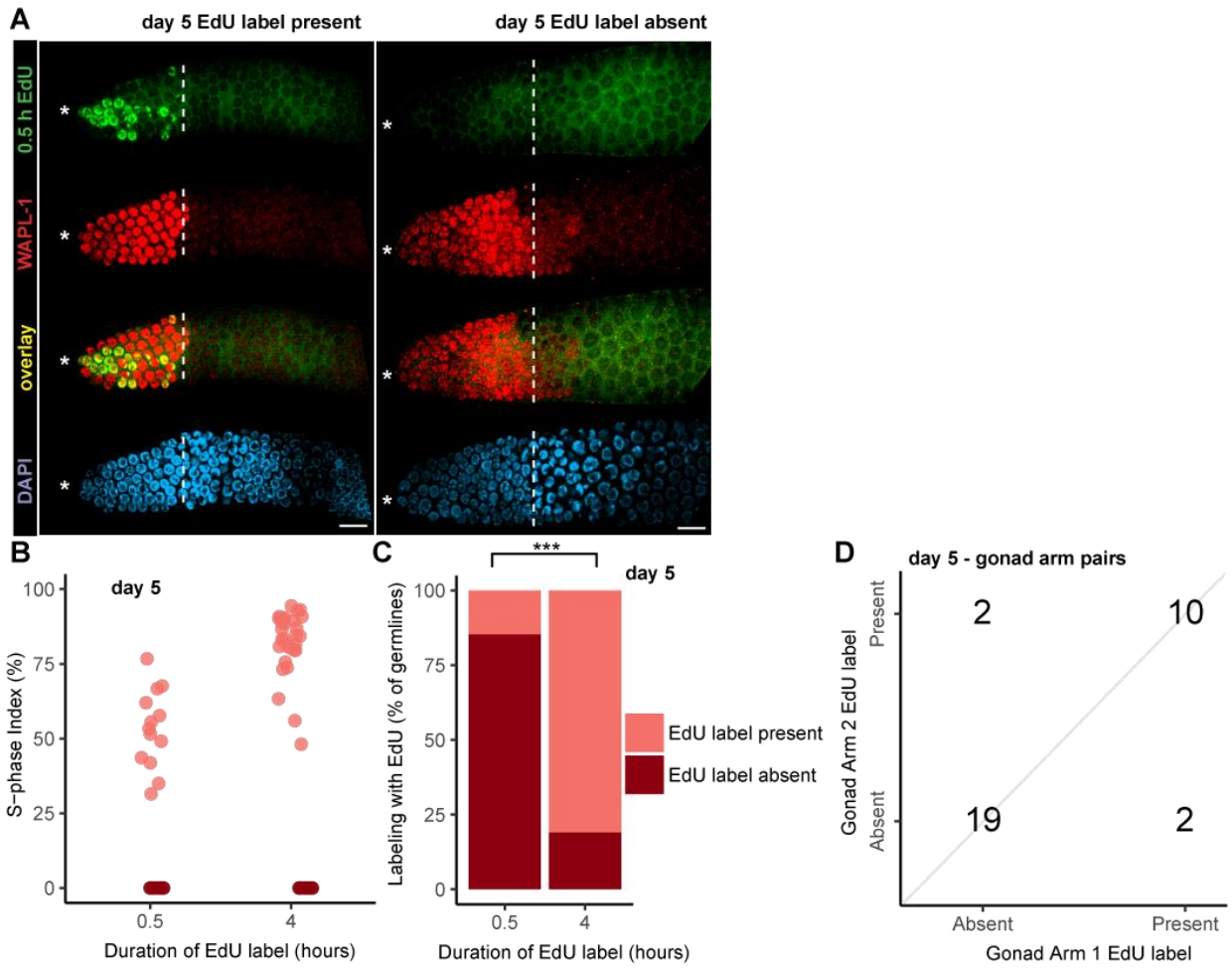

Supplemental Figure 6: A fraction of sperm-replete day 5 animals displayed no EdU labeling. A) Representative fluorescence micrographs of two germlines from day 5 adults fed EdU for 0.5 hours and subsequently stained for EdU (green, row 1), WAPL-1 (red, row 2), EdU and WAPL-1 (row 3) and DAPI (blue, row 4). Panels on the left show an animal that successfully labeled with EdU; panels on the right show an animal that failed to label with EdU. Asterisks indicate the position of the DTC nucleus, and white dashed lines indicate the proximal boundary of WAPL-1-positive cells. Scale bar = 10 μm. **B)** Each data point indicates the S-phase index (number of EdU positive cells divided by the number of progenitor zone WAPL-1-positive cells) of day 5 animals fed EdU for either 0.5 or 4 hours. Both data sets display a bimodal distribution. **C)** The proportion of day 5 adults that labeled with EdU in 0.5 or 4 hours. Dark red indicates germlines with no detectable EdU labeled cells, and light red indicates germlines with multiple EdU labeled cells. n=130, 63; three or more biological replicates. Comparison by Pearson's Chi-squared test. **D)** To investigate co-occurrence of EdU labeling in the two gonad arms in day 5 adults, we took advantage of a subset of animals in which both gonad arms were visible after dissection following feeding EdU for 0.5 h. 19 animals displayed two germlines lacking EdU labeling, 10 animals displayed two germlines positive for EdU labeling, and 4 animals displayed discordant germlines. There was a significant intraclass correlation (intraclass correlation coefficient=0.75, $p<0.0001$), suggesting a systemic cause of germline non-labeling. (See Supplemental Table S6 for statistics)

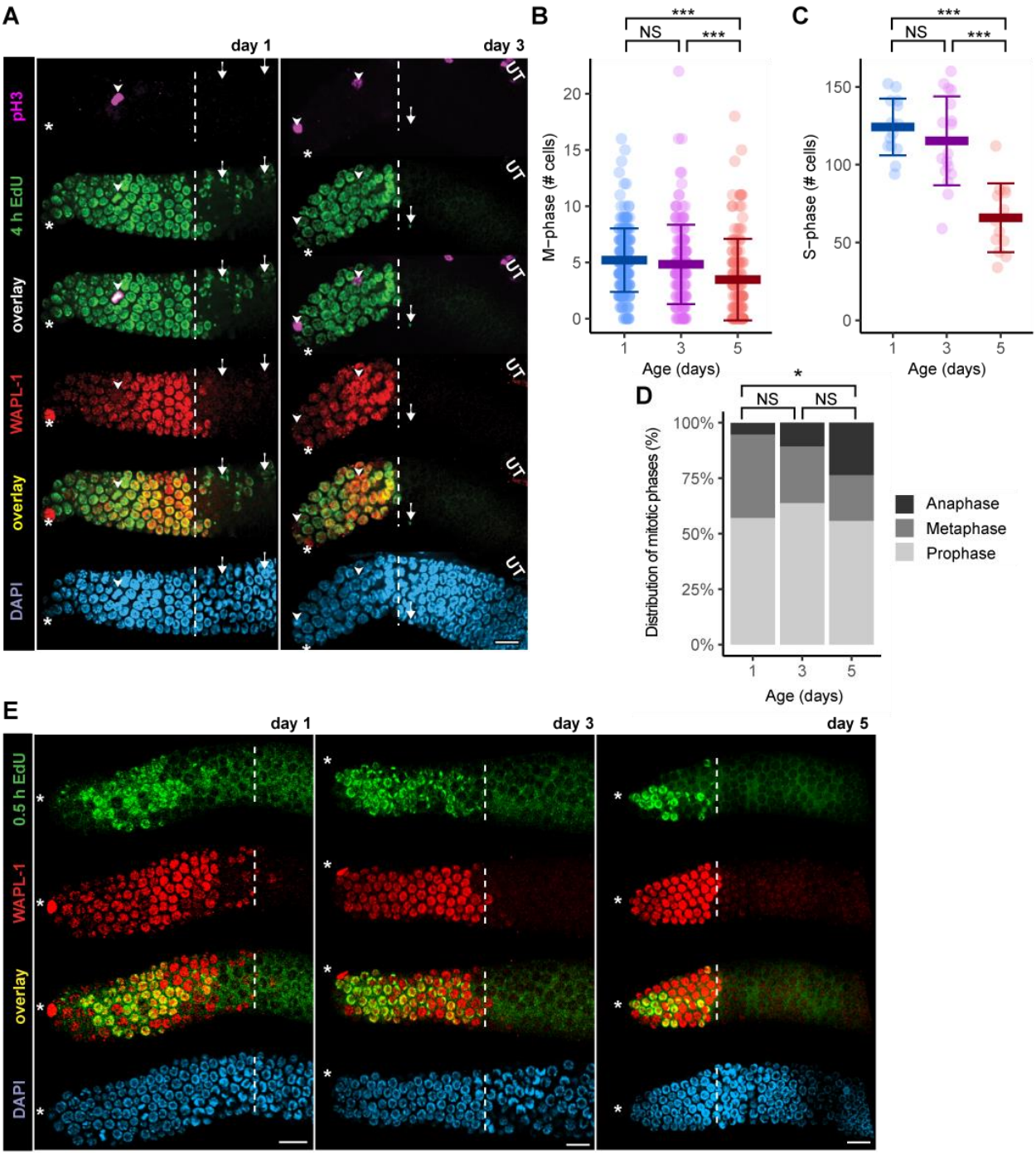

Supplemental Figure 7: Age-related change in the numbers of M-phase and S-phase cells. A) Representative fluorescence micrographs of germlines from day 1 (left) and day 3 (right) adults fed EdU for 4 hours and subsequently stained for pH3 (magenta, row 1), EdU (green, row 2), pH3 and EdU (overlay, row 3), WAPL-1 (red, row 4), EdU and WAPL-1 (overlay, row 5), and DAPI (blue, row 6). Asterisks indicate the position of the DTC nuclei, and white dashed lines indicate the proximal boundary of WAPL-1-positive cells. Arrowheads indicate pH3-positive cells. Arrows indicate examples of EdU-positive, WAPL-1-negative cells. UT indicates the uterus, where Major Sperm Protein positive sperm are visible in magenta. Scale bar = 10 μm. **B)** Each data point indicates the number of M-phase (pH3-positive) cells per gonad arm of day 1, 3, and 5 adults. Bars represent the average, and whiskers represent the standard deviation. n=213, 155, 134 in 4 or more biological replicates. Comparison by

Kruskal-Wallis test. **C)** Each data point indicates the number of S-phase (EdU-positive) cells per gonad arm of day 1, 3, and 5 adults fed EdU for 0.5 hours. Bars represent the average, and whiskers represent the standard deviation. n= 14, 17, 13 in two or more biological replicates. Comparison by Kruskal-Wallis test. **D)** Distribution of mitotic phases among pH3 immunoreactive cells was determined by DAPI morphology in day 1, 3, and 5 adults and characterized as anaphase (black), metaphase (dark gray) or prophase (light gray). n=77, 47, 34. Comparison by Pearson's Chi-squared test. NS indicates P>0.05, * P<0.05, ** P<.001. **E)** Representative fluorescence microscope images of germlines from day 1, 3, and 5 adults fed EdU for 0.5 hours and subsequently stained for EdU (green, row 1), WAPL-1 (red, row 2), EdU and WAPL-1 (overlay, row 3) and DAPI (blue, row 4). Asterisks indicate the position of the DTC nuclei, and white dashed lines indicate the proximal boundary of WAPL-1-positive cells. Scale bar = 10 µm. Some of these images appear in **Fig.3A** and **Fig.4E**. (See Supplemental Table S7 for statistics)

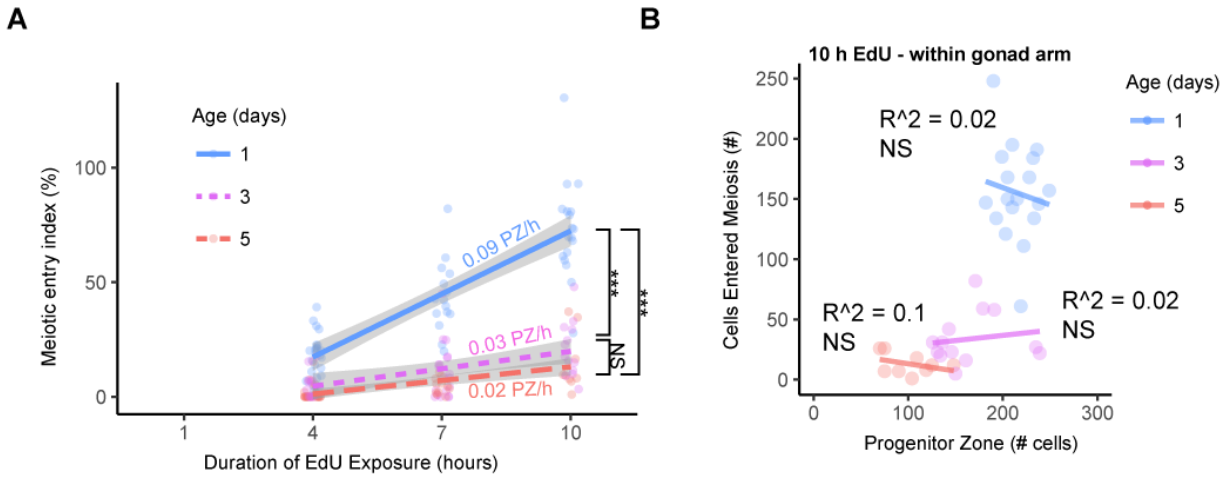

Supplemental Figure 8: Age-related decrease in the rate of meiotic entry A) Mated hermaphrodites at day 1 (blue), 3 (purple), or 5 (red) were exposed to EdU for 4, 7, or 10 hours, and germlines were dissected and stained with anti-WAPL-1 antibody and EdU click chemistry. The meiotic entry index was calculated by dividing the number of cells that entered meiosis (EdU positive, WAPL-1 negative) by the number of progenitor zone cells (WAPL-1-positive). The normalized rate of meiotic entry (% of progenitor zone per hour) was calculated from the slope of the linear regression of the meiotic entry index versus the duration of the EdU exposure. Gray range indicates 95% confidence interval on linear regression. Comparison by Kruskal-Wallis test compared the meiotic entry index at 10 hours. NS indicates P>0.05, *** P<.0001. **B)** To investigate the relationship between the rate of cells entering meiosis and the progenitor zone size in individual animals, we measured both values in the same gonad arm. Data points represent the two values expressed as number of cells. There was no significant correlation between the number of cells that entered meiosis (in a 10 hour EdU label) and the number of progenitor zone cells within day 1, 3, or 5 adults. n=18, 13, 9. Comparison by Pearson Correlation. (See Supplemental Table S8 for statistics)

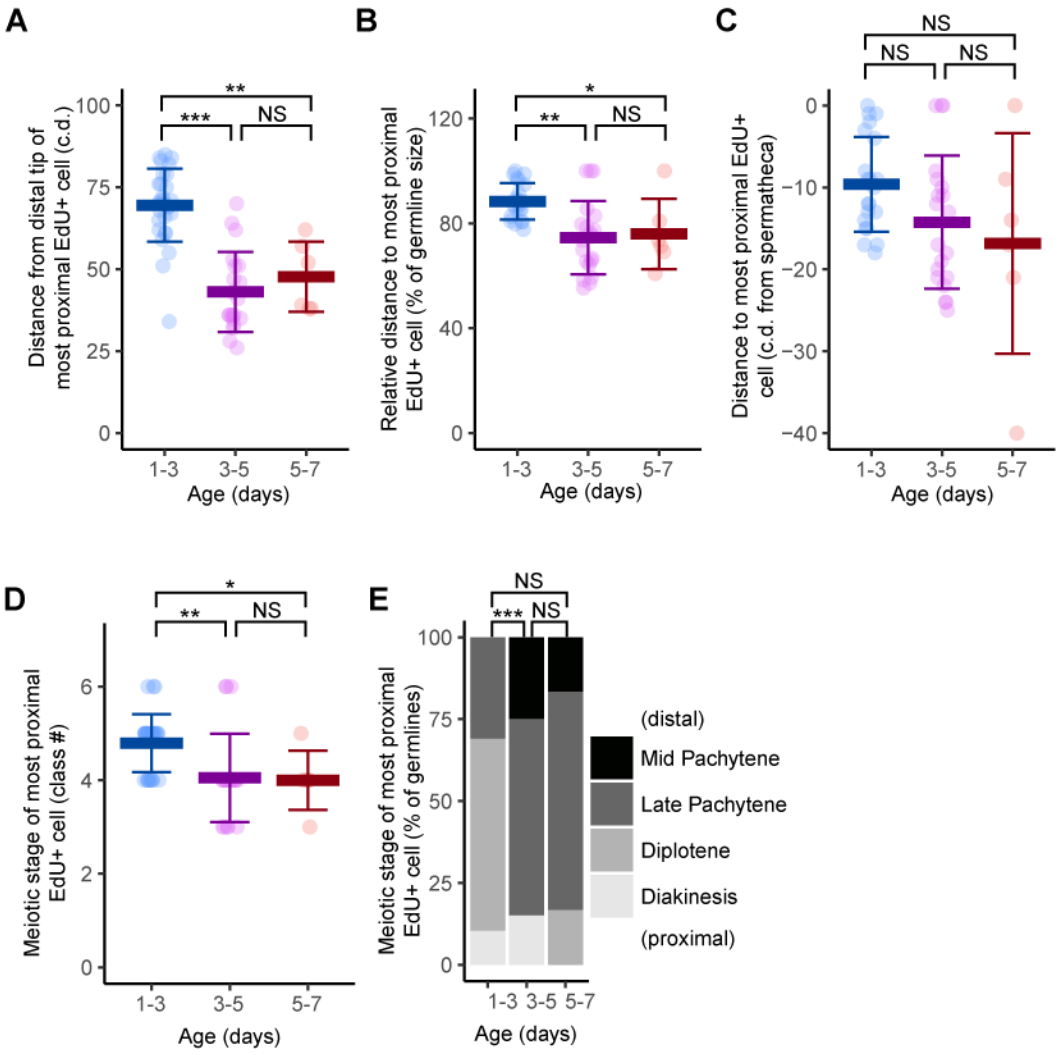

Supplemental Figure 9: Age-related decrease in the rate of meiotic progression. Mated hermaphrodites at day 1 (blue), 3 (purple), or 5 (red) were exposed to EdU labeled bacteria for 4 hours ("pulse"), transferred to unlabeled bacteria for 48 hours ("chase"), and germlines were dissected and stained with anti-WAPL-1 antibody and EdU click chemistry. The most proximal EdU positive cells were identified, and their position and meiotic stage were determined. **A)** Each data point indicates the distance from the distal tip of the gonad arm to the most proximal EdU positive cell in cell diameters. **B)** Each data point indicates the distance from the distal tip of the gonad arm to the most proximal EdU positive cell, divided by the distance from the distal tip of the gonad arm to the spermatheca (size of the germline). **C)** Each data point indicates the distance from the spermatheca to the most proximal EdU positive cell in cell diameters. We defined the position of the spermatheca as 0, and negative values indicate positions distal to the spermatheca. Comparison by Kruskal-Wallis test. **D)** To facilitate statistical tests of an ordered categorical variable, we defined mid-pachytene = 3, late-pachytene = 4, diplotene = 5, and diakinesis = 6, similar to Jaramillo-Lambert et al., (2007). Each data point indicates the numeric meiotic stage of the most proximal EdU positive cell. Comparison by Kruskal-Wallis test. **E)** In each germline, the most proximal EdU labeled cell was identified and categorized as mid pachytene, late pachytene, diplotene or diakinesis stage of meiosis. Comparison by Pearson's Chi-squared test. Only a small number of germlines were included in the day 5-7 data, which may contribute to the lack of significance in comparisons with that age (See Supplemental Table S9 for statistics).

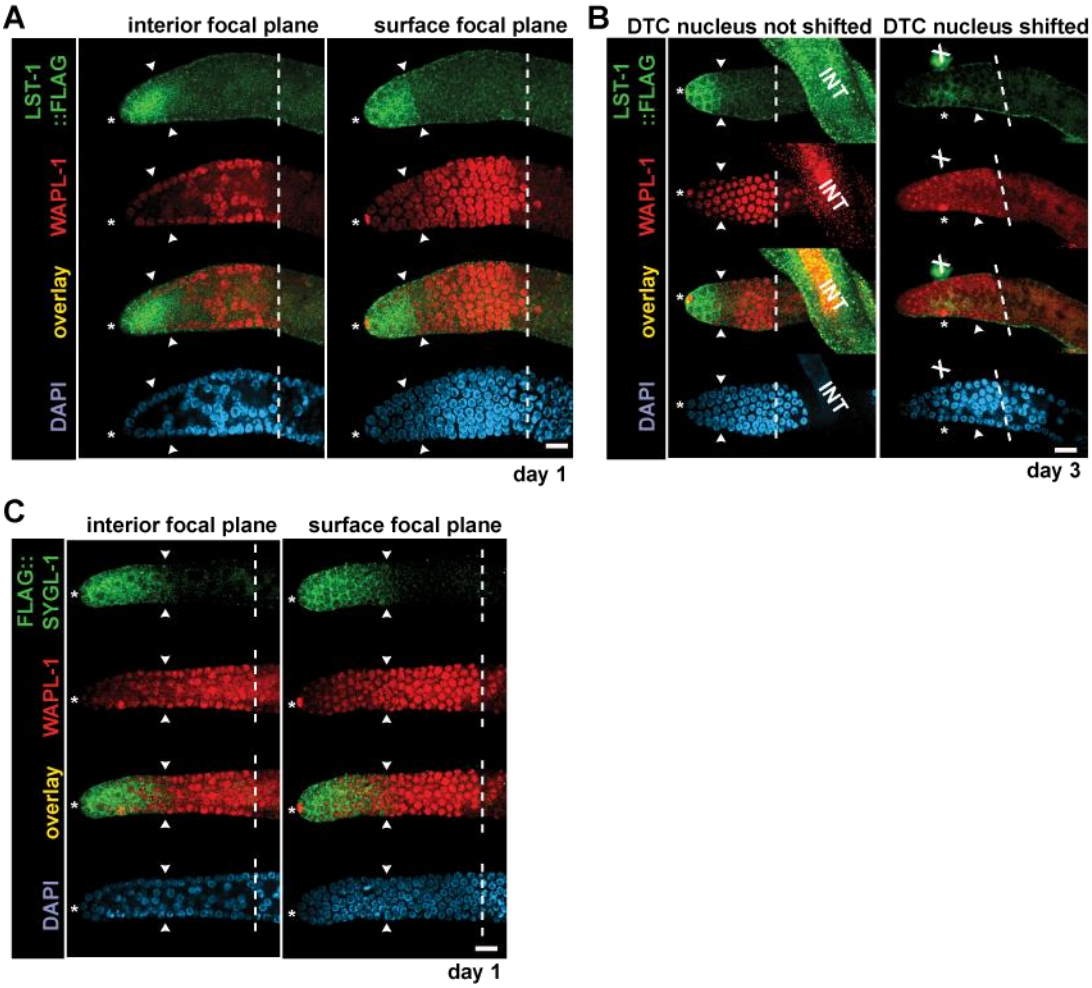

Supplemental Figure 10: Distribution of LST-1::FLAG and FLAG::SYGL-1 in the surface and interior of germlines and relative to the position of the DTC nucleus. A-C) Representative fluorescence microscope image of one germline stained for FLAG (green, row 1), WAPL-1 (red, row 2), FLAG and WAPL-1 (overlay, row 3) and DAPI (blue, row 4). Asterisk indicates the position of the DTC nucleus, white arrowheads indicate the proximal boundary of FLAG staining, and white dashed lines indicate the proximal boundary of WAPL-1-positive cells. Scale bar = 10 μm. **A)** Day 1 germline with LST-1::FLAG. Panels on left display a focal plane from the interior of the germline, whereas panels on right display a focal plane from the surface of the germline. **B)** Day 3 germlines with LST-1::FLAG. Panels on left show a germline with the DTC nucleus at position 1. Panels on right show a germline with the DTC nucleus shifted to position 6. Note that LST-1::FLAG signal is positioned near the shifted DTC nucleus, not near the distal tip of the germline. INT indicates intestine; X indicates a speck of green dust. **C)** Day 1 germline with FLAG::SYGL-1. Panels on left display a focal plane from the interior of the germline, whereas panels on right display a focal plane from the surface of the germline.

Appendix 3: Supplemental data for Chapter 6

Tables are available as supplemental .xlsx files

Supplemental Table 1: Statistical analysis of daily progeny production in the genus *Caenorhabditis*

Genotype			Mothers	Progeny	Bagging Propensity[1]	total brood size					early brood size (5-)					late brood size (6+)					late brood size (8+)					late brood size (10+)				
Strain	Species	Mating	n	n	% of mated animals	n	average	s.d.	CV	P-value	n	average	s.d.	CV	P-value	n	average	s.d.	CV	P-value	n	average	s.d.	CV	P-value	n	average	s.d.	CV	P-value
BS553	elegans	cont	20	11268	90%	20	**563**	210	37%		**20**	**517**	185	36%		15	**62**	29	47%		**5**	**11**	8	68%		--	--	--	--	
SB146	remanei	re cont	20	7770	5%	20	**389**	273	70%	0.0210	20	**311**	195	63%	0.0015	18	**86**	99	115%	0.8100	18	**19**	31	163%	0.6800	18	**3**	5	170%	--
VX02253	brenneri	cont	10	2553	0%	10	**255**	137	53%		10	**252**	136	54%		10	**4**	6	171%		9	**1**	3	265%		9	**0.2**	0.7	300%	
VX02253	brenneri	d5 cont	10	354	0%	10	**35**	35	100%	--	--	--	--	--	--	10	**35**	35	100%	0.0024	9	**8**	18	226%	0.1746	6	**0.3**	0.5	155%	0.4480
VX02253	brenneri	d7 cont	10	253	0%	10	**25**	33	130%	--	--	--	--	--	--	10	**25**	33	130%	--	10	**25**	33	130%	0.0026	8	**5**	7	139%	0.0640
VX02253	brenneri	d9 cont	10	21	0%	10	**2**	4	210%	--	--	--	--	--	--	10	**2**	4	210%	--	10	**2**	4	210%	--	10	**2**	4	210%	0.3310
CB4855	elegans	self-ferti	8	2393	13%	8	**299**	16	5%		8	**299**	16	6%		8	**1**	2	283%		8	**1**	2	283%		7	**0**	0	--	
VX02253	brenneri	cont	10	1827	0%	8	**222**	85	39%		8	**208**	95	46%		7	**16**	31	187%		7	**4**	7	204%		6	**1**	2	147%	
VX02253	brenneri	L4	10	2575	0%	10	**258**	129	50%	0.5148	10	**253**	124	49%	0.4200	10	**5**	10	192%	0.2243	10	**0.1**	0.3	316%	0.0338	10	**0**	0	--	0.0211
VX02253	brenneri	L4	10	1816	10%	10	**182**	101	56%		10	**182**	101	56%		9	**0**	0	--		9	**0**	0	--		9	**0**	0	--	
VX02253	brenneri	d5	35	2523	3%	33	**76**	57	74%	--	--	--	--	--	--	33	**76**	57	74%	0.0000	30	**14**	19	139%	0.0004	23	**1**	2	295%	0.1445
VX02253	brenneri	d7	24	838	4%	24	**35**	43	123%	--	--	--	--	--	--	24	**35**	43	123%	--	24	**35**	43	123%	0.0002	17	**9**	14	154%	0.0033
VX02253	brenneri	d9	24	448	0%	24	**19**	26	138%	--	--	--	--	--	--	24	**19**	26	138%	--	24	**19**	26	138%	--	24	**19**	26	138%	0.0006
VX02253	brenneri	L4d5	12	1652	0%	10	**162**	129	80%		10	**145**	120	83%		10	**17**	30	175%		10	**8**	15	195%		8	**1**	2	168%	
VX02253	brenneri	L4d7	12	2470	0%	11	**224**	69	31%	0.1600	11	**195**	83	43%	0.1700	11	**29**	39	134%	0.1300	11	**16**	18	116%	0.1407	11	**4**	7	166%	0.4000
VX02253	brenneri	L4d9	12	2378	0%	11	**216**	62	29%	0.1700	11	**203**	70	34%	0.1100	11	**13**	23	180%	0.8800	11	**2**	7	289%	0.3096	10	**1**	1	254%	0.4300
VX02253	brenneri	cont	12	3240	0%	12	**270**	112	41%		12	**255**	104	41%		12	**15**	15	99%		12	**3**	3	102%		11	**0**	1	254%	
VX02253	brenneri	L4	16	3132	0%	16	**196**	96	49%	0.1313	16	**196**	96	49%	0.1900	14	**0**	0	374%	0.0000	12	**0**	0	346%	0.0010	12	**0**	0	--	0.1480
VX02253	brenneri	L4d5	8	1535	0%	7	**219**	64	29%	0.3978	7	**187**	76	41%	0.1600	7	**32**	32	100%	0.1380	6	**15**	20	136%	0.3188	6	**0**	0	--	0.3240
VX02253	brenneri	d5	12	1112	0%	10	**111**	97	87%	--	--	--	--	--	--	10	**111**	97	87%	0.0030	9	**49**	56	115%	0.0240	9	**8**	18	220%	0.3180
BS553	elegans	L4d5	17	5957	76%	16	**353**	119	34%		16	**304**	87	28%		12	**66**	41	63%		9	**25**	21	84%		7	**9**	13	153%	
BS553	elegans	d5	2	161	50%	2	**81**	30	38%	--	--	--	--	--	--	2	**81**	30	38%	0.5800	1	**2**	--	--	0.4000	1	**1**	NA	--	1.0000
PX439	remanei	re L4d5	9	707	44%	9	**79**	63	80%		9	**64**	45	70%		4	**34**	29	85%		4	**6**	6	110%		4	**0**	1	200%	
PX439	remanei	re d5	4	242	0%	4	**61**	86	142%	--	--	--	--	--	--	4	**61**	86	142%	0.8900	3	**23**	40	173%	0.8500	2	**7**	9	141%	0.5800
BS553	elegans	L4d5	10	3249	30%	10	**325**	237	73%		10	**295**	223	76%		8	**37**	41	111%		6	**9**	10	107%		4	**0**	1	200%	
BS553	elegans	d5	10	816	20%	10	**82**	89	109%	--	--	--	--	--	--	10	**82**	89	109%	0.2000	8	**24**	42	172%	0.9500	3	**0**	0	--	0.5640
PX439	remanei	re L4d5	6	690	33%	6	**113**	91	80%		6	**58**	49	84%		6	**55**	51	92%		5	**9**	16	176%		4	**3**	6	200%	
PX439	remanei	re d5	13	653	38%	13	**50**	58	115%	--	--	--	--	--	--	13	**50**	58	115%	0.7600	10	**25**	41	164%	0.4600	8	**7**	14	205%	0.3320

[1]Propensity to die by matricidal hatching was calculated as percent of mated animals.

Supplemental Table 2: Statistical analysis of daily progeny production in *C. elegans* mutants

Genotype			Mothers	Progeny	Bagging Propensity[1]	self brood size					brood size					early brood size (4-)					late brood size (5+)					very late brood size (8+)				
Strain	Gene	allele	n	n	% of mated animals	n	average	s.d.	CV	P-value	n	average	s.d.	CV	P-value	n	average	s.d.	CV	P-value	n	average	s.d.	CV	P-value	n	average	s.d.	CV	P-value
N2	wt	wt	25	7994	47%	10	**264**	22	8%		9	**487**	116	24%		**9**	**396**	87	22%		8	**103**	36	36%		4	**11**	11	98%	
CB1370	daf-2	e1370	25	8376	84%	0	--	--	--	--	22	**364**	67	18%	0.0007	22	**178**	26	15%	0.0000	22	**186**	53	28%	0.0013	20	**61**	28	47%	0.0067
DA465	eat-2	ad465	25	4810	42%	6	**169**	24	14%	0.0003	15	**245**	81	33%	0.0003	15	**107**	41	38%	0.0001	15	**139**	51	37%	0.1006	15	**65**	32	49%	0.0037
WU1686	phm-2	am117	25	3214	53%	8	**124**	57	46%	0.0000	17	**131**	58	45%	0.0000	17	**72**	29	40%	0.0000	15	**66**	34	52%	0.0235	15	**26**	26	99%	0.2109
N2	wt	wt	30	12359	83%	5	**262**	41	16%		22	**485**	121	25%		22	**383**	86	22%		22	**102**	41	40%		12	**16**	9	54%	
DR1572	daf-2	e1368	30	10256	94%	10	**262**	34	13%	0.7593	18	**424**	71	17%	0.0419	18	**304**	46	15%	0.0004	18	**120**	43	36%	0.3209	11	**22**	13	59%	0.2671
CB502	sma-2	e502	30	5008	65%	3	**170**	16	9%	0.0357	24	**183**	84	46%	0.0000	24	**104**	44	43%	0.0000	21	**90**	36	40%	0.3882	17	**24**	18	72%	0.4780
YT17	crh-1	tz2	30	9932	86%	8	**275**	35	13%	0.6216	21	**350**	86	25%	0.0002	21	**247**	50	20%	0.0000	20	**108**	50	47%	0.7338	12	**18**	16	86%	0.6645
WT5434	tph-1	mg280	30	9534	85%	17	**241**	24	10%	0.0416	12	**445**	126	28%	0.3581	12	**325**	74	23%	0.0254	12	**120**	57	47%	0.2204	4	**17**	13	74%	0.9515
VC222	raga-1	ok386	30	5470	32%	7	**123**	37	30%	0.0025	21	**216**	90	41%	0.0000	21	**131**	37	28%	0.0000	20	**90**	53	60%	0.5372	20	**11**	11	103%	0.0899
PR801	che-3	p801	30	14540	67%	2	**283**	23	8%	0.8571	19	**555**	82	15%	0.0712	19	**385**	43	11%	0.7437	19	**170**	54	32%	0.0002	15	**24**	14	57%	0.1122
JK5500	sygl-1	transgene	30	14619	55%	7	**382**	47	12%	0.0025	17	**557**	109	20%	0.0673	17	**398**	65	16%	0.6709	17	**159**	65	41%	0.0060	13	**15**	13	85%	0.3541
N2	wt	wt	35	17422	66%	6	**306**	23	7%		23	**611**	61	10%		23	**508**	30	6%		23	**102**	43	42%		9	**9**	7	78%	
JK5500	sygl-1	transgene	35	22592	50%	5	**476**	91	19%	0.0130	27	**727**	87	12%	0.0000	27	**530**	40	7%	0.0580	27	**197**	71	36%	0.0000	22	**23**	22	97%	0.0580
N2	wt	wt	61	437	41%	--	--	--	--		--	--	--	--		--	--	--	--		--	--	--	--		18	**22**	15	67%	
DR1572	daf-2	e1368	52	940	69%	--	--	--	--	--	--	--	--	--	--	--	--	--	--	--	--	--	--	--	--	33	**28**	13	48%	0.1215
TJ1052	age-1	hx546	60	95	57%	--	--	--	--	--	--	--	--	--	--	--	--	--	--	--	--	--	--	--	--	3	**11**	7	66%	0.2472
WU710	age-1	am88	46	524	50%	--	--	--	--	--	--	--	--	--	--	--		--	--	--	--	--	--	--	--	21	**23**	18	76%	0.9888
CB502	sma-2	e502	69	917	93%	--	--	--	--	--	--	--	--	--	--	--	--	--	--	--	--	--	--	--	--	31	**29**	23	78%	0.3186
NU3	dbl-1	nk3	71	169	51%	--	--	--	--	--	--	--	--	--	--	--	--	--	--	--	--	--	--	--	--	12	**8**	8	100%	0.0026
YT17	crh-1	tz2	48	495	63%	--	--	--	--	--	--	--	--	--	--	--	--	--	--	--	--	--	--	--	--	15	**27**	13	47%	0.2326
PR801	che-3	p801	62	643	66%	--	--	--	--	--	--	--	--	--	--	--	--	--	--	--	--	--	--	--	--	17	**36**	16	44%	0.0139
WU968	osm-3	am177	57	568	46%	--	--	--	--	--	--	--	--	--	--	--	--	--	--	--	--	--	--	--	--	29	**18**	8	42%	0.6454
CX3410	odr-10	ky225	59	216	64%	--	--	--	--	--	--	--	--	--	--	--	--	--	--	--	--	--	--	--	--	8	**18**	13	76%	0.4043
N2	wt	wt	58	272	57%	--	--	--	--	--	--	--	--	--	--	--	--	--	--	--	--	--	--	--	--	8	**18**	12	67%	
CB1370	daf-2	e1370	64	1625	92%	--	--	--	--	--	--	--	--	--	--	--	--	--	--	--	--	--	--	--	--	45	**36**	15	42%	0.0046
WU1024	osm-3	am172	59	556	86%	--	--	--	--	--	--	--	--	--	--	--	--	--	--	--	--	--	--	--	--	19	**21**	9	41%	0.4729
PR802	osm-3	p802	62	41	90%	--	--	--	--	--	--	--	--	--	--	--	--	--	--	--	--	--	--	--	--	4	**10**	5	45%	0.2662
PR813	osm-5	p813	60	55	47%	--	--	--	--	--	--	--	--	--	--	--	--	--	--	--	--	--	--	--	--	5	**11**	9	85%	0.2716
CB1124	che-3	e1124	60	251	65%	--	--	--		--	--	--	--	--	--	--	--	--	--	--	--	--	--	--	--	8	**13**	9	68%	0.3717
WU1026	che-3	am162	62	178	84%	--	--	--	--	--	--	--	--	--	--	--	--	--	--	--	--	--	--	--	--	11	**16**	6	40%	0.7098
PR678	tax-4	p678	65	139	89%	--	--	--	--	--	--	--	--	--	--	--	--	--	--	--	--	--	--	--	--	10	**14**	9	66%	0.5329
N2	wt	wt	24	8410	55%	10	**244**	134	55%		11	**540**	183	34%		11	**209**	79	38%		11	**331**	128	39%		10	**113**	59	52%	
BS3164	glp-1	ar202	24	5426	25%	12	**237**	46	20%	0.5300	12	**215**	91	43%	0.0001	12	**131**	43	33%	0.0116	12	**84**	56	66%	0.0003	9	**10**	12	125%	0.0003
DG2389	glp-1	bn18	24	5314	42%	10	**251**	59	23%	0.6800	11	**247**	110	44%	0.0006	11	**103**	32	31%	0.0086	11	**144**	87	61%	0.0004	8	**58**	31	53%	0.0831
N2	wt	wt	10	3737	20%	5	**291**	45	15%		5	**456**	103	23%		5	**201**	31	15%		5	**256**	75	29%		5	**89**	51	57%	
BS3164	glp-1	ar202	10	2553	25%	2	**268**	110	41%	1.0000	8	**252**	101	40%	0.0016	8	**124**	40	32%	0.0082	8	**128**	80	63%	0.0451	7	**41**	35	84%	0.1040
DG2389	glp-1	bn18	10	2633	60%	0	--	--	--	--	10	**263**	68	26%	0.0007	10	**128**	39	30%	0.0013	10	**135**	40	29%	0.0007	10	**47**	22	47%	0.0990

[1]Propensity to die by matricidal hatching was calculated as percent of mated animals.

Supplemental Table 3: Statistical analysis of daily progeny production in *C. elegans* mutants on various bacterial diets

Genotype				Mothers	Progeny	Bagging Propensity[1]	self brood size					brood size					early brood size (4-)					late brood size (5+)					very late brood size (8+)				
Strain	Gene	allele	diet	n	n	% of mated animals	n	average	s.d.	CV	P-value	n	average	s.d.	CV	P-value	n	average	s.d.	CV	P-value	n	average	s.d.	CV	P-value	n	average	s.d.	CV	P-value
N2	wt	wt	OP50	20	9502	69%	7	**324**	38	12%		13	**556**	139	25%		**13**	**456**	87	19%		13	**100**	70	70%		10	**13**	16	118%	
WS2277	hus-1	op241	OP50	20	8873	23%	7	**295**	37	13%	0.2100	12	**557**	119	21%	1.0000	12	**470**	80	17%	0.6600	12	**87**	54	62%	0.6400	11	**10**	15	153%	0.3700
N2	wt	wt	OP50	20	10134	42%	8	**312**	30	10%		12	**637**	172	27%		12	**558**	108	19%		11	**86**	97	113%		6	**0**	0	245%	
WS2277	hus-1	op241	OP50	20	12376	24%	3	**299**	55	18%	0.6300	14	**682**	191	28%	0.2080	14	**554**	135	24%	0.7600	14	**127**	74	58%	0.2100	10	**2**	3	148%	0.0360
N2	wt	wt	HB101	20	10756	27%	3	**100**	171	171%	0.0480	14	**728**	226	31%	0.1600	14	**599**	143	24%	0.1200	12	**150**	122	81%	0.1900	11	**7**	11	155%	0.1950
WS2277	hus-1	op241	HB101	20	15191	16%	1	**271**	--	--	1.0000	19	**785**	171	22%	0.5290	19	**612**	64	10%	0.5600	19	**173**	123	71%	0.5900	16	**9**	23	248%	0.6980
N2	wt	wt	OP50	20	9558	36%	3	**310**	15	5%		11	**784**	163	21%		11	**689**	104	15%		10	**105**	69	66%		7	**2**	3	161%	
WU1686	phm-2	am117	OP50	20	1962	17%	--	--	--	--	--	10	**171**	62	36%	0.0000	10	**141**	56	39%	0.0000	10	**30**	24	81%	0.0100	8	**6**	8	122%	0.2998
N2	wt	wt	Comamonas	20	10863	20%	--	--	--	--	--	15	**724**	207	29%	0.3800	15	**643**	151	23%	0.5070	14	**87**	88	102%	0.3639	10	**0**	1	316%	0.1316
WU1686	phm-2	am117	Comamonas	20	2653	0%	--	--	--	--	--	14	**190**	40	21%	0.0000	14	**189**	39	21%	0.0000	14	**0**	1	219%	0.0003	14	**0**	0	--	0.2719

[1]Propensity to die by matricidal hatching was calculated as percent of mated animals.

Supplemental Table 4: Statistical analysis of germline phenotypes, including meiotic entry

Age and	Meiotic Entry (cell diameters)			Progenitor Zone (c.d.)			DTC position (c.d.)			Oocytes (number)			sygl-1 expression (c.d.)			lst-1 expression (c.d.)		
Genotype	mean	s.d.	n	mean	s.d.	n	mean	s.d.	n	mean	s.d.	n	mean	s.d.	n	mean	s.d.	n
1_wt	18.05769	3.268468	52	20.41566	2.304566	166	1.01227	0.110427	163	10.90625	1.78451	32	10.6875	1.558578	16	5.95098	0.960494	51
1_e1370	9.395833	1.943232	48	17.34507	2.557275	142	1.028169	0.204338	142	6.178571	0.944911	28	11.75862	1.527257	29	5.586957	1.221513	23
1_ad465	4.925926	1.959708	27	13.74603	3.237722	63	1.142857	0.395831	63	6.28125	1.396641	32	9.555556	2.351123	9	4.904762	0.830949	21
1_am117	6.695652	2.601307	23	15.05882	3.202572	51	1.12963	0.390756	54	6.466667	1.641718	15	8.795455	1.694944	22	5.125	1.433029	8
3_wt	6.027027	3.547194	37	13.89744	3.013346	78	2.438202	1.67844	89	10.34211	2.441492	38	7.464286	2.44528	14	4.948276	0.9387	29
3_e1370	10.19048	2.787062	42	15.09859	2.982954	142	2.345455	1.647817	165	6.577778	1.876758	45	9.363636	1.187051	22	5.438597	1.382513	57
3_ad465	4.793103	3.143921	29	11.65254	2.412139	118	2.349206	1.375892	126	5.565217	1.408613	23	7.080645	0.949533	31	4.625	0.527645	12
3_am117	3.592593	2.40607	27	11.61957	2.820032	92	2.081395	1.129447	86	4.0625	1.507517	48	7.092593	1.91169	27	4.138889	0.81601	36
5_wt	3.470588	2.786522	17	10.775	3.925508	40	2.310345	1.416824	29	6.266667	1.760355	30	6	0.707107	7	4.416667	0.792962	12
5_e1370	6.882353	2.409133	34	13.8875	2.899121	80	2	1.345185	85	6.038462	1.148243	26	8.466667	3.176176	15	4.693548	1.339636	31
5_ad465	3.375	2.268295	32	11.13333	3.243534	105	2.777778	1.949359	81	4.192308	1.600481	26	7.30303	1.832601	33	3	NA	1
5_am117	2.566667	1.654322	30	14.36667	2.97673	30	3.111111	2.339448	36	4.272727	1.695423	22	--	--	--	--	--	--
7_wt	0	NA	1	14	NA	1	8	NA	1	5	NA	1	--	--	--	--	--	--
7_e1370	7.24	3.072458	25	15.04	3.034249	25	2.444444	1.5525	27	4.92	1.255654	25	--	--	--	--	--	--
7_ad465	3.2	2.598076	25	13.08	2.596793	25	2.15	1.496487	20	3.470588	1.624717	17	--	--	--	--	--	--
7_am117	2.857143	2.544836	7	13.28571	2.288689	7	3.875	1.457738	8	4.125	1.642081	8	--	--	--	--	--	--

Supplemental Figures 1-22: Detailed analysis of progeny production and brood size in *C. brenneri, C. remanei,* and *C. elegans* mutants.

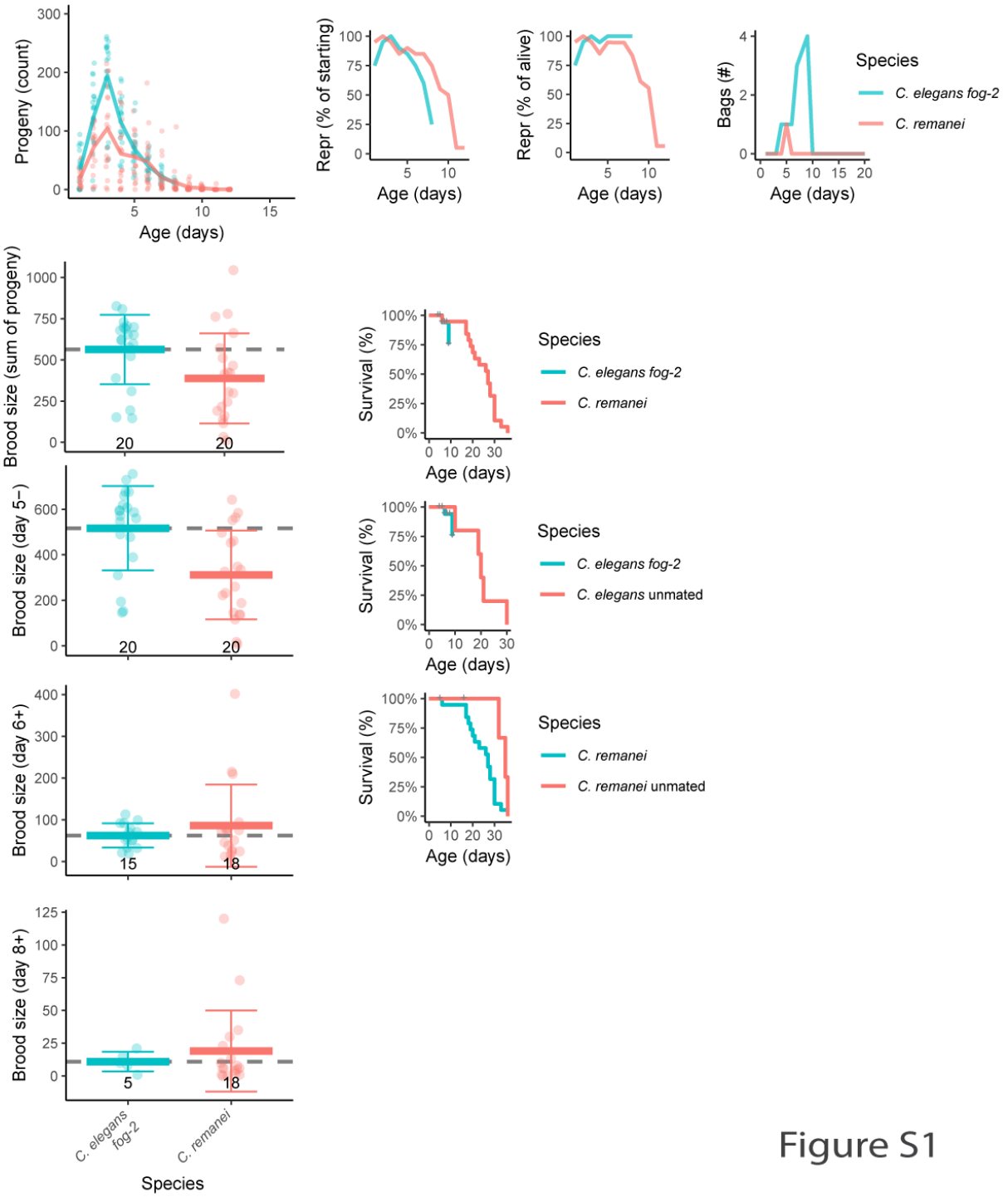
Progeny (count)
Age (days)
Repr (% of starting)
Repr (% of alive)
Bags (#)
Species
C. elegans fog-2
C. remanei
Brood size (sum of progeny)
Brood size (day 5−)
Brood size (day 6+)
Brood size (day 8+)
Survival (%)
C. elegans unmated
C. remanei unmated
C. elegans fog-2
C. remanei
Species

Figure S1

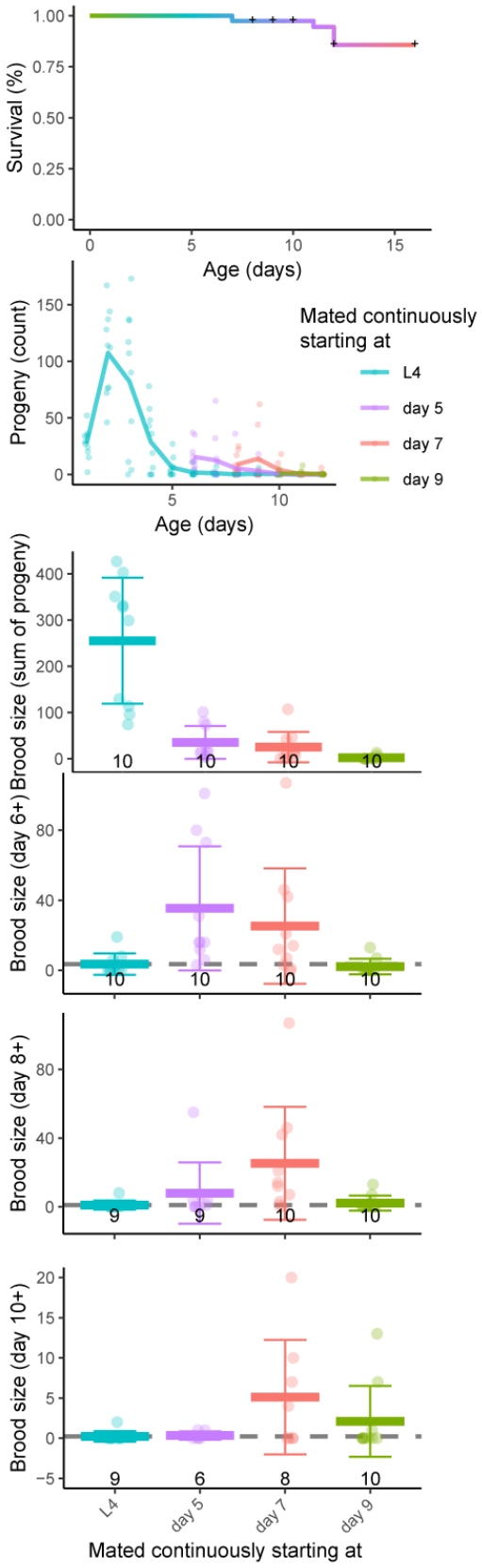

Figure S2

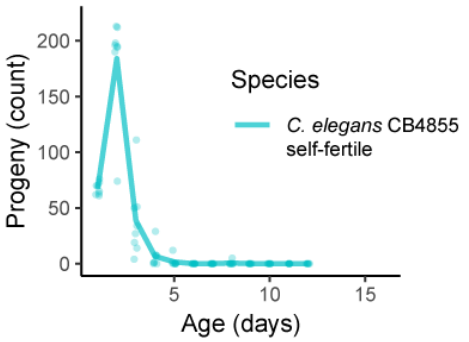

Figure S3

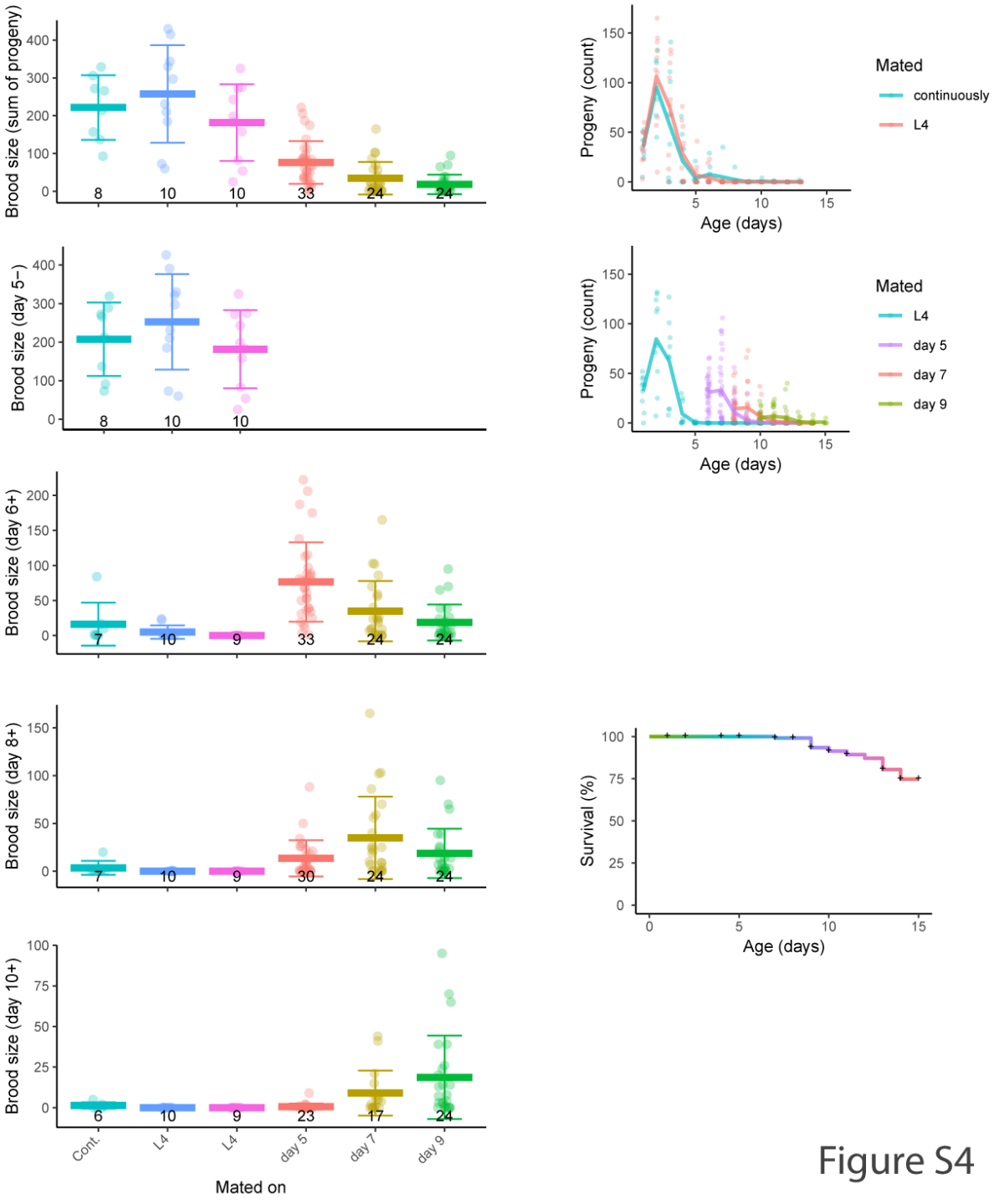
Brood size (sum of progeny)
Brood size (day 5−)
Brood size (day 6+)
Brood size (day 8+)
Brood size (day 10+)
8 10 10 33 24 24
8 10 10
7 10 9 33 24 24
7 10 9 30 24 24
6 10 9 23 17 24
Cont. L4 L4 day 5 day 7 day 9
Mated on
Progeny (count)
Age (days)
Mated
continuously
L4
day 5
day 7
day 9
Survival (%)

Figure S4

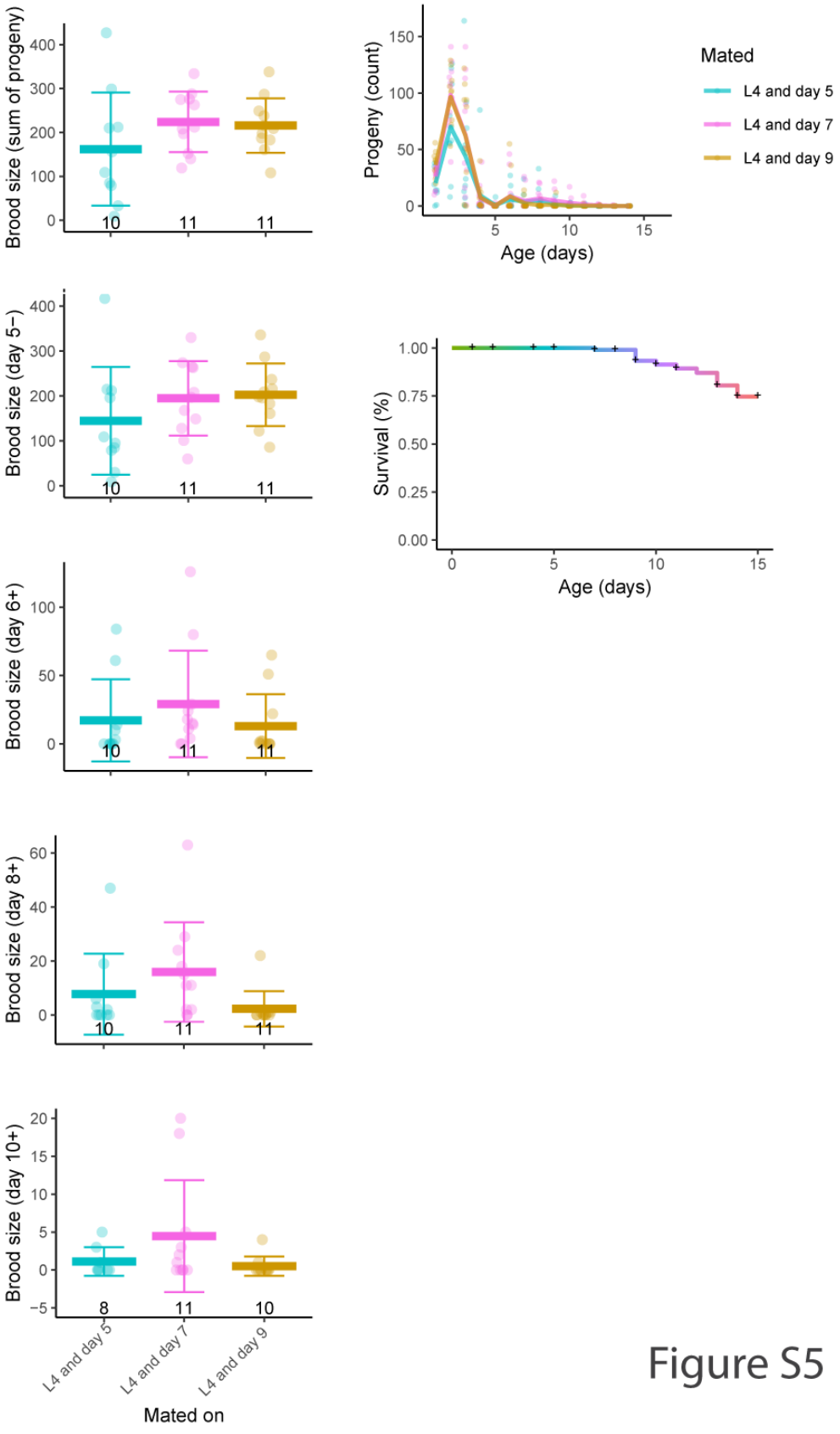
Brood size (sum of progeny)
Progeny (count)
Age (days)
Mated
L4 and day 5
L4 and day 7
L4 and day 9
Brood size (day 5−)
Survival (%)
Age (days)
Brood size (day 6+)
Brood size (day 8+)
Brood size (day 10+)
Mated on

Figure S5

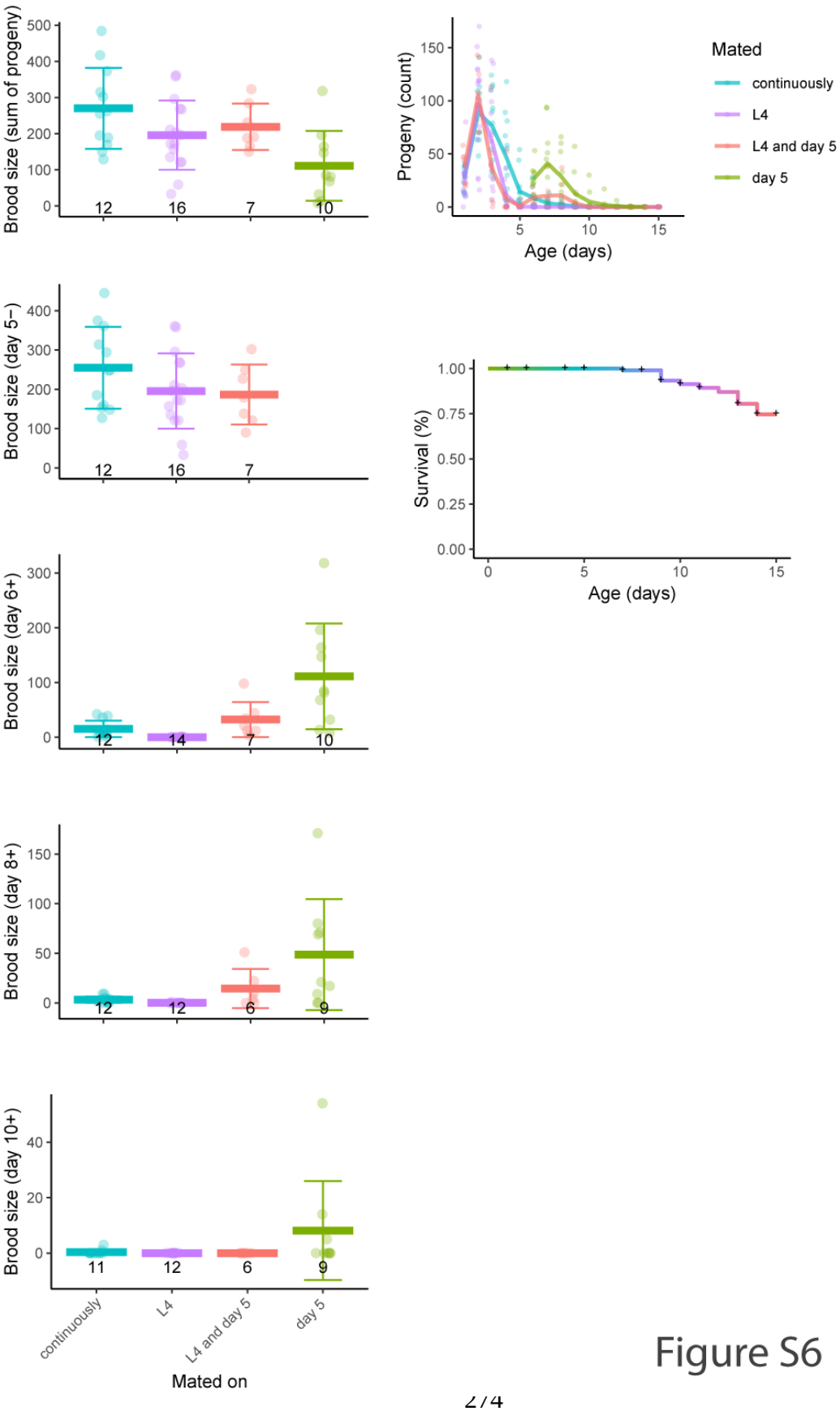
Brood size (sum of progeny)
500
400
300
200
100
0
12
16
7
10
Progeny (count)
150
100
50
0
5
10
15
Age (days)
Mated
continuously
L4
L4 and day 5
day 5
Brood size (day 5−)
400
300
200
100
0
12
16
7
Survival (%)
1.00
0.75
0.50
0.25
0.00
0
5
10
15
Age (days)
Brood size (day 6+)
300
200
100
0
12
14
7
10
Brood size (day 8+)
150
100
50
0
12
12
6
9
Brood size (day 10+)
40
20
0
11
12
6
9
continuously
L4
L4 and day 5
day 5
Mated on

Figure S6

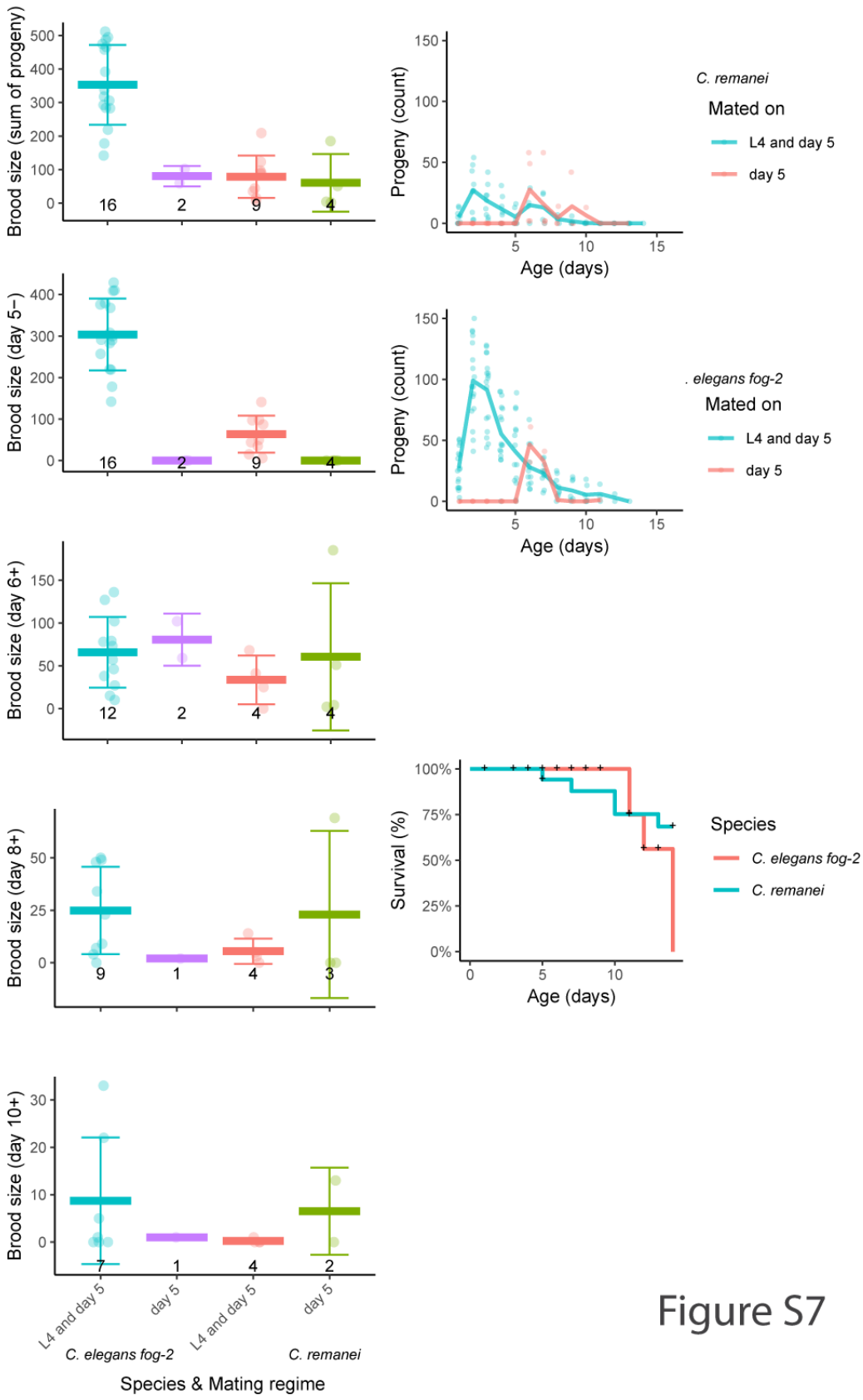
Brood size (sum of progeny)
Brood size (day 5−)
Brood size (day 6+)
Brood size (day 8+)
Brood size (day 10+)
16
2
9
4
16
2
9
4
12
2
4
4
9
1
4
3
7
1
4
2
L4 and day 5
day 5
L4 and day 5
day 5
C. elegans fog-2
C. remanei
Species & Mating regime
Progeny (count)
Age (days)
C. remanei
Mated on
L4 and day 5
day 5
Progeny (count)
Age (days)
. elegans fog-2
Mated on
L4 and day 5
day 5
Survival (%)
Age (days)
Species
C. elegans fog-2
C. remanei

Figure S7

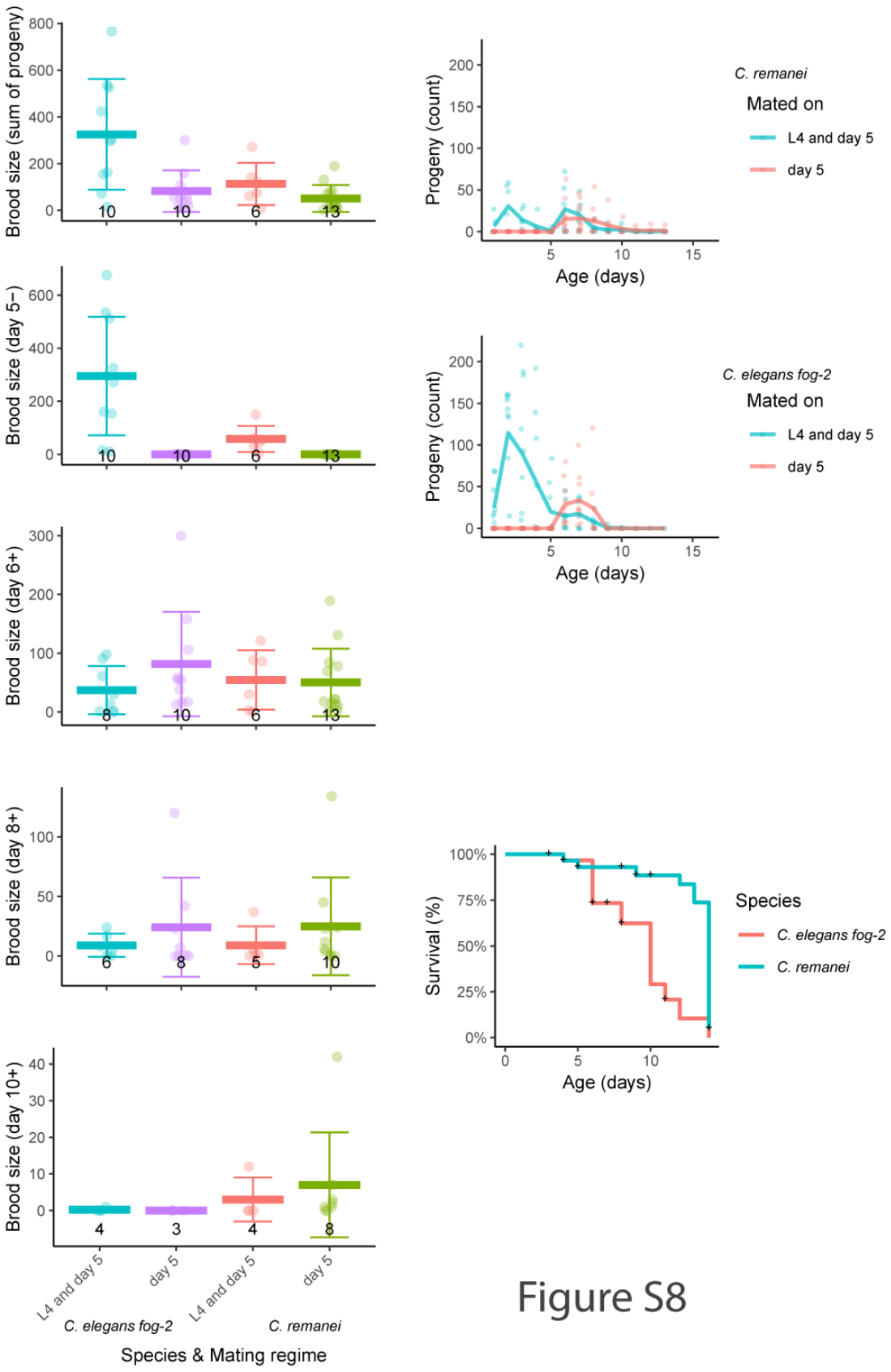
Brood size (sum of progeny)
Brood size (day 5−)
Brood size (day 6+)
Brood size (day 8+)
Brood size (day 10+)
10
10
6
13
8
3
4
5
L4 and day 5
day 5
C. elegans fog-2
C. remanei
Species & Mating regime
Progeny (count)
Age (days)
C. remanei
Mated on
L4 and day 5
day 5
C. elegans fog-2
Survival (%)
Species

Figure S8

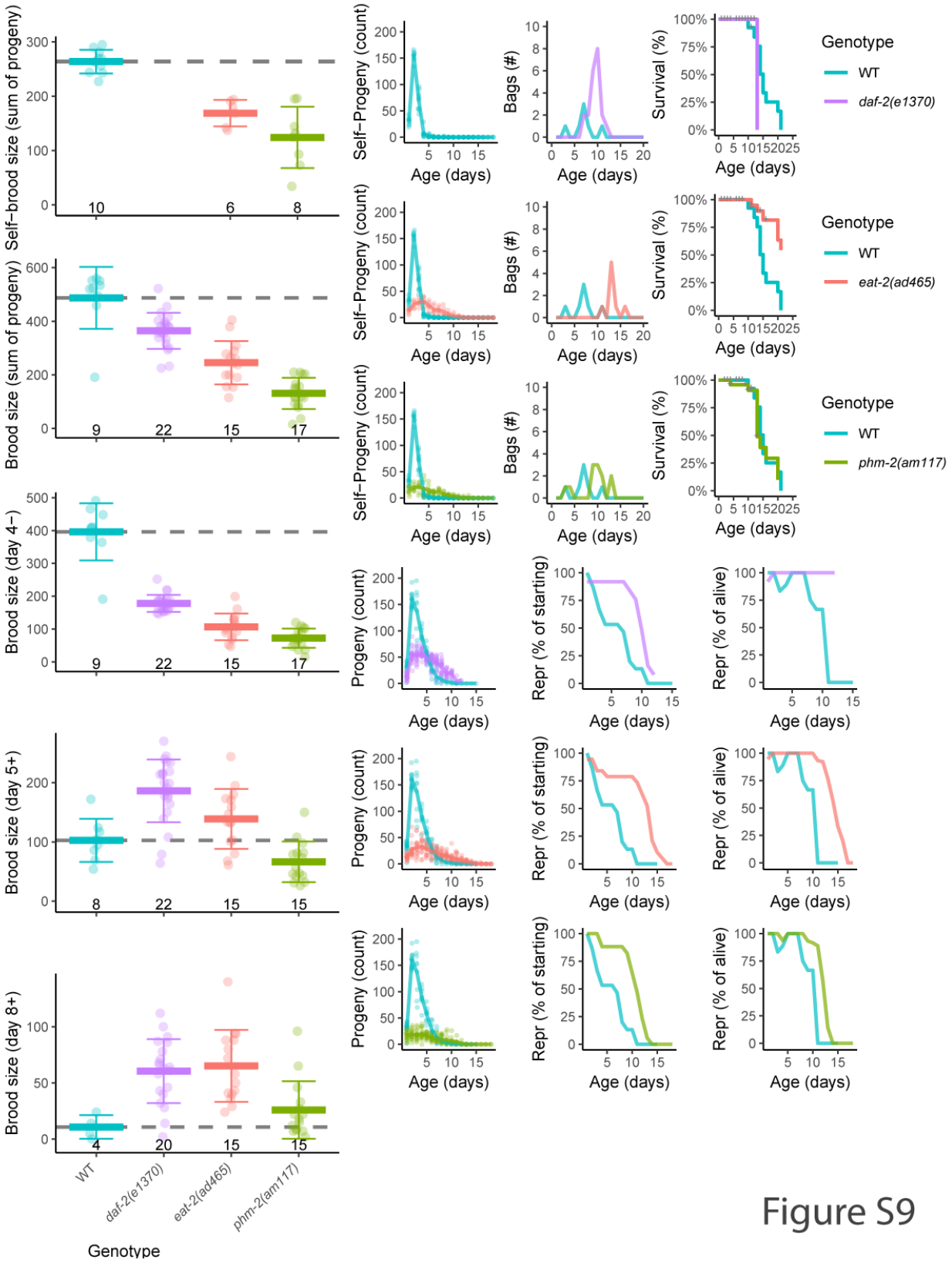
Self−brood size (sum of progeny)
Brood size (sum of progeny)
Brood size (day 4−)
Brood size (day 5+)
Brood size (day 8+)
Self−Progeny (count)
Bags (#)
Survival (%)
Progeny (count)
Repr (% of starting)
Repr (% of alive)
Age (days)
Genotype
WT
daf-2(e1370)
eat-2(ad465)
phm-2(am117)

Figure S9

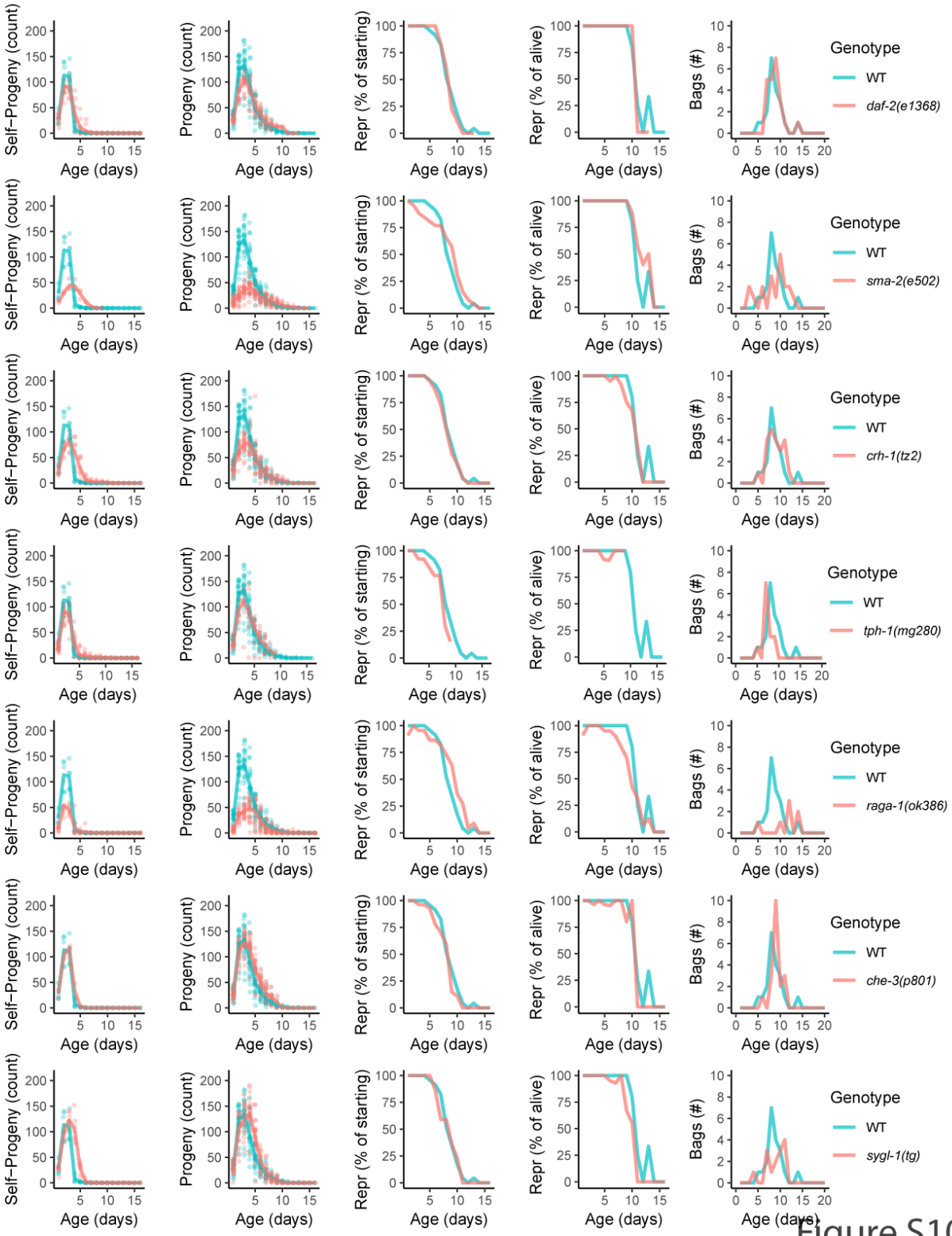
Self−Progeny (count)
Progeny (count)
Repr (% of starting)
Repr (% of alive)
Bags (#)
Age (days)
Genotype
WT
daf-2(e1368)
sma-2(e502)
crh-1(tz2)
tph-1(mg280)
raga-1(ok386)
che-3(p801)
sygl-1(tg)

Figure S10

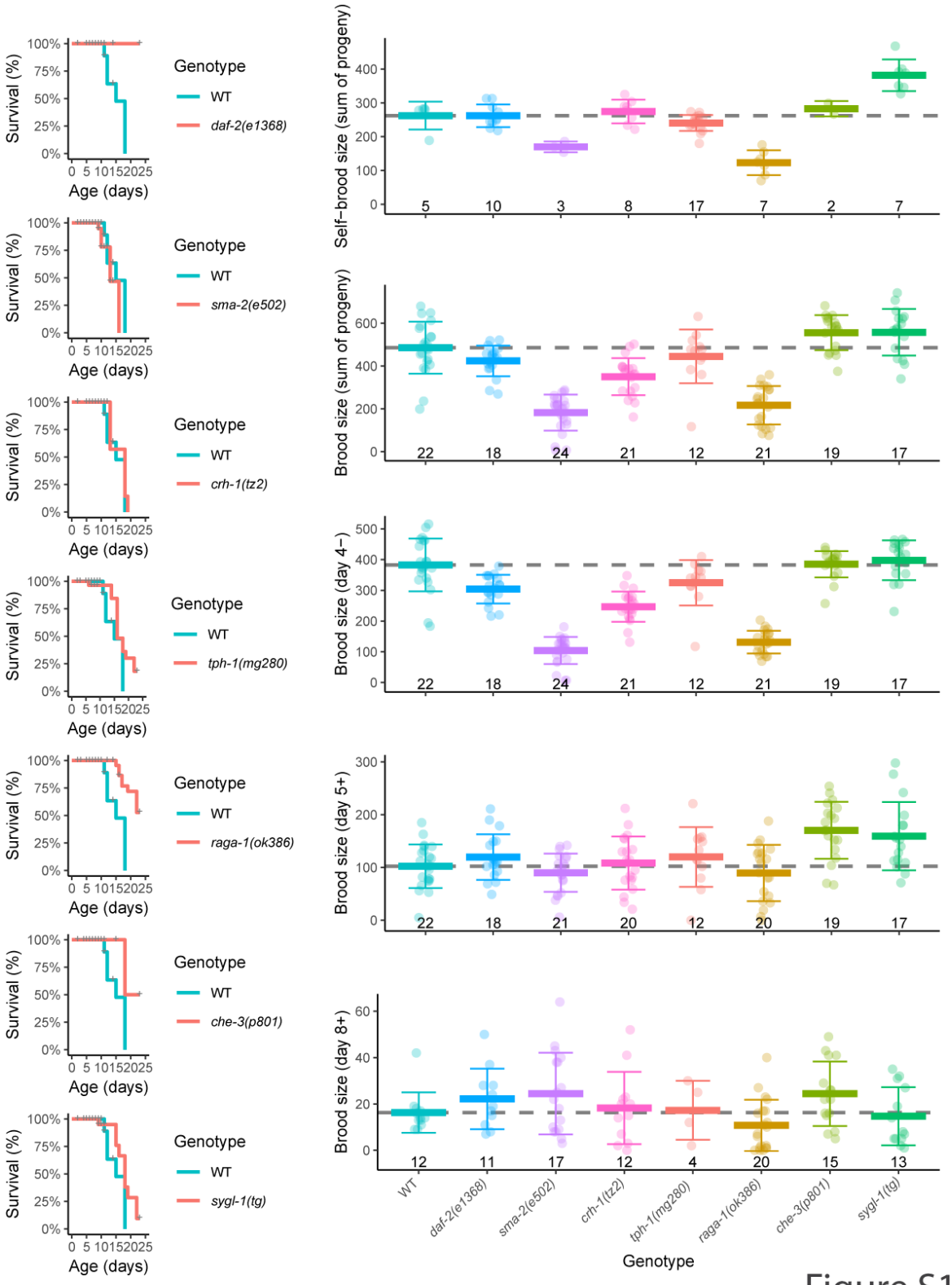
Survival (%)
100%
75%
50%
25%
0%
0 5 10 15 20 25
Age (days)
Genotype
WT
daf-2(e1368)
sma-2(e502)
crh-1(tz2)
tph-1(mg280)
raga-1(ok386)
che-3(p801)
sygl-1(tg)
Self−brood size (sum of progeny)
Brood size (sum of progeny)
Brood size (day 4−)
Brood size (day 5+)
Brood size (day 8+)
5 10 3 8 17 7 2 7
22 18 24 21 12 21 19 17
22 18 24 21 12 21 19 17
22 18 21 20 12 20 19 17
12 11 17 12 4 20 15 13
WT
daf-2(e1368)
sma-2(e502)
crh-1(tz2)
tph-1(mg280)
raga-1(ok386)
che-3(p801)
sygl-1(tg)
Genotype

Figure S11

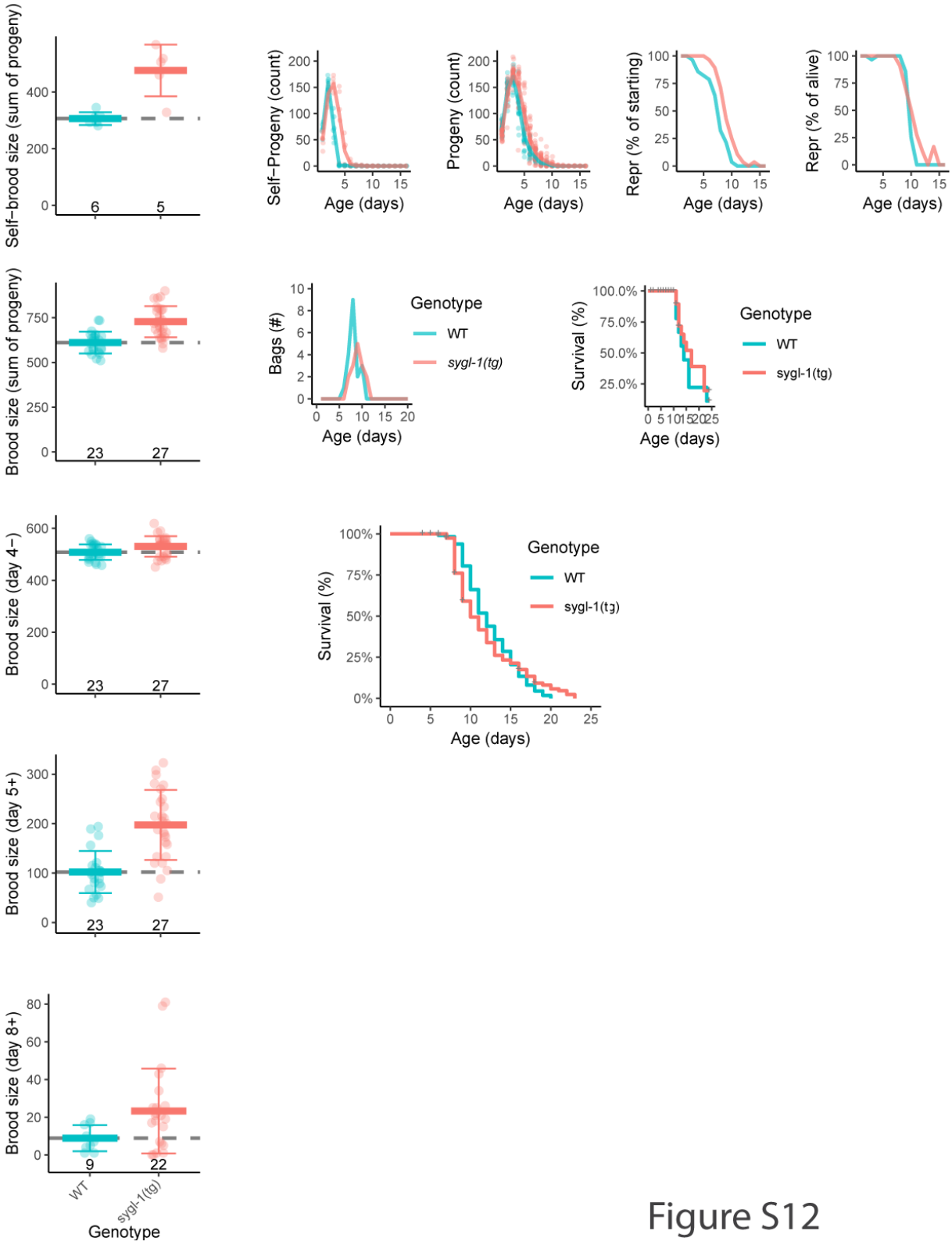
Self−brood size (sum of progeny)
Brood size (sum of progeny)
Brood size (day 4−)
Brood size (day 5+)
Brood size (day 8+)
Genotype
WT
sygl-1(tg)
Self−Progeny (count)
Progeny (count)
Repr (% of starting)
Repr (% of alive)
Bags (#)
Survival (%)
Age (days)

Figure S12

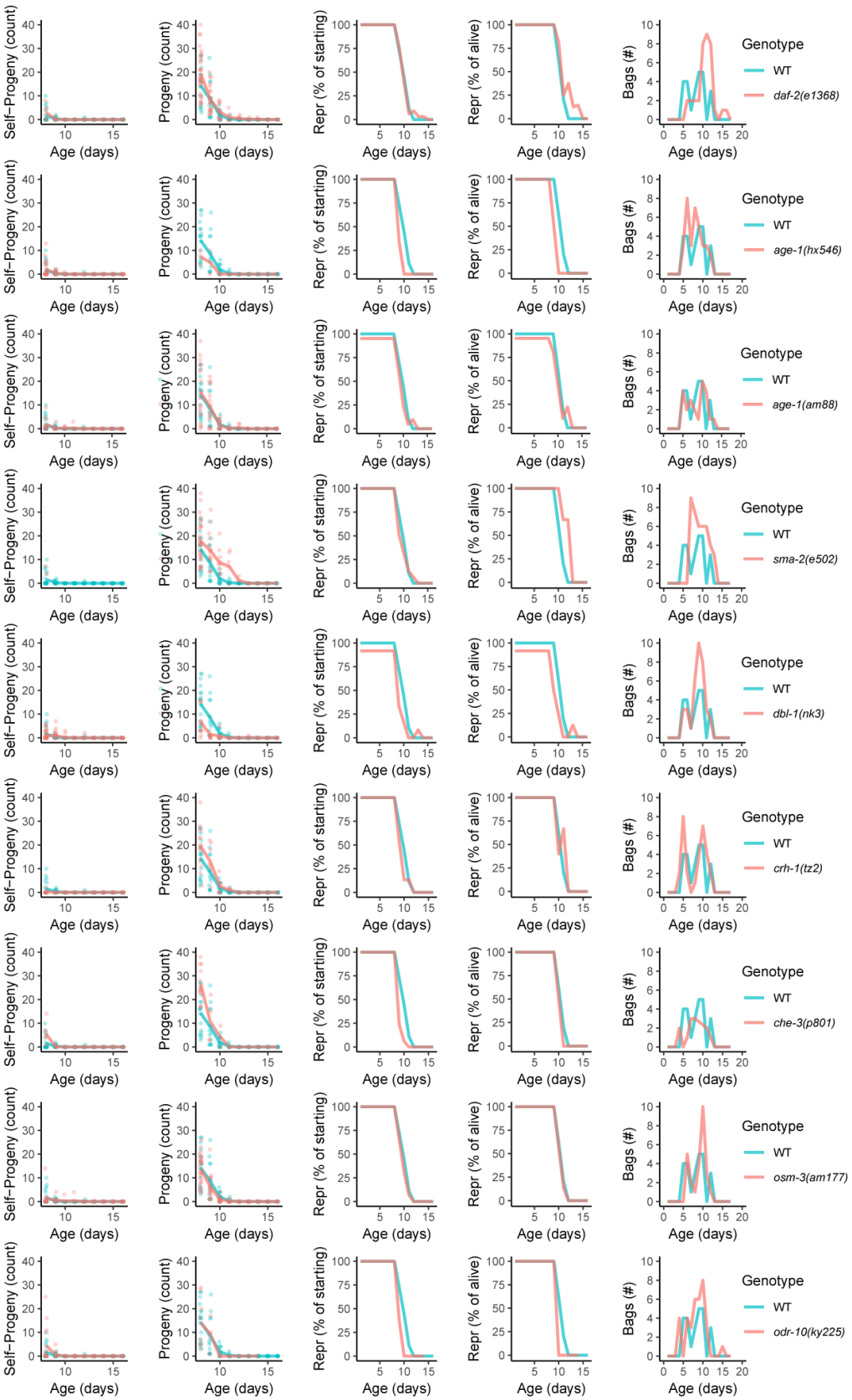
Self−Progeny (count)
Progeny (count)
Repr (% of starting)
Repr (% of alive)
Bags (#)
Age (days)
Genotype
WT
daf-2(e1368)
age-1(hx546)
age-1(am88)
sma-2(e502)
dbl-1(nk3)
crh-1(tz2)
che-3(p801)
osm-3(am177)
odr-10(ky225)

Figure S13

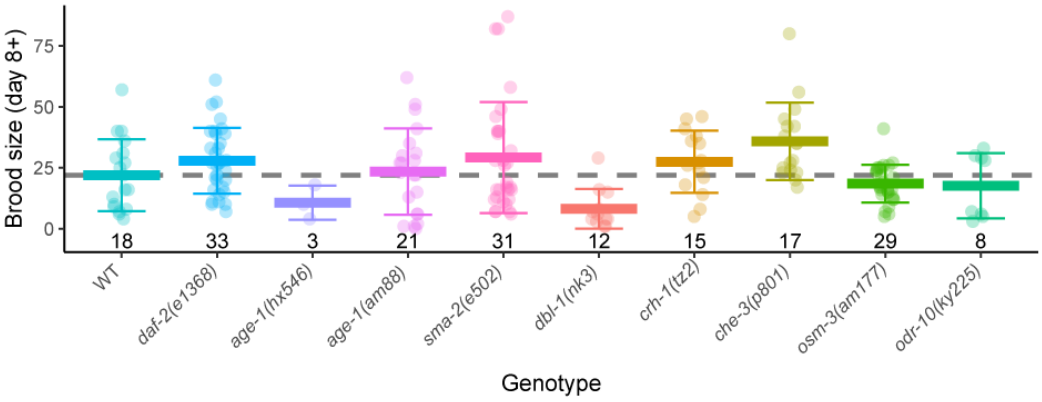
Brood size (day 8+)
75
50
25
0
18
33
3
21
31
12
15
17
29
8
WT
daf-2(e1368)
age-1(hx546)
age-1(am88)
sma-2(e502)
dbl-1(nk3)
crh-1(tz2)
che-3(p801)
osm-3(am177)
odr-10(ky225)
Genotype

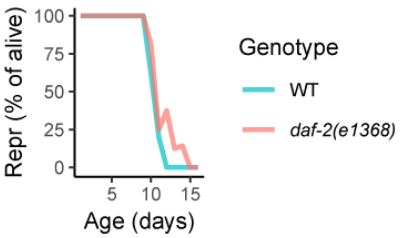
Repr (% of alive)
100
75
50
25
0
5
10
15
Age (days)
Genotype
WT
daf-2(e1368)

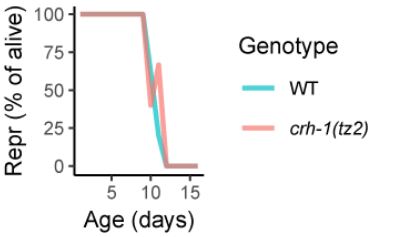
Repr (% of alive)
100
75
50
25
0
5
10
15
Age (days)
Genotype
WT
crh-1(tz2)

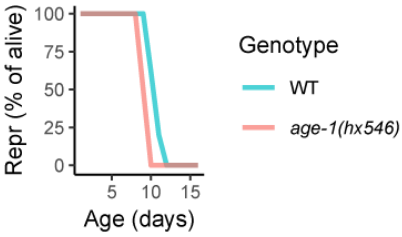
Repr (% of alive)
100
75
50
25
0
5
10
15
Age (days)
Genotype
WT
age-1(hx546)

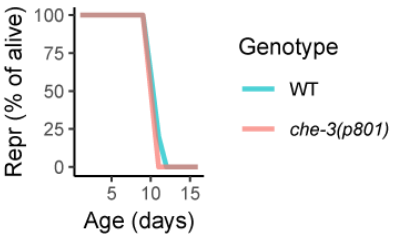
Repr (% of alive)
100
75
50
25
0
5
10
15
Age (days)
Genotype
WT
che-3(p801)

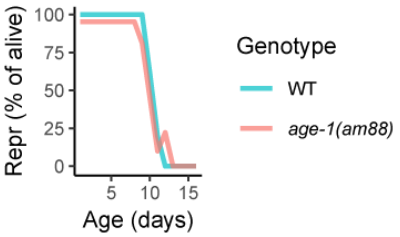
Repr (% of alive)
100
75
50
25
0
5
10
15
Age (days)
Genotype
WT
age-1(am88)

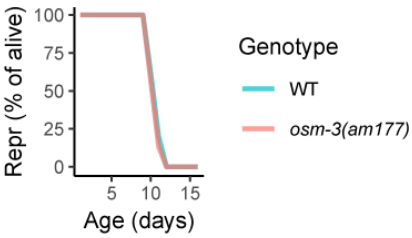
Repr (% of alive)
100
75
50
25
0
5
10
15
Age (days)
Genotype
WT
osm-3(am177)

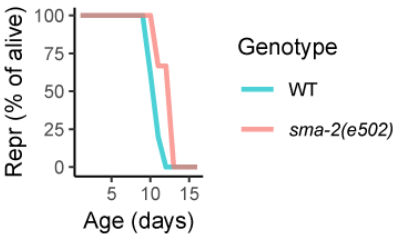
Repr (% of alive)
100
75
50
25
0
5
10
15
Age (days)
Genotype
WT
sma-2(e502)

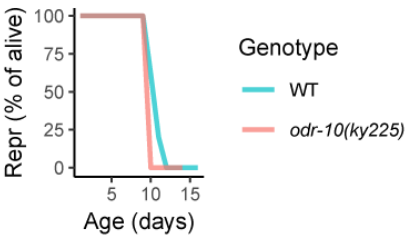
Repr (% of alive)
100
75
50
25
0
5
10
15
Age (days)
Genotype
WT
odr-10(ky225)

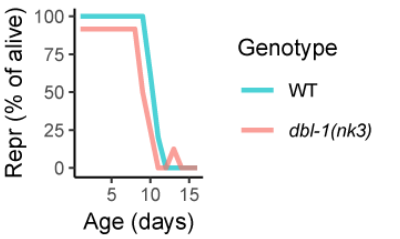
Repr (% of alive)
100
75
50
25
0
5
10
15
Age (days)
Genotype
WT
dbl-1(nk3)

Figure S14

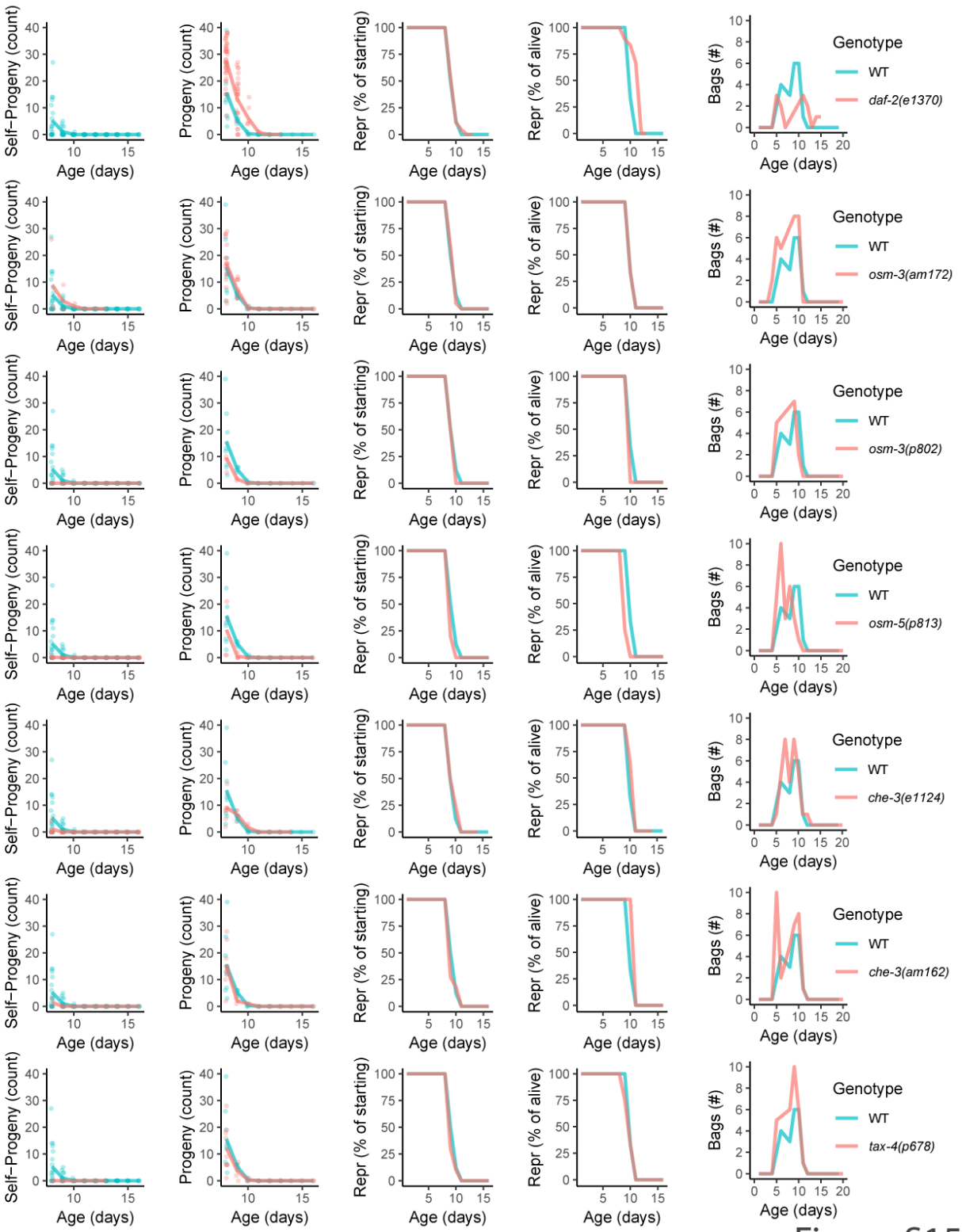
Self−Progeny (count)
Progeny (count)
Repr (% of starting)
Repr (% of alive)
Bags (#)
Age (days)
Genotype
WT
daf-2(e1370)
osm-3(am172)
osm-3(p802)
osm-5(p813)
che-3(e1124)
che-3(am162)
tax-4(p678)

Figure S15

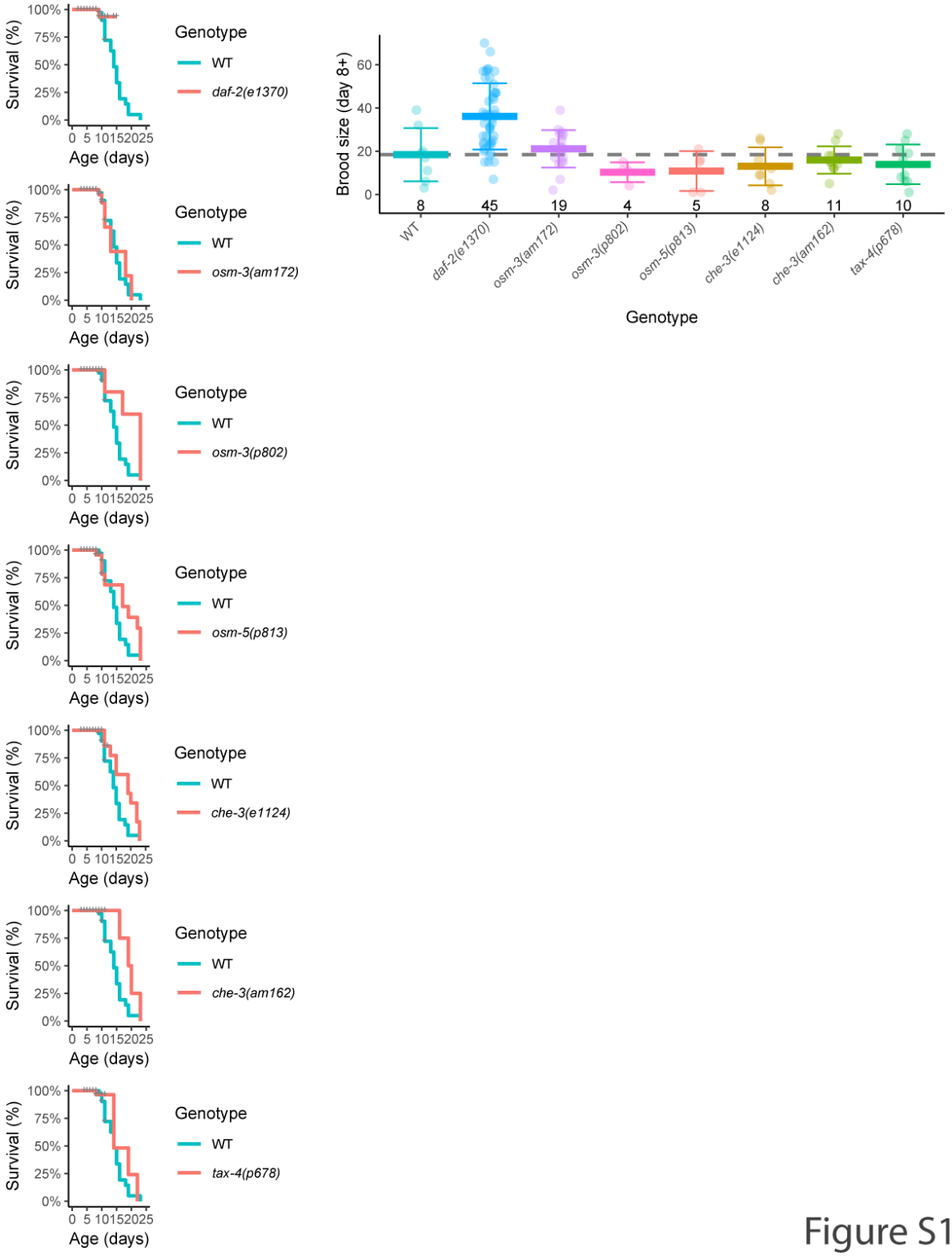
Survival (%)
100%
75%
50%
25%
0%
0 5 10 15 20 25
Age (days)
Genotype
WT
daf-2(e1370)
osm-3(am172)
osm-3(p802)
osm-5(p813)
che-3(e1124)
che-3(am162)
tax-4(p678)
Brood size (day 8+)
0
20
40
60
8
45
19
4
5
8
11
10
WT
daf-2(e1370)
osm-3(am172)
osm-3(p802)
osm-5(p813)
che-3(e1124)
che-3(am162)
tax-4(p678)
Genotype

Figure S16

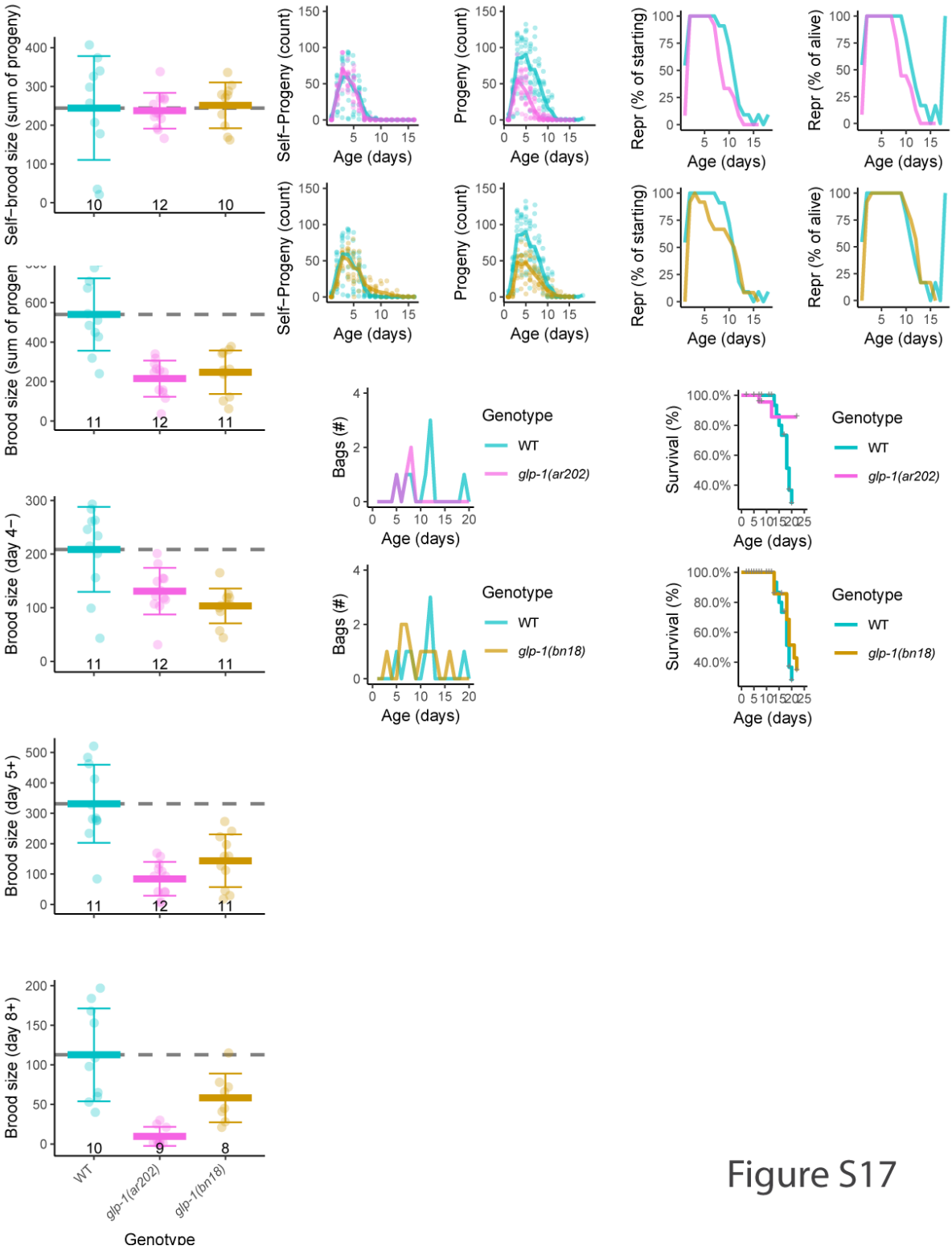
Self−brood size (sum of progeny)
Brood size (sum of progen
Brood size (day 4−)
Brood size (day 5+)
Brood size (day 8+)
10 12 10
11 12 11
11 12 11
11 12 11
10 9 8
WT
glp-1(ar202)
glp-1(bn18)
Genotype
Self−Progeny (count)
Progeny (count)
Repr (% of starting)
Repr (% of alive)
Age (days)
Bags (#)
Survival (%)
Genotype
WT
glp-1(ar202)
glp-1(bn18)

Figure S17

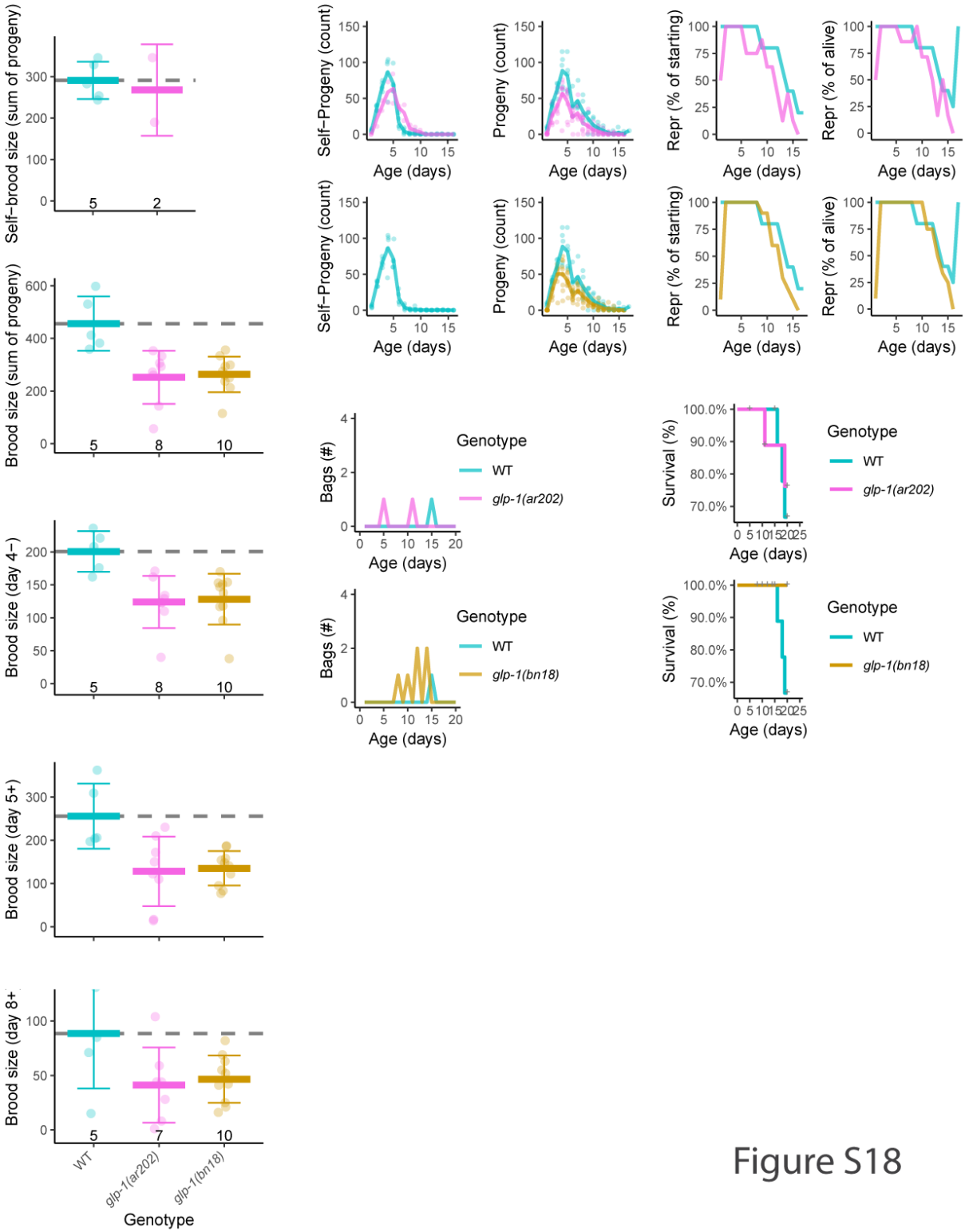
Self−brood size (sum of progeny)
Brood size (sum of progeny)
Brood size (day 4−)
Brood size (day 5+)
Brood size (day 8+)
Genotype
WT
glp-1(ar202)
glp-1(bn18)
Self−Progeny (count)
Progeny (count)
Repr (% of starting)
Repr (% of alive)
Age (days)
Bags (#)
Survival (%)
Genotype
WT
glp-1(ar202)
glp-1(bn18)

Figure S18

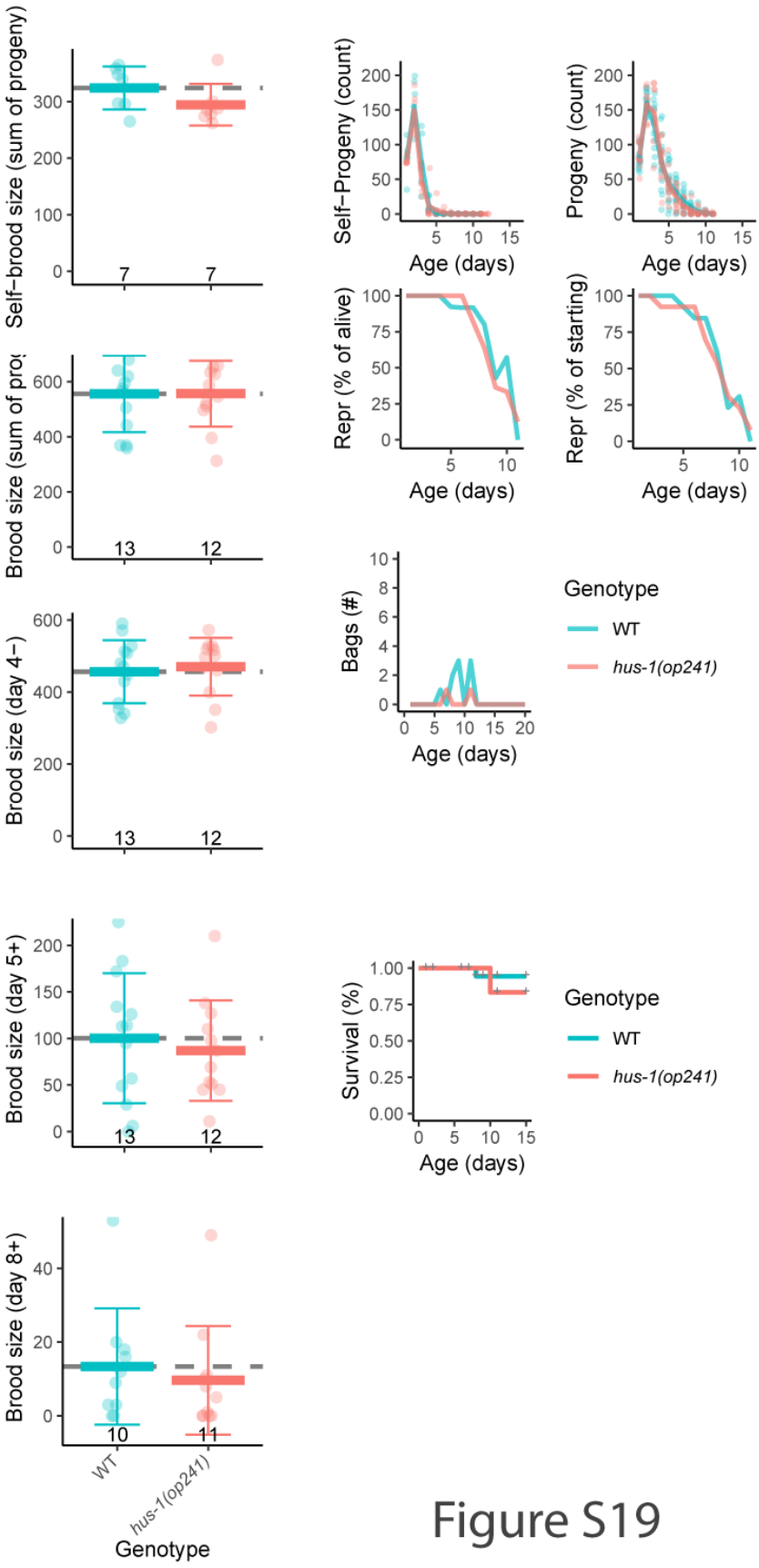
Self−brood size (sum of progeny)
Brood size (sum of pro
Brood size (day 4−)
Brood size (day 5+)
Brood size (day 8+)
7
7
13
12
13
12
13
12
10
11
WT
hus-1(op241)
Genotype
Self−Progeny (count)
Progeny (count)
Repr (% of alive)
Repr (% of starting)
Bags (#)
Survival (%)
Age (days)
Genotype
WT
hus-1(op241)

Figure S19

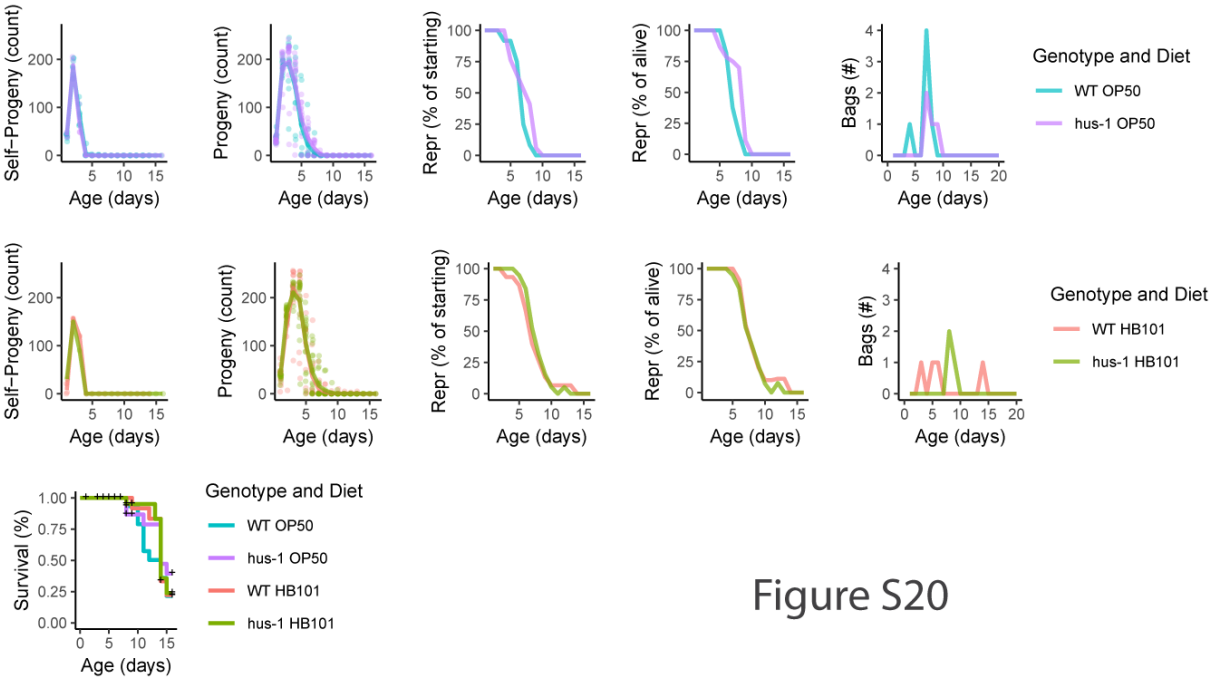
Self−Progeny (count)
Progeny (count)
Repr (% of starting)
Repr (% of alive)
Bags (#)
Age (days)
Genotype and Diet
WT OP50
hus-1 OP50
WT HB101
hus-1 HB101

Survival (%)
Age (days)
Genotype and Diet
WT OP50
hus-1 OP50
WT HB101
hus-1 HB101

Figure S20

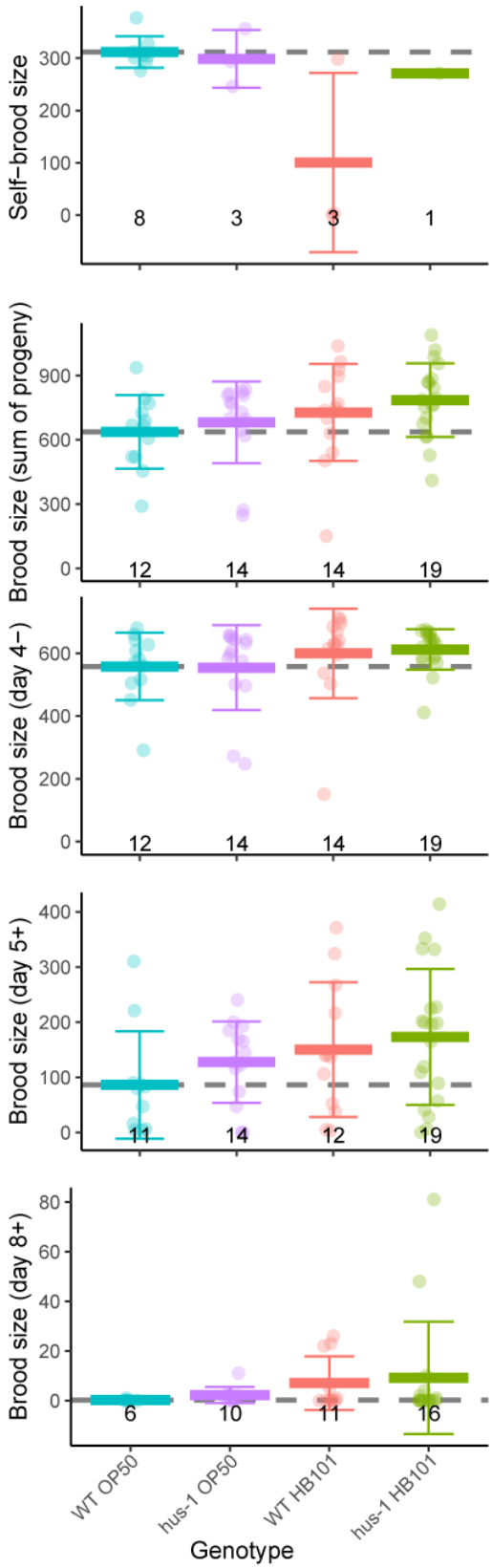
Self−brood size
300
200
100
0
8
3
3
1
Brood size (sum of progeny)
900
600
300
0
12
14
14
19
Brood size (day 4−)
600
400
200
0
12
14
14
19
Brood size (day 5+)
400
300
200
100
0
11
14
12
19
Brood size (day 8+)
80
60
40
20
0
6
10
11
16
WT OP50
hus-1 OP50
WT HB101
hus-1 HB101
Genotype

Figure S21

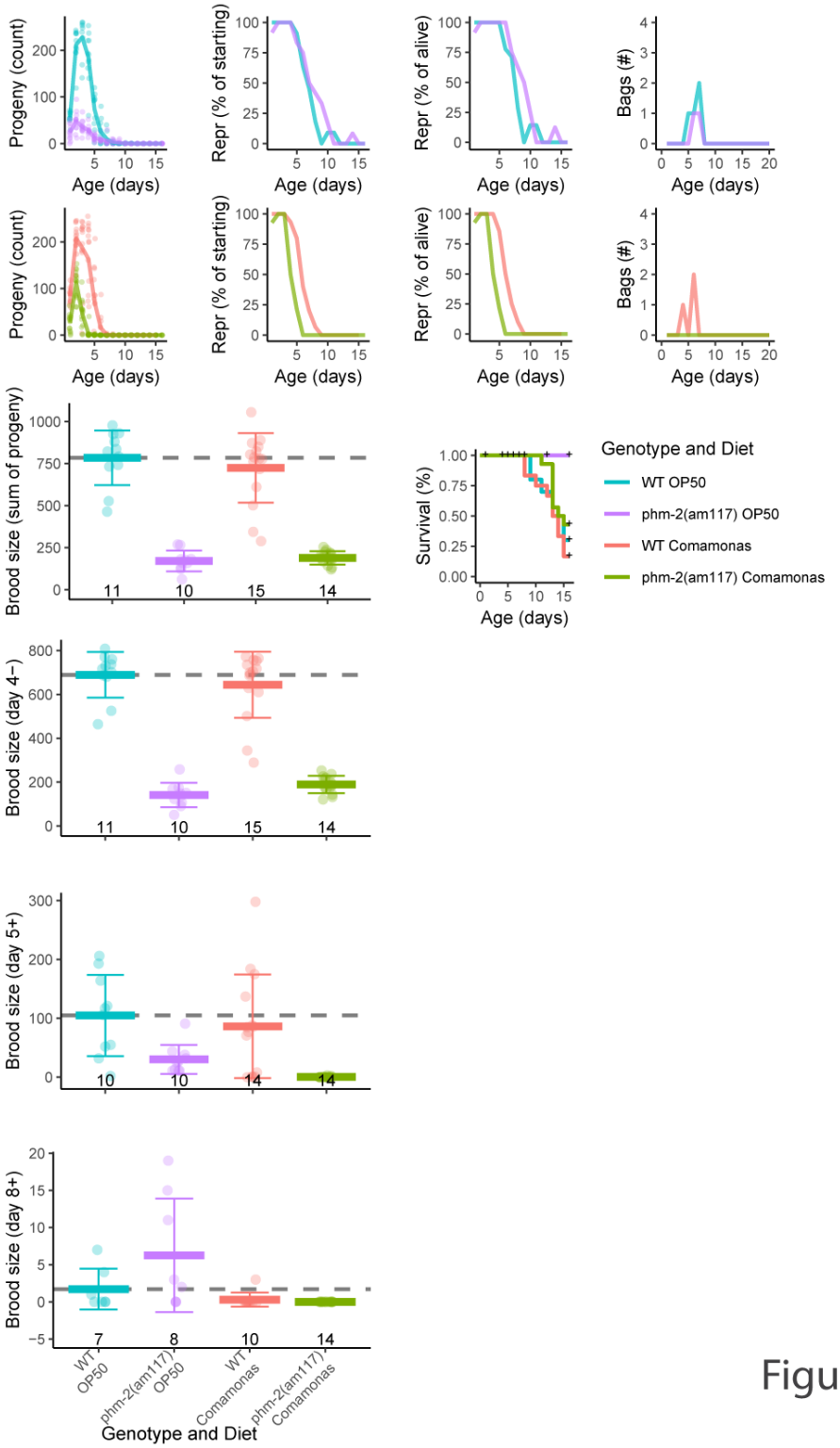
Progeny (count)
Repr (% of starting)
Repr (% of alive)
Bags (#)
Age (days)
Brood size (sum of progeny)
Brood size (day 4–)
Brood size (day 5+)
Brood size (day 8+)
Survival (%)
11
10
15
14
7
8
10
14
Genotype and Diet
WT OP50
phm-2(am117) OP50
WT Comamonas
phm-2(am117) Comamonas

Figure S22